Subdivision Surfaces: C^2 schemes and generalized control nets.

Vom Fachbereich Mathematik
der Technischen Universität Darmstadt
zur Erlangung des Grades eines
Doktors der Naturwissenschaften
(Dr.rer.nat.)
genehmigte

Dissertation

von
Dipl. Math. René Hartmann
aus Penang Island/Malaysia.

Referent:	Prof. Dr. U. Reif.
Korreferent:	Prof. Dr. H. Prautzsch
Tag der Einreichung:	10. Dezember 2010
Tag der mündlichen Prüfung:	17. März 2011

Darmstadt 2011
D 17

German abstract / Deutsches Abstract

Wir führen neue Basen für C^2-Splines der Ordnungen sieben und acht ein, inkl. Masken für binäre Unterteilung. Diese Basen zerlegen den Funktionenraum in die direkte Summe des Raums der kubischen Splines, sowie von "Details", die vorrangig für Krümmungsstetigkeit an irregulären Punkten im bivariaten Fall notwendig sind. Wichtige Eigenschaften wie Konvergenz des kubischen Teils werden gezeigt. Weiterhin werden neue Aspekte polynomialer Unterteilung im regulären Fall aufgezeigt. Das dritte Kapitel beschäftigt sich mit der Konstruktion von Charakteristischen Abbildungen; des weiteren wird ein Weg präsentiert, wie deren Injektivität sich für undendlich viele Wertigkeiten nachweisen lässt. Konstruktion und Diskussion von uns konstruierter C^2-Verfahren sind Gegenstand von Kapitel 4. Kapitel 5 beschäftigt sich mit Konvergenzgeschwindigkeiten von parametrischer und Hausdorff-Distanz zwischen Kontrollnetzen und Subdivisionsfläche in der Umgebung von irregulären Punkten, wobei die dafür verantwortlichen Eigenschaften der Netze im Begriff der (irregulären) Proxies abstrahiert werden. Weiterhin analysiert werden Konvergenz-Geschwindigkeit von Einheitsnormalen. Ein Konzept, langsame Konvergenz zu vermeiden, sowie seine Diskussion, schließen diese Betrachtungen ab.

Contents

Contents **5**

1 Introduction **9**

2 Polynomial Subdivision in the Regular Setting **11**
2.1 General terms and notations 12
Relations on function spaces 12
2.2 Subdivision of polynomials 15
Outlook 26
2.3 Cardinal cubic B-splines 26
Multivariate setting 32
2.4 B-splines of orders 7–8 33
Binary subdivision 36
Designer's viewpoint 37
2.5 A_7/A_8-spline basis 39
Decomposing the function space 39
Definition 41
Masks for binary Subdivision 44
2.6 Change of B- to A_7/A_8-basis 44
Univariate scenario 44
The domain $\mathbb{R}^2 \setminus (-\frac{1}{2}, \frac{1}{2})^2$ (in preparation of extraordinary points) 53
2.7 Convergence of the cubic part 58
2.8 The bundle-paradigm in the bi-variate tensor scenario 65

2.9 How the non-cubic part of a spline comes into play—outlook 67

3 The Characteristic Map 71
3.1 Setup for non-regular points 72
3.2 Tools for the study of non-regular points 75
The OOP-class `irP` 76
The OOP-class `PolarRing` 81
3.3 How to construct χ 81
Schemes on L-domains 82
Polar schemes 86
3.4 How injectivity can be verified for infinitely many valencies 88
Prerequisite of the technique 89
Showing that the premises of the theorem are fulfilled 90
Verifying positivity of $\mathbb{R} \cap \operatorname{image} c$ 92
3.5 Topology of the image of χ 94
Continuity of the extension 95
The signed distance function 97
Inheritance of injectivity onto ψ 99
Properties of the $\psi(r\,\mathbf{S}_n)$, such as simple-connectedness . . 101

4 C^2 schemes 105
4.1 Historical note 106
4.2 Extending splinerings by the PTER-scheme 110
Revised PTER-scheme 110
Accelerating schemes 112
Calculating derivatives of $\mathbf{x} \circ \chi^{-1}$ 113
4.3 Extension by quadratic forms 115
A sufficient condition for quadratic precision 116
Route to a stationary subdivision matrix 118
Restriction to homogeneous quadratic forms 119
The Euler-Lagrange equation 122
Sufficient conditions for invariance under Euclidean motions 123
4.4 Implementation of the extension 128
Numerical integration on a single ring 130
Minimizing the quadratic functional 132
4.5 Results 133
Differential operators of degree 3 133
Differential operators of degree 2 138

5 Proxies of subdivision surfaces **151**
5.1 Defining extraordinary proxies 152
5.2 Parametric distance 156
5.3 Lipschitz continuity of the eigenfunctions 162
5.4 Hausdorff distance 169
The fundament 170
Estimate of Hausdorff distance 176
5.5 Graphs over the subdominant component 177
5.6 Super-converging proxies 180
Super-convergent, piecewise (bi-) linear proxies imply unusable central surfaces 186
5.7 Convergence class of unit normals 190
Assumptions 190
Goal of the section 190
Dissection 191
The stepping stone 195
Regular region on outermost rings 196
Towards the central point 197
Region of Transition 198
5.8 Postproxies: how convergence for Catmull-Clark proxies can be put straight 200
Basic principles 201
Constructing a subdominant postproxy 203
Reasoning behind the construction 206

6 Conclusion and outlook **213**

A Additional contents **215**
A.1 Tools for univariate splines 215

Bibliography **217**

Chapter 1

Introduction

In 1978, spline subdivision was generalized for bi-cubic splines to meshes with extraordinary points by Catmull and Clark [4]. Near-simultaneously, Doo and Sabin generalized subdivision of quadratic box splines [11] in a similar fashion. Although sometimes slow convergence rates of control nets to limit surface were certainly observed even back then, subdivision surfaces rapidly gained popularity in computer graphics. In 1987, Charles Loop introduced a scheme for triangular-meshes [34], which generalized box splines[1] to extraordinary points.

A number of works on C^1 continuity of subdivision surfaces at extraordinary points followed [2, 64]. But it was only until 1993 that C^1 continuity of subdivision surfaces was fully understood [55]. Further, it was realized that curvature continuity at extraordinary points needs polynomials of degree at least six. Two related techniques for such C^2 schemes were developed: *Freeform Splines*, and *TURBS*. Both were published near-simultaneously. Unfortunately, neither of the competing concepts gained broader acceptance.

Then, in spring 2006, guided subdivision surfaces [27], developed by J. Peters and K. Karciauskas, and the PTER-scheme that was derived from it by U. Reif [50], opened new avenues toward C^2 surfaces. The crucial new element was the extension of more functions onto the next spline ring than

[1]The book *Box Splines* [9] is a good introduction to box splines.

merely the polynomials $\chi_1^i \chi_2^j$, $i + j \leq 2$: higher order terms were permitted to decay more slowly. As a consequence, the technique relied on infinitely many surface rings towards the singularity.

This work began shortly after the appearance of guided subdivision schemes.

In Chapter 2 we introduce and discuss a new basis for C^2 splines of orders seven–eight. Cardinal cubic B-splines are among the generating elements of this basis, which allows to decompose the space of polynomials of high degree into the direct sum of the subspace of cubic splines, and some "details", whose purpose is to allow for curvature continuity at extraordinary points in the bivariate setting. Masks for binary subdivision are provided. We also prove convergence rates of the cubic part of the spline under repeated refinement. We show how it is possible to change from B-spline representations to this basis.
Besides this main topic of the chapter, we point out new insights into polynomial subdivision in the regular setting. The analysis leads to techniques of a general nature that allow to deduce convergence rates for generalized control structures toward the limit curve, or surface.

The third chapter centers on the characteristic map of a subdivision scheme. We present a method by which characteristic maps to arbitrary eigenvalues $0 < \lambda < 1$ can be constructed, which is, for instance, needed for the PTER-scheme. Further, a solution to verifying injectivity of a characteristic map for infinitely many valencies is presented and executed at hand of a sample characteristic map.

In Chapter 4 we construct and test C^2-subdivision schemes based on the PTER-principle by minimizing quadratic functionals. We discuss some selected differential operators that can be used, and example surfaces, as well as generating splines derived by them.

Convergence rates of control nets have been studied extensively only in recent years. Chapter 5 further develops the concept of extraordinary proxies from *Subdivision Surfaces* [50]. Proxies abstract the relevant properties that make control nets converge to the limit surface. Parametric and Hausdorff distances are estimated, with sharpness established for each. We continue by analyzing convergence speed of unit normals in the vicinity of extraordinary points. Finally, we conclude by pointing out how slow convergence—of distance or of normals—can be circumvented in situations where the Catmull-Clark algorithm is still used. This also provides a new perspective on using control-nets as approximations to the limit surface.

Chapter 2

Polynomial Subdivision in the Regular Setting

In this chapter, we examine splines, as well as their subdivision in the regular setting. For these schemes, under repeated subdivision the control polygon converges toward the original spline. Thus, a separate analysis of the smoothness of the limit curve or surface is superfluous.

For the more general case of linear, stationary subdivision, including the bi-variate case, an extensive theory can be found in [14, 13, 20, 29, 41, 40, 42]; the book [5] is available at no cost at http://books.google.com/. Conversely, for non-linear or non-stationary schemes, see [15, 39, 30, 32]. More recent examples that produce curves of superior visual fairness are [61, 1]. It should be noted, however, that for non-linear or non-stationary schemes, such as [1], still few is known.

2.1 General terms and notations

Let $|\cdot|$ be a norm on $\mathbb{C}^{1\times d}$. We also denote by it the matrix norm that it induces. $\langle a, b\rangle$ denotes the product of vectors $a, b \in \mathbb{C}^d$. Concatenation and stacking of matrices $M_1, \ldots, M_n$ of appropriate sizes are written in MATLAB notation,

$$[M_1, \ldots, M_n] := (M_1, \ldots, M_n), \quad [M_1; \ldots; M_n] := \begin{pmatrix} M_1 \\ \vdots \\ M_n \end{pmatrix}.$$

Relations on function spaces

Definition 2.1 ($\preccurlyeq, \sim$ and congruencies on spaces of bounded functions)**.** Let $\mathcal{L}_\infty(\mathcal{D})$ be the space of bounded functions from some domain $\mathcal{D}$ to $\mathbb{C}$. Then

$$\begin{aligned} f \preccurlyeq g\colon &\Leftrightarrow \exists c > 0\, \forall z \in \mathcal{D}:\ |f(z)| \le c|g(z)| \\ f \sim g\colon &\Leftrightarrow f \preccurlyeq g \wedge f \succcurlyeq g \\ f \precnsim g\colon &\Leftrightarrow f \preccurlyeq g \wedge f \not\succcurlyeq g \\ f \equiv g \bmod h\colon &\Leftrightarrow f - g \preccurlyeq h. \end{aligned}$$

$\succcurlyeq$ and $\succnsim$ are defined canonically: $f \succcurlyeq g \Leftrightarrow g \preccurlyeq f$ and $f \succnsim g \Leftrightarrow g \precnsim f$.

In this work, $\mathcal{D}$ will usually be $\mathbf{S}_n \times \mathbb{N}$, $\mathbb{N}$, or some subset thereof, which may be interpreted as sequences of functions, or, simply, sequences. Here, it makes sense to read $f \preccurlyeq g$ as "f decays at least as fast as g".

Back to general $\mathcal{D}$, though. $\mathcal{L}_\infty(\mathcal{D})$ with standard operations $+, -, \cdot$ is an algebraic ring. For any $h \in \mathcal{L}_\infty(\mathcal{D})$ the set of all $f \in \mathcal{L}_\infty(\mathcal{D})$ that are $\preccurlyeq h$ is an ideal. Going over to the factor ring yields the congruence relation $\equiv \bmod h$ in Definition 2.1. Further, $\sim$ is an equivalence relation. The equivalence class of f under it is called *convergence class* of f. When two terms are mapped from $\mathbb{C}^d$ to $\mathbb{R}$ by a norm $|\cdot|$, equivalence of norms on $\mathbb{C}^d$ implies the relation $\preccurlyeq, \sim, \precsim, \equiv$ of images is independent of the choice of norm. Consequently, convergence classes do not depend on the norm either.

$\preccurlyeq, \sim, \precsim$ can be defined for arbitrary function spaces. The restriction to bounded functions is only necessary if one wants to calculate modulo certain convergence classes.

An equivalent definition of $\preccurlyeq$ that is sometimes useful can be made by means of

Definition 2.2 (Set of zeros)**.** Denote by

$$\mathcal{Z}_f := \{x \in \mathcal{D} : \quad f(x) = 0\}$$

the *set of zeros* of a function $f \in \mathcal{L}_\infty(\mathcal{D})$.

Lemma 2.3. *Let $f, g \in \mathcal{L}_\infty(\mathcal{D})$. Then*

$$f \preccurlyeq g \Leftrightarrow \left(\begin{array}{r} \sup\limits_{x \in \mathcal{D} \setminus \mathcal{Z}_g} \dfrac{|f(x)|}{|g(x)|} < \infty \\ \wedge\ \mathcal{Z}_g \subseteq \mathcal{Z}_f \end{array} \right).$$

Proof. "$\Rightarrow$": If $f \preccurlyeq g$, there is some $C > 0$ such that

$$C|g(x)| \geq |f(x)| \quad \text{for all } x \in \mathcal{D}. \tag{2.1}$$

Hence, $|f(x)|/|g(x)| \leq C$ if $g(x) \neq 0$. When $g(x) = 0$, by (2.1) $f(x)$ follows to be zero, thus $\mathcal{Z}_g \subseteq \mathcal{Z}_f$.

"$\Leftarrow$": On the other hand, if C is the supremum, $C \geq |f(x)|/|g(x)|$ holds for all $x \in \mathcal{D} \setminus \mathcal{Z}_g$. Thus, $C|g(x)| \geq |f(x)|$ is true for all these x. This last inequality also holds for $x \in \mathcal{Z}_g$: because of $\mathcal{Z}_g \subseteq \mathcal{Z}_f$, $f(x)$ is zero whenever $g(x)$ is. □

In most cases, the relation $f \precsim g$ will not capture strongly enough how much two convergence classes differ. $f \not\asymp g$ within $f \precsim g$ merely means that the supremum

$$\sup_{x \in \mathcal{D} \setminus \mathcal{Z}_f} \frac{|g(x)|}{|f(x)|} = \infty \tag{2.2}$$

does not exist. This is equivalent only to the existence of a series of $(x_n) \subseteq \mathcal{D}$ which makes the quotient in (2.2) diverge.

Let us consider a typical example from practice to point out what we expect instead. Let $\mathcal{D} = \mathbb{R} \times \mathbb{N}$ and

$$f_\ell(x) = \mu^\ell F(x), \quad g_\ell(x) = \lambda^\ell G(x), \quad \ell \in \mathbb{N},$$

for some bounded functions $F, G : \mathbb{R} \to \mathbb{R}$. $0 < \mu < \lambda < 1$ might be eigenvalues of some matrix. The quotient in (2.2) diverges uniformly then, i.e. it does so for *all* $x \in \mathbb{R}$. Note that we have a specialized type of domain here, and that part of it, $\mathbb{N}$, is taken out and plays a special role.

This—as we will see shortly, stronger— convergence allows to deduce far more conclusions of a combination of f, g. We define

Definition 2.4. Let $\mathcal{D} = \widetilde{\mathcal{D}} \times \mathbb{N}$ and $f, g \in \mathcal{L}_\infty(\mathcal{D})$. Instead of $f(x, \ell)$ where $x \in \widetilde{\mathcal{D}}$ and $\ell \in \mathbb{N}$, we also write $f_\ell(x)$ here, similarly for g.
We say f *converges uniformly faster* than g, written as

$$f \prec g$$

if and only if $\mathcal{Z}_g \subseteq \mathcal{Z}_f$ and $S_\ell := \sup_{(x,\ell)\in\mathcal{D}\setminus\mathcal{Z}_g} \frac{|f_\ell(x)|}{|g_\ell(x)|}$ satisfy

1. $S_\ell < \infty$ is true for all $\ell \in \mathbb{N}$, and
2. $\lim_{\ell\to\infty} S_\ell = 0$.

As mentioned previously, $\prec$ and $\precsim$ are related by

Lemma 2.5. *Let $f, g \in \mathcal{L}_\infty(\mathcal{D})$. Then $f \prec g \implies f \precsim g$.*

Proof. With S_ℓ as in Definition 2.4, it is

$$\begin{aligned}\sup_{(x,\ell)\in\mathcal{D}\setminus\mathcal{Z}_g} \frac{|f_\ell(x)|}{|g_\ell(x)|} &= \sup_{\ell\in\mathbb{N}} \sup_{(x,\ell)\in\mathcal{D}\setminus\mathcal{Z}_g} \frac{|f_\ell(x)|}{|g_\ell(x)|} \\ &= \sup_{\ell\in\mathbb{N}} S_\ell.\end{aligned}$$

It follows from $\lim_{\ell\to\infty} S_\ell = 0$ that the sequence S_ℓ is bounded. Thus, $\sup_{(x,\ell)\in\mathcal{D}\setminus\mathcal{Z}_g} \frac{|f_\ell(x)|}{|g_\ell(x)|} < \infty$. The assertion is now implied by Lemma 2.3. □

2.2 Subdivision of polynomials

To begin with

Definition 2.6 ((Non-degenerate) knot vectors)**.** $K = [\kappa_1, \ldots, \kappa_{m+n}]$ with $m \geq n$ is a (non-degenerate) *knot vector* if and only if

1. its components are ascending reals, $\kappa_j \leq \kappa_{j+1}$ for $j \in \{1, \ldots, m+n-1\}$,
2. for every $j \in \{1, \ldots, m\}$, it is $\kappa_j < \kappa_{j+n}$, and
3. the two intervals (κ_n, κ_{n+1}), (κ_m, κ_{m+1}) are both non-empty.

In the following, we will always assume K to be a non-degenerate knot vector. We assume the reader is familiar with the definition and associated terms of B-splines.

Introduction

Although B-splines were introduced in 1946 by Schoenberg [62], it has only been about ten years that a tight estimate of the distance between Bézier control polygon and its curve was found, see [35]. Technique and results were transferred to B-splines and extended by Ulrich Reif [60], showing that

$$\|(B - \breve{B})\mathbf{Q}\|_\infty \leq \max \frac{\sigma_j^2}{8(n-2)} |\triangle^2 \mathbf{Q}|_\infty.$$

Here,

n**:** is the order of the spline,

B**:** the row vector of B-spline basis functions b_j to knot vector K,

$\breve{b}_j$**:** the B-spline control polygon to control points $\mathbf{p}_i = \delta_{ij} = \begin{cases} 1 & \text{if } i = j, \\ 0 & \text{otherwise.} \end{cases}$

$\breve{B}$**:** the row vector of all $\breve{b}_j$.

Q: initial control points,

σ_j^2**:** variance of knots $\kappa_{j+1}, \ldots, \kappa_{j+n-1}$ (depends on n also),

$\triangle^2$**:** the second-difference operator to the respective knot vector K, at order n.

One corollary of this strong statement is that the control polygon converges under a-ary refinemnt ($a \in \mathbb{N}$) toward the spline at a rate of $1/a^{2\ell}$, where ℓ denotes the refinement level. The central part of the proof builds on spline values being convex combinations of the control points.

This fact also follows from interpreting control polygons as quasi interpolants, a tool first introduced by Carl de Boor in [3]. Cohen and Schumaker [6] use this technique; it should be noted that convexity is also crucial to their argumentation.

Both these approaches share that

1. They are specific to B-splines and cannot be directly transferred to functions obtaining values outside the interval $[0, 1]$.

2. They give no insight into the process simultaneously happening in the space of functions during subdivision.

We address both issues by a generalization of B-spline control polygons. The definition of these *proxies* abstracts the relevant properties. We examine the specific situation of B-splines, using them to depict the underlying process in the function space.

We assume the reader is already familiar with B-splines. Classical introductions are *A Practical Guide to Splines* [8], *Box Splines* [9], or *Spline Functions: Basic Theory* [63]. For more recent books, consult *The NURBS Book* [52], *Bézier and B-Spline techniques* [24], or [36, 43]. The e-books [17, 16] are available at http://books.google.com at no cost.

Proxies

Let $B_K = [b_{K,1}, \ldots, b_{K,m}]$ be a basis of the space $\mathcal{S}_n^{(K)}$ of splines of order n with knot intervals[1] $[\kappa_j, \kappa_{j+1})$, $n \leq j \leq m$. It shall depend on its knot vector $K = [\kappa_1, \ldots, \kappa_{m+n}]$ in the manner

$$B_K = B_{c+K}(\cdot + c), \quad c \in \mathbb{R}, \tag{2.3}$$

$$B_K = B_{cK}(\cdot c), \quad c > 0. \tag{2.4}$$

[1]It is typical that multiple knots denote decrease in smoothness in the transition between knot intervals.

A spline basis with these properties is called *consistent under translation of knots*, respectively *consistent under dilation of knots*.

Further, let the $b_{K,j}$ be a *local basis*, too:

1. on each non-empty knot interval $(\kappa_j, \kappa_{j+1}), n \leq j \leq m$, exactly n of the $\{b_{K,i} : 1 \leq i \leq m\}$ take values different from zero and

2. $b_{K,j-n+1}, \ldots, b_{K,j}$ are a basis for the space of polynomials of order n restricted to the interval (κ_j, κ_{j+1}).

The truncated power basis is consistent under translation of knots, but not under dilation. The latter one could easily be remedied, but it still lacks the local basis property.

For univariate splines, essentially only B-splines have all the properties. Our purpose is to point out and name those properties that lead to the following two theorems, 2.8 and 2.13. We begin with an example

Example 2.7 (Binary refinement)**.** Suppose we have a spline that is defined over the unit interval $[0, 1]$. The coarse knot vector be given by

$$K_0 = (-3, -2, -1, 0, 1, 2, 3, 4)\$k,$$

for some $k \in \mathbb{N}$ denoting the knots' joint multiplicity[2]. After two steps of "binary" subdivision, we have knots

$$K_2 = (-0.75, -0.5, -0.25, \ldots, 1.5, 1.75)\$k.$$

Those knots of K_2 which define the spline's values on the sub-interval [0.5, 0.75], are given by $\varphi(K_0)$, where

$$\varphi(x) = \frac{1}{4}x + \frac{1}{2}, \quad x \in \mathbb{R}.$$

This mapping is the composition of a dilation and a translation! Something of similar nature is applicable for the remaining sub-intervals, and, ultimately, at all refinement levels.

Now let us see what happens behind the scenes in the world of functions,

[2]For $k > 1$, not all of the knots of K_0 are needed for the space of splines over $[0, 1]$. We did not like a complex formula distracting the reader - simply ignore the superfluous knots. The same is true for K_2.

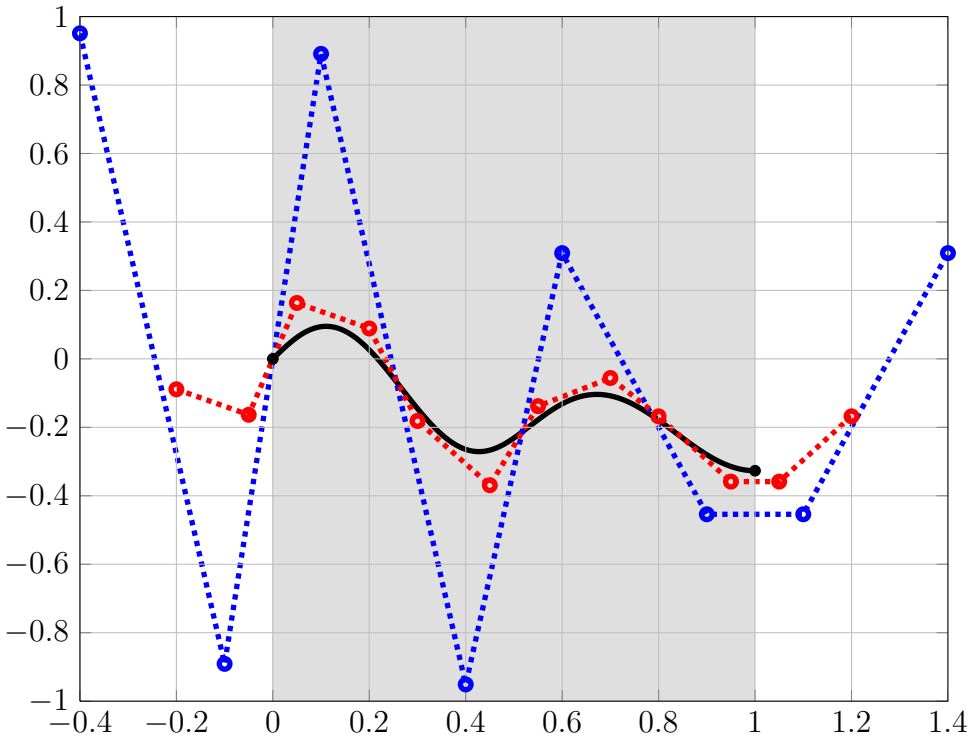

Figure 2.1: Part of a spline of order six (*black*) with knots $\frac{1}{2}\mathbb{Z}\$2$ (the appended \$2 denotes multiplicity). *Blue:* (coarse) control polygon. *Red:* control polygon with refined knots $\frac{1}{4}\mathbb{Z}\$2$. The shaded area indicates the domain of the spline where the various distances are examined.

Theorem 2.8 (Eigenfunctions of refinement)**.** *Let φ be an affine-linear mapping,*

$$\varphi(x) = \varphi_0 + wx, \quad x \in \mathbb{R}$$

for $\varphi_0, \varphi_0 + w \in [0,1]$ with $w \in (0,1)$. Further, $K = [\kappa_1, \ldots, \kappa_{2n}]$ be a non-degenerate knot vector with $(\kappa_n, \kappa_{n+1}) = (0,1)$. For some initial control points $\mathbf{P}_K$ let $\mathbf{P}_{\varphi(K)}$ be defined by

$$B_K(t)\mathbf{P}_K =: B_{\varphi(K)}(t)\mathbf{P}_{\varphi(K)}, \quad t \in \varphi([0,1)).$$

Then the linear mapping $\mathbf{P}_K \mapsto \mathbf{P}_{\varphi(K)}$ has eigenvalues

$$1, w^1, w^2, \ldots, w^{n-1}.$$

Calling the associated eigen-vectors and -functions $\mathbf{v}_j$*, respectively* $f_j := B_K\mathbf{v}_j$*, we have*

$$f_j(t) = (t - \operatorname{Fix}\varphi)^j, \quad j = 0, \ldots, n-1.$$

Here, $\varphi_\star := \operatorname{Fix}\varphi = \frac{\varphi_0}{1-w} \in \varphi([0,1])$ *is* φ*'s unique fixpoint.*

Proof. Simple algebra yields the formula for (and uniqueness of) $\varphi_\star := \operatorname{Fix}\varphi$,

$$x = \varphi(x) = \varphi_0 + wx \;\Leftrightarrow\; x = \frac{\varphi_0}{1-w}.$$

To see that $\varphi_\star \in \varphi([0,1])$: if $\varphi(0) = \varphi_0 = 0$ it is $\varphi_\star = \varphi_0$ and similarly for $\varphi(1) = \varphi_0 + w = 1$: $\varphi_\star = 1$. Otherwise, the continuous function $\varphi(x) - x$ is greater than zero at $x = 0$ and negative at $x = 1$, hence has a root between $\varphi_0 = \varphi(0)$ and $\varphi_0 + w = \varphi(1)$. Since $\varphi_\star$ is unique, this has to be $\varphi_\star$ itself.

We now have

$$\varphi\left(\varphi_\star + \frac{h}{w}\right) = \varphi_\star + h, \quad h \in \mathbb{R}. \tag{2.5}$$

By (2.3) and (2.4) it follows that

$$B_K = B_{\varphi(K)} \circ \varphi. \tag{2.6}$$

With $\mathbf{v}_j$ the control points of $(t - \varphi_\star)^j_{|[0,1]}$ in terms of B_K,

$$\left(\frac{h}{w}\right)^j = B_K(\varphi_\star + \frac{h}{w})\mathbf{v}_j = B_{\varphi(K)}(\varphi_\star + h)\mathbf{v}_j,$$

where h is any real with $\varphi_\star + \frac{h}{w} \in [0,1]$. Multiplying with w^j yields the claim. □

The eigenvectors $\mathbf{v}_j$ of $\mathbf{P}_K \mapsto \mathbf{P}_{\varphi(K)}$ depend on the knot vector K. Likewise, the specific components of the $\mathbf{v}_j$ are not known in general. But *the eigenfunctions* $f_j := B_K\mathbf{v}_j$ *and -values remain the same*, regardless which K they are based on.

The theorem can easily be used to advantage,

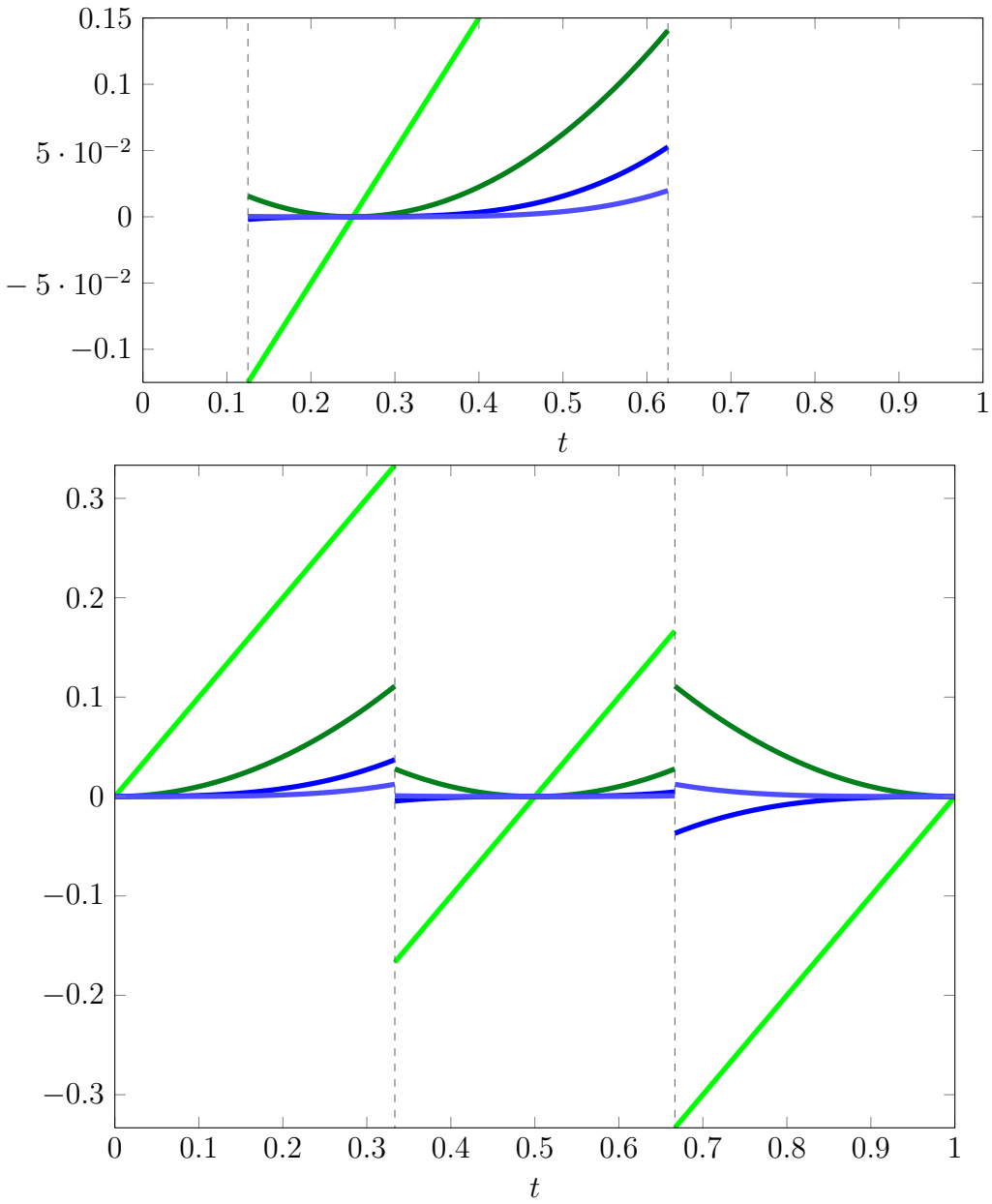

Figure 2.2: *Above:* eigenfunctions of the refinement $\varphi(x) = 0.125 + 0.5x$. *Bottom:* multiple intervals in case of ternary subdivision. The eigenfunctions of degree zero, $t \mapsto 1$, are not shown in either display.

Example 2.9 (Outermost intervals under binary refinement)**.** Revisiting Example 2.7, we turn our attention to the left-most interval. After $\ell \in \mathbb{N}$ steps of binary subdivision, the left-most interval is the image of $[0, 1]$ under

$$\varphi(x) = wx, \quad x \in \mathbb{R}.$$

The width is then given by $w = 2^{-\ell}$. From Theorem 2.8 we know that in the world of functions the refinement operation has eigenfunctions $1, t, t^2, \ldots, t^{n-1}$ and that their eigenvalues are $1, 2^{-\ell}, 2^{-2\ell}, \ldots, 2^{-(n-1)\ell}$. By linear precision, the B-spline control polygons of the first two eigenfunctions are identical to their respective spline. Therefore, the distance between control polygon and spline on $\varphi([0, 1]) = [0, 2^{-\ell}]$ decays at least as fast as $2^{-2\ell}$.

The example raises further questions: does convergence occur solely on the outermost intervals (an analogue case can be made for $[1 - 2^{-\ell}, 1]$)? What about derivatives?

The underlying principle, which makes both values and derivatives of a B-spline control polygon converge toward the spline, is not unique to B-splines. Its more general nature gives it an own right to exist. Therefore, we abstract the crucial properties into

Definition 2.10 ((Regular) generating proxy)**.** Let the order n of the splines be fixed. A univariate *generating proxy* $\breve{b}_{K,j}$ to knots K is a mapping from $\mathbb{R} \to \mathbb{R}$

1. which is consistent under both translation as well as dilation of knots

$$\breve{b}_{K,j} = \breve{b}_{c+K,j}(c + \cdot), \quad c \in \mathbb{R}, \tag{2.7}$$

$$\breve{b}_{K,j} = \breve{b}_{cK,j}(c\cdot), \quad c > 0 \tag{2.8}$$

   in the same way the basis functions $b_{K,j}$ are,

2. whose support is a subset of the support of its associated b_j,

3. that is piecewise C^{m_j-1} for some $m_j \geq 1$ on each of finitely many pieces, the maximal number of which does not depend on the knots themselves.

Definition 2.11 ((Regular) proxies & tupels of generating proxies)**.** Let $f(t) = \sum_{j=1}^{m} b_j \mathbf{p}_j$. Replacing the basis splines b_j by their respective generating proxies $\breve{b}_j$—keeping the coefficients—gives the spline's *proxy* $\breve{f}(t) := \sum_{j=1}^{m} \breve{b}_j \mathbf{p}_j$ *for any* tuple $\breve{B}_K := (\breve{b}_{K,1}, \ldots, \breve{b}_{K,m})$ of generating proxies.

Note that the knots K of the spline space need not be themselves knots of the generating proxies. For the latter ones, they are merely considered parameters. Generating proxies are not required to be piecewise polynomials, either (though most times, they are). Tuples of generating proxies usually have the additional property of being $\breve{n}$-precise for some $\breve{n} \in \mathbb{N}$:

Definition 2.12 ($\breve{n}$-precision)**.** For $\breve{n} \in \{1, \dots, n-1\}$, a tuple $\breve{B}_K$ of generating proxies $\breve{b}_{K,1}, \dots, \breve{b}_{K,m}$ is called *$\breve{n}$-precise* or *has $\breve{n}$-precision* if and only if

1. replacing the spline basis by the tuple of generating proxies leaves all polynomials of order $\breve{n}$ the same, i.e. if $f(t) = \sum_j b_j \mathbf{p}_j$ is a polynomial of order $\breve{n}$, then $\breve{f}(t) = \sum_j \breve{b}_j \mathbf{p}_j = f(t)$, but
2. there is some polynomial of order $\breve{n}+1$ for which $f(t)$ and $\breve{f}(t)$ are not identical, and
3. each of its generating proxies is piecewise $C^{\breve{n}-1}$, i.e. $m_j \geq \breve{n}$ in Definition 2.10(3) above.

Before we proceed, some further terms should be introduced. Let $\mathbf{Q}$ be the vector of initial control points to the n basis functions $b_{K,j}$ that are the local basis for the polynomials of order n on $[0,1)$ to the knot vector K. From the interval $[0,1]$, K may contain 0 and 1 as knots, but none of the points in between.

Let $\mathbf{P} = [\mathbf{p}_0; \dots; \mathbf{p}_{n-1}]$ denote the representation of $B_K\mathbf{Q}$ in the monomial (Taylor) basis t^j, $j \in \{0, \dots, n-1\}$, that is,

$$\mathbf{P} := M\mathbf{Q}, \quad B_K(t)M^{-1} = \begin{bmatrix} 1 \\ \vdots \\ t^{n-1} \end{bmatrix}^T, \ t \in (0,1), \tag{2.9}$$

for some invertible M. Translating the center point t_0 of any *Taylor basis* $(t-t_0)^j$, $j = \{0, \dots, n-1\}$ by s_0 leads to coefficients $T^{(s_0)}\mathbf{P}$ in the new basis $(t-(t_0+s_0))^j$. Note that by its definition, $T^{(-s_0)}$ is the inverse of $T^{(s_0)}$ (conveniently allowing to write the former instead), so

$$B_K(t)M^{-1}T^{(-s_0)} = \begin{bmatrix} 1 \\ \vdots \\ (t-s_0)^{n-1} \end{bmatrix}^T, \ t \in (0,1). \tag{2.10}$$

Theorem 2.13 (Main theorem of proxies: approximation errors)**.** *Suppose we have a tuple of generating proxies that is $\breve{n}$-precise for some $\breve{n} \in \{1, \dots, n-1\}$. Let $\mathbf{P}, \mathbf{p}_j$ be defined from $\mathbf{Q}$ as in equation (2.9).*

a) Let φ be as in Theorem 2.8 and $k \in \{0, \dots, \breve{n}-1\}$. Then the difference of k-th derivatives of spline $\mathbf{x}(t) = B_K(t)\mathbf{Q}$ and proxy $\breve{\mathbf{x}}_{\varphi(K)}(t) = \breve{B}_{\varphi(K)}(t)\mathbf{Q}_{\varphi(K)}$ converges at least as fast as $w^{\breve{n}-k}$, i.e. there is a constant $C > 0$ such that

$$\max_{t \in \varphi([0,1])} \left| \partial^k \left(\mathbf{x} - \breve{\mathbf{x}}_{\varphi(K)} \right)(t) \right| \leq C \max_{\breve{n} \leq j < n} |\mathbf{p}_j| \cdot w^{\breve{n}-k}, \tag{2.11}$$

holds for all widths $w \in (0, 1]$ of the subdivided interval, $\varphi_0 \in [0, 1-w]$ and initial control points $\mathbf{Q}$.

b) Conversely, to $\varphi_\star \in [0, 1]$ and $w \in (0, 1)$ let $\varphi(x) = \varphi_\star + w(x - \varphi_\star)$. Assume $\mathbf{Q}$ and $\varphi_\star$ are fixed with $(\partial^{\breve{n}-1}\mathbf{x})(\varphi_\star) \neq 0$; again $k \in \{0, \dots, \breve{n}-1\}$. Then there is a constant $C > 0$ and $\bar{w} \in (0, 1]$ such that

$$C \max_{t \in \varphi([0,1])} \left| \partial^k \left(\mathbf{x} - \breve{\mathbf{x}}_{\varphi(K)} \right)(t) \right| \geq w^{\breve{n}-k}$$

holds for all $w \in (0, \bar{w})$. If $\mathbf{x}(t)$ restricted to $(0, 1)$ is a polynomial of degree $\breve{n}$, one can choose $\bar{w} = 1$.

Proof. We can assume $\mathbf{P} \neq 0$ and $t \in \varphi([0, 1])$. By the local basis property of $B_{\varphi(K)}$, Theorem 2.8 and (2.11), the coarse spline $B_K(t)M^{-1}T^{(-\varphi_\star)} \cdot T^{(\varphi_\star)}\mathbf{P}$ has refinement

$$B_{\varphi(K)}(t)M^{-1}T^{(-\varphi_\star)}WT^{(\varphi_\star)}\mathbf{P},$$

where $W = \operatorname{diag}(1, w, w^2, \dots, w^{n-1})$. Thus, the control points

$$\mathbf{Q} = M^{-1}T^{(-\varphi_\star)}T^{(\varphi_\star)}\mathbf{P}$$

of the coarse spline map to

$$\mathbf{Q}_{\varphi(K)} = M^{-1}T^{(-\varphi_\star)}WT^{(\varphi_\star)}\mathbf{P}$$

under refinement and

$$\begin{aligned} \partial^k \left(\mathbf{x} - \breve{\mathbf{x}}_{\varphi(K)} \right) &= \partial^k \left(B_{\varphi(K)} - \breve{B}_{\varphi(K)} \right) \cdot M^{-1}T^{(-\varphi_\star)}WT^{(\varphi_\star)}\mathbf{P} \\ &= \sum_{j=0}^{n-1} \left(\partial^k \left(B_{\varphi(K)} - \breve{B}_{\varphi(K)} \right) \cdot M^{-1}T^{(-\varphi_\star)}e_j \right) \cdot w^j \cdot e_j^T T^{(\varphi_\star)}\mathbf{P}, \end{aligned}$$

where $e_j = [0_{j\times 1}; 1; 0_{(n-1-j)\times 1}]$ (indices start at zero: the column vectors $e_0, \dots, e_{n-1}$ are $\mathbb{R}^n$'s standard basis). Due to $\breve{n}$-precision, the summands to $j \in \{0, \dots, \breve{n}-1\}$ in the last line are all zero. Applying ∂_t^k to (2.6) yields $\partial^k B_{\varphi(K)} = w^{-k}\left(\partial^k B_K\right) \circ \varphi^{-1}$. The generating proxies change the same way under translation and scaling of the knot vector as the B_K, cf. equations (2.7)-(2.8). Therefore, $\partial^k \breve{B}_{\varphi(K)} = w^{-k}(\partial^k \breve{B}_K) \circ \varphi^{-1}$, too.
The previous equation thus becomes

$$\begin{aligned}
&\partial^k \left(\mathbf{x} - \breve{\mathbf{x}}_{\varphi(K)}\right) \\
&= \sum_{j=\breve{n}}^{n-1} w^{j-k} \left(\partial^k \left(B_K - \breve{B}_K\right) \cdot M^{-1} T^{(-\varphi_\star)} e_j\right) \circ \varphi^{-1} \cdot e_j^T T^{(\varphi_\star)} \mathbf{P}, \qquad (2.12) \\
&\leq \sum_{j=\breve{n}}^{n-1} w^{j-k} \max_{\substack{\breve{n}\leq j<n \\ \varphi_\star, s\in[0,1]}} \left|\left(\partial^k \left(B_K - \breve{B}_K\right) \cdot M^{-1} T^{(-\varphi_\star)} e_j\right)(s)\right| \max_{\substack{\breve{n}\leq j<n \\ \varphi_\star\in[0,1]}} \left|e_j^T T^{(\varphi_\star)} \mathbf{P}\right|.
\end{aligned}$$

$T^{(\varphi_\star)}\mathbf{P}$ is the column-vector of coefficients under the Taylor basis $1, (t-\varphi_\star), \dots, (t-\varphi_\star)^{n-1}$. Note that

- none of the coefficients $e_{\breve{n}}^T T^{(\varphi_\star)}\mathbf{P}, \dots, e_n^T T^{(\varphi_\star)}\mathbf{P}$ depends on the values $\mathbf{p}_0, \dots, \mathbf{p}_{\breve{n}-1}$,
- both sides of the last display are linear in $\max_{\breve{n}\leq j<n} |\mathbf{p}_j|$. The same is true for the estimate we aim to prove, (2.11). Restricting both to $\max_{\breve{n}\leq j<n} |\mathbf{p}_j| = 1$ (the case $\mathbf{P} = 0$ already being done), (2.11) simply turns into

$$\max_{t\in\varphi([0,1])} \left|\partial^k \left(\mathbf{x} - \breve{\mathbf{x}}_{\varphi(K)}\right)(t)\right| \leq w^{\breve{n}-k} C. \qquad (2.13)$$

- now both maximas are taken over finitely many piecewise continuous functions with finitely many pieces, on compact domains,

$$s, \varphi_\star \in [0,1],\ \mathbf{p}_{\breve{n}}, \dots, \mathbf{p}_{n-1} \in [-1,1] \text{ s.t. } \max_{\breve{n}\leq j<n} |\mathbf{p}_j| = 1.$$

  This is why they exist.

Finally, $w \in (0,1]$ allows to estimate w^{j-k} by $w^{\breve{n}-k}$ when $j \geq \breve{n}$. Hence, (2.13) follows and part a) of the theorem is shown.

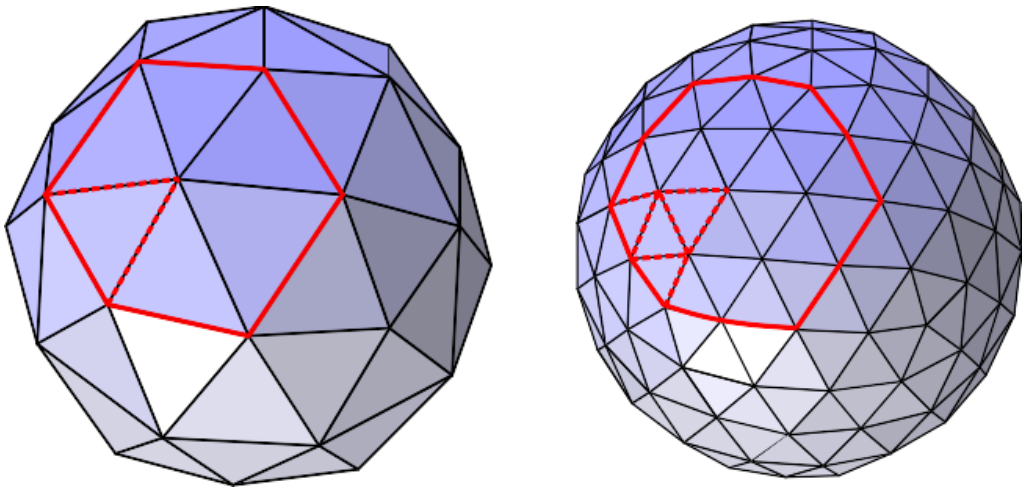

Figure 2.3: Loop-subdivision scheme at its regular valency, six. With modifications (and permission) from Wikipedia.

For part b), let us go back to inequality (2.12). As noted above, $(\partial^{\breve{n}}\mathbf{x})(\varphi_\star)$ is some multiple of $e_{\breve{n}}^T T^{(\varphi_\star)}\mathbf{P}$, so the latter term is different from zero, too. By the inverse triangle inequality,

$$\begin{aligned}
&\partial^k\left(\mathbf{x}-\breve{\mathbf{x}}_{\varphi(K)}\right)\\
&\quad\geq w^{\breve{n}-k}\left[\left|\left(\partial^k\left(B_K-\breve{B}_K\right)\cdot M^{-1}T^{(-\varphi_\star)}e_{\breve{n}}\right)\circ\varphi^{-1}\right|\cdot\left|e_{\breve{n}}^T T^{(\varphi_\star)}\mathbf{P}\right|\right.\\
&\qquad\qquad\left.-w\tilde{C}\sum_{j=\breve{n}+1}^{n-1}w^{j-\breve{n}}\left|e_j^T T^{(\varphi_\star)}\mathbf{P}\right|\right]
\end{aligned}$$

where

$$\tilde{C}:=\max_{s\in\varphi([0,1])}\left(\partial^k\left(B_K-\breve{B}_K\right)\cdot M^{-1}T^{(-\varphi_\star)}e_{j+\breve{n}+1}\right)(s).$$

By definition of $\breve{n}$-precision, the first term is not the zero function, so there is some $t_0\in[0,1]$ at which it is strictly positive. For $w\to 0$, the second term vanishes. Hence, there exists $\bar{w}>0$ such that it is less than half the former's magnitude m at $t=t_0$, for all $0<w<\bar{w}$. The constant C can be chosen as $2/m$ to set proper scaling. Finally, if $\mathbf{x}$ is a polynomial of degree $\breve{n}$, all $e_j^T T^{(\varphi_\star)}\mathbf{P}$ in the second sum are zero. □

Outlook

The argumentation for Theorem 2.8 and Theorem 2.13 can be transferred to regular regions of almost every multivariate subdivision scheme. This also includes box-splines and their triangle-based variants. While *translation of knots* directly translates into higher dimensions, *dilation of knots* should include—as its name hints to—only dilations, i.e. linear mappings that preserve orientation of the knot lines.

Consider the regular regions of Loop's scheme, for instance (illustrated by Figure 2.3 on page 25). In each refinement step, the width of polynomial pieces is halved. It should therefore have convergence class $1/4^\ell$ of the control polygon to limit surface, while the derivatives converge at the rate $1/2^\ell$, ℓ the refinement level.

2.3 Cardinal cubic B-splines

As we are going to see now, univariate cardinal, cubic B-spline control polygons are special in the sense that the distance shrinks *exactly* by the factor 1/4 at *every* refinement step. A similar statement is true for first derivatives, except that the factor is 1/2, here.

Along the way, the same is true for cardinal quadratic splines in B-form. However, for the latter it is not very surprising. Let us apply the argumentation of Section 2.2 to them.

On each knot interval of refinement level zero, the spline is a quadratic polynomial. Out of that polynomial up to linear terms have error zero, due to linear precision. Hence, these can be disregarded. When we translate the taylor polynomials, the coefficient of the quadratic one remains the same because it belongs to the highest order term here. Then, if we subdivide in a binary fashion, that coefficient gets scaled by $2^{-2\ell}$ (see Theorem 2.8 on page 18). It is therefore no surprise for cardinal quadratic splines that the new error is $2^{-2\ell}$ times the old one.

Conversely, for cardinal cubic splines there are *two* taylor coefficients to terms of order ≥ 3: the ratio of the coefficients of the quadratic and cubic taylor polynomials could change. Hence, for cardinal cubic B-splines, this shrinkage of error can *not* be expected, at least not by the same argumentation.

Let us begin with the univariate case:

Theorem 2.14 (Binary subdivision of univariate cardinal cubic splines in B-form)**.** *Let $f(t) = B(t)P$ be a scalar-valued cubic spline, $B = [b_1, \dots, b_4]$ the vector of cubic B-splines to knots $K_0 = [-3, \dots, 4]$. Further, let $\tilde{P}$ be the control points of its binary refinement, to the knots $K_1 = [-3, \dots, 5]/2$. Let $k_\ell(t)$ denote the respective control polygon at level $\ell \in \{0, 1\}$. We parametrize the $k_\ell(t)$ as splines in B-form of order two, to the respective control points of their refinement level, and to knot vectors given by the Greville abczissas, i.e. $[-1, \dots, 2]$ at level zero and $[-1, \dots, 3]/2$ at $\ell = 1$. Then*

$$\max_{t\in[0,1]} |f(t) - k_1(t)| = \frac{1}{4} \max_{t\in[0,1]} |f(t) - k_0(t)|, \tag{2.14}$$

$$\max_{t\in[0,1]} |\frac{\partial f}{\partial t}(t) - \frac{\partial k_1}{\partial t}(t)| = \frac{1}{2} \max_{t\in[0,1]} |\frac{\partial f}{\partial t}(t) - \frac{\partial k_0}{\partial t}(t)|. \tag{2.15}$$

Furthermore, there exists $t^* \in \{0, 1\}$ that simultaneously maximizes the distances at both refinement levels in the j-th derivative, $j \in \{0, 1\}$. Suppose we have integer knots $K_0 = [\kappa_1, \dots, \kappa_{m+4}]$ and repeatedly subdivide binary. Then, after ℓ additional refinement steps, the errors are given by

$$\max_{t\in[\kappa_4,\kappa_{m+1}]} |f(t) - k_\ell(t)| = \left(\frac{1}{4}\right)^\ell \max_{t\in\{\kappa_4,\dots,\kappa_{m+1}\}} |f(t) - k_0(t)|,$$

$$\max_{t\in[\kappa_4,\kappa_{m+1}]} |\frac{\partial f}{\partial t}(t) - \frac{\partial k_\ell}{\partial t}(t)| = \left(\frac{1}{2}\right)^\ell \max_{t\in\{\kappa_4,\dots,\kappa_{m+1}\}} |\frac{\partial f}{\partial t}(t) - \frac{\partial k_0}{\partial t}(t)|.$$

Proof. For affine-linear maps the errors are always zero. Thus, we only need to prove the case where the degree of $f_{|[0,1]}$ is two or three. It turns out that for $f(t)_{|[0,1]} = t^2$

$$\Delta_0^{(2)}(t) := f(t) - k_0(t) = t^2 - (t - \frac{1}{3})$$

$$\Delta_1^{(2)}(t) := f(t) - k_1(t) = t^2 - \begin{cases} (\frac{t}{2} - \frac{1}{12}) & \text{if } t \in [0, \frac{1}{2}] \\ (\frac{3}{2}t - \frac{7}{12}) & \text{if } t \in (\frac{1}{2}, 1]. \end{cases}$$

Similarly, for $f(t)_{|[0,1]} = t^3$ it is

$$\Delta_0^{(3)}(t) := f(t) - k_0(t) = t^3$$

$$\Delta_1^{(3)}(t) := f(t) - k_1(t) = t^3 - \begin{cases} 0 & \text{if } t \in [0, \frac{1}{2}] \\ \frac{3}{4}(2t - 1) & \text{if } t \in (\frac{1}{2}, 1]. \end{cases}$$

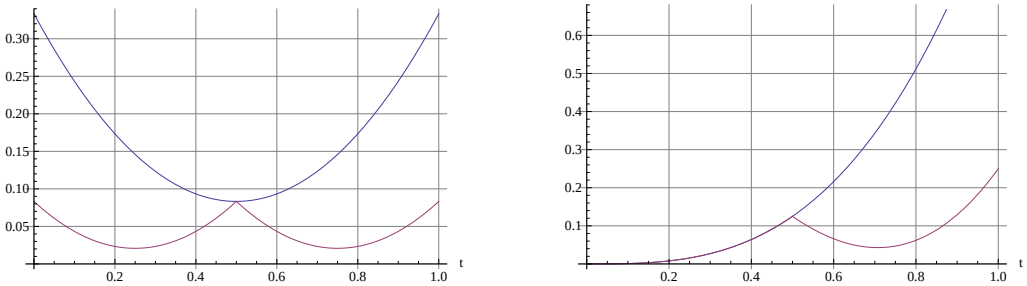

Figure 2.4: *Left:* differences $\Delta_\ell^{(2)}$ corresponding to $f(t) = t^2$ at refinement level 0 (blue), respectively level 1 (red). *Right:* the same when $f(t) = t^3$.

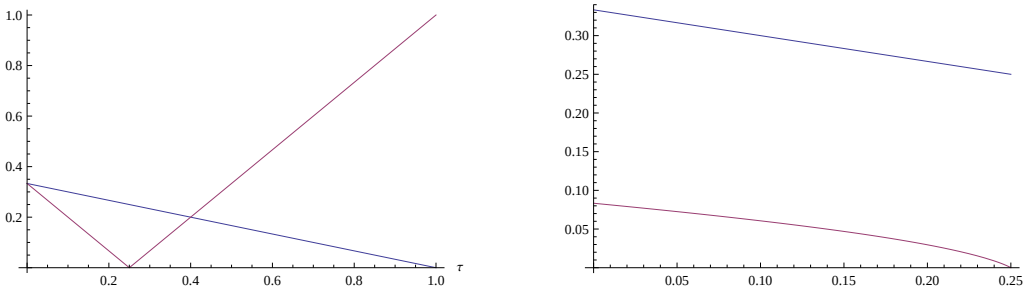

Figure 2.5: *Left:* function values $|F_0(-1, \tau, t)|$ at the boundaries $t = 0$ (blue), $t = 1$ (purple). *Right:* comparison with the function values at the t-extremal values (purple).

First, consider refinement level $\ell = 0$. We need the values $M_\ell(\sigma, \tau) := \max_{t\in[0,1]} |F_\ell(\sigma, \tau, t)|$, where $F_\ell(\sigma, \tau, t) := (1 - \tau)\Delta_\ell^{(2)}(t) + \sigma\tau\Delta_\ell^{(3)}(t)$, for all $\sigma \in \{\pm 1\}, \tau \in [0, 1]$. It is $|\Delta_0^{(g)}(t)| \le \Delta_0^{(g)}(1)$ for both $g \in \{2, 3\}$. Hence, $M_0(1, \tau) = (1 - \tau)\frac{1}{3} + \tau$. Now, let $\sigma = -1$. Differentiating $F_0(-1, \tau, t)$ for t yields the possible extrema $t = (1 - \tau - \sqrt{1 - 5\tau + 4\tau^2})/(3\tau), 0 < \tau \le 1$. As further examined in Figure 2.5 on page 28, this leads to

$$M_0(-1, \tau) = \begin{cases} \frac{1-\tau}{3} & , \tau \in [0, \frac{2}{5}] \\ \frac{4\tau-1}{3} & , \tau \in (\frac{2}{5}, 1]. \end{cases}$$

Now to refinement level one. As in the case $\ell = 0$, it is $|\Delta_1^{(g)}(t)| \le \Delta_1^{(g)}(1)$ for both $g \in \{2, 3\}$. Thus, $M_1(1, \tau) = (1 - \tau)\frac{1}{12} + \tau\frac{3}{4}$. Next, let $\sigma = -1$.

$\partial F_1(-1,\tau,t)/\partial t$ has the zeros

$$t_1(\tau) = \left((1-\tau) + \sqrt{(2-13\tau+20\tau^2)/2}\right)/(3\tau), \quad 0 < \tau \leq \frac{1}{4},$$
$$t_2(\tau) = \begin{cases} \left((1-\tau) - \sqrt{(2-7\tau+5\tau^2)/2}\right)/(3\tau) & \text{if } 0 < \tau \leq \frac{2}{5}, \\ \left((1-\tau) + \sqrt{(2-13\tau+20\tau^2)/2}\right)/(3\tau) & \text{if } \frac{2}{5} < \tau \leq 1 \end{cases}$$

(also see Figure 2.6 on page 30). $\partial^2 F_1(-1,\tau,t)/\partial t^2 = 2(1-\tau) - 6t\tau$ at these $t_j(\tau)$ is greater than zero, so we have local minima. The reductions are somewhat lengthy. Hence they are not included here; we arrive at

$$M_1(-1,\tau) = \begin{cases} \frac{1-\tau}{12} & ,\tau \in [0,\frac{2}{5}] \\ \frac{4\tau-1}{12} & ,\tau \in (\frac{2}{5},1], \end{cases}$$

which shows our claims for the 0^{th} derivative (concerning t_0^*: the maximum distance is in each of the cases $\tau \in [0,2/5] \vee \tau \in [2/5,1]$ the function value $F_\ell(-1,\tau,t)$ at the boundary $t = 0 \vee t = 1$).

The proof for the first derivatives is shorter. For $f(t)_{|[0,1]} = t^2$ it is

$$\tilde{\Delta}_0^{(2)}(t) := \frac{\partial\,(f-k_0)}{\partial t}(t) = 2t - 1$$
$$\tilde{\Delta}_1^{(2)}(t) := \frac{\partial\,(f-k_1)}{\partial t}(t) = 2t - \begin{cases} \frac{1}{2} & \text{if } t \in [0,\frac{1}{2}] \\ \frac{3}{2} & \text{if } t \in (\frac{1}{2},1]. \end{cases}$$

Similarly, for $f(t)_{|[0,1]} = t^3$

$$\tilde{\Delta}_0^{(3)}(t) := \frac{\partial\,(f-k_0)}{\partial t}(t) = 3t^2$$
$$\tilde{\Delta}_1^{(3)}(t) := \frac{\partial\,(f-k_1)}{\partial t}(t) = 3t^2 - \begin{cases} 0 & \text{if } t \in [0,\frac{1}{2}] \\ \frac{3}{2} & \text{if } t \in (\frac{1}{2},1] \end{cases}$$

(refer to Figure Figure 2.7 on page 31 for a quick overview). Let $\tilde{M}_\ell(\sigma,\tau) := \max_{t\in[0,1]} |\tilde{F}_\ell(\sigma,\tau,t)|$, where $\tilde{F}_\ell(\sigma,\tau,t) := \sigma(1-\tau)\tilde{\Delta}_\ell^{(2)}(t) + \tau\tilde{\Delta}_\ell^{(3)}(t)$. When $\sigma = +1$ we have again $\tilde{M}_\ell(1,\tau) = \tilde{F}_\ell(1,\tau,1) = (1-\tau)\left(\frac{1}{2}\right)^\ell + 3\tau\left(\frac{1}{2}\right)^\ell$, for the same reasons as before. The lemma's claim follows directly.

Now, let $\sigma = -1$. Consider refinement level 0: $\tilde{F}_0(-1,\tau,t) = -2(1-\tau) + 6t\tau$ has zeros $t_1(\tau) := (1/\tau - 1)/3, 1/4 < \tau < 1$. Comparison with the

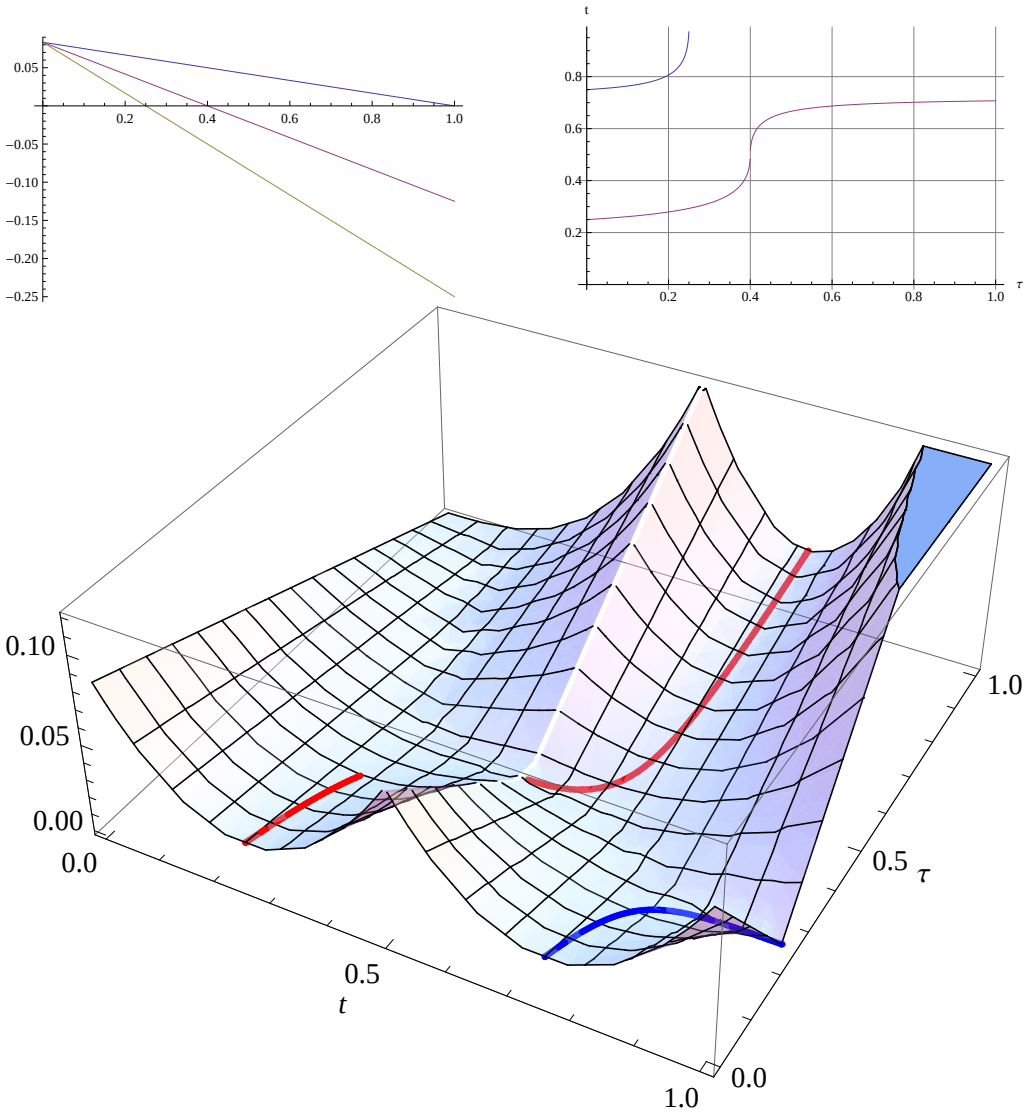

Figure 2.6: *Above, left:* function values $F_1(-1, \tau, t)$ at the transition of polynomial pieces, $t \in \{0, 1/2, 1\}$ (respective colors: blue,purple,yellow). The maximum in modulus changes from the blue to the yellow line at $\tau = 2/5$. *Above, right:* pairs (τ, t) for which $\partial F_1(-1, \tau, t)/\partial t$ vanishes; $t_1(\tau)$ shown in blue, $t_2(\tau)$ purple. *Bottom:* overview of function values for all pairs (τ, t), including those of $t \in \{0, 1/2, 1\}$.

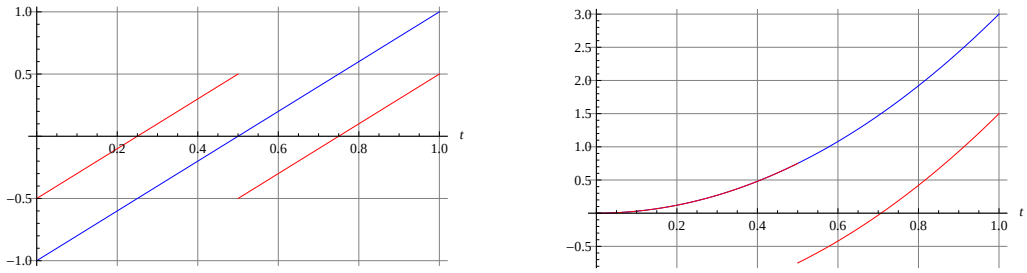

Figure 2.7: *Left:* differences $\tilde{\Delta}_\ell^{(2)}$ corresponding to $f(t) = t^2$ at refinement level 0 (blue), respectively level 1 (red). *Right:* the same when $f(t) = t^3$.

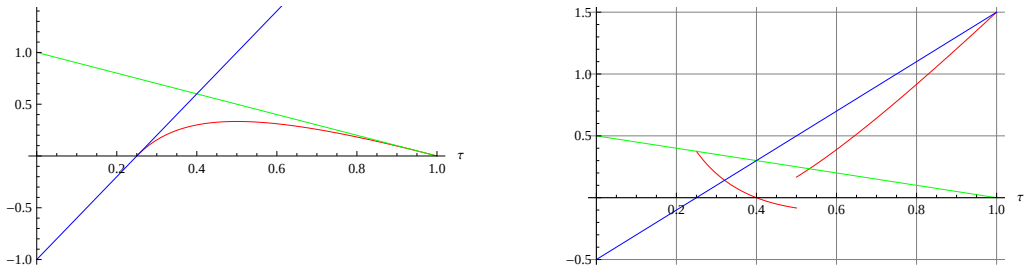

Figure 2.8: *Left:* function values $\tilde{F}_0(-1,\tau,0), \tilde{F}_0(-1,\tau,1)$ at the t-boundary, compared to $\tilde{F}_0(-1,\tau,t_1(\tau)), 1/4 < \tau < 1$, the values at the local extremes. *Right:* Comparison between function values $\tilde{F}_1(-1,\tau,0)$, $\tilde{F}_1(-1,\tau,1)$ and $-\tilde{F}_1(-1,\tau,t_2(\tau))$.

function values at the boundary leads to

$$\tilde{M}_0(-1,\tau) = \begin{cases} 1-\tau & ,0 < \tau < \frac{2}{5}, \\ 4\tau - 1 & ,\frac{2}{5} \le \tau \le 1 \end{cases}$$

(see Figure 2.8 on page 31). For refinement level 1 it is

$$\frac{\partial \tilde{F}_1}{\partial t}(-1,\tau,t) = \begin{cases} 3t^2\tau - \left(2t - \frac{1}{2}\right)(1-\tau), & 0 \le t < \frac{1}{2}, \\ \left(3t^2 - \frac{3}{2}\right)\tau - \left(2t - \frac{3}{2}\right)(1-\tau), & \frac{1}{2} < t \le 1, \end{cases}$$

which results in local extremes $t_2(\tau)\frac{1-\tau}{3\tau}, \frac{1}{4} \le \tau \le \tau$. As illustrated in Figure 2.8 on page 31, again function values at the boundary dominate the

maximum in modulus, which leads to

$$\tilde{M}_1(-1,\tau) = \begin{cases} \frac{1-\tau}{2}, & 0 \le \tau \le \frac{2}{5} \\ \frac{4\tau-1}{2}, & \frac{2}{5} < \tau \le 1. \end{cases}$$

Comparison with $\tilde{M}_0(-1,\tau)$ yields the lemma's claim. □

Multivariate setting

Having finished the univariate case, we now consider bi-variate cardinal cubic tensor product splines in B-form of ≥ 2 variables. These contain (non-trivial-)subspaces that are isomorphic to the bivariate case, which we are going to study now. Thus, the differences to the univariate setting we will establish also apply to splines in B-form in any number of variables greater than one:

- We store the scalar-valued control points in the 4×4 matrix $\mathbf{P}$.
- Control polygon and spline are identical if the latter one is a polynomial whose degree in each variable is at most one. Therefore, when studying the difference between the two, without loss of generality we may assume that the "inner" 2×2 control points are zero,

$$\mathbf{P} = \begin{bmatrix} * & * & * & * \\ * & 0 & 0 & * \\ * & 0 & 0 & * \\ * & * & * & * \end{bmatrix}$$

  (one could also argue with affine invariance of the B-spline representation).
- $B(s)$ is the row-vector of four univariate, cubic, cardinal B-splines in the first variable s, similarly $B(t)$ for the second variable t.
- Let $\breve{B}_\ell(s)$, $\breve{B}_\ell(t)$ be the analogous terms for the univariate control polygon.

Spline and control polygon of the bivariate setting at refinement level ℓ are given by

$$F(s,t) = B(s)\mathbf{P}B^T(t),$$

respectively

$$\breve{F}_\ell(s,t) = \breve{B}_\ell(s)\mathbf{P}\breve{B}_\ell^T(t).$$

Their difference is

$$\Delta_\ell(s,t) := B(s)\mathbf{P}B^T(t) - \breve{B}_\ell(s)\mathbf{P}\breve{B}_\ell^T(t).$$

As far as we could see, the univariate case is of no help here. To directly bring univariate control polygons into play, one needs terms $B(s)\mathbf{P}\breve{B}_\ell^T(t)$ or $\breve{B}_\ell(s)\mathbf{P}B^T(t)$. Yet these do not appear in $\Delta_\ell(s,t)$ except for when $B(s) = \breve{B}_\ell(s)$ or $B(t) = \breve{B}_\ell(t)$, i.e. Δ is linear in either s, or t. Then, we could swap those variable's B-splines with the control polygon. But essentially, one would be in the univariate setting.

Systematic experiments gave insight as presented in Table 2.1. An analogous approach as we have done in the univariate case can not be taken. Even for the bivariate case, determining the zeros of $\operatorname{grad}\Delta_\ell(s,t)$ with a computer algebra system—we used MATHEMATICA—proved impracticable. Therefore, we formulate only

Conjecture 2.15. *The difference function Δ_ℓ between cardinal cubic tensor product splines in B-form and their control polygon at binary refinement level $\ell \in \mathbb{N}$ can be estimated safely by the restriction of Δ_ℓ to the knot lines (of the respective refinement level). The same is true for derivatives of multi-degree one.*

2.4 B-splines of orders 7–8

As is known since Reif's Degree Estimate [57], stationary C^2 schemes in the irregular setting cannot be realized without polynomial order of at least seven. We take a look at univariate, C^2 B-splines of orders $n \in \{7, 8\}$.

In this and the next section, masks were calculated with the computer algebra system MAPLE. Some techniques and routines are briefly described in Appendix A.1.

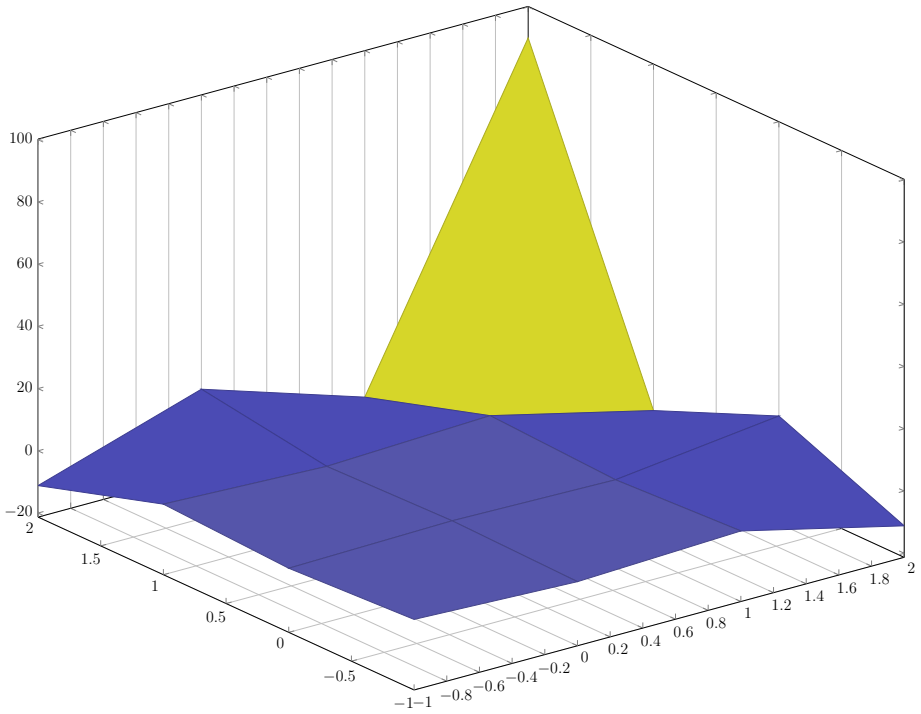

(a) B-control-mesh.

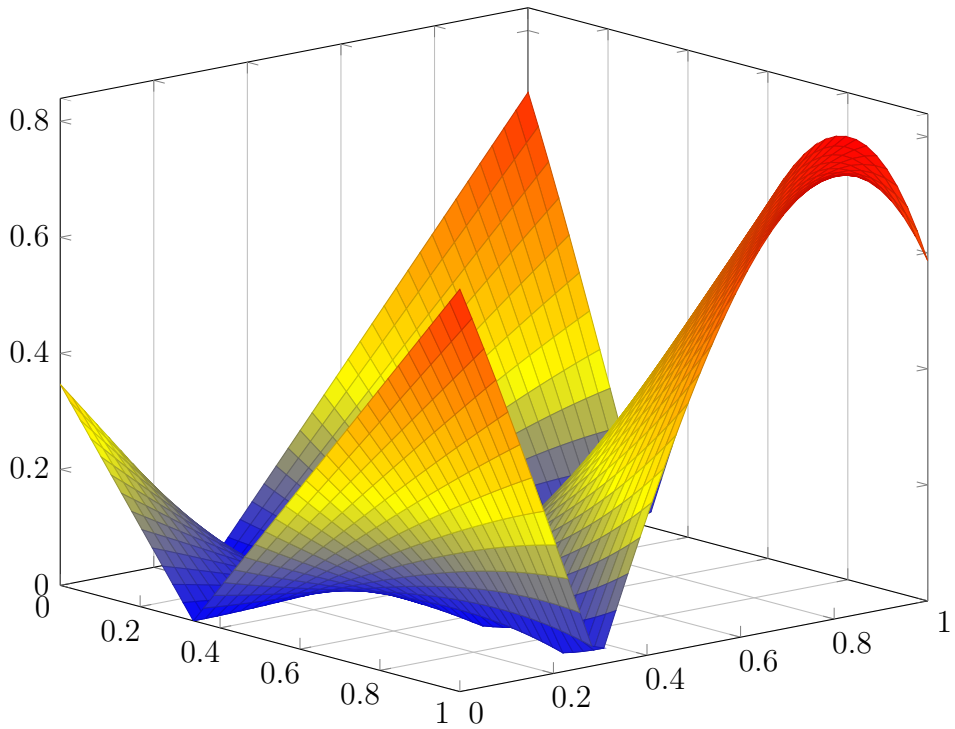

(b) $|\Delta_\ell(s,t)|$.

Figure 2.9: For the tensor-product of cubic splines in more than one variable the largest deviation between spline and B-spline control polygon always seems to happen at the boundaries of the polynomial pieces.

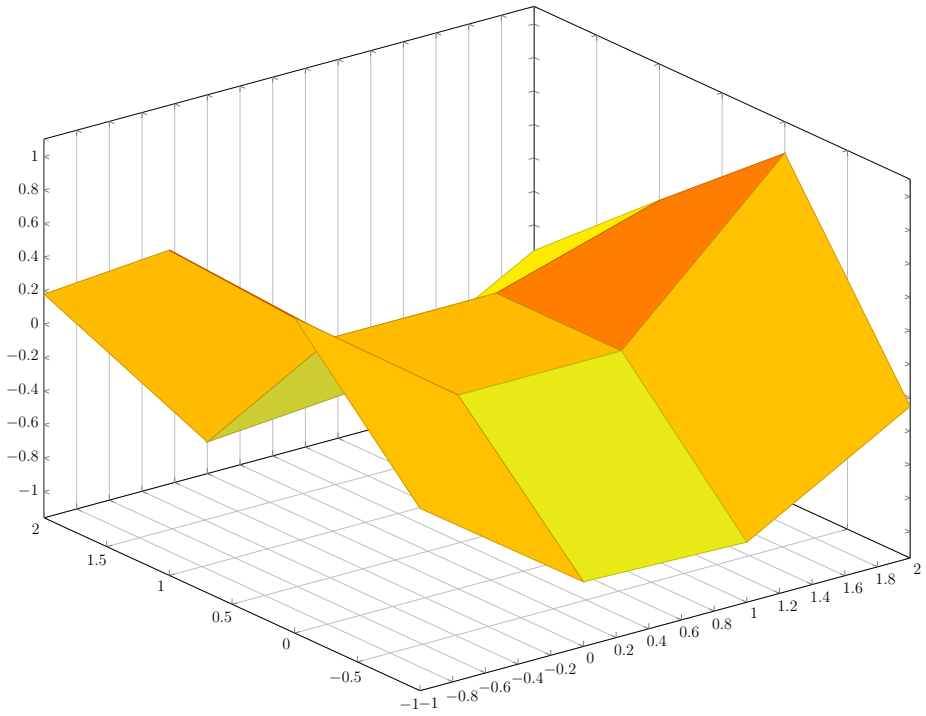

(a) Coarse control mesh.

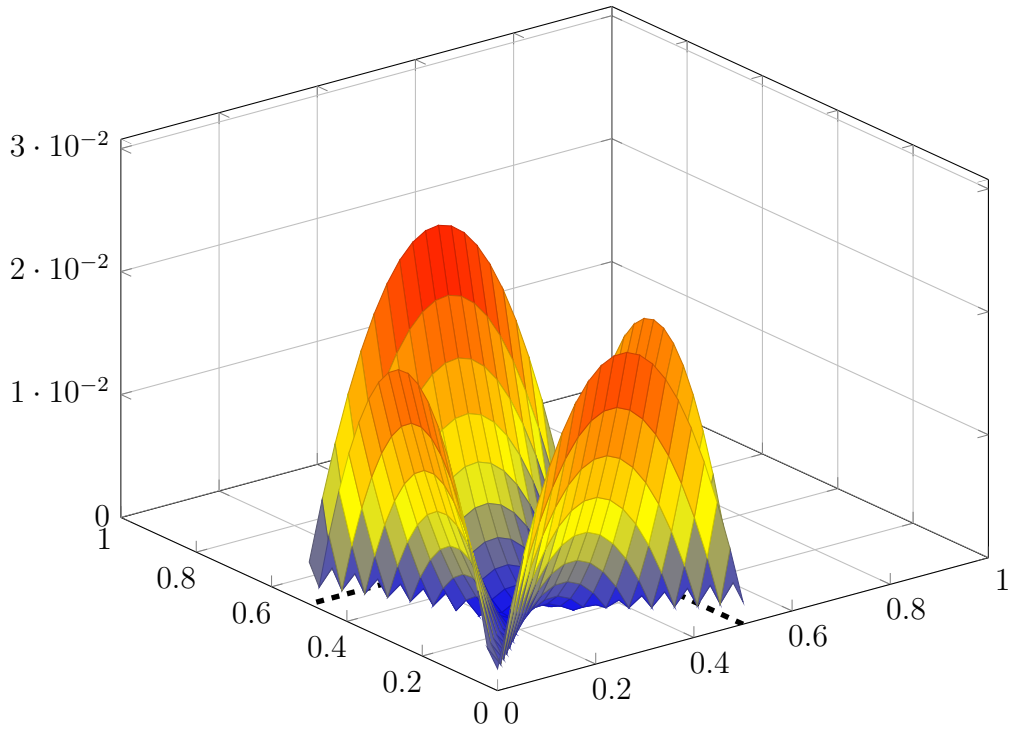

(b) $|\Delta_\ell(s,t)|$.

Figure 2.10: In contrast to the univariate setting, for bi-cubic splines in B-form the maximum of $|\Delta_\ell(s,t)|$ also occurs at transitions between subdivided polynomial pieces. In this case, the control net—with Greville abscissas for x-/y-components—corresponds to a saddle.

Δ_ℓ	univ.	$\geq$bivariate	Refer to
has max. always at knot	✓	↯	Fig. 2.9
. . . -lines	✓	✓	Conj. 2.15
. . . of level 0	✓	↯	Fig. 2.10
shrinks by $\frac{1}{4}$ exactly	✓	↯	-
simult. max. with derivatives	✓	↯	-

Table 2.1: Overview of properties of the difference function between cardinal cubic splines and their B-spline control mesh (defined analogously as in Theorem 2.14). Unfortunately, most properties of the univariate case do not carry over to the general setting of more than one variable.
For derivatives of bi-degree at most one, we made similar observations.

Binary subdivision

We presuppose bi-infinte integer knots $\mathbb{Z}$ of multiplicities four, respectively five for order eight. It is convenient to partition the B-splines into blocks b_j, or *bundles*, of four/five elements; see Figure 2.11 on page 38 (it is a good idea to keep the term "block" available for descriptions and for terms of broader scope; for instance, a block may be used to refer to several bundles).

Going up one refinement level to bundles $\widetilde{b}_j$, the coarser B-bundles b_j are represented by

$$b_j = \begin{bmatrix} \widetilde{b}_{2j-1}, & \widetilde{b}_{2j}, & \widetilde{b}_{2j+1} \end{bmatrix} \cdot S. \tag{2.16}$$

The matrices $S = S_B^{(n)}$ can be found in Table 2.2 on page 37, due to their size.

With likewise partitioning of $S = [S_{-1}; S_0; S_1]$ the substitution $i = 2j + k \Leftrightarrow j = (i - k)/2$ produces

$$\sum_j b_j p_j = \sum_j \sum_{k\in\{-1,0,1\}} \tilde{b}_j S_k p_{j+k} = \sum_i \sum_{\substack{k\in\{-1,0,1\},\\ i-k \text{ even}}} \tilde{b}_i S_k p_{(i-k)/2}$$

$$= \sum_i \tilde{b}_i \begin{cases} S_0 p_{i/2} & \text{if } i \text{ is even,} \\ \sum_{k\in\{\pm1\}} S_k p_{(i-k)/2} & \text{if } i \text{ is odd.} \end{cases}$$

Hence, the control bundles $\widetilde{p}_j$ of the subdivided spline are

$$\widetilde{p}_j = \begin{cases} S_0 p_{j/2} & \text{if } j \text{ is even} \\ S_{+1} p_{(j-1)/2} + S_{-1} p_{(j+1)/2} & \text{if } j \text{ is odd.} \end{cases} \tag{2.17}$$

$$S_B^{(7)} = \frac{1}{64}\left[\begin{array}{cccc} 8 & 0 & 0 & 0 \\ 16 & 4 & 0 & 0 \\ 24 & 18 & 2 & 0 \\ 16 & 33 & 10 & 1 \\ \hline 8 & 38 & 16 & 2 \\ 0 & 36 & 24 & 4 \\ 0 & 12 & 40 & 12 \\ 0 & 4 & 24 & 36 \\ \hline 0 & 2 & 16 & 38 \\ 0 & 1 & 10 & 33 \\ 0 & 0 & 2 & 18 \\ 0 & 0 & 0 & 4 \end{array}\right], \quad S_B^{(8)} = \frac{1}{128}\left[\begin{array}{ccccc} 8 & 0 & 0 & 0 & 0 \\ 20 & 4 & 0 & 0 & 0 \\ 40 & 22 & 2 & 0 & 0 \\ 40 & 51 & 12 & 1 & 0 \\ 32 & 66 & 20 & 2 & 0 \\ \hline 16 & 76 & 32 & 4 & 0 \\ 0 & 72 & 48 & 8 & 0 \\ 0 & 24 & 80 & 24 & 0 \\ 0 & 8 & 48 & 72 & 0 \\ 0 & 4 & 32 & 76 & 16 \\ \hline 0 & 2 & 20 & 66 & 32 \\ 0 & 1 & 12 & 51 & 40 \\ 0 & 0 & 2 & 22 & 40 \\ 0 & 0 & 0 & 4 & 20 \\ 0 & 0 & 0 & 0 & 8 \end{array}\right].$$

Table 2.2: Matrices $S = S^{(n)}$ for binary subdivision of C^2 B-splines of orders 7–8, as per equation (2.16).

Notice that masks for the "correction" of old bundles are even smaller than they are for the Catmull-Clark scheme. On the other hand, newly inserted bundles are obtained by masks of identical size. This leads to a scheme as illustrated in Figure 2.12 on page 38.

Designer's viewpoint

A subdivision scheme based on these B-splines entails severe disadvantages for a designer:

Microscopic: Control of the surface is of differing—much smaller—scope

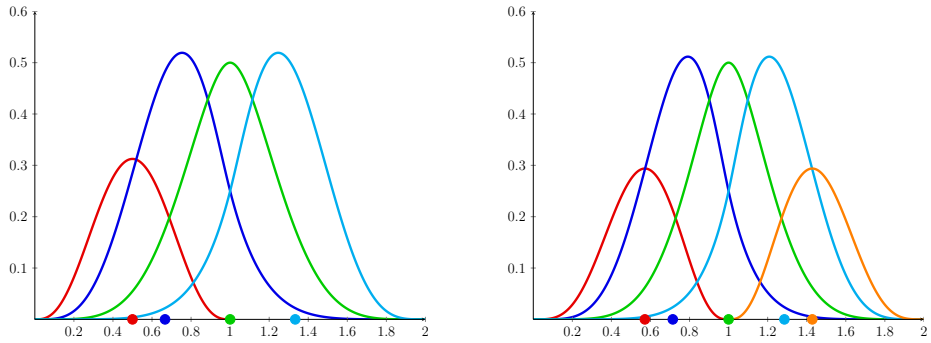

Figure 2.11: One bundle b_j of B-spline basis functions for $\mathcal{S}_7$ *(left)* and $\mathcal{S}_8$ *(right)*. Associated Greville-abscissa are marked as circles on the axes.

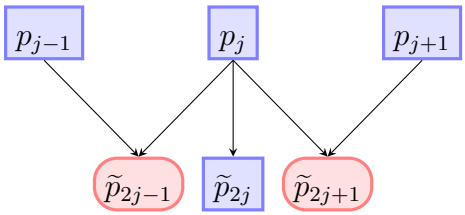

Figure 2.12: Refinement scheme for C^2 B-bundles of orders seven–eight. Notice that, in contrast to cardinal cubic B-splines, we need only bundle p_j, but *not* p_{j-1} and p_{j+1} to caclculate the "correction" of p_j to $\tilde{p}_{2j}$.

when compared with cardinal cubics. Supports are only one–two knot intervals wide; for cardinal cubic splines, it is four.

Non-equidistant Greville-abscissae: Greville-abscissae do *not* form an evenly spaced grid. For example, refer to Figure 2.13 on page 39, which provides an illustration of the control net that corresponds to the identity on $[0, 2] \times [0, 1]$.

Non-translates: While B-splines could easily be replaced by linear combinations that restore equidistant Greville-abscissae, the problem remains that the scalar valued functions attached to the control points are no longer pairwise translates of another. Designers face a longer learning

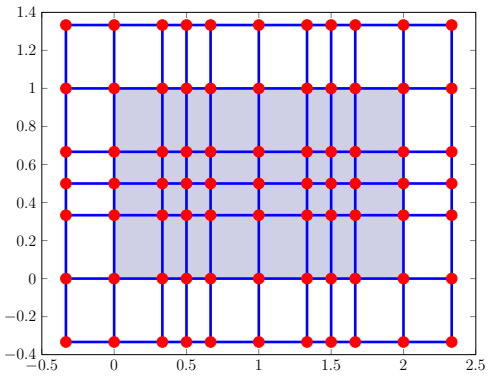

Figure 2.13: A designer would want the control points of the identity on the (shaded) domain $[0, 2] \times [0, 1]$ to be evenly spaced. But this is not the case for B-splines of orders seven and eight, of which the latter one is not illustrated.

curve. Even after that, the process remains more complex—ultimately, time-consuming—than it is with cardinal cubics. Additionally, we should keep in mind that the latter ones are still present in the dominating, regular regions of the mesh.

The question is: if cubic splines form a subspace of those of order seven, is the hassle truly necessary? We might simply let designers work with what they are used to model with: cardinal, cubic splines.

2.5 A_7/A_8-spline basis

Decomposing the function space

To counter the B-basis' shortcomings discussed in Subsection 2.4, we need a decomposition of $\mathcal{S}_7$ into a direct sum[3]

$$\mathcal{S}_n = \mathcal{S}_4 \oplus \mathcal{D}_n, \quad n \in \{7, 8\}. \tag{2.18}$$

$\mathcal{S}_n$ is the space of C^2 splines of order n. Designers will interact with $\mathcal{S}_4$ only. On the other hand, splines in $\mathcal{D}_n$ are considered *details*, needed solely for C^2

[3]In the interest of good readability, we usually refer to $\mathcal{S}_7$ only. The same applies to $\mathcal{S}_8$.

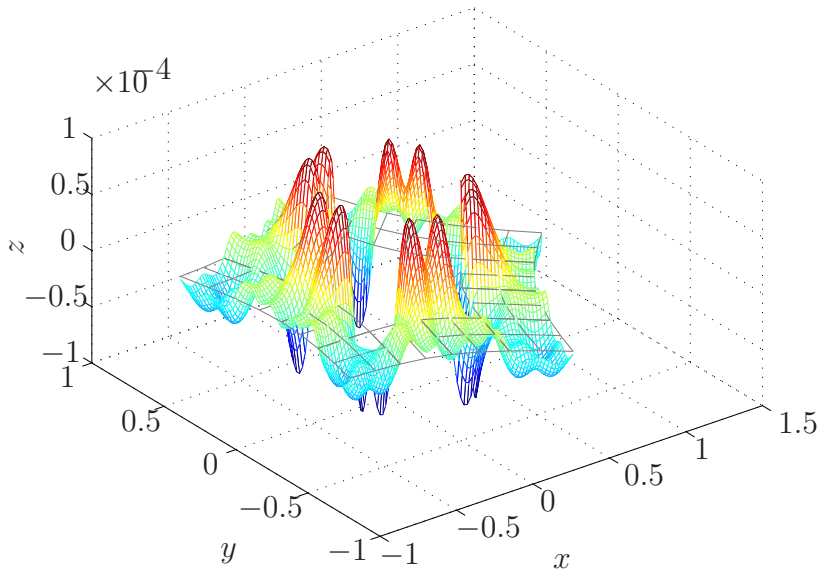

Figure 2.14: Taking the two component functions x, y of the splinering χ, we set z to some purely quadratic polynomial of x and y. $z = x^2 + y^2$ can be decomposed into cubic-, and non-cubic parts ("details"), by $z = z^{[4]} + d$.
The details of $x^2 + y^2$ presented here are produced by the A_7-basis, which will be introduced in Section 2.5. They are of typical size for the purely quadratic polynomials. Notice that the non-cubic spline d is less than *two thousand times* as large in magnitude as z itself. This very tiny bit is decisive to C^2 continuity at non-regular points.

continuity at the extraordinary point in the bi-variate case. These details will be adjusted automatically.

There are some requirements for a decomposition (2.18) to be acceptable in practice:

intuitive (geometrically): the cubic spline should be a good approximation of the full spline,

***convergent*:** under repeated subdivision, the cubic part is to converge quickly towards the spline.

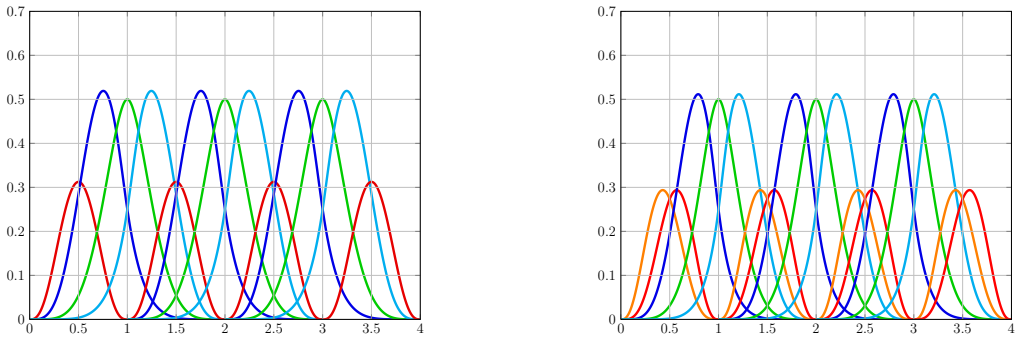

Figure 2.15: *Left:* the 13 B-splines that are combined to one bundle of the A-basis for order seven. *Right:* the same for order eight.

Definition

We give the new basis of $\mathcal{S}_n$ in terms of the B-basis. For this, let us denote by $B^{(7)}$ and $B^{(8)}$ the row-vectors of 13, resp. 17 B-splines of orders $n \in \{7, 8\}$, with knots

$$K_7 = (-2\$4, \ldots, 2\$4),\ K_8 = (-2\$5, \ldots, 2\$5)$$

(see Figure 2.15 on page 41).

K_7 and K_8 should not to be confused with the knot vectors of a spline space. For instance, when $n = 7$ the first of the 13 B-splines has the knots $-2\$4, -1\$4$ (the left-most, red function in Figure 2.15). Conversely, the last one of the B-splines has knots $1\$4, 2\$4$ (analogously, the right-most, red function in the figure).

Then

$$\widetilde{a}_j^{(n)} := \widetilde{a}_0^{(n)}(\cdot - j),$$

$$\widetilde{a}_0^{(7)} = \frac{B^{(7)}}{120}\left[\begin{array}{cccc} 0 & 0 & 1 & 0 \\ 0 & 0 & 4 & 0 \\ 0 & 0 & 16 & 0 \\ 0 & 0 & 44 & 0 \\ \hline 120 & 59 & 59 & 1 \\ 0 & 44 & 72 & 4 \\ 0 & 16 & 88 & 16 \\ 0 & 4 & 72 & 44 \\ \hline 0 & 1 & 59 & 59 \\ 0 & 0 & 44 & 0 \\ 0 & 0 & 16 & 0 \\ 0 & 0 & 4 & 0 \\ \hline 0 & 0 & 1 & 0 \end{array}\right], \widetilde{a}_0^{(8)} = \frac{B^{(8)}}{210}\left[\begin{array}{ccccc} 0 & 0 & 1 & 0 & 0 \\ \hline 0 & 0 & 4 & 0 & 0 \\ 0 & 0 & 10 & 0 & 0 \\ 0 & 0 & 30 & 0 & 0 \\ 0 & 0 & 70 & 0 & 0 \\ 0 & 0 & 92 & 1 & 0 \\ \hline 210 & 92 & 113 & 4 & 0 \\ 0 & 70 & 130 & 10 & 0 \\ 0 & 30 & 150 & 30 & 0 \\ 0 & 10 & 130 & 70 & 0 \\ 0 & 4 & 113 & 92 & 210 \\ \hline 0 & 1 & 92 & 0 & 0 \\ 0 & 0 & 70 & 0 & 0 \\ 0 & 0 & 30 & 0 & 0 \\ 0 & 0 & 10 & 0 & 0 \\ 0 & 0 & 4 & 0 & 0 \\ \hline 0 & 0 & 1 & 0 & 0 \end{array}\right], \tag{2.19}$$

defines one bundle (centered at j) of a basis with masks that are—under the bundle paradigm—identical in size to those of cardinal cubic splines (we will get to the masks shortly). An illustration of the functions is provided in Figure 2.16 on page 43.

The third columns in (2.19) represent the order-raised, cardinal, cubic B-spline. Colors match those in the figures.

Figure 2.16 on page 43 shows this *pre-stage* of the A_7/A_8-bases. Notice that by setting the coefficients of all details to one, for every bundle, the sum of "details" is close to the constant function 0.55 (and clearly bounded away from zero!). Regardless what the cubic part of the spline actually were, we can give a far better representation of the overall shape: one simply expects the center of mass to be entirely in the cubic part[4]. "Details", in contrast, *must* have zero mean.

To achieve this while maintaining size of the masks, we turn the L^2-

[4]If we used some other decomposition of the function space, derived from some product different from the L^2 one, "center of mass" would be defined in an analogue fashion. This is why the requirement of zero mean is made at this point, instead of the enumeration in *Decomposing the function space*.

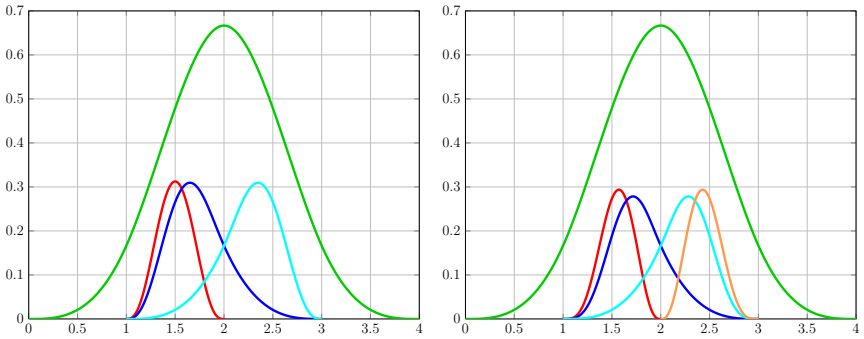

(a) Order 7. **(b)** Order 8.

Figure 2.16: Pre-stage functions of the A_7/A_8-basis, before details are turned to zero-mean. The first (left) half of the function to the right of the center is the same as the first quarter of the cardinal cubic B-spline. Similarly, on $[2, 3]$, the dark blue function is a translation of the last quarter of the cubic B-spline. Allthough they are never directly used to represent a surface, the pre-stage functions of the A_n-bases are important when the domain contains boundaries.

projections onto the cardinal, cubic B-spline to zero within each bundle:

$$a_j^{(n)} := \tilde{a}_j^{(n)} W^{(n)}, \tag{2.20}$$

where

$$W^{(7)} := \begin{bmatrix} 1 & 0 & 0 \\ 0 & 1 & 0 \\ -w_1^{(7)} & -w_2^{(7)} & 1 & -w_4^{(7)} \\ 0 & 0 & 1 \end{bmatrix},$$

$$W^{(8)} := \begin{bmatrix} 1 & 0 & 0 & 0 \\ & 1 & 0 & 0 \\ -w_1^{(8)} & -w_2^{(8)} & 1 & -w_4^{(8)} & -w_5^{(8)} \\ 0 & 0 & 1 & 0 \\ 0 & 0 & 0 & 1 \end{bmatrix},$$

$$w_j^{(n)} := \frac{\int_{\mathbb{R}} B^{(n)}(s) \tilde{P}_{\mathrm{All},j}^{(n)} \mathrm{d}s}{\int_{\mathbb{R}} B^{(n)}(s) \tilde{P}_{\mathrm{All},3}^{(n)} \mathrm{d}s},$$

$$w^{(n)} = \begin{cases} (\frac{1}{7}, \frac{47}{210}, 1, \frac{47}{210}), & \text{for order } n = 7, \\ (\frac{1}{8}, \frac{317}{1680}, 1, \frac{317}{1680}, \frac{1}{8}), & \text{for order } n = 8. \end{cases}$$

$\widetilde{P}^{(n)}$ are the control points used in equation (2.19) to define the $\widetilde{a}_j$. $\widetilde{P}^{(n)}_{\mathrm{All},j}$ refers to the j-th column of $\widetilde{P}^{(n)}$. The $a^{(n)}_j$ finally yield the A_7/A_8-basis, of which one respective bundle is presented in Figure 2.17 on page 46.

Masks for binary Subdivision

We can increase the subdivision level by

$$a_j = \left[\underline{a}_{2j-2}, \ldots, \underline{a}_{2j+2}\right] \cdot S.$$

Due their size, the matrices $S = S^{(n)}_A$ are listed in Table 2.3 on page 45.

2.6 Change of B- to A_7/A_8-basis

In this subsection, we examine how one may change from the B-spline basis, that we have discussed in Section 2.4, to our new A_7/A_8-basis.

Univariate scenario

We consider domains without boundaries as well as finite intervals. The case of real intervals with only a lower bound, or an upper one, can be constructed thereof.

Bi-infinite knots

If we have bi-infinite knots, i.e. the domain is without boundaries, the B-bundle $b^{(n)}_j$ is given by

$$b^{(n)}_j = [a^{(n)}_{j-1}, a^{(n)}_j, a^{(n)}_{j+1}]\, T^{\mathrm{A}_n;\mathrm{B}}. \tag{2.21}$$

The matrices $T^{\mathrm{A}_n;\mathrm{B}}$ can be found in Table 2.4 on page 48.

A spline $f(t) = \sum_j b_j \mathbf{p}^{\mathrm{B}}_j$ can be converted into the A_n-basis as follows: first, we partition $T^{\mathrm{A}_n;\mathrm{B}} = [T^{\mathrm{A}_n;\mathrm{B}}_{-1}; T^{\mathrm{A}_n;\mathrm{B}}_0; T^{\mathrm{A}_n;\mathrm{B}}_1]$ into blocks corresponding

$$S_A^{(7)} = \begin{bmatrix}
0 & 0 & 0 & 0 \\
0 & 0 & 0 & 0 \\
-\frac{53}{336} & -\frac{235}{2016} & \frac{1}{8} & -\frac{47}{1680} \\
-\frac{5}{8} & -\frac{19}{48} & 0 & 0 \\
\hline
\frac{9}{32} & \frac{187}{960} & 0 & 0 \\
-\frac{5}{16} & -\frac{53}{192} & 0 & 0 \\
\frac{305}{672} & \frac{103}{360} & \frac{1}{2} & -\frac{47}{420} \\
-\frac{5}{16} & \frac{31}{192} & 0 & 0 \\
\hline
\frac{9}{32} & -\frac{17}{240} & 0 & 0 \\
-\frac{5}{8} & \frac{5}{48} & 0 & 0 \\
-\frac{139}{672} & -\frac{299}{10080} & \frac{3}{4} & -\frac{197}{10080} \\
0 & 0 & 0 & \frac{5}{48} \\
\hline
0 & 0 & 0 & -\frac{17}{240} \\
0 & 0 & 0 & \frac{31}{192} \\
-\frac{1}{14} & -\frac{47}{420} & \frac{1}{2} & \frac{5003}{20160} \\
0 & 0 & 0 & -\frac{53}{192} \\
\hline
0 & 0 & 0 & \frac{187}{960} \\
0 & 0 & 0 & -\frac{19}{48} \\
-\frac{1}{56} & -\frac{47}{1680} & \frac{1}{8} & -\frac{1789}{20160} \\
0 & 0 & 0 & 0
\end{bmatrix},$$

$$S_A^{(8)} = \begin{bmatrix}
0 & 0 & 0 & 0 & 0 \\
0 & 0 & 0 & 0 & 0 \\
-\frac{365}{3072} & -\frac{22433}{322560} & \frac{1}{8} & -\frac{317}{13440} & -\frac{1}{64} \\
-\frac{35}{64} & -\frac{31}{128} & 0 & 0 & 0 \\
0 & -\frac{169}{80640} & 0 & 0 & 0 \\
\hline
\frac{1}{128} & \frac{155}{16128} & 0 & 0 & 0 \\
-\frac{35}{64} & -\frac{53}{192} & 0 & 0 & 0 \\
\frac{387}{1024} & \frac{6655}{43008} & \frac{1}{2} & -\frac{317}{3360} & -\frac{1}{16} \\
0 & \frac{121}{384} & 0 & 0 & 0 \\
-\frac{13}{384} & -\frac{1081}{80640} & 0 & 0 & 0 \\
\hline
\frac{49}{384} & \frac{197}{40320} & 0 & 0 & 0 \\
-\frac{35}{64} & \frac{33}{128} & 0 & 0 & 0 \\
-\frac{139}{768} & \frac{21121}{645120} & \frac{3}{4} & \frac{21121}{645120} & -\frac{139}{768} \\
0 & 0 & 0 & \frac{33}{128} & -\frac{35}{64} \\
0 & 0 & 0 & \frac{197}{40320} & \frac{49}{384} \\
\hline
0 & 0 & 0 & -\frac{1081}{80640} & -\frac{13}{384} \\
0 & 0 & 0 & \frac{121}{384} & 0 \\
-\frac{1}{16} & -\frac{317}{3360} & \frac{1}{2} & \frac{6655}{43008} & \frac{387}{1024} \\
0 & 0 & 0 & -\frac{53}{192} & -\frac{35}{64} \\
0 & 0 & 0 & \frac{155}{16128} & \frac{1}{128} \\
\hline
0 & 0 & 0 & -\frac{169}{80640} & 0 \\
0 & 0 & 0 & -\frac{31}{128} & -\frac{35}{64} \\
-\frac{1}{64} & -\frac{317}{13440} & \frac{1}{8} & -\frac{22433}{322560} & -\frac{365}{3072} \\
0 & 0 & 0 & 0 & 0 \\
0 & 0 & 0 & 0 & 0
\end{bmatrix}.$$

Table 2.3: Refinement matrices for the A-basis. As is already known from the cubic subspace, cardinal, cubic B-splines are the linear combination of $\frac{1}{8}$, $\frac{1}{2}$, $\frac{3}{4}$, $\frac{1}{2}$, $\frac{1}{8}$ times their siblings one refinement level higher. This identity reappears in the third column. For order eight we have point symmetry within the refinement matrix.

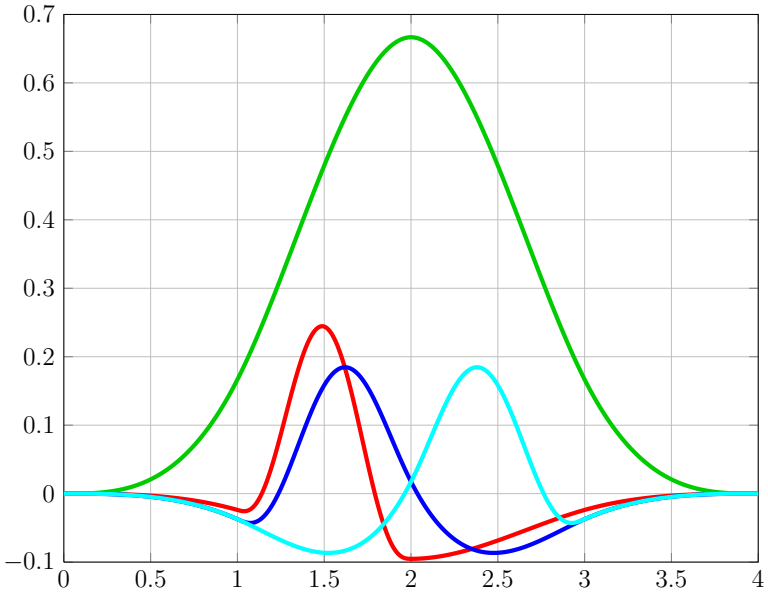

(a) A_7-basis.

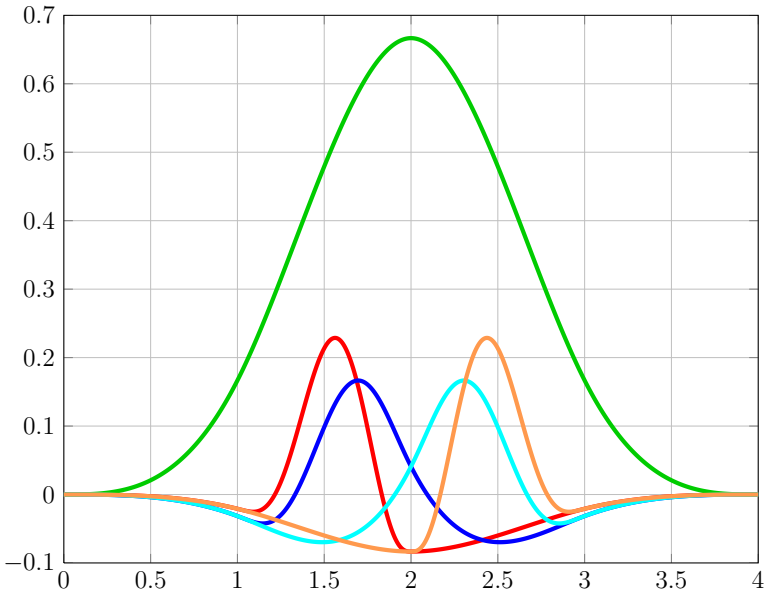

(b) A_8-basis.

Figure 2.17: One bundle of the A_7/A_8-basis, where "details" are of zero-mean. Notice that we have symmetry within a bundle only for order eight.

to bundles (also indicated in Table 2.4 on page 48). Simple algebra yields

$$\begin{aligned}\sum_j b_j \mathbf{p}_j^{\mathrm{B}} &= \sum_j \sum_{k=-1}^{1} a_{j+k} T_k^{\mathrm{A}_n;\mathrm{B}} \mathbf{p}_j^{\mathrm{B}}, \\ &= \sum_j a_j \mathbf{p}_j^{\mathrm{A}_n;\infty},\end{aligned}$$

with

$$\mathbf{p}_j^{\mathrm{A}_n;\infty} := \sum_{k=-1}^{1} T_{-k}^{\mathrm{A}_n;\mathrm{B}} \mathbf{p}_{j+k}^{\mathrm{B}}. \tag{2.22}$$

It might be surprising that a B-bundle is given by a suitably weighted 1-neighborhood of the A_7/A_8- basis – the supports being four knot intervals wide for the latter. But we should keep in mind that the supports of the pre-stage functions of the A_7/A_8- basis are a lot smaller (cf. Figure 2.16 on page 43).

The basis for finite intervals as domain

Suppose we have integer knots and the domain $[0, m]$ for some $m \geq 2, m \in \mathbb{N}$. The space of splines is spanned by the B-bundles centered at $0, \ldots, m$. The first function of the bundle at zero is superfluous (for order eight, the last one of the bundle at m is so, too). We could simply replace the respective B-bundles by their A_7-cousins in order to span the spline space (see Figure 2.18a on page 49) Yet, if we did that, our basis would be lacking the two cardinal cubic B-splines centered at -1 and $m + 1$. To include them

1. in the bundle centered at zero, we replace the (blue) function directly to the left of the cardinal cubic by the cardinal cubic of the bundle centered at -1,

2. analogously for the bundle centered at m, replace the cyan function to the right of the cardinal cubic by the cardinal cubic of the bundle centered at $m + 1$.

The pre-stage pendants of these functions are identical on $[0, m]$ with the cubic spline we replace them by. This is directly obvious from equation (2.19). The process is illustrated in Figure 2.18 on page 49, colors used match the figures throughout the section.

$$
\underbrace{\left[\begin{array}{cccc}
0 & 0 & 0 & 0 \\
0 & 0 & 0 & 0 \\
0 & \frac{47}{210} & -\frac{47}{70} & \frac{47}{210} \\
0 & 1 & -3 & 1 \\
\hline
1 & -\frac{21}{10} & \frac{9}{4} & -\frac{13}{20} \\
0 & \frac{17}{4} & -\frac{9}{2} & \frac{5}{4} \\
\frac{1}{7} & -\frac{29}{420} & \frac{183}{140} & \frac{29}{210} \\
0 & \frac{5}{4} & -\frac{9}{2} & \frac{17}{4} \\
\hline
0 & -\frac{13}{20} & \frac{9}{4} & -\frac{21}{10} \\
0 & 1 & -3 & 1 \\
0 & \frac{11}{84} & -\frac{7}{20} & -\frac{8}{105} \\
0 & 0 & 0 & 0
\end{array}\right]}_{T^{\mathrm{A}_7;\mathrm{B}}},
\underbrace{\left[\begin{array}{ccccc}
0 & 0 & 0 & 0 & 0 \\
0 & 0 & 0 & 0 & 0 \\
0 & \frac{947}{3360} & -\frac{841}{1120} & \frac{47}{168} & 0 \\
0 & \frac{3}{2} & -4 & \frac{3}{2} & 0 \\
0 & -\frac{1}{105} & \frac{13}{420} & -\frac{11}{420} & 0 \\
\hline
1 & -\frac{689}{420} & \frac{86}{105} & -\frac{73}{420} & 0 \\
0 & \frac{11}{2} & -\frac{13}{2} & 2 & 0 \\
\frac{1}{8} & -\frac{349}{1120} & \frac{981}{560} & -\frac{349}{1120} & \frac{1}{8} \\
0 & 2 & -\frac{13}{2} & \frac{11}{2} & 0 \\
0 & -\frac{73}{420} & \frac{86}{105} & -\frac{689}{420} & 1 \\
\hline
0 & -\frac{11}{420} & \frac{13}{420} & -\frac{1}{105} & 0 \\
0 & \frac{3}{2} & -4 & \frac{3}{2} & 0 \\
0 & \frac{47}{168} & -\frac{841}{1120} & \frac{947}{3360} & 0 \\
0 & 0 & 0 & 0 & 0 \\
0 & 0 & 0 & 0 & 0
\end{array}\right]}_{T^{\mathrm{A}_8;\mathrm{B}}}
$$

Table 2.4: Representations of a single B-bundle by a 1-neighborhood of the $\mathrm{A}_7/\mathrm{A}_8$- basis, per equation (2.21).

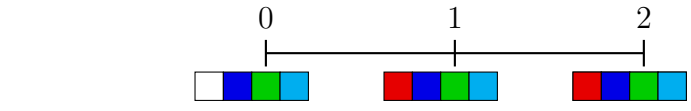

(a) $B^{(7)}$-bundles.

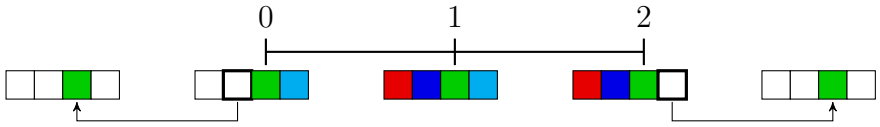

(b) A_7-bundles.

Figure 2.18: a) The space of splines could be spanned by simply using the A_7-bundles in place of B-bundles (white indicates parts of a bundle which is not within the basis). But if we did so, the basis would be lacking the two outermost cardinal, cubic B-splines. b) On the left, we replace the function whose pre-stage pendant is identical on $[0, m]$ with the cardinal cubic spline centered at -1, by the latter one. We proceed in the same manner at the right end of the interval.

Converting to $\mathbf{A_7/A_8}$ on finite intervals

As in the bi-infinite case, let

$$f(t) = \sum_{j=0}^{m} b_j(t)\mathbf{p}_j^{\mathrm{B}}, \quad t \in [0, a],$$

be a spline in B-bundle form, of order $n \in \{7, 8\}$. We are looking for its representation with respect to the A_n-basis, i.e.

$$f(t) = \sum_{j=-1}^{m+1} a_j(t)\mathbf{p}_j^{\mathrm{A}_n}, \quad t \in [0, a] \tag{2.23}$$

for the unknowns $\mathbf{p}_j^{\mathrm{A}_n}$. This can easily be done by interpolation. The results can be found in Tables 2.5 (order seven), respectively Table 2.6 (order eight).

Using interpolation has several shortcomings:

- It provides little insight and thus no guidance for non-tensor domains.
- Finding the $\mathbf{p}_j^{\mathrm{A}_n}$ by interpolation can only be done for finitely many such intervals $[0, m]$. Is the solution presented in tables 2.5–2.6 really correct for any m?

$$\mathbf{p}_{-1}^{\mathrm{A}_7} = \begin{bmatrix} 0 & 0 & 0 & 0 \\ 0 & 0 & 0 & 0 \\ 0 & \frac{17}{4} & -\frac{9}{2} & \frac{5}{4} \\ 0 & 0 & 0 & 0 \end{bmatrix} \mathbf{p}_0^{\mathrm{B}},$$

$$\mathbf{p}_0^{\mathrm{A}_7} = \begin{bmatrix} 0 & 0 & 0 & 0 \\ 0 & 0 & 0 & 0 \\ 0 & -\frac{121}{168} & \frac{279}{140} & -\frac{41}{840} \\ 0 & \frac{5}{4} & -\frac{9}{2} & \frac{17}{4} \end{bmatrix} \mathbf{p}_0^{\mathrm{B}} + \begin{bmatrix} 0 & 0 & 0 & 0 \\ 0 & 0 & 0 & 0 \\ 0 & \frac{47}{210} & -\frac{47}{70} & \frac{47}{210} \\ 0 & 1 & -3 & 1 \end{bmatrix} \mathbf{p}_1^{\mathrm{B}},$$

$$\mathbf{p}_j^{\mathrm{A}_7} = \mathbf{p}_j^{\mathrm{A}_{7;\infty}}, \quad \text{for } j = 1, \ldots, m-1,$$

$$\mathbf{p}_m^{\mathrm{A}_7} = \begin{bmatrix} 0 & -\frac{13}{20} & \frac{9}{4} & -\frac{21}{10} \\ 0 & 1 & -3 & 1 \\ 0 & \frac{11}{84} & -\frac{7}{20} & -\frac{8}{105} \\ 0 & 0 & 0 & 0 \end{bmatrix} \mathbf{p}_{m-1}^{\mathrm{B}} + \begin{bmatrix} 1 & -\frac{21}{10} & \frac{9}{4} & -\frac{13}{20} \\ 0 & \frac{17}{4} & -\frac{9}{2} & \frac{5}{4} \\ \frac{1}{7} & -\frac{293}{840} & \frac{81}{35} & -\frac{683}{840} \\ 0 & 0 & 0 & 0 \end{bmatrix} \mathbf{p}_m^{\mathrm{B}},$$

$$\mathbf{p}_{m+1}^{\mathrm{A}_7} = \begin{bmatrix} 0 & 0 & 0 & 0 \\ 0 & 0 & 0 & 0 \\ 0 & \frac{5}{4} & -\frac{9}{2} & \frac{17}{4} \\ 0 & 0 & 0 & 0 \end{bmatrix} \mathbf{p}_m^{\mathrm{B}}.$$

Table 2.5: Formulas to calculate A_7-control points for equation (2.23) when the domain is given by a finite interval $[0, m]$.

Some argumentation seems in order. How can the $\mathbf{p}_j^{\mathrm{A}_n}$ be derived from the $\mathbf{p}_j^{\mathrm{A}_n;\infty}$?

Changing to $\mathbf{A}_7$-basis by systematic course of action

We describe the process for order 7 only, as it is mostly identical for order eight. In fact, the reader should find the latter case easier, as it is fully symmetric then.

1. Calculate $\mathbf{p}_j^{\mathrm{A}_7;\infty}$. Away from the boundaries, $\mathbf{p}_j^{\mathrm{A}_7;\infty}$ and $\mathbf{p}_j^{\mathrm{A}_7}$ are identical: $\mathbf{p}_j^{\mathrm{A}_7;\infty} = \mathbf{p}_j^{\mathrm{A}_7}$, $j = 1, \ldots, m-1$.

2. Denoting by $a_{0,1}, a_{0,2}$ the first two functions of the bundle centered at

$$\mathbf{p}_{-1}^{\mathrm{A}_8} = \begin{bmatrix} 0 & 0 & 0 & 0 & 0 \\ 0 & 0 & 0 & 0 & 0 \\ 0 & \frac{11}{2} & -\frac{13}{2} & 2 & 0 \\ 0 & 0 & 0 & 0 & 0 \\ 0 & 0 & 0 & 0 & 0 \end{bmatrix} \mathbf{p}_0^{\mathrm{B}},$$

$$\mathbf{p}_0^{\mathrm{A}_8} = \begin{bmatrix} 0 & 0 & 0 & 0 & 0 \\ 0 & 0 & 0 & 0 & 0 \\ 0 & -\frac{769}{672} & \frac{3221}{1120} & -\frac{1121}{1680} & \frac{1}{8} \\ 0 & 2 & -\frac{13}{2} & \frac{11}{2} & 0 \\ 0 & -\frac{73}{420} & \frac{86}{105} & -\frac{689}{420} & 1 \end{bmatrix} \mathbf{p}_0^{\mathrm{B}} + \begin{bmatrix} 0 & 0 & 0 & 0 & 0 \\ 0 & 0 & 0 & 0 & 0 \\ 0 & \frac{947}{3360} & -\frac{841}{1120} & \frac{47}{168} & 0 \\ 0 & \frac{3}{2} & -4 & \frac{3}{2} & 0 \\ 0 & -\frac{1}{105} & \frac{13}{420} & -\frac{11}{420} & 0 \end{bmatrix} \mathbf{p}_1^{\mathrm{B}},$$

$$\mathbf{p}_j^{\mathrm{A}_8} = \mathbf{p}_j^{\mathrm{A}_{8;\infty}}, \quad \text{for } j = 1, \ldots, m-1,$$

$$\mathbf{p}_m^{\mathrm{A}_8} = \begin{bmatrix} 0 & -\frac{11}{420} & \frac{13}{420} & -\frac{1}{105} & 0 \\ 0 & \frac{3}{2} & -4 & \frac{3}{2} & 0 \\ 0 & \frac{47}{168} & -\frac{841}{1120} & \frac{947}{3360} & 0 \\ 0 & 0 & 0 & 0 & 0 \\ 0 & 0 & 0 & 0 & 0 \end{bmatrix} \mathbf{p}_{m-1}^{\mathrm{B}} + \begin{bmatrix} 1 & -\frac{689}{420} & \frac{86}{105} & -\frac{73}{420} & 0 \\ 0 & \frac{11}{2} & -\frac{13}{2} & 2 & 0 \\ \frac{1}{8} & -\frac{1121}{1680} & \frac{3221}{1120} & -\frac{769}{672} & 0 \\ 0 & 0 & 0 & 0 & 0 \\ 0 & 0 & 0 & 0 & 0 \end{bmatrix} \mathbf{p}_m^{\mathrm{B}}$$

$$\mathbf{p}_{m+1}^{\mathrm{A}_8} = \begin{bmatrix} 0 & 0 & 0 & 0 & 0 \\ 0 & 0 & 0 & 0 & 0 \\ 0 & 2 & -\frac{13}{2} & \frac{11}{2} & 0 \\ 0 & 0 & 0 & 0 & 0 \\ 0 & 0 & 0 & 0 & 0 \end{bmatrix} \mathbf{p}_m^{\mathrm{B}}.$$

Table 2.6: Formulas to calculate A_8-control points of equation (2.23). The domain is given by a finite interval $[0, m]$. Notice that the process is completely symmetric for order eight.

zero, we revert $a_{0,1}, a_{0,2}$ and a_{-1} to pre-stage by (2.20),

$$\hat{a}_1 := \widetilde{a}_1 = a_1 \left(W^{(7)}\right)^{-1}, \quad \hat{a}_0 := [\widetilde{a}_{0,1}, \widetilde{a}_{0,2}, a_{0,3}, a_{0,4}],$$

$$\hat{\mathbf{p}}_{-1}^{\mathrm{A}_7} = \begin{bmatrix} 0 & 0 & 0 & 0 \\ 0 & 0 & 0 & 0 \\ -w_1 & -w_2 & 1 & -w_4 \\ 0 & 0 & 0 & 0 \end{bmatrix} \mathbf{p}_{-1}^{\mathrm{A}_7;\infty} + \begin{bmatrix} 0 & 0 & 0 & 0 \\ 0 & 0 & 0 & 0 \\ 0 & 1 & 0 & 0 \\ 0 & 0 & 0 & 0 \end{bmatrix} \mathbf{p}_0^{\mathrm{A}_7;\infty},$$

$$\hat{\mathbf{p}}_0^{\mathrm{A}_7} = \begin{bmatrix} 0 & 0 & 0 & 0 \\ 0 & 0 & 0 & 0 \\ -w_1 & -w_2 & 1 & 0 \\ 0 & 0 & 0 & 1 \end{bmatrix} \mathbf{p}_0^{\mathrm{A}_7;\infty}.$$

The supports

a) of $\widetilde{a}_{-1,k}, k \neq 3$, are given by the interval $[-2, 0]$,

b) of $\widetilde{a}_{0,1}$ is $[-1, 0]$

(see Figure 2.16 on page 43). Since they are zero on the spline domain, $[0, m]$, we can change their coefficients to zero.

3. $\widetilde{a}_{-1,3}$ and $\widetilde{a}_{0,2}$ are the same when restricted to $[0, m]$. We turn the coefficient of $\widetilde{a}_{0,2}$ to zero, too, by moving it into $\mathbf{p}_{-1,3}^{\mathrm{A}_7}$:

$$\begin{bmatrix} \mathbf{p}_{-1,3}^{\mathrm{A}_7} \\ \mathbf{p}_{0,2}^{\mathrm{A}_7} \end{bmatrix} = \begin{bmatrix} 1 & 1 \\ 0 & 0 \end{bmatrix} \begin{bmatrix} \hat{\mathbf{p}}_{-1,3}^{\mathrm{A}_7} \\ \hat{\mathbf{p}}_{0,2}^{\mathrm{A}_7} \end{bmatrix}.$$

4. Out of the bundle $\hat{a}_{-1}$, all but the cardinal cubic have zero coefficients now. Both $\hat{a}_{0,1}, \hat{a}_{0,2}$ do as well. We can therefore replace $\hat{a}_{-1}$ by a_{-1}, and $\hat{a}_0$ by a_0, as desired.

5. Apart from that $a_{0,1}$ has no pendant at the right end of the interval which must be treated (contrary to order eight), we take an analogous course of action as in steps 2–4 for the bundles centered at m and $m + 1$.

In matrix notation, we have

$$\begin{bmatrix} \mathbf{p}_{-1}^{\mathrm{A}_7} \\ \mathbf{p}_0^{\mathrm{A}_7} \end{bmatrix} = M_1 M_2 \begin{bmatrix} \mathbf{p}_{-1}^{\mathrm{A}_7;\infty} \\ \mathbf{p}_0^{\mathrm{A}_7;\infty} \end{bmatrix},$$

where M_1M_2 represent the cumulative steps 2–3 above. M_1 and M_2 are

$$\left(\begin{array}{cccc|cccc} 0&0&0&0&0&0&0&0\\ 0&0&0&0&0&0&0&0\\ 0&0&1&0&0&1&0&0\\ 0&0&0&0&0&0&0&0\\ \hline 0&0&0&0&0&0&0&0\\ 0&0&0&0&0&0&0&0\\ 0&0&0&0&0&0&1&0\\ 0&0&0&0&0&0&0&1 \end{array}\right), \left(\begin{array}{cccc|cccc} 1&0&0&0&0&0&0&0\\ 0&1&0&0&0&0&0&0\\ -w_1&-w_2&1&-w_4&0&0&0&0\\ 0&0&0&1&0&0&0&0\\ \hline 0&0&0&0&1&0&0&0\\ 0&0&0&0&0&1&0&0\\ 0&0&0&0&-w_1&-w_2&1&0\\ 0&0&0&0&0&0&0&1 \end{array}\right).$$

Expanding products and substituting the expressions for the $\mathbf{p}_j^{\mathrm{A}_7;\infty}$ gives the formulas of Table 2.5.

The domain $\mathbb{R}^2 \setminus (-\frac{1}{2}, \frac{1}{2})^2$ (in preparation of extraordinary points)

Recall that we want the A_n-bases to represent subdivision surfaces near extraordinary points. To both $n = 7$ and $n = 8$ more that n basis functions have values different from zero on each knot interval. Hence, can its regular setting be generalized to extraordinary points[5]? That depends on whether masks draw on small neighborhoods only, when we change from $B^{(n)}$ to A_n-basis. Suppose we have knots $\frac{1}{4}\mathbb{Z}\$(n-3)$, and a spline $f : \mathbb{R}^2 \setminus (-\frac{1}{2}, \frac{1}{2})^2$ in B-bundle form,

$$f(s,t) = \sum_{|(i,j)|_\infty \geq \frac{1}{2}} b_i(s)\mathbf{p}^{\mathrm{B}}_{i,j}b_j(t).$$

In the notation, (i, j) is also the point in the domain, $\mathbb{R}^2$, to which its B-bundle is centered. We consider control bundles $\mathbf{p}^{\mathrm{B}}_{i,j}$ as submatrices of the (complete) B-spline control net here. The function space is sketched in Figure 2.19 on page 54.

The function space

Notice that the domain of f is not a tensor product and that it has an inner boundary. Analogously to the univariate setting, we could span the

[5]The setup for extraordinary points of subdivision surfaces is presented in Section 3.1. For the purpose of the current section, however, it is sufficient to consider the domain $\mathbb{R}^2 \setminus (-\frac{1}{2}, \frac{1}{2})^2$.

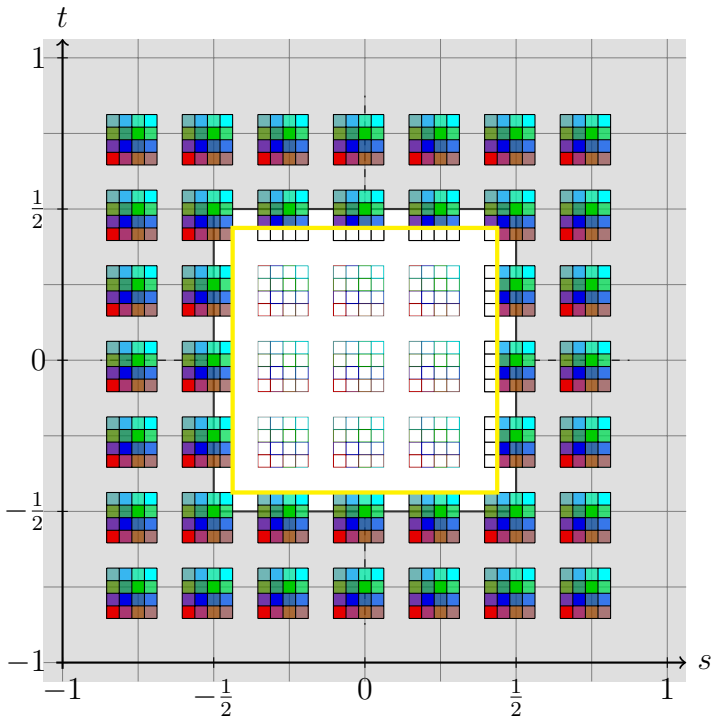

Figure 2.19: The two innermost rings of $B^{(7)}$-control bundles used to span the space of C^2 splines of order seven for the domain $\mathbb{R}^2 \setminus (-\frac{1}{2}, \frac{1}{2})^2$ (shaded gray). Thin lines mark knot lines. All B-splines in the yellow rectangle are excluded, as their support is disjoint from the domain. As before, white indicates these "deactivated" parts of a bundle, required to have all-zero coefficients.

function space by simply using A_n- instead of $B^{(n)}$-bundles. Again, this is not desireable because one would wish to have the tensor product cardinal cubic splines of the bundles (i, j), $|(i, j)|_\infty = 1/4$, in the basis. We can use the same trick: we replace some of the generating functions by cardinal cubic splines. Figure 2.20 on page 55 illustrates the process.

Changing basis by systematic course of action

Changing to A_n-bases can be done similarly as for finite intervals. As there, we describe the process for order seven, as the absence of symmetry within

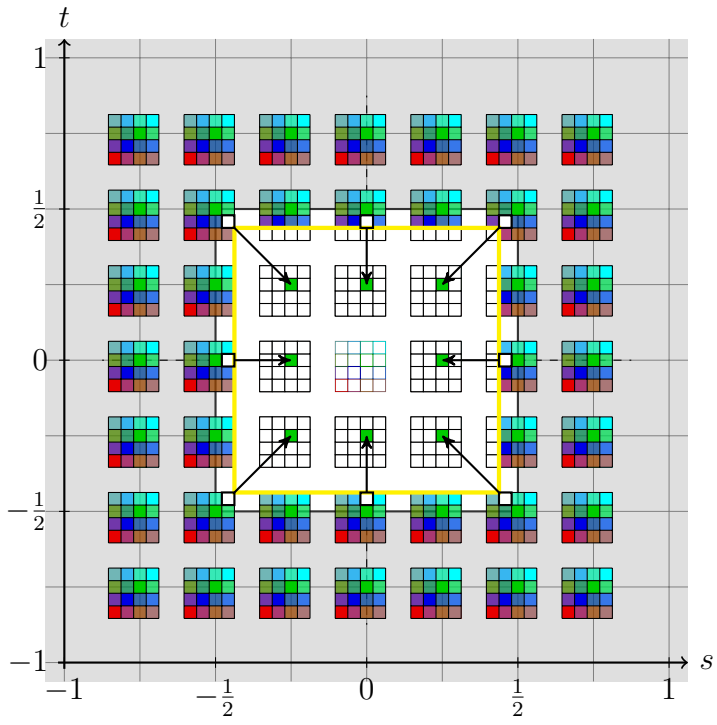

Figure 2.20: The three innermost rings of A_7-bundles that are used to span the space of splines for the domain $\mathbb{R}^2 \setminus (-\frac{1}{2}, \frac{1}{2})^2$. As in the univariate case, we replace functions at the—here, inner—boundary by the cardinal cubics of the next ring; the coefficients of the former ones therefore become those of the latter ones (or, if the latter ones are non-zero, are added to these). The pre-stage pendants of the deactivated functions are identical, when restricted to $\mathbb{R}^2 \setminus (-\frac{1}{2}, \frac{1}{2})^2$, with the cardinal cubic B-splines they are replaced with. The yellow rectangle is repeated from Figure 2.19, in order to assist orientation.

a bundle makes the task more treacherous[6].

The steps are:

1. Change to control points $\mathbf{p}_{(i,j)}^{\mathrm{A}_7;\infty}$. By (2.22), we have

$$\mathbf{p}_{(i,j)}^{\mathrm{A}_n;\infty} := \sum_{k,m=-1}^{1} T_{-k}^{\mathrm{A}_n;\mathrm{B}} \mathbf{p}_{(j+\frac{k}{4},i+\frac{m}{4})}^{\mathrm{B}} \left(T_{-m}^{\mathrm{A}_n;\mathrm{B}}\right)^T.$$

   Superfluous B-splines, whose support is a subset of the hole $(-\frac{1}{2},\frac{1}{2})^2$ in the domain, are to be assigned zero coefficients, of course. It is

$$\mathbf{p}_{(i,j)}^{\mathrm{A}_n} = \mathbf{p}_{(i,j)}^{\mathrm{A}_n;\infty}, \quad \text{for all } |(i,j)|_\infty \geq \frac{3}{4}.$$

2. Revert to pre-stage the functions that are replaced by some other functions in Figure 2.20, as well as all functions within the yellow rectangle. The control bundles to be converted fully can be handled by

$$\hat{\mathbf{p}}_{(i,j)}^{\mathrm{A}_n} = W^{(n)} \mathbf{p}_{(i,j)}^{\mathrm{A}_n;\infty} \left(W^{(n)}\right)^T, \quad |(i,j)|_\infty = \frac{1}{4}.$$

   In order to change only part of a univariate bundle, say function i, back to pre-stage, let $W_i^{(n)}$ be the identity matrix with i-th column replaced by the one of $W^{(n)}$. To give an example, for the bundle centered at $(\frac{1}{2},0)$, we have

$$\hat{\mathbf{p}}_{(\frac{1}{2},0)}^{\mathrm{A}_n} = W_1^{(n)} \mathbf{p}_{(\frac{1}{2},0)}^{\mathrm{A}_n;\infty} \left(W^{(n)}\right)^T.$$

3. We transfer coefficients as indicated in Figure 2.21 on page 57. After that, the tensor product cardinal cubic B-splines are the only functions within the yellow rectangle whose coefficient is not either zero, or whose support is disjoint from our domain.

[6] 1) As to "symmetry within a bundle", cf. Figure 2.17 on page 46. 2) Behind this absence of symmetry is that, for order seven, there is only one C^2 spline whose support is exactly one knot interval wide. Consequently, one cannot have symmetry within the bundle-paradigm for $n = 7$.

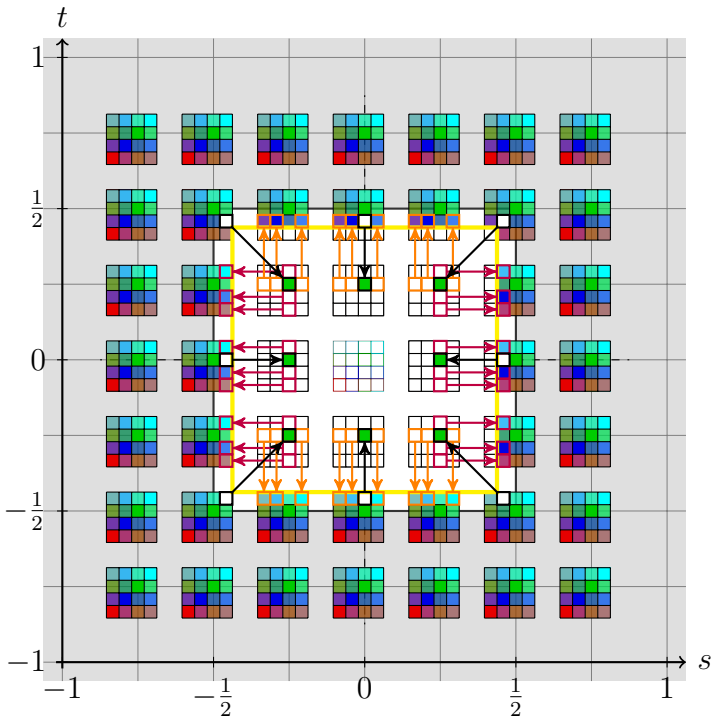

Figure 2.21: The figure shows which pre-stage functions are pairwise identical on the domain $\mathbb{R}^2 \setminus (-\frac{1}{2}, \frac{1}{2})$ (it might be a good idea to revisit Figure 2.16 on page 43 for the pre-stage functions' support).
There is a one-to-one relationship between the functions and their coefficients. Hence, we do not repeat the same figure with squares denoting coefficients instead. Let us simply agree that a square can represent the function as well as its coefficient. Returning to the current problem, we add the coefficient where an arrow starts to the one its tip points at, for all arrows. After that, we must turn the coefficients of the former ones to zero.
Notice that, for example for the bundle centered at $(s,t) = (0, -\frac{1}{2})$, the support of the functions attached to the orange squares in the t-direction is $[-\frac{3}{2}, \frac{1}{2}]$. This is due to the fact that the functions attached to the orange squares are all tensor products of the cubic B-spline (in the variable t) centered at $t = -\frac{1}{2}$ with the corresponding (pre-stage) function in the variable s.

Changing basis using interpolation

The A_n-representation can be calculated by interpolation, too. Since $\mathbf{p}^{A_n}_{(i,j)} = \mathbf{p}^{A_n;\infty}_{(i,j)}$ holds for $|(i,j)|_\infty \geq \frac{3}{4}$, we changed the domain to $[-1,1]^2 \setminus (-\frac{1}{2},\frac{1}{2})^2$, so that outer boundaries—anticipating spline rings—are covered as well.

If there is both an inner, as well as an outer, boundary, we use the function space shown in Figure 2.22.

The results of the interpolation are stored in MATLAB (ASCII) `.mat` format, using 16 digit double precision and tab-delimeters. This should be very easy to read, even by someone who does not have access to MATLAB. After that, to do the conversion, say, for order seven, we simply put the 35×35 B-spline -coefficients within a single vector x^{B}, using rowwise ordering (which is the standard in MATHEMATICA). We can then compute the corresponding vector x^{A_7} of 44×44 A_7-coefficients by

$$x^{A_7} = M^{(7)} x^{\mathrm{B}},$$

where $M^{(7)}$ is the matrix from the `.mat` file.

Figure 2.24 provides an example showing how good the cubic part approximates a surface.

Masks still draw on 1-neighborhoods only

Finally, it is easily verified that changing from $B^{(n)}$- to A_n-basis can be realized by 1-neighborhoods (i.e. the coefficients of a bundle in the new basis result from a 1-neighborhood of bundles of coefficients in the old basis). The animation in Figure 2.25 on page 62 illustrates which old coefficients determine a particular coefficient in the new basis (indicated in red). We conclude that the A_n-bases can indeed serve to model subdivision surfaces near extraordinary points (whose domain is similar to $\mathbb{R}^2 \setminus (-\frac{1}{2},\frac{1}{2})^2$, cf. Section 3.1).

2.7 Convergence of the cubic part

In this section, we are going to examine convergence of the cubic part, as well as its control polygon, to the full spline of order seven or eight.

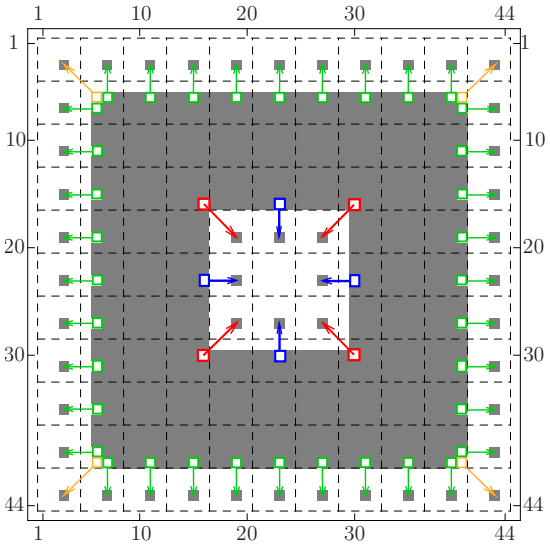

(a) Order 7.

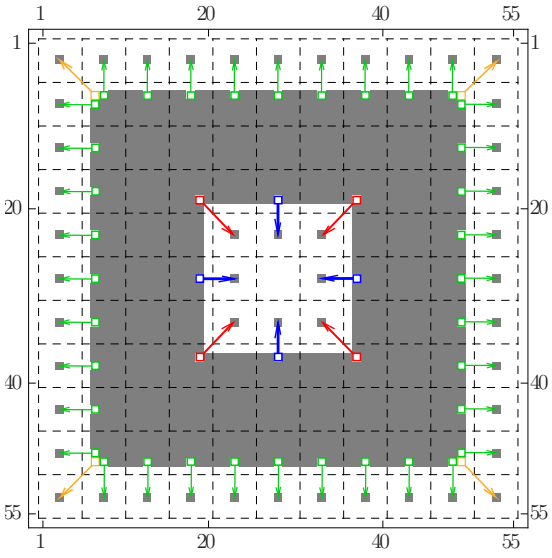

(b) Order 8.

Figure 2.22: If the domain is given by a single spline *ring*, i.e. the domain is $[-1,1]^2 \setminus (-\frac{1}{2},\frac{1}{2})^2$, at the outer boundary, the replacement of functions is as indicated by yellow and green arrows. At the inner boundary, the situation remains the same as if there was no outer boundary (red and blue arrows). Free coefficients are shaded, while "deactivated" ones (those that are always zero) remain white. Be careful, these figures were produced (in part) by MATHEMATICA'S routine `MatrixPlot` – in contrast to preceding figures, the vertical axes go from top to bottom. 2.22b) The reversion of the vertical axis by `MatrixPlot` is unproblematic here, due to symmetry within bundles.

order n	name of attached file	#B-splines	#A_n-splines
7	`B7-to-A7-on-splinering.mat`	35×35	44×44
8	`B8-to-A8-on-splinering.mat`	43×43	55×55.

Figure 2.23: The files that contain the results of the symbolic calculation for changing from $B^{(n)}$ to A_n-basis. The domain is $[-1,1]^2 \setminus (-\frac{1}{2},\frac{1}{2})^2$, and the knots are given by $\frac{1}{4}(-5\$(n-3),\ldots,+5\$(n-3))$.

Which tool to use?

There are some problems that would make it necessary to adapt and expand the theory on proxies, which we have presented in Subsection 2.2:

Non-local basis: the A_n-bases are not local bases – on every knot interval, more than n of the basis functions are different from the zero polynomial.

Not a 1:1 relationship: every bundle a_j contains four (for $n = 7$), respectively five (for $n = 8$) functions.

Neither of these obstacles is insurmountable. But while they would require some effort, using the theory that is available for quasi interpolants allows to answer the foremost questions concerning the cubic part very quickly.

Quasi interpolants

Let $K = [\kappa_1, \ldots, \kappa_{m+n}]$ be a non-degenerate knot vector as defined in Section 2.2. Further, $\mathcal{S}_K^{(n)}$ is the space of splines of order n defined over it, with domain

$$\mathrm{dom}(K) := [\kappa_n, \kappa_{m+1}).$$

Definition 2.16 (Quasi-interpolants)**.** A *quasi-interpolant*[7] *of order* $\nu \in \mathbb{N}$ is a linear mapping

$$g \mapsto \sum_{j=1}^{m} b_j^{K,n}(Q_j g)$$

from $C(\mathrm{dom}(K))$ into $\mathcal{S}_K^{(n)}$ with the four properties

[7] *As noted earlier, quasi interpolants were introduced by C. de Boor [3].*

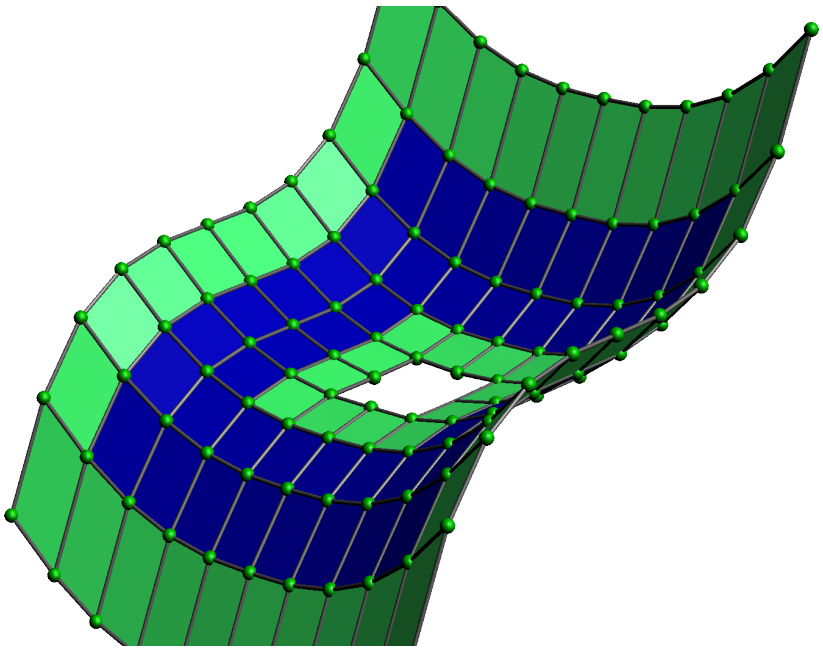

Figure 2.24: Putting the cubic decomposition of the A_7-basis to the test: with x_j-/y_j- the x- and y- components of the identity, we have set $z_j = x_j^3 - \frac{1}{2}|y_j|^{2.5}$. *Top:* As we can see from the cubic control net, the cubic part is a very good representation of the surface. Blue color indicates facets of the control polygon whose domain coincides with that of the spline ring. *Bottom:* accompanying non-cubic part. Click the figures to explore in interactive (3D) view.

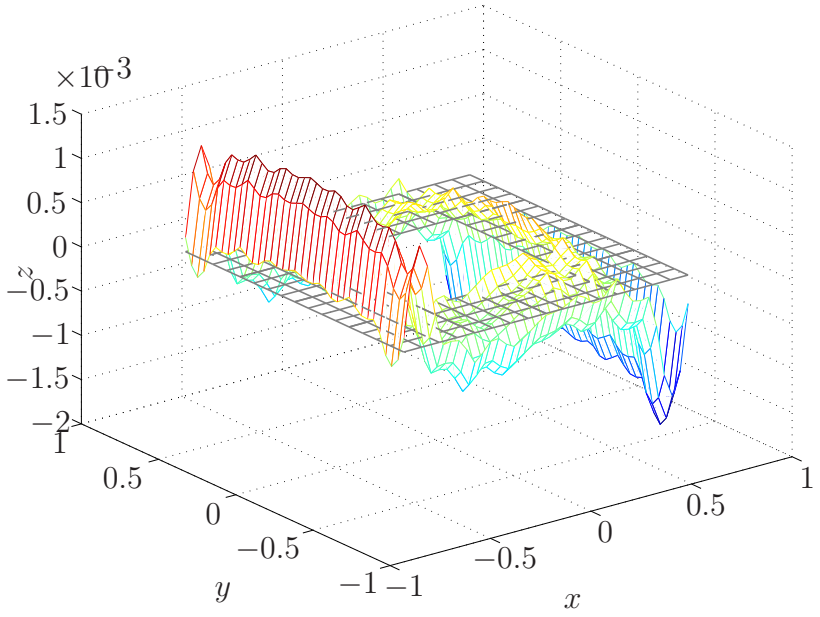

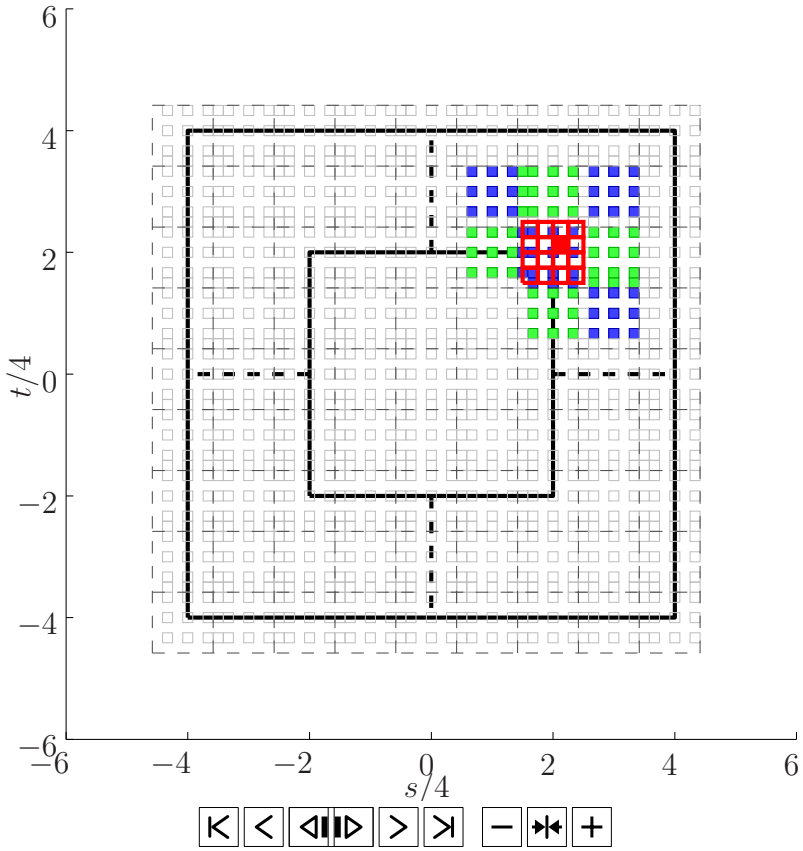

Figure 2.25: The figure shows which $B^{(7)}$-coefficients (blue and green checkerboard) enter a particular coefficient of the A_7-basis (red), when we change from $B^{(7)}$- to A_7-basis. In this figure, B-splines are represented by their Greville abscissas. Dashed lines mark the partitioning into bundles. Only the inner rings of A_7-bundles are covered in the animation, as the remaining ones are unaffected by the inner boundary. For order eight, the change of basis turns out to be local, too, allthough this is not illustrated here.

1. that it is the identity on polynomials of order ν,
2. every $Q_j g$ depends solely on the restriction of g to the support of its corresponding B-spline $b_j^{K,n}$,
3. the Q_j are linear functionals on $C(\mathrm{dom}(K))$, and
4. all Q_j are bounded operators in terms of the sup-norm on the interval $\mathrm{dom}(K)$.

When $f(t)$ is a suitable C^2 spline of order $n = 7, 8$, we denote by

$$f_\ell^{[4]}(t), \quad \breve{f}_\ell^{[4]}(t)$$

its cubic part in the A_n-basis, respectively the control polygon of the latter. Both are dependent on the binary- refinement level ℓ.

Let K_ℓ be the knot-vector at binary refinement level ℓ. Since K_0 will be fixed in all of the following, we abbreviate

$$\mathcal{S}_\ell^{(n)} := \mathcal{S}_{K_\ell}^{(n)}.$$

Theorem 2.17. *There is a quasi interpolant $\mathcal{Q}^{(\ell)}$ which projects onto $\mathcal{S}_\ell^{(4)}$ with $\mathcal{Q}^{(\ell)} f = f_\ell^{[4]}$. Its order is four.*

Theorem 2.18. *There is a quasi interpolant $\breve{\mathcal{Q}}^{(\ell)}$ which projects onto $\mathcal{S}_\ell^{(2)}$ with $\breve{\mathcal{Q}}^{(\ell)} f = \breve{f}_\ell^{[4]}$. The order of $\breve{\mathcal{Q}}^{(\ell)}$* is two.

Before we do the proofs, we should give some preparative explanations:

1. Let $\mathcal{Q} : C^2(\mathrm{dom}\, K) \to \mathcal{S}_K^{(n)}$ be any quasi interpolant of order ν. We can append some mapping $\mathcal{M} : \mathcal{S}_K^{(n)} \to \mathcal{S}_K^{(n)}$ to it. If $\mathcal{M}$ preserves properties 1–4 in the definition of quasi interpolants, the decomposition $\mathcal{M} \circ \mathcal{Q}$ again is a quasi interpolant of order ν. If $\mathcal{M}$ has properties 2–4 but preserves only polynomials of order $\tilde{\nu} < \nu$, then $\mathcal{M} \circ \mathcal{Q}$ is still a quasi interpolant, but its order is $\tilde{\nu}$ ($\mathcal{Q}$ is also a quasi interpolant of order $\tilde{\nu}$ for any $\tilde{\nu} < \nu$).
2. The quasi-interpolant $\widehat{\mathcal{Q}}$ we use here is well known for its use in showing stability of the B-basis. It is also a projector onto B-splines of order n. To define $\widehat{\mathcal{Q}}_j$, we take the largest knot interval of the B-spline b_j

associated to $\widehat{\mathcal{Q}}_j$ (if there is more than one such interval, we might take, say, the center- or left-most every time). We interpolate the function g to be mapped by the quasi interpolant at n points distributed equidistantly in this interval. The coefficient of b_j then is returned as the value of $\widehat{\mathcal{Q}}_j g$.

3. For the purpose of Theorem 2.17, $\mathcal{M}$ returns only the cubic part of the image of Q, as defined by the A_n-basis of that order.

4. In the proof of Theorem 2.18, $\mathcal{Q}$ is a mapping $C^2(\operatorname{dom} K) \to \mathcal{S}_K^{(n)} \subseteq \operatorname{span}(\mathcal{S}_K^{(n)} \cup \mathcal{S}_{\mu(\tilde{K},n)}^{(2)})$. Here, $\mu(\tilde{K}, n)$ is the vector of Greville absciassae to the knot vector $\tilde{K}$, which contains each knot of K only once. $\mathcal{M}$ now returns the control polygon of the cubic part, i.e. one can view this as an additional function appended to the $\mathcal{M}$ of the previous item.

5. Finally, notice that any quasi interpolant that projects onto a space of splines of order $n \in \mathbb{N}$ is inherently of order n. Thus, provided $\mathcal{Q}^{(\ell)}, \breve{\mathcal{Q}}^{(\ell)}$ exist and are projectors, their orders are as asserted in Theorems 2.17–2.18.

Proof of Theorem 2.17. Let the order $n \in \{7, 8\}$ be fixed. We must verify the four properties required in the definition of quasi interpolants.

Due to their basis property, the cubic part $f_\ell^{[4]}$ of the A_n-generating system defines a projector onto $\mathcal{S}_{4,\ell}$. By Tables 2.5–2.6, this mapping is linear and obviously is the identity on cubic polynomials. Properties 1 and 3 follow.

Regarding 2.: As we have seen in Section 2.6, when we change from $B^{(n)}$ to A_n-basis, all new coefficients can be calculated by 1-neighborhoods (bundlewise). Without loss of generality, we may assume integer knots, and bundles indexed by their central knot. Hence, the support of b_j (of order n) is $[j-1, j+1]$, while the cardinal cubic B-spline of the bundle a_k has support $[k-2, k+2]$. Obviously, for $j \in \{k-1, k, k+1\}$, the support of b_j is contained within that of a_k.

Finally, we must show that all $\mathcal{Q}_j^{(\ell)}$ are bounded operators. The $\widehat{\mathcal{Q}}_{\ell,j}$ are such ones. The $\mathcal{Q}_j^{(\ell)}$ evolve from the former ones by Tables 2.5–2.6, that is, by operations that are linear as well as bounded. The composition of linear, bounded operators is again linear and bounded.

□

Proof of Theorem 2.18. Due to $\mathcal{Q}_j^{(\ell)} = \breve{\mathcal{Q}}_j^{(\ell)}$, properties 3.–4. hold for $\breve{\mathcal{Q}}_j^{(\ell)}$.

If b_j is the B-spline of (any) order n to knots $(\kappa_j, \kappa_{j+1}, \ldots, \kappa_{j+n})$, then for the Greville-abscissas $\mu_l = \sum_{k=1}^{n-1} \kappa_{k+l}/(n-1)$ we have $\kappa_j \leq \mu_{j-1} \leq \mu_{j+1} \leq \kappa_{j+n}$ automatically. This means the support of its control polygon $\breve{b}_j$, which is given by $[\mu_{j-1}, \mu_{j+1}]$, is a subset of the support $[\kappa_j, \kappa_{j+n}]$ of b_j. Property 2. required for quasi interpolants follows. Finally, $\breve{\mathcal{Q}}^{(\ell)}$ has order two because of linear precision.

□

The desired convergence estimates now follow directly:

Corollary 2.19. *Let $k \in \{0, 1\}$. Then it is*

$$\|\partial^k (f - f_\ell^{[4]})\|_\infty \preccurlyeq 2^{-(4-k)\ell},$$
$$\|\partial^k (f - \breve{f}_\ell^{[4]})\|_\infty \preccurlyeq 2^{-(2-k)\ell}, \quad \|\partial^k (f_\ell^{[4]} - \breve{f}_\ell^{[4]})\|_\infty \preccurlyeq 2^{-(2-k)\ell}.$$

Proof. The first two estimates follow from the approximation properties of quasi interpolants of the respective orders, $\nu \in \{2, 4\}$. The triangle inequality yields $2^{-(2-k)\ell} \succcurlyeq \|\partial^k (f - f_\ell^{[4]})\|_\infty + \|\partial^k (f - \breve{f}_\ell^{[4]})\|_\infty \succcurlyeq \|\partial^k (f_\ell^{[4]} - \breve{f}_\ell^{[4]})\|_\infty$, i.e. the third claim of the corollary. □

2.8 The bundle-paradigm in the bi-variate tensor scenario

We can view bundles under any of the two internal, logical structures[8]

matrix structure: the bundle is interpreted as a 4×4 matrix, or

vector structure: the bundle is considered a column vector. Its 16 elements are given by reading the 4×4 matrix either along the rows, or the columns.

For the first option, we can transfer Equation (2.17) directly to the tensor setting. Table 2.7 describes binary subdivision for the bivariate A_n-bases.

[8]We mean the internal logical structure of the control bundles, i.e. each of its 4×4 entries is considered a single entity. For 3D-surfaces, these entities are given by points in three-dimensional Euclidean space.

$i \setminus j$	**odd**	**even**
odd	$\sum_{\substack{k\in\{\pm1\}\\ l\in\{\pm1\}}} S_{-k} p_{\frac{i+k}{2},\frac{j+l}{2}} S^T_{-l}$	$\sum_{\substack{k\in\{\pm1\}\\ l\in\{-2,0,2\}}} S_{-k} p_{\frac{i+k}{2},\frac{j+l}{2}} S^T_{-l}$
even	$\sum_{\substack{k\in\{-2,0,2\}\\ l\in\{\pm1\}}} S_{-k} p_{\frac{i+k}{2},\frac{j+l}{2}} S^T_{-l}$	$\sum_{\substack{k\in\{-2,0,2\}\\ l\in\{-2,0,2\}}} S_{-k} p_{\frac{i+k}{2},\frac{j+l}{2}} S^T_{-l}$

Table 2.7: Rules to calculate new control bundles $\widetilde{p}_{i,j}$ for bi-variate, tensor product A_7/A_8-splines. $[S_{-2}; S_{-1}; S_0; S_1; S_2]$ are the blocks of the binary-subdivision matrices $S = S^{(n)}$ given in Table 2.3 on page 45. A matrix-like internal, logical structure of control bundles $p_{i,j}, \widetilde{p}_{i,j}$ is presupposed here.

Keeping to the internal matrix structure—ideally suited for working with tensor-product splines—the subdivision rules can be derived quite easily. However, notice that we need *two* matrix multiplications to calculate subdivided bundles, even though the latter ones are still produced linearly from coarse bundles. So, what is the matrix essentially describing $X \mapsto LXR^T$?

Matrix notation for $X \mapsto LXR^T$

Two-dimensional indices of $m \times m$ matrices are usually transformed into one dimensional ones by either of two ways:

$$\widehat{\varphi}(i,j) := \begin{cases} im + j, & \text{if reading rowwise,} \\ i + jm, & \text{if reading columnwise.} \end{cases}$$

Presupposing $\mathrm{mod}(a + bm, m) = a$, $a \in \{0, \ldots, m-1\}, b \in \mathbb{Z}$, the inverse function is

$$\varphi(\widehat{i}) := \begin{cases} (\left\lfloor \frac{\widehat{i}}{m} \right\rfloor, \mathrm{mod}(\widehat{i}, m)), & \text{if reading rowwise,} \\ (\mathrm{mod}(\widehat{i}, m), \left\lfloor \frac{\widehat{i}}{m} \right\rfloor), & \text{if reading columnwise.} \end{cases}$$

For the current situation,

$$m := \begin{cases} 4, & \text{if } n = 7, \\ 5, & \text{if } n = 8, \end{cases} \qquad = n - 3$$

is the number of functions per univariate bundle at spline order n.

To given $L, X, R \in \mathbb{R}^{m\times m}$ we are searching for the $m^2 \times m^2$ matrix M such that $(LXR^T)_{i,j}$ and

$$\left(M \begin{bmatrix} X_{\psi(0)} \\ \vdots \\ X_{\psi(m^2-1)} \end{bmatrix} \right)_{\varphi(i,j)}$$

are identical for all $i, j \in \{0, \ldots, m-1\}$. We start with

$$(LXR^T)_{i,j} = \sum_{k,l=0}^{m-1} L_{i,k} X_{k,l} R_{j,l}.$$

Transforming indices by

$$(i, j) = \varphi(\widehat{i}), \quad (k, l) = \varphi(\widehat{j})$$

yields

$$(LXR)_{i,j} = \sum_{\widehat{j}=0}^{m^2-1} L_{\varphi_1(\widehat{i}),\varphi_1(\widehat{j})} X_{\varphi(\widehat{j})} R_{\varphi_2(\widehat{i}),\varphi_2(\widehat{j})},$$

and so

$$M_{\widehat{i},\widehat{j}} = L_{\varphi_1(\widehat{i}),\varphi_1(\widehat{j})} R_{\varphi_2(\widehat{i}),\varphi_2(\widehat{j})}, \quad \widehat{i}, \widehat{j} \in \{0, \ldots, m^2 - 1\}. \tag{2.24}$$

A last word concerning bundles

With equation (2.24), binary subdivision can be done with a single matrix multiplication. Thus, involved bundles are combined linearly by $(m^2 \times m^2)$ matrices. This is simply a generalization of the scenario of bundle size $m = 1$, where control-points are linear-combined with scalar weights.

2.9 How the non-cubic part of a spline comes into play—outlook

Let us denote the subdivision level ℓ by a second subscript. The decomposition of $\mathcal{S}_{7,\ell}$ enters stage in the following situation only:

1. The user begins by defining control points that lie in $\mathcal{S}_{4,0}$. She can directly add and modify cubic splines only.

2. Suppose some extraordinary point is created in the mesh. All cardinal cubic splines on $\mathbf{S}_n^0$ are automatically supplemented by details on $\frac{1}{2}\mathbf{S}_n$ for C^2 continuity of the surface. *Details are tiny* when compared to the cardinal cubic splines, to which they are coupled—the shape of the surface is determined by the latter ones.

3. The mesh is subdivided $\ell \geq 1$ times towards the extraordinary point. By "convergence" above, in the new, finer spline space $\mathcal{S}_{4,\ell}$, part of the details "flow" into the cubic subspace.

The cubic mesh we are being offered at this point depends on the nature of the decomposition used for $\mathcal{S}_{7,\ell}$. A palpable example may be found in Figure 2.26 on page 69.

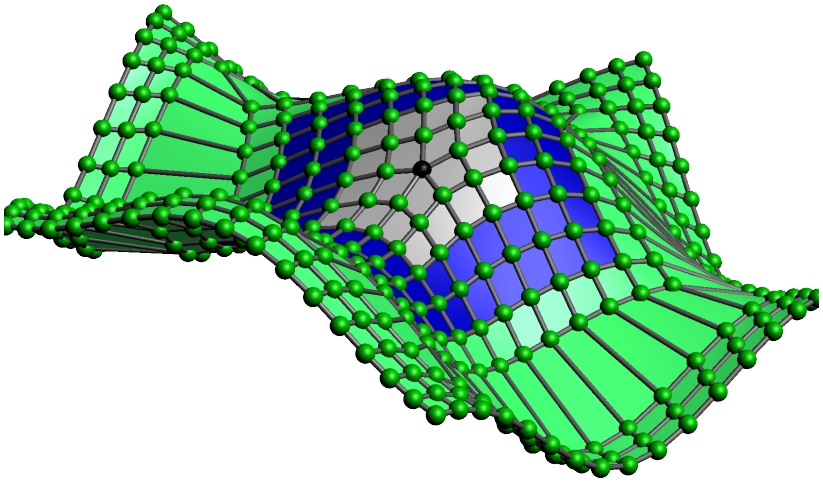

(a) Level 0.

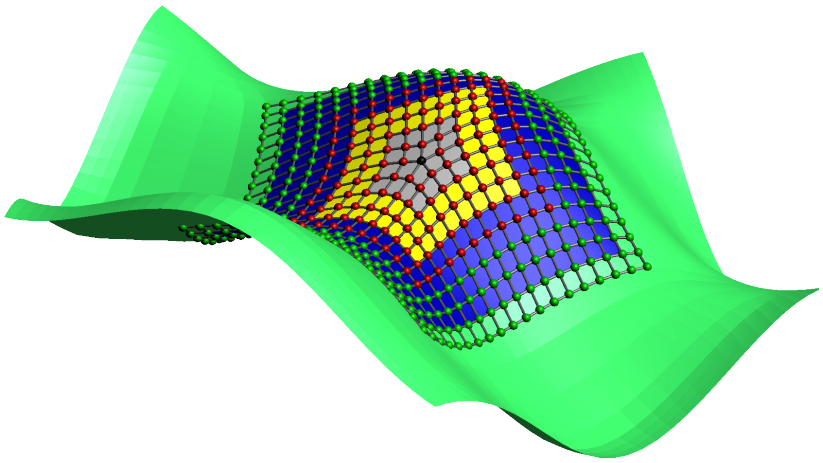

(b) Level 1.

Figure 2.26: The Figure illustrates how higher-order splines enter a subdivision surface. At level zero, the subdivision surface is a purely cubic spline (Subfigure 2.26a). From level one onwards, it exhibits spline rings of order seven ❖ around extraordinary points ●.
Control points: "normal", cardinal cubic B-splines are ●. Conversely, ● are control bundles that contain C^2 information. Only their cubic part is displayed, so the mesh is indistinguishable from a purely cubic one. The black central point ● of the mesh is, strictly speaking, not a control point, as no generating function is affixed to it (allthough one could do that). We have simply set it to the value of the surface at the central point here, thus closing the mesh while simultaneously providing additional information.
Control polygons: in the regular region ❖, cardinal, cubic B-splines are used. The first spline ring surrounding the extraordinary point is marked blue ❖. It is still cubic, however. All successive spline rings are of order seven, ❖. Finally, ❖ indicates rings of the underlying *surface* that are not yet defined at the respective refinement level (note the distinction from control polygon).

Chapter 3

The Characteristic Map

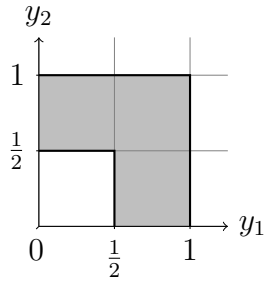

Figure 3.1: Single segment of the domain $\mathbf{S}_n^0$.

The characteristic map can be considered as central to any subdivision scheme at extraordinary points. This is why in this chapter we make it our (near-)exclusive topic. Before we address it, however, we introduce terms and notations for extraordinary points, and also efficient techniques to model them in a computer program.

3.1 Setup for non-regular points

In this section, we introduce the basic terms that are needed for the discussion of extraordinary points in all the following chapters.

With $\mathbb{Z}_n := \mathbb{Z}/(n\mathbb{Z})$, define the domain

$$\mathbf{S}_n := [0,1]^2 \times \mathbb{Z}_n.$$

$\mathbf{S}_n$ is partitioned into the nested rings

$$\mathbf{S}_n^m := 2^{-m}\left([0,1]^2 \setminus [0,\frac{1}{2})^2\right) \times \mathbb{Z}_n, \quad m \in \mathbb{N},$$

(refer Figure 3.1 on page 72).

We relate by an additional subscript j the *closure of segment* $j \in \mathbb{Z}_n$ *of ring* m,

$$\mathbf{S}_{n,j}^m := \{(u,v,k) \in \mathbf{S}_n^0 : \ k = j\}.$$

Because each segment visually resembles a (rotated) capital letter "L", this setting–as opposed to the polar setting that we will briefly present in 3.2 and 3.3–is sometimes referred to as the setting of "L-domains".

Further, let any $\tau \geq 0$ act on the u, v- components of triples $(u, v, j) \in \mathbf{S}_n$ only,

$$(u, v, j)\tau := (\tau u, \tau v, j),$$

i.e. τ does not act on the part that stems from $\mathbb{Z}_n$. We denote by $\varrho \colon \mathbf{S}_n \to \mathbb{N} \cup \{\infty\}$,

$$\varrho(t) := \begin{cases} \infty & \text{if } t = 0, \\ m & \text{if } t \in \mathbf{S}_n^m \setminus \mathbf{S}_n^{m+1}, \end{cases}$$

the *ringindex* of $t \in \mathbf{S}_n$.

The *generating splines* $B = [b_0, \ldots, b_{\bar{k}}] \in C^1(\mathbf{S}_n, \mathbb{R}^{1\times(\bar{k}+1)})$ define a *spline* $\mathbf{x} := B\mathbf{Q}$ for any matrix $\mathbf{Q} := [\mathbf{q}_0; \ldots; \mathbf{q}_{\bar{k}}]$ of *control points* $\mathbf{q}_k \in \mathbb{R}^{1\times d}$ (which are row vectors). Alternatively, we will also refer to the $\mathbf{q}_k$ as *initial* or *input coefficients*.

For $m = 0, 1, 2, \ldots$ the (spline) *ring*

$$\mathbf{x}^m = x(2^{-m}\cdot)_{|\mathbf{S}_n^0}$$

is the restriction of the whole spline to $\mathbf{S}_n^m$ and replacing this domain subsequently by $\mathbf{S}_n^0$. $\mathbf{x}$ can then be regarded as the union of the *central point* $\mathbf{x}(0)$ and a nested sequence of annuli formed by these rings,

$$\mathbf{x}(\mathbf{S}_n) = \mathbf{x}(0) \cup \bigcup_{m\in\mathbb{N}} \mathbf{x}^m(\mathbf{S}_n^0).$$

Analogously to $\mathbf{x}^m$, (spline-) *rings* are denoted by a single supscript

$$b_j^m := b_j(2^{-m}\cdot)_{|\mathbf{S}_n^0}, \quad B^m := [b_0^m, \ldots, b_{\bar{k}}^m]. \tag{3.1}$$

We examine *stationary* subdivision schemes, that is

$$B^m = B^0 A^m, \tag{3.2}$$

where A is a real, square matrix.

Let the Jordan decomposition of A be VJV^{-1} for $V = [v_0, \ldots, v_{\bar{k}}]$. Let $|\lambda_0| \geq |\lambda_1| \geq \ldots \geq |\lambda_{\bar{k}}|$ be its eigenvalues, counted by multiplicity and sorted by modulus. $E := [e_0, \ldots, e_{\bar{k}}] := BV$ are called *eigensplines.* Let

$$\mathbf{P} := V^{-1}\mathbf{Q} =: [\mathbf{p}_0; \ldots; \mathbf{p}_{\bar{k}}] \in \mathbb{C}^{(\bar{k}+1)\times d}$$

be the representation of the initial coefficients $\mathbf{Q}$ in the eigen basis $v_0, \ldots, v_{\bar{k}}$. We will call $\mathbf{p}_k$ *eigen-coefficients*, respectively $\mathbf{P}$ *(vector of) eigen-coefficients*. For real eigenvalues corresponding eigenvectors of the subdivision matrix can be chosen real. We will henceforth assume they are such ones.

Further, we presuppose that

1. (A, B^0) is a *standard subdivision algorithm*, as per Definition 5.3 in [50]. In particular, this guarantees that

   a) A is free of ineffective eigenvectors. An *eigenvector* v of A to some eigenvalue $\kappa \neq 0$ *is called ineffective*[1] if $B^0 v = 0$.

2. The subdivision algorithm (A, B^0) is both normal continuous and single-sheeted, according to Definition 3.11 in [50].

3. The eigenvalues $\lambda_0, \lambda_1, \lambda_3$ have full geometric multiplicity[2] with

$$1 = \lambda_0 \ > \ \lambda := \lambda_1 = \lambda_2 \ > \ \mu := \lambda_3 = \ldots = \lambda_{2+\sharp\mu} \ > \ |\lambda_{3+\sharp\mu}|\,,$$
$$v_0 = [1;\ \ldots; 1]\,,$$

4. In three dimensions, we assume that the eigen-coefficients $\mathbf{P}$ are *generic*, that is

$$\det[\mathbf{p}_1; \mathbf{p}_2; \sum_{k=3}^{2+\sharp\mu} \mathbf{p}_k] \neq 0$$

   ($\sharp\mu$ denotes the multiplicity of the eigenvalue).

5. The *characteristic map*

$$\chi := B\,[v_1, v_2] : \mathbf{S}_n \to \mathbb{R}^{1\times 2}$$

   is injective with $\det D\chi^0 > 0$ (Jacobian determinant).[3]

[1] The notion of ineffective eigenvectors was first introduced 1999, [59]. The definition in [50] is identical, however, and we recommend the latter source for a detailed study of ineffective eigenvectors.

[2] A standard subdivision algorithm does not require full geometric multiplicity for the subsubdominant eigenvalue μ. It should be possible to prove all of the subsequent theorems under these slightly weaker conditions. However, discussing this general but inevitably far more sophisticated case makes the plot of the argumentation less clear while adding nothing significant to the theory.

[3] As noted above, for real eigenvalues corresponding eigenvectors of the subdivision matrix can be chosen real, and we assume they are such ones. Thus, χ is a mapping from $\mathbf{S}_n$ to $\mathbb{R}^2$.

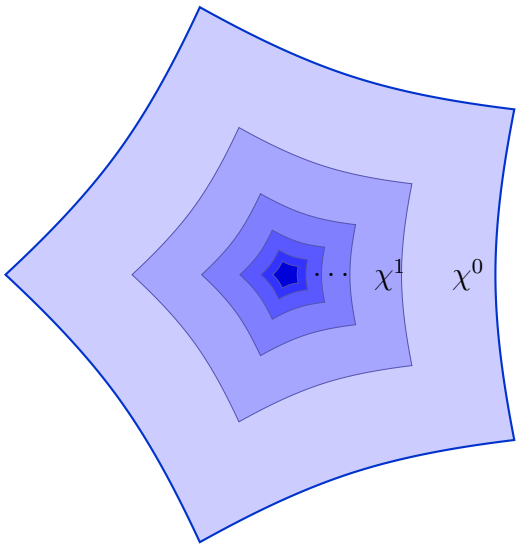

Figure 3.2: The image of the *characteristic map* χ of the Catmull-Clark algorithm. Shadings indicate the images of successive *rings* χ^m, $m = 0, 1, 2 \ldots$.

6. The subdivision algorithm (A, B^0) is symmetric, i.e. both shift- and flip-invariant (refer to [50, Def. 5.13 and Def. 5.21]).

3.2 Tools for the study of non-regular points

In this section we outline techniques for programs and data structures that a practical study of subdivision schemes must incorporate. The implementation needs to accommodate two conflicting goals:

1. **Easy-to-apply mathematical operations:** calculating spline values and derivatives, or inserting knots should be as easy as in the regular case. `irP` and `PolarRing`'s *redundant representation* has been designed for this. Typically, we perform per-segment access to all relevant control points.

2. **Easy to compute with:** applying subdivision matrices to control points, determining operators that yield derivatives at various lists of

points or even calculating the quadratic form on a spline ring essentially requires the control points $\mathbf{q}_0, \ldots, \mathbf{q}_{\bar{k}} \in \mathbb{R}^{1\times d}$ to be stored in a vector

$$\mathbf{Q} = \begin{bmatrix} \mathbf{q}_0 \\ \vdots \\ \mathbf{q}_{\bar{k}} \end{bmatrix} \tag{3.3}$$

in order to be practical. Characteristic here is an one-to-one correspondence between control points and rows of $\mathbf{Q}$. `irP` and `PolarRing` refer to it as *vector representation*.

Object oriented programming (OOP) is of particular advantage as both data structures and the program code that is to handle the data are encapsulated within a single entity.

The redundant representation is the internal format of the classes `irP` and `PolarRing`. Both exhibit a method `VecRep`, which allows exporting to, as well as importing back from, vector representation (3.3). Further, they are based on tensor-product B-Splines (short TPB) of arbitrary degrees and knot vectors. We designed the routines to be inherently symmetric in handling knots and degrees, and to preserve that property. There seems little value in the construction of non-symmetric subdivision schemes.

The OOP-class `irP`

The fundamental, low-level procedure to create `irP` objects is

```
P = irP(0, Order, Tge0, [s1 s2], valency, CPdim);
```

The first parameter—`0`, here—specifies the subfunction to be accessed. Most functions consolidate a lot of subfunctions, as well as slightly varied "sub" versions, which are all centered around a specific theme. In this case, the class-constructor `irP` creates new objects of its type. The remaining parameters passed to it are

Order: the spline order around the extraordinary point. For L-domains, both tensor directions have to be of the same order (in contrast to the polar setting).

Tge0: vector of knots greater than or equal zero for both variables. Knots less than zero are added automatically since they are implicit for symmetric schemes. The complete knot-vector together with `[s1 s2]` is indispensable to most methods.

[s1,s2]: Domain of the spline ring. The analysis uses $[\frac{1}{2}, 1]$ exclusively for spline rings. To avoid rounding errors and for better facility of inspection, we preferred integer-valued knots and `s1,s2` in the implementation. Additionally, the class can accommodate proxies[4] of subdivision surfaces, too, which necessitate other ratios than $1:2$.

valency: Valency of the extraordinary point and the number of segments stored within `P`.

CPdim: The dimension of the control points which are initialized to zeros.

The returned object `P` has a property `CP`, which is a two-dimensional cell-array. In MATLAB, cell arrays are indexed by curled braces { }. Element `{j,d}` of `P` stores the control mesh of segment j and coordinate d. We can store sparse matrices when calculating discrete versions of operators.
Let us consider a simple case.

Example 3.1 (`irP` object for the Catmull-Clark scheme)**.** To create an `irP` object for the Catmull-Clark scheme with integer valued knots, we use `Order`$= 4$, `Tge0`$= (0, 1, \ldots, 5)$, `[s1 s2]`$= (1, 2)$.

On the other hand, aiming for a C^2 scheme to the subdominant eigenvalue $1/2$, we might proceed via

Example 3.2 (Cardinal cubic characteristic ring to $\lambda = 1/2$ and accompanying spline ring of degree six)**.** We need 3×4 polynomial pieces to construct a characteristic ring based on cubic, cardinal TPB with $\lambda = 1/2$, cf. Figure 3.3 on page 78. In order to create the `irP` object for χ^0, we use $(s_1, s_2) :=$`[s1 s2]`$= (2, 4)$ and

$$\texttt{Order} = 4, \quad \texttt{Tge0} = (0, 1, 2, \ldots, 7).$$

[4] *Proxies* (at extraordinary points) are a generalization of control polyhedrons and are our main topic in Chapter 5.

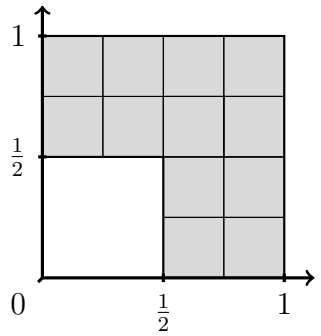

Figure 3.3: Layout of polynomial pieces we use for our characteristic map to $\lambda = 1/2$.

For the spline ring,

$$\texttt{Order} = 7, \quad \texttt{Tge0} = (0x4, 1x4 \ldots, 4x4, 5x3)$$

proves suitable.

It can be tricky to handle all polynomial orders and knot multiplicities at once. We will briefly describe the central idea.

A generally valid vector representation

We assign each segment its own, local coordinate system $x^{(j)}, y^{(j)}$. Then there is only one way by which consecutive segments can be connected such that the generator functions are C^1 – the one that is shown in Figure 3.4 on page 79. Coordinates in directly neighboring systems can be converted either way by

$$(x^{(j)}, y^{(j)}) = (-y^{(j+1)}, x^{(j+1)}), \quad j \in \mathbb{Z}_n. \tag{3.4}$$

Let us consider the tensor product spline at (regular) valency four of Example 3.2. Figure 3.5a on page 80 shows the control points by their Greville abscissae over the rectangular domain $[-s_2, +s_2]$. In the figure, axes are labelled by the respective knot vector that goes along it—S_j for the $x^{(j)}$-axis, T_j the $y^{(j)}$-one. The coordinates of its Greville abscissae allow to assign each generator function a unique segment number. A generator function is assigned to segment j if and only if both

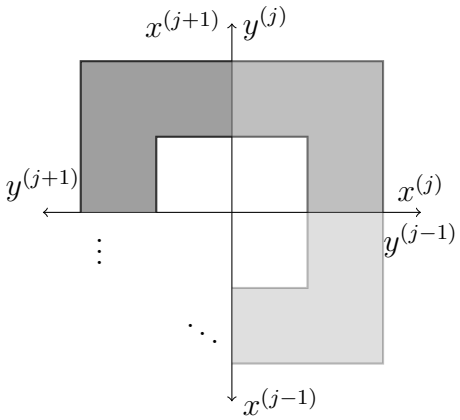

Figure 3.4: Connection of segment j with segments $j-1$ and $j+1$. The segment to which the respective axis belongs is noted as a superscript.

1. the $x^{(j)}$-component of its Greville abscissa is non-negative (≥ 0), and

2. its $y^{(j)}$-component is strictly positive (> 0)

(see Figure 3.5b).

We can easily determine from the order and knot vectors which B-splines' support extends to a current segment's "L". Combining both criteria provides the control points of a particular segment of the spline *ring* (Figure 3.5d).

The redundant representation

Conversely, the redundant representation saves a complete, square-matrix-like block of control points (corresponding to the regular valency) for every segment (as in Figure 3.5a). Unless the valency is three, the lower left quadrant's control points have no meaning–it simply is easier to work with a matrix-like structure of the mesh.

Evaluation, integration (used in constructing χ^0) and knot insertion, for instance to increase the refinement level, are directly inherited from the regular valency.

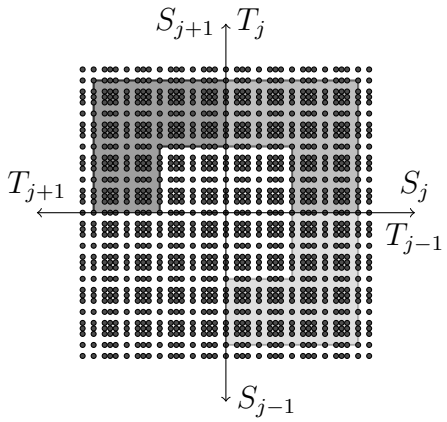

(a) Redundant representation.

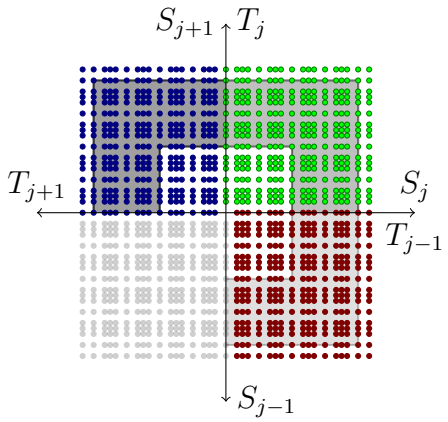

(b) Assigning segments to control points.

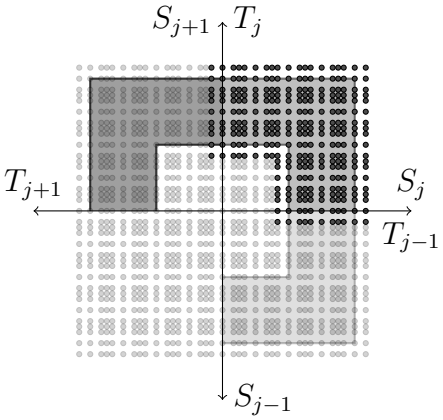

(c) B-splines with support on segment j's "L".

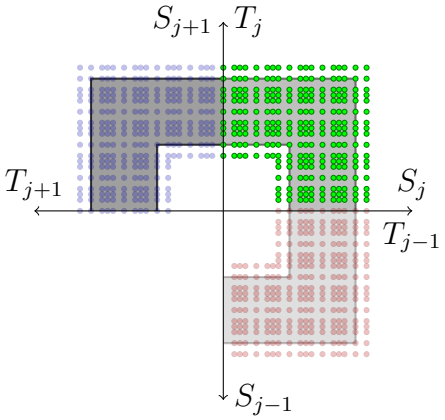

(d) Control points of segment zero.

Figure 3.5: *3.5a)* the regular valency is basis for `irP's` redundant representation. *Subfigures 3.5b-3.5c)* assigning segment numbers and identifying which B-splines are indeed generator functions of the spline ring. *3.5d)* intersecting both masks produces the control points of segment j of the spline ring.

Changing between both representations

It should be clear how to export to vector representation. To re-import into the redundant representation, we chose this three step strategy:

1. Read in exactly those control points into segment j which would have been stored in the vector-representation when exporting.

2. Equation (3.4) describes how to transfer coordinates between adjacent segments. Get from the two neighboring segments $j \pm 1$ those control points that have already been assigned there, but have not been assigned to the current segment in previous steps .

3. Repeat step two once.

Of course, the process in step two is always the same in every segment.

The OOP-class `PolarRing`

Unlike the quite challenging situation for L-domains, implementing an efficient class structure for the polar TPB setting can be done in a very short time. We are assuming here that there are routines available which provide basic functionality for univariate splines:

1. evaluation

2. differentiation

3. insertion of knots

Contrary to L-domains, the polar setting allows the redundant representation to encompass all segments' control points within a single matrix, for each dimension of the control points. The example in Subsection 3.3 should make this obvious.

3.3 How to construct χ

When designing subdivision algorithms, the characteristic map is an important part. Usually, we want it to be as "close" to an affine-linear mapping as possible. In this section we present a route that one can take here. It

could easily be adapted to non-symmetric schemes; however, since symmetry is preferred in practice exclusively, there seems little point in discussing non-symmetric schemes here.

Again, for a thorough introduction to symmetric schemes we refer the reader to [50]. For these schemes, the control points $\mathbf{Q}$ can be partitioned into blocks $\mathbf{Q}_k$, i.e. $\mathbf{Q} = [\mathbf{Q}_0; \ldots; \mathbf{Q}_{n-1}]$, n the valency of the irregular point. The control points of the characteristic map are points in the Euclidean plane. Its blocks must be related by

$$\mathbf{Q}_k = R^k(\mathbf{Q}_0), \tag{3.5}$$

where R^k rotates each 2-dimensional row-vector of a matrix counterclockwise by $2\pi k/n$. Only the control points of a single block remain free variables.

Schemes on L-domains

Let T be a linear differential operator on functions $f : [0,1]^2 \setminus [0, \frac{1}{2})^2 \to \mathbb{R}$. Recall that $\mathbf{S}^0_{n,j}$ denotes the *closure of segment* $j \in \mathbb{Z}_n$ of[5] $\mathbf{S}^0_n$.

We define $\chi^0 = [\chi^0_1, \chi^0_2]$ by the constrained quadratic optimization

$$\sum_{j\in\mathbb{Z}_n} \sum_{d=1}^{2} \int_{[0,1]^2\setminus[0,\frac{1}{2})^2} \left(T\chi^0_d(\cdot,\cdot,j)\right)^2 \mathrm{d}S \to \min, \tag{3.6}$$

subject to (3.5) and

$$\begin{aligned} \chi(1,1,0) &= (1,0), \\ (\partial_1^{k_1}\partial_2^{k_2}\chi)(2^{-1}s) &= \lambda 2^{k_1+k_2}(\partial_1^{k_1}\partial_2^{k_2}\chi)(s), \quad s \in \partial\mathbf{S}_n,\ k_1,k_2 = 0,\ldots,\overline{k}. \end{aligned} \tag{3.7}$$

$\overline{k}$ is the degree of smoothness that we want the scheme to have at non-extraordinary points[6]. The first condition, $\chi(1,1,0) = (1,0)$, fixes rotation and scaling so that our characteristic map will be a normalized one. Regarding the second equation: presupposing $\chi(2^{-1}\cdot) = \lambda\chi$ and $t \in 2^{-1}\mathbf{S}_n$ we

[5] In a more general context, one wants the term "segment index" to be well-defined. This means that the intersection of two segments must be empty.

[6] Note that the total degree $k_1 + k_2 \le \overline{k}$ would actually be enough for this. However, when the generator functions are tensor products (as it is in our case) it is more convenient to demand $C^{\overline{k}}$-smoothness independently in every variable.

have

$$\begin{aligned}\partial_1^{k_1}\partial_2^{k_2}\chi(t) &= \partial_1^{k_1}\partial_2^{k_2}\lambda\chi(2t)\\ &= \lambda 2^{k_1+k_2}\left(\partial_1^{k_1}\partial_2^{k_2}\chi\right)(2t).\end{aligned}$$

With $s = 2t$ this is equivalent to (3.7).

Only the integral over one segment needs to be calculated

Let us momentarily relate the control point of sub-index k of segment j by $\mathbf{q}_{j,k}$, and its dimension $d \in \{1, 2\}$ by $\mathbf{q}_{j,k,d}$. Further, $b_{j,k}$ be the generator function attached to $\mathbf{q}_{j,k}$. Since the generating system B is shift-symmetric, we have

$$b_{i,k}(\cdot,\cdot,j) = b_{i-j,k}(\cdot,\cdot,0)$$

and therefore $Tb_{i,k}(\cdot,\cdot,j) = Tb_{i-j,k}(\cdot,\cdot,0)$. Further, (3.5) ensures that $\mathbf{q}_{j,k} = R^j(\mathbf{q}_{0,k})$, and so

$$\sum_{d=1}^{2}(T\chi_d^0(\cdot,\cdot,j))^2 = \sum_{d=1}^{2}(T\chi_d^0(\cdot,\cdot,0))^2.$$

Hence, the integrals

$$\sum_{d=1}^{2}\int_{[0,1]^2\setminus[0,\frac{1}{2})^2}\left(T\chi_d^0(\cdot,\cdot,j)\right)^2\mathrm{d}S$$

in our ansatz are the same for all $j \in \mathbb{Z}_n$.

Flip-invariance

Let $\rho(x, y) := (y, x)$ be the reflection on the line $\mathbb{R}(1, 1)$ (swapping x and y). It is sensefull to require of T that

$$(Tf)^2 = (T(f \circ \rho))^2 \tag{3.8}$$

holds for all $f : \mathbb{R}^2 \to \mathbb{R}$, because this ensures flip-invariance of χ, for an uniquely determined solution.

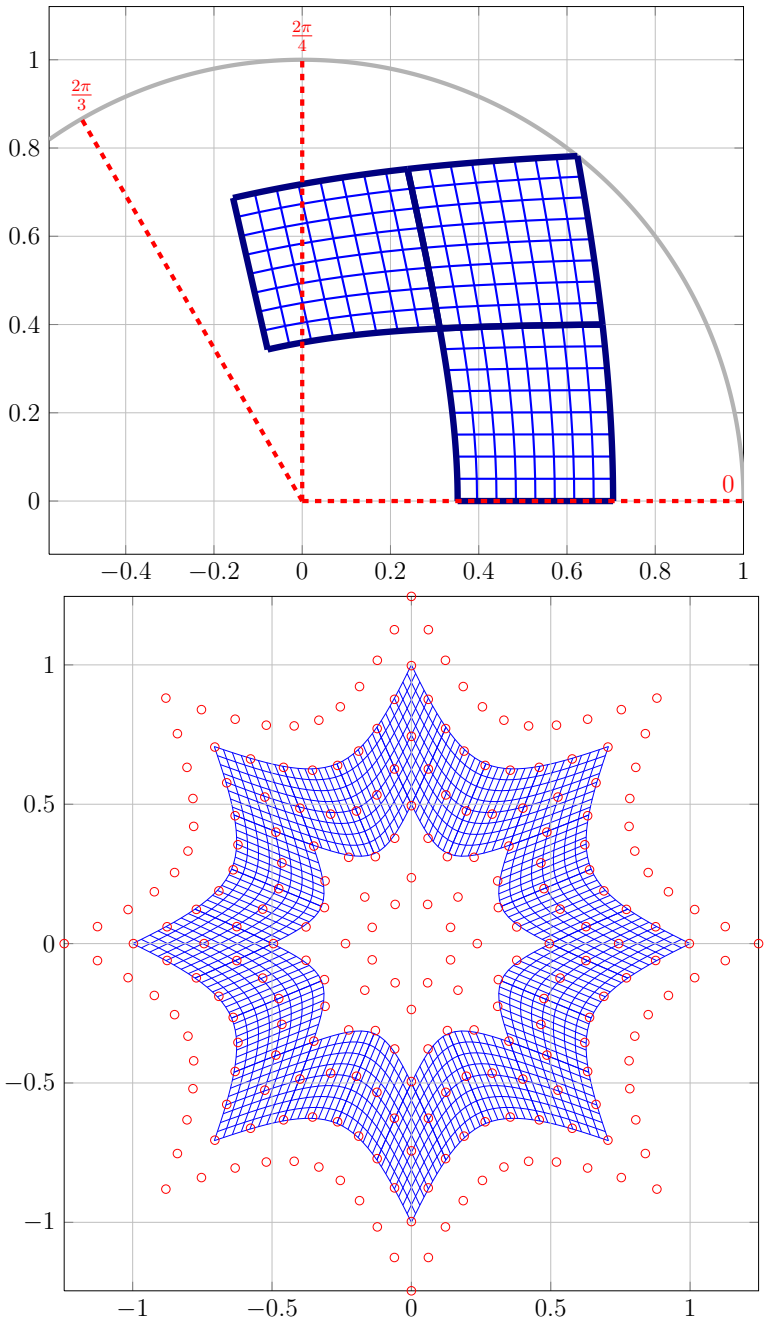

Figure 3.6: *Top*: the characteristic map we have computed symbolically in this section depends continuously on the valency n, as this figure illustrates for $n = 3.5$. *Bottom*: of course, only for integer valencies $n \in \mathbb{N}^{\geq 2}$ can we connect the remaining, suitably rotated $n - 1$ segments without self-intersections. The lower figure shows the result for $n = 8$.

Minimization within the finite function space

Naturally, χ has to be contained in the finite function space that is generated by the rings $b_0^0, \ldots, b_k^0$ we have introduced in Section 3.1.

We put the associated x- and y- control points into a single vector

$$\tilde{\mathbf{Q}} = [\mathbf{x}_0; \mathbf{y}_0].$$

This is very sensible, because the next step will be solving the minimization problem over $\tilde{\mathbf{Q}}$. Correspondingly, we gather $\tilde{B}^0 := [B^0, B^0]$.

In this finite scenario, the Gramnian G of the system reduced by rotation-invariance is given by

$$G_{i,j} := \int_{[0,1]^2 \setminus [0,\frac{1}{2})^2} \left(T\tilde{B}^0(u,v,0)\tilde{R}_n e_i\right)\left(T\tilde{B}^0(u,v,0)\tilde{R}_n e_j\right) \mathrm{d}(u,v).$$

The row-vectors $e_1, \ldots, e_{\#\mathrm{rows}(\tilde{\mathbf{Q}})}$ are the standard basis in whose span $\tilde{\mathbf{Q}}$ lies. i and j both go from 1 to the number of rows in $\tilde{\mathbf{Q}}$. Finally, $\tilde{R}_n$ denotes the rotation by $2\pi/n$, transferred to this notation.

This leads to the minimization problem

$$\tilde{\mathbf{Q}}^T G \tilde{\mathbf{Q}} \to \min \quad \text{s.t. } C\tilde{\mathbf{Q}} = 0, \tag{3.9}$$

where the constraints C directly derive from (3.5) and (3.7).

We refrain from an – by necessity – overly detailed description on how to calculate the Gramnian G, and the constraints C, of the reduced system. The particular steps are simply not very interesting.

Problem (3.9) can be solved with Lagrangian multipliers Λ,

$$\underbrace{\left(\begin{array}{c|c} G + G^T & C^T \\ \hline C & 0 \end{array}\right)}_{H} \left[\begin{array}{c} \tilde{\mathbf{Q}} \\ \Lambda \end{array}\right] = \left[\begin{array}{c} 0 \\ c \end{array}\right].$$

With M given by $MH = \tilde{I}$, $\tilde{I}$ the first (#CP) columns of the identity matrix of same size as H, we can compute $\tilde{\mathbf{Q}}$ without having to calculate the Λ as well by $\tilde{\mathbf{Q}} = M[0; c]$. In MATLAB, M can be computed with $M = \tilde{I}/H$.

Using the Symbolic Toolbox of MATLAB as well as MATHEMATICA proved very convenient here. Using the patch layout we have indicated in Figure 3.3 on page 78 in Section 3.2, we computed a symbolic, generic formula of the control points of the first segment of χ for $\lambda = 1/2$. As the solution is a rational function, it is too large to present here completely. Figure 3.7 on page 86 presents part of it, and gives some more details to its nature. In the digital attachments, B4C2_chi.txt contains the full solution.

```
Out[89]= {{15 120 (-9 247 496 818 917 674 909 210 037 315 552 180 - 7 043 386 899 647 777 976 931 042 633 130 417 c +
        2 064 585 452 347 978 798 358 350 418 455 388 c^2 - 138 702 382 400 834 146 474 532 216 328 107 c^3 +
        827 951 253 133 937 925 782 233 165 640 c^4 + 5 870 021 127 856 048 822 495 673 628 c^5 + 3 289 077 905 569 152 310 146 256 c^6), -15 120
      (-9 247 496 818 917 674 909 210 037 315 552 180 + 2 204 109 919 269 896 932 278 994 682 421 763 c - 139 524 466 921 918 133 920 644 263 966 375 c^2 +
        822 084 521 083 987 446 112 047 638 268 c^3 + 5 866 732 049 950 479 670 185 527 372 c^4 + 3 289 077 905 569 152 310 146 256 c^5) s},
     {-336 (832 274 713 702 590 741 828 903 358 399 696 200 + 759 066 507 571 471 959 691 001 538 522 847 350 c -
        84 657 139 333 823 581 167 343 531 695 175 501 c^2 - 11 407 879 855 407 810 118 048 223 215 642 226 c^3 +
        40 992 351 658 814 564 444 746 266 752 825 c^4 - 60 871 864 030 231 129 160 969 663 076 c^5 + 123 774 144 115 819 581 366 268 524 c^6),
      336 (832 274 713 702 590 741 828 903 358 399 696 200 - 73 208 206 131 118 782 137 901 819 876 848 850 c -
        11 448 933 202 704 799 029 441 711 818 326 651 c^2 + 41 053 347 296 988 911 393 488 602 684 425 c^3 -
        60 995 638 174 346 948 742 335 931 600 c^4 + 123 774 144 115 819 581 366 268 524 c^5) s}}
```

(a) Numerator.

```
Out[90]= 32 (-34 955 537 975 508 811 156 813 941 052 787 240 400 - 16 211 256 457 405 525 723 655 465 763 566 648 520 c +
     3 821 744 297 570 652 106 190 989 816 600 835 848 c^2 - 28 585 704 612 947 784 456 188 183 758 234 777 c^3 +
     38 673 603 451 271 651 622 562 206 773 785 c^4 + 153 912 939 667 982 773 916 056 126 908 c^5 + 17 662 893 530 983 185 723 807 828 c^6)
```

(b) Denominator.

Figure 3.7: Numerator and denominator of the first two control points of the symbolic solution (x- as well as y-coordinates) we computed by minimizing the Laplacian. *Top*: the denominator is a polynomial in both $c = \cos\frac{2\pi}{n}$ and $s = \sin\frac{2\pi}{n}$ and of degree $(6, 1)$. *Bottom*: the joint denominator of all control points is a polynomial of degree 6 in c only.

Polar schemes

Here, no optimization is necessary. The characteristic map can be constructed in a straightforward manner from two univariate functions, the radial and circular components. We proceed as follows:

1. We find any univariate approximation $c(t) = B^{\text{circ}}(t)\mathbf{Q}^{\text{circ}}$ of the unit circle. $\mathbf{Q}^{\text{circ}}$ is a column vector of two-dimensional control points (row vectors). Note that, if the scheme is to have only one polynomial piece per segment circular-wise, the value of the corresponding control point is already determined by symmetry. Conversely, if there is more than one polynomial piece per segment it is possible that there is still some freedom and a particular approximation of the unit circle must be decided on (under the constraint of maintaining reflection symmetry, of course).

2. With $\lambda \in (0, 1)$ the eigenvalue that we want our characteristic map to have, we define $r(s) = B^{\text{rad}}(s)\mathbf{Q}^{\text{rad}}$ to be the polynomial of order two such that

$$r(\frac{1}{2}) = \lambda, \quad r(1) = 1.$$

3. The x- and y-components of the matrix of control points can be obtained by taking tensor products,

$$X = \mathbf{Q}^{\text{rad}} \left(\mathbf{Q}^{\text{circ}}(:,1) \right)^T$$
$$Y = \mathbf{Q}^{\text{rad}} \left(\mathbf{Q}^{\text{circ}}(:,2) \right)^T$$

(MATLAB-notation: $\mathbf{Q}^{\text{circ}}(:,j)$ denotes column j of the matrix $\mathbf{Q}^{\text{circ}}$).

The last step is actually done only to stay within the mesh structure of subdivision surfaces. One can evaluate χ more easily by

$$\chi(s,t) = r(s)\, c(t). \tag{3.10}$$

Let us finish the section with an example:

Example 3.3 (Polar χ from cardinal, cubic splines)**.** Let $\lambda \in (0,1)$ and $n \geq 3$. The knot vectors $T^{\text{circ}}, T^{\text{rad}}$ and control points be defined by

$$\begin{aligned}
T^{\text{circ}} &= \mathbb{Z}_n, \\
\mathbf{Q}^{\text{circ}} &= \begin{bmatrix} \cos(0 \cdot \frac{2\pi}{n}), & \sin(0 \cdot \frac{2\pi}{n}) \\ \vdots & \vdots \\ \cos((n+2) \cdot \frac{2\pi}{n}), & \sin((n+2) \cdot \frac{2\pi}{n}) \end{bmatrix} \\
T^{\text{rad}} &= (-2, \ldots, 5)/2, \quad \mu^{\text{rad}} = (0,1,2,3)^T/2, \\
\mathbf{Q}^{\text{rad}} &= \lambda + 2(\mu^{\text{rad}} - 1/2)(1-\lambda).
\end{aligned}$$

Here, we have chosen each segment to consist of a single polynomial piece in the circular direction. The same holds true in the radial direction. For the circular component the first and last three control points coincide, in order to C^2-connect the ends of the curve. We arrive at

$$X = \begin{bmatrix} 0 \cdot \cos(0 \cdot \frac{2\pi}{n}), & \ldots, & \cos((n+2) \cdot \frac{2\pi}{n}) \\ 1 \cdot \cos(0 \cdot \frac{2\pi}{n}), & \ldots, & \cos((n+2) \cdot \frac{2\pi}{n}) \\ 2 \cdot \cos(0 \cdot \frac{2\pi}{n}), & \ldots, & \cos((n+2) \cdot \frac{2\pi}{n}) \\ 3 \cdot \cos(0 \cdot \frac{2\pi}{n}), & \ldots, & \cos((n+2) \cdot \frac{2\pi}{n}) \end{bmatrix},$$

$$Y = \begin{bmatrix} 0 \cdot \sin(0 \cdot \frac{2\pi}{n}), & \ldots, & \sin((n+2) \cdot \frac{2\pi}{n}) \\ 1 \cdot \sin(0 \cdot \frac{2\pi}{n}), & \ldots, & \sin((n+2) \cdot \frac{2\pi}{n}) \\ 2 \cdot \sin(0 \cdot \frac{2\pi}{n}), & \ldots, & \sin((n+2) \cdot \frac{2\pi}{n}) \\ 3 \cdot \sin(0 \cdot \frac{2\pi}{n}), & \ldots, & \sin((n+2) \cdot \frac{2\pi}{n}) \end{bmatrix},$$

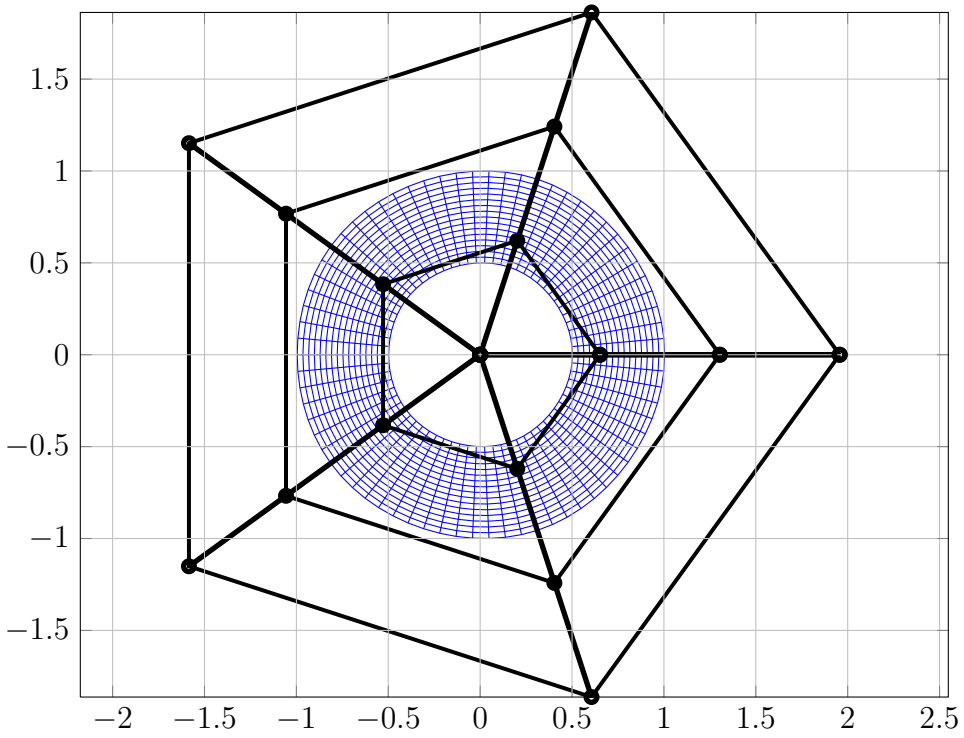

Figure 3.8: Polar characteristic map χ from Example 3.3 with $\lambda = 1/2$. *blue*: parameter lines. *Black, thick:* control net. The innermost control points coincide in the origin if we use cardinal cubic splines in the radial direction.

as x- and y-components of the control net. Note that the radial direction corresponds to going along the rows in X, Y; the circular one along the columns. See Figure 3.8 on page 88 for an illustration.

3.4 How injectivity can be verified for infinitely many valencies

For polar schemes, injectivity of χ can usually be shown by verifying strict monotonicity[7] of the component functions of the characteristic map in polar

[7]Some straightforward tricks can be used but we do not wish to stray here.

coordinates, cf. (3.10). For L-domains, however, the situation is more complex. A useful tool here is

Theorem 3.4. *Let (A, G) be a symmetric standard subdivision algorithm (as wee have generally persupposed in Section 3.1). Further, the Fourier indices of the subdominant eigenvalue shall be exactly $\{-1, +1\}$. We assume the complex characteristic ring χ^0 to be normalized and regular (i.e. $\det D\chi^0 \neq 0$).*

Then (A, G) is a C_1^k-subdivision algorithm if and only if *all real points on the curve*

$$c(u) := \chi(u, 1, 0), \quad u \in [0, 1],$$

are strictly positive:

$$\text{image}\, c \cap \mathbb{R} \subseteq (0, \infty). \tag{3.11}$$

The Fourier indices of a symmetric subdivision matrix are defined via the latter one's discrete Fourier transformation; see Definition 5.15 of [50, p. 100] for a full formal definition.
The theorem and its proof can be found in [50, as Theorem 5.24 p. 105f]. Its prerequisites are usually not so hard to verify, especially when the scheme is a polynomial one. However, one faces the problem of infinitely many valencies $3, 4, 5 \ldots$ here.

For the Catmull-Clark scheme and its generalizations – which all have the same characteristic map – injectivity was first shown in Peters and Reif [48]. However, only valencies up to 10,000 were covered[8]. We present a method to verify injectivity for all valencies, using symbolic calculation. We use the characteristic map from Section 3.3 as an example. Some select lines of MATHEMATICA code are given for a more complete picture.

Prerequisite of the technique

The only prerequisite needed is that we have a parametrized form of the control points of χ. This form typically contain rationals in $c := \cos\frac{2\pi}{n}, s := \sin\frac{2\pi}{n}$, n the valency. We observed that it is preferable to leave the two

[8] In [59], U. Reif argued the remaining cases for that scheme.

parameters c,s in χ untouched; and to merely append $c^2 + s^2 = 1, \cos\frac{2\pi}{3} \leq c \leq 1, s \geq 0$ to the global assumptions. Substituting, for instance,

$$c = \cos(2\pi\tau), \quad s = \sin(2\pi\tau) \tag{3.12}$$

or $s = \sqrt{1 - c^2}$ only increased time and memory needed for subsequent computations, without obtaining substantial benefits.

When the control points stem from an eigen-problem in lieu of the minimization of a quadratic, the parametrized form may include radicals in c, s. Our technique should be implementable just the same then, but might require more computing power to carry through.

Showing that the premises of the theorem are fulfilled

For the characteristic map from Section 3.3, Fourier indices $\{\pm 1\}$ and normalization of χ are a direct consequence of the way we constructed χ. It remains to verify that the Jacobian determinant does not vanish. In contrast to (3.11), this requires by far the most work.

We abbreviate segment zero of the characteristic ring by

$$\psi := \chi^0(\cdot, \cdot, 0) : [0,1]^2 \setminus [0, \frac{1}{2}]^2 \to \mathbb{R}^2.$$

Further, with c, s as in (3.12), we define the local coordinate-system

$$\gamma(\tau) : \begin{bmatrix} 1 \\ 0 \end{bmatrix}, \begin{bmatrix} 0 \\ s \end{bmatrix}. \tag{3.13}$$

We will refer representatives of control points or functions in this system by a superscript $\gamma(\tau)$. Let $\mathbf{P}^{\gamma(\tau)}$ be the control points of $\psi^{\gamma(\tau)}$.

Vital to showing regularity of ψ is that $\mathbf{P}^{\gamma(\tau)}$ converges to a non-degenerate mesh[9] for $\tau \to 0$. Figure 3.9 on page 91 provides an illustration. Due to symmetry, we have to do only the proof for either the upper or lower half of the segment. The Jacobian determinant of bi-orders six can easily be interpolated into a B-spline representation.

After substituting $s = \sqrt{1 - c^2}$ and canceling terms, its control points turn out to be differentiable in $c \in [\cos\frac{2\pi}{3}, 1]$. MATHEMATICA's function

[9] The function $\tau \mapsto \mathbf{P}^{\gamma(\tau)}$, $\tau \in [0, 1/3]$, is typically continuous at all $\tau \in [0, 1/3]$, but in our situation, continuity at zero is sufficient.

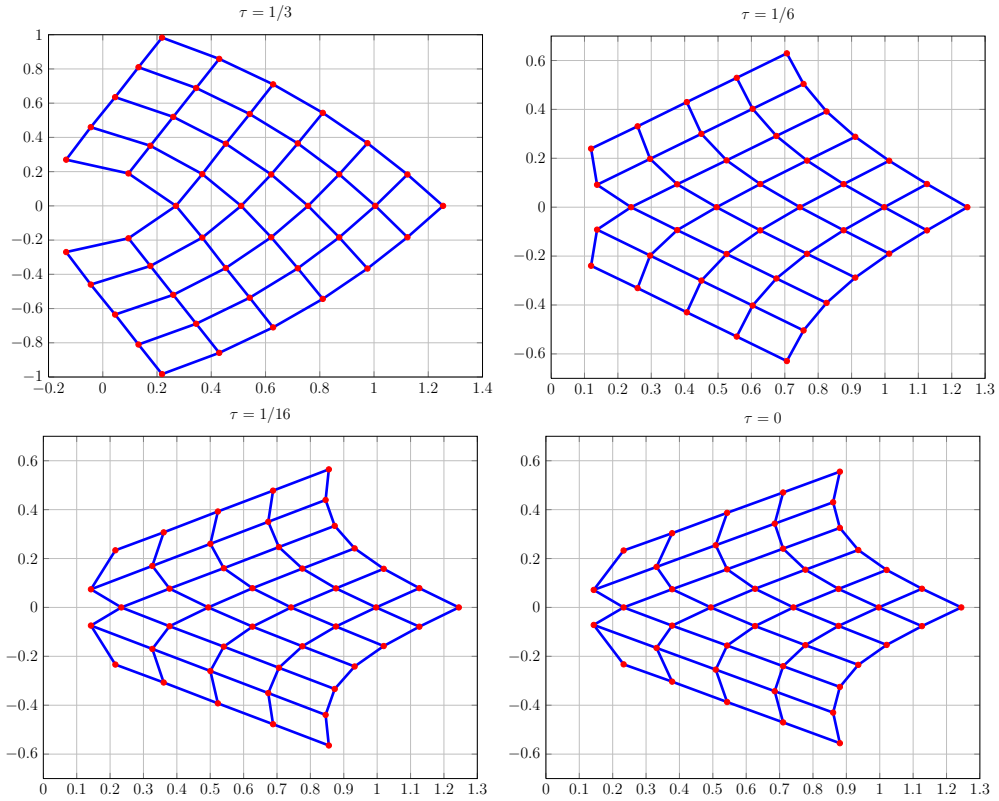

Figure 3.9: The control points of ψ in the local coordinate system $\gamma(\tau)$; $\mathbf{P}^{\gamma(\tau)}$ shown for $\tau \in \{\frac{1}{3}, \frac{1}{6}, \frac{1}{18}, 0\}$ (upper left to lower right). Something similar is obtained for the Catmull-Clark or Doo-Sabin algorithms, although not shown here.

`MinValue` can determine the minimums of the control points symbolically (the nominators and denominators are too large to present here). We easily verify that these minimums are greater than zero:

```
In[400]:= Union[Map[(# > 0 &), Flatten[MinValsJacDetChiCP]]]
Out[400]= {True}
```

The MATHEMATICA-code above checks each control point for positivity, flattening the dimensions of the array and joining the results by the set-operation `Union`, thereby removing duplicates of the value "`True`". Figure 3.10 on page 92 shows the trace of the control points under the parameter c as an additional, visual check.

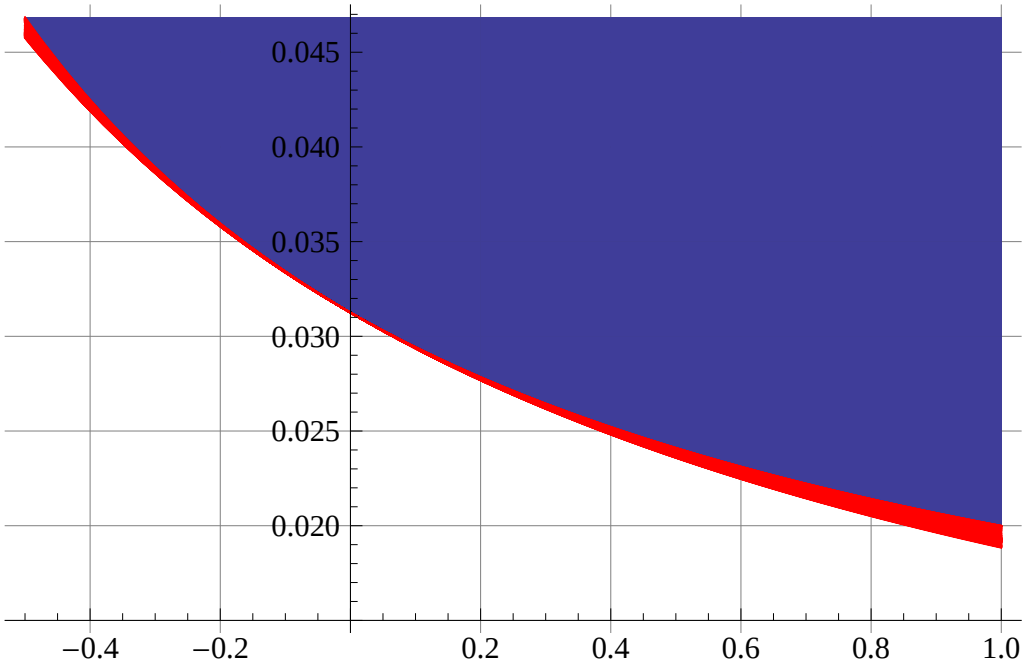

Figure 3.10: The B-Spline control points $\mathbf{P}^{\gamma(\tau(c))}$ (red) of the Jacobian determinant as a function of $c \in [\cos\frac{2\pi}{3}, 1] = [-0.5, 1]$. The plot has been flooded blue from above – we can easily see that the $\mathbf{P}^{\gamma(\tau(c))}$ are bounded away from zero.

Verifying positivity of $\mathbb{R} \cap \operatorname{image} c$

To show that $\mathbb{R} \cap \operatorname{image} c \subseteq (0, \infty)$, we expand block zero's 30 control points to the 7×7 (minus 2×2) mesh which defines the function values on segment 0 (multiplying with c, s where appropriate). We set the 2×2 control points towards the central point to coordinates $(1, 0)$, so they do not get into the way of the verifications. Substituting $s = \sqrt{1 - c^2}, c = \cos\frac{2\pi}{3}$ yields something as presented in Figure 3.11 on page 93, *left*.
For $n \geq 5$, we can directly verify positivity of the x-component of the control points with MATHEMATICA. In our MATHEMATICA notebook, $\chi[[i, j, 1]]$ refers the x-coordinate of control point indexed $(i, j) \in \{1, \ldots, 7\}^2$.

We replace s by $\sqrt{1 - c^2}$. The MATHEMATICA routine `Reduce` simplifies

$$\chi[[i, j, 1]] > 0 \quad \wedge \quad \cos\frac{2\pi}{5} \leq c \leq 1,$$

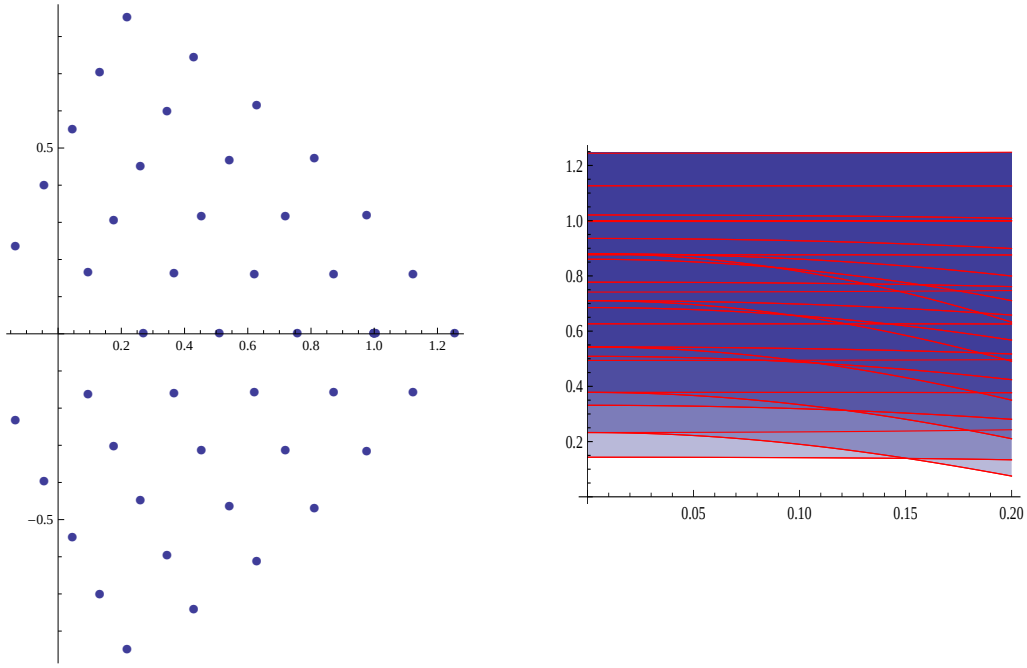

Figure 3.11: *Left:* the control points needed to evaluate χ in segment 0 for valency $n = 3$. *Right:* x-components of χ's control points (red lines) versus fraction $\tau \in [0, \frac{1}{5}]$ of 2π on the abscissa. The second plot has been flooded blue from the top: indeed, all red lines keep away from the abszissa.

finding that the first inequality is implied by the second one. This becomes apparent when we use the set-wise `Union` over all indices (i, j):

```
Clear[chiXposVerified];
chiXposVerified = With[{d = Dimensions[χ[[All, All, 1]]]},
   Table[
    Reduce[(χ[[i, j, 1]] /. s → Sqrt[1 - c^2]) > 0 && Cos[2 π / 5] ≤ c ≤ 1, c],
    {i, d[[1]]}, {j, d[[2]]}]];
```

```
In[164]:= Union[Flatten[chiXposVerified]]
```

$$\text{Out[164]=}\quad \left\{\frac{1}{4}\left(-1+\sqrt{5}\right) \le c \le 1\right\}$$

It is $\cos\frac{2\pi}{5} = \frac{1}{4}(-1+\sqrt{5})$: as can be directly observed, only the inequality $\cos\frac{2\pi}{5} \le c \le 1$ remains.

Figure 3.11 on page 93 (*right*) provides an illustration.

For valencies $n < 5$ we have to subdivide the control points in order to

show that the intersections with $(t, 0)$, $t \geq 0$, have all x-coordinates > 0; we do not present the result of this detail here.

3.5 Topology of the image of χ

Our initial motivation to examine the topological properties of the image of χ was that 0 has to be an interior point of its image. This is something one would clearly expect, and so it seemed moot to include the additional assumption. In pursuing the matter, our purpose expanded to

- provide a solid groundwork for latter proofs, such as for the continuity of χ^{-1},
- show certain properties are implied by minimal indispensable ones and need not be presupposed therefore,
- give a rigorous overview on the topology of the image of χ.

One of our two main tools in this section will be

Theorem (Jordan Curve theorem, JCT)**.** *Let C be a simple closed curve in $\mathbb{R}^2$. Then C separates $\mathbb{R}^2$ into precisely two components W_1 and W_2, exactly one of which is bounded. Each of the sets W_1 and W_2 has C as its boundary; that is, $C = \overline{W}_i$ for $i = 1, 2$.*

A proof can be found in [44]: Theorem 63.4 (JCT for $\mathbb{S}^2$) and Lemma 61.1 (connects theorems on $\mathbb{S}^2$ and $\mathbb{R}^2$); historically, [66] is considered the first rigorous proof, while [38] is an alternative, more modern proof via the Brouwer Fixed Point Theorem.

Let

$$\partial \mathbf{S}_n := \{(x, y, j) \in \mathbf{S}_n : \ \|(x, y)\|_\infty = 1, \ j \in \mathbb{Z}_n\}.$$

Throughout the section, we presuppose

Assumption 3.5. *Let $\psi^0 : \mathbf{S}_n^0 \to \mathbb{R}^2$ be continuous. Further, let*

$$\psi^0(2^{-1}s) = \lambda \psi^0(s), \tag{3.14}$$

for all $s \in \partial \mathbf{S}_n$ and some fixed parameter $\lambda \in (0, 1)$.

Leveraging (3.14), ψ^0 can be extended to all of $\mathbf{S}_n$ by setting

$$\psi(s) := \begin{cases} \lambda^m \psi^0(2^m s), & \text{if } s \in \mathbf{S}_n^m, m \in \mathbb{N}, \\ 0, & \text{if } s = 0. \end{cases} \tag{3.15}$$

Continuity of the extension

While continuity of χ is usually presupposed, it should be pointed out that χ is such automatically, if χ^0 is continuous and χ is derived from the former by (3.15):

Theorem 3.6. *The extension $\psi : \mathbf{S}_n \to \mathbb{R}$ from (3.15) is uniformly continuous.*

By the Jordan Curve Theorem (JCT), any Jordan curve $\gamma : [0,1] \to \mathbb{R}^2$ divides the Euclidean plane into two disjoint, connected components: one that is bounded, and the other unbounded.

For every parameter $r \in (\frac{1}{2}, 1]$, we have a Jordan curve

$$\gamma_r(h) := \psi(rh), \quad h \in \partial \mathbf{S}_n.$$

Denote by I_r the bounded, open[10], connected component that is enclosed by γ_r, thus

$$\operatorname{image} \gamma_r = \partial I_r \neq \emptyset, \quad r > 0. \tag{3.16}$$

Proof of Theorem 3.6. Continuity at $s = 0$: the sets $A_j = \{(x, y, j) : \|(x, y)\|_\infty \in [1/2, 1]\} \subset \mathbf{S}_n$, $j \in \mathbb{Z}_n$ are compact under the induced topology, by continuity of ψ^0, $\operatorname{image} \psi^0 = \bigcup_{j=1}^n \psi^0(A_j)$ is compact. Therefore it is bounded and by

$$\psi(2^{-m} \cdot) = \lambda^m \psi, \quad m \in \mathbb{N}, \tag{3.17}$$

for every $\varepsilon > 0$ there is an $m \in \mathbb{N}$ such that $\|\psi(t)\| \leq \varepsilon$ for all $t \in 2^{-m}\mathbf{S}_n$. But $t = (x, y, j) \in 2^{-m}\mathbf{S}_n \Leftrightarrow \|(x, y)\|_\infty \leq 2^{-m}$, so ψ is continuous at 0 if and only if $\psi(0) = 0$, as claimed.

[10]The image M of γ_r is compact, so when we take any x from I_r, it has minimal distance $\varepsilon > 0$ to all points in M. The ball around x with radius $\varepsilon/2$ is also contained in I_r. An analogous argument can be made for $\mathbb{R}^2 \setminus \overline{I_r}$.

Continuity at $s \neq 0$: let $k \in \mathbb{N}$ be the ringindex of s, i.e. $s \in \mathbf{S}_n^k$. Then s lies in

$$\begin{aligned} T &= (\mathbf{S}_n^k \cup \mathbf{S}_n^{k-1}) \setminus 2^{-(k-1)}\partial\mathbf{S}_n \\ &= \{(x, y, j) \in \mathbf{S}_n : 2^{-(k+1)} < \|(x, y)\|_\infty < 2^{-(k-1)}\}, \end{aligned}$$

which is open in $\mathbf{S}_n$. By (3.20) $\psi_{|M}$, $M = \overline{\mathbf{S}_n^k} \cup \overline{\mathbf{S}_n^{k-1}}$, is continuous, and so is $\varphi = \psi_{|T}$. Thus for any open $U \subset \mathbb{R}^2$ containing $\psi(s)$, there is a V that is open in $\mathbf{S}_n$ such that $V \cap T = \varphi^{-1}(U)$ is open in $\mathbf{S}_n$ and contains s. $\varphi^{-1}(U) \subseteq \psi^{-1}(U)$ shows that ψ is continuous at s, too.
Under the induced topology, $\mathbf{S}_n$ is compact (union of $U \times \{j\}$, U the unit square, $j = 1 \dots n$) and the sets $r\,\partial\mathbf{S}_n = \{(x, y, j) \in \mathbf{S}_n : \|(x, y)\|_\infty = r\}$, $r \in [0, 1]$, are closed, hence are compact within $\mathbf{S}_n$, too. Continuous mappings on compact domains $\subset \mathbb{R}^m, m \in \mathbb{N}$, are uniformly continuous. Thus, the restriction of ψ to segment j's unit square is uniformly continuous. Because $\mathbf{S}_n$ consists of only finitely many segments (n such), ψ is uniformly continuous on all of $\mathbf{S}_n$.

□

Now that the extension of ψ^0 has been proven to be sensible, for the remainder of this section, we presuppose

Assumption 3.7. *ψ is defined from ψ^0 via equation* (3.15).

In principle, one could argue similarly for generalized eigenvectors of the subdivision matrix. This result would be superseded by Theorem 5.14, which, building on continuity of χ, shows Lipschitz continuity of all eigenfunctions.

A direct consequence of Theorem 3.6 is

Corollary 3.8. *$\psi(\mathbf{S}_n)$ and the images of every γ_r, $r \in [0, 1]$, are compact.*

Proof. By Theorem 3.6, ψ is continuous, so the images of the compact sets $\mathbf{S}_n$ and $\partial\mathbf{S}_n$ are compact. □

Corollary 3.9. *ψ^{-1} is continuous, i.e. $\psi : \mathbf{S}_n \to \psi(\mathbf{S}_n)$ is a homeomorphism.*

Proof. The claim follows from continuity of ψ, Corollary 3.8 and the following Lemma 3.10 from topology. (Every subspace of a Hausdorff space is a Hausdorff space, thus, $\psi(\mathbf{S}_n)$ is Hausdorff.) □

Lemma 3.10. *Let X be a compact topological space and Y a Hausdorff space. Then every continuous, bijective mapping $f : X \to Y$ is an homeomorphism, i.e. f^{-1} is continuous, too.*

As we could not locate a proof in the widely-spread literature, and it is quite short, we give it here:

Proof. Let $U \subseteq X$ be closed. Since X is compact, U is compact as well. It follows from continuity of f that $f(U)$ is compact. In Hausdorff spaces, compact sets are closed, hence f^{-1} is continuous. □

Corollary 3.11. 0 *is an interior point of the image of ψ.*

Proof. 0 is an interior point in $\mathbf{S}_n$, and by Corollary 3.9, ψ is an open mapping. It follows that zero is an interior point of $\psi(\mathbf{S}_n)$. □

For the following, we extend the definition of $\gamma_r(h)$ and I_r to all $r \in (0, 1]$.

The signed distance function

The next topic we are aiming toward is how ψ inherits injectivity from ψ^0. We need to construct a tool first, which will also be useful later on. An intermediate step is

Lemma 3.12. *The mapping*

$$\tilde{d}(x, r) := \min_{f \in \partial \mathbf{S}_n} \|\gamma_r(f) - x\|, \quad x \in \mathbb{R}^2, r \in [0, 1],$$

is continuous.

Proof. The minimum in the definition of $\tilde{d}(x, r)$ exists, since $\gamma_r(\partial \mathbf{S}_n)$ is compact (Corollary 3.8). Recall that per definition,

$$\gamma_r(f) = \psi(rf).$$

Let $\varepsilon > 0, x \in \mathbb{R}^2, r \in [0, 1]$ and $f \in \mathbf{S}_n$ be a point where the minimum is attained. Because ψ is uniformly continuous, there is $\delta_1 = \delta_1(\varepsilon) > 0$ such that

$$|\psi(rf) - \psi(\tilde{r}f)| < \varepsilon/2, \quad |r - \tilde{r}| < \delta_1, \tilde{r} \in [0, 1].$$

Hence, for $\|x - \tilde{x}\| < \varepsilon/2$ it is

$$\begin{aligned}\tilde{d}(\tilde{x}, \tilde{r}) &= |(\psi(\tilde{r}f) - \tilde{x}) - (\psi(rf) - x) + (\psi(rf) - x)| \\ &\leq \underbrace{|\psi(\tilde{r}f) - \psi(rf)|}_{<\varepsilon/2} + \underbrace{|\tilde{x} - x|}_{<\varepsilon/2} + \underbrace{|\psi(rf) - x|}_{\tilde{d}(x,r)}.\end{aligned}$$

Thus, $\tilde{d}(\tilde{x}, \tilde{r}) - \tilde{d}(x, r) < \varepsilon$, i.e.

$$\tilde{d}(\tilde{x}, \tilde{r}) < \tilde{d}(x, r) + \varepsilon, \quad \text{if } |x - \tilde{x}|, |r - \tilde{r}| < \varepsilon/2.$$

Changing the roles of (r, x) and $(\tilde{r}, \tilde{x})$ and applying the same argument again—at this point, uniform continuity of ψ is used—shows $\tilde{d}(x, r) - \varepsilon \leq \tilde{d}(\tilde{x}, \tilde{r})$. Combining both yields

$$\tilde{d}(\tilde{x}, \tilde{r}) \in \tilde{d}(x, r) + [-\varepsilon, \varepsilon], \quad \text{for } |x - \tilde{x}|, |r - \tilde{r}| < \varepsilon/2.$$

Consequently, $\tilde{d}$ is continuous. □

With J_- and J_+ given by

$$\begin{aligned}J_- &:= \overline{I_r} \times [0, 1], \\ J_+ &:= \left(\mathbb{R}^2 \setminus I_r\right) \times [0, 1],\end{aligned}$$

let

$$\begin{aligned}d_-(x, r) &:= -\min_{f \in \partial \mathbf{S}_n} \|x - \gamma_r(f)\|, \quad (x, r) \in J_- \\ d_+(x, r) &:= +\min_{f \in \partial \mathbf{S}_n} \|x - \gamma_r(f)\|, \quad (x, r) \in J_+.\end{aligned}$$

Building on Lemma 3.12, we can construct the second central tool,

Lemma 3.13. *The "signed distance function to (the image of) γ_r"*

$$d(x, r) := \begin{cases} d_-(x, r), & \text{if } (x, r) \in J_-, \\ d_+(x, r), & \text{if } (x, r) \in J_+, \end{cases} \tag{3.18}$$

is continuous and

$$d(x, r) \begin{cases} > 0 & \Leftrightarrow x \in \mathbb{R}^2 \setminus \overline{I_r}, \\ = 0 & \Leftrightarrow x \in \operatorname{image} \gamma_r = \partial I_r, \\ < 0 & \Leftrightarrow x \in I_r. \end{cases} \tag{3.19}$$

holds. (d and $\tilde{d}$ from Lemma 3.12 are related by $\tilde{d} = |d|$.)

Proof. An easy exercise from topology is: for arbitrary topological spaces X, Y

1. if $A, B \subseteq X$ are closed and $f : A \to Y$, $g : B \to Y$ continuous with $f_{|A\cap B} = g_{|A\cap B}$, then

$$e(x) := \begin{cases} f(x) & \text{if } x \in A, \\ g(x) & \text{if } x \in B \setminus A \end{cases} \tag{3.20}$$

   is continuous.
2. $e : X \to Y$ is continuous $\Leftrightarrow e^{-1}(C)$ is closed in X when C is closed in Y.

By Lemma 3.12 $\tilde{d}$ is continuous, its restrictions $d_\pm = \pm\tilde{d}_{|J_\pm}$inherit that property. Notice that d_-, d_+ vanish on the intersection image $\gamma_r, \times[0, 1]$ of their domains. The $J_\pm$ are closed under the induced topology, therefore d is continuous.

Finally, from compactness of image γ_r, (3.16) and by the way d is defined, (3.19) follows. □

Inheritance of injectivity onto ψ

The next issue we look into is

Theorem 3.14. *Injectivity of ψ^0 paired with $0 \notin$ image ψ^0 is equivalent to injectivity of ψ.*

The proof of Theorem 3.14 mostly breaks down into the following three lemmas:

Lemma 3.15. *If 0 does not lie in $\overline{I_1}$, then $I_{\frac{1}{2}}$ is not contained in I_1.*

Proof. Let $0 \notin \overline{I_1}$. Since $\overline{I_1}$ is compact, it contains some m with minimal norm. It is $m \in \partial I_1$ because otherwise there would be $\varepsilon > 0$ such that $(1 - \varepsilon)m \in I_1$, whose norm is smaller. So far, $0 < \|m\| \leq \|x\|$ for all $x \in \overline{I_1}$. The norm of $\lambda m \in \overline{I_{\frac{1}{2}}}$ is smaller than that of m, so $\lambda m \in \mathbb{R}^2 \setminus \overline{I_1}$. By injectivity of ψ^0 and the Jordan Curve Theorem, image $\gamma_{\frac{1}{2}} \subseteq \mathbb{R}^2 \setminus \overline{I_1}$, therefore $I_1 \not\supseteq I_{\frac{1}{2}}$. □

Lemma 3.16. *If ψ^0 is injective, I_1 cannot be a subset of $I_{\frac{1}{2}}$.*

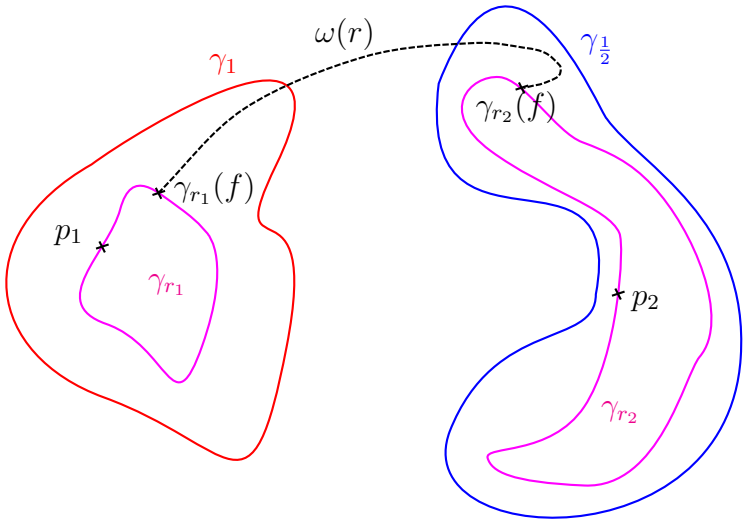

Figure 3.12: The situation that we take to contradiction in Lemma 3.17. It is $r_1, r_2 \in (1/2, 1)$, yet $\omega(r) = \gamma_r(f)$, for all $r \in [r_1, r_2] \cup [r_2, r_1]$, is a path connecting the interiors of γ_1 and $\gamma_{1/2}$. It follows that ψ^0 cannot be injective.

Proof. Suppose ψ^0 is injective and I_1 were a subset of $I_{\frac{1}{2}}$. Then it follows that $\overline{I_{\frac{1}{2}}} \supseteq \overline{I_1}$, which implies

$$\max_{x \in \overline{I_{\frac{1}{2}}}} \|x\| \geq \max_{x \in \overline{I_1}} \|x\| > 0. \tag{3.21}$$

If m is a maximizer of the leftmost side, it is $\frac{m}{\lambda} \in \overline{I_1}$. But $\|\frac{m}{\lambda}\| = \|m\|/\lambda > \|m\|$ contradicts (3.21). □

Lemma 3.17. *If neither $I_{\frac{1}{2}}$ is contained in I_1, nor the latter contained in the former one, ψ^0 cannot be injective.*

Proof. Suppose that ψ^0 were injective. By (3.16) we can take $p_1 \in I_1$, $p_2 \in I_{1/2}$. Since d is continuous, there are some $r_j \in (1/2, 1)$ such that $p_j \in \operatorname{image} \gamma_{r_j}$, $j \in \{1, 2\}$.

Since ψ^0 is injective, it follows that the image of γ_{r_1} is contained in I_1, and the image of γ_{r_2} in $I_{1/2}$. If we take any $f \in \mathbf{S}_n$,

$$\omega(r) := \gamma_r(f), \quad r \in [r_1, r_2] \cup [r_2, r_1],$$

is a path from I_1 to $I_{1/2}$ (see Figure 3.12 on page 100).

By the JCT this path must intersect the images of γ_1 and $\gamma_{1/2}$, contradicting that ψ^0 is injective. 3.12 offers a schematic view of the situation. □

Now we are ready for the

Proof of Theorem 3.14. Regarding "⇐": by Theorem 3.6, $\psi(0) = 0$ is necessary. Hence, $0 \notin \operatorname{image} \psi^0$ and if ψ is injective, then ψ^0 is, too.

"⇒": The assertion follows from Theorem 3.6 and Lemmata 3.15,3.16 and 3.17.

□

Properties of the $\psi(r\,\mathbf{S}_n)$, such as simple-connectedness

An important property of the image of ψ is that it contains no "holes", or more precisely, that it is simply connected. Before we go into this, we should pluck some nearby, low-hanging fruits that might come in handy at some time:

Theorem 3.18. *If ψ^0 is injective with $0 \notin \operatorname{image} \psi^0$, then*

a) all I_r are open when $r \in (0, 1]$,

b) $\overline{I_r} = \psi(r\mathbf{S}_n)$, for all $r \in (0, 1]$,

c) $\{0\} \subset I_r \subset I_s$ for all $0 < r < s \leq 1$.

For the proof of the theorem, we use

Lemma 3.19. *Let $\frac{1}{2} \leq a < b < c \leq 1$. If ψ^0 is injective and $I_a \subset I_c$, then $I_a \subset I_b \subset I_c$.*

Proof. By the JCT it is either $\operatorname{image} \gamma_b \subset I_c$ or $\subset \mathbb{R}^2 \setminus \overline{I_c}$. First, let us discuss the latter one. For any fixed $f \in \partial\mathbf{S}_n$, $\tau \mapsto \gamma_\tau(f), \tau \in [a, b]$, there is a path from $\mathbb{R}^2 \setminus \overline{I_c}$ to I_c, which has to intersect $\operatorname{image} \gamma_c$ by the JCT. This contradicts injectivity of ψ^0, so it must be $I_b \subset I_c$. An analogous argument shows $I_a \subset I_b$. □

Proof of Theorem 3.18. a) by their very definition at the beginning of this section, the I_r are open.
b) by the JCT, $\psi(\mathbf{S}_n) \setminus \operatorname{image}\gamma_1$ is either contained in I_1, or in $\mathbb{R}^2 \setminus \overline{I_1}$. Lemmas 3.16-3.17 show that it is the former.
c) let $0 < r < s \leq 1$; first we will show $I_r \subset I_s$. By Lemmas 3.16–3.17 it is $I_{1/2} \subset I_1$, hence all we have to do is to show the claim if r and s are in the same ring. Because of $\psi(2^{-1}\cdot) = \lambda\psi$ we may assume $1/2 \leq r < s \leq 1$ without loss of generality.
Now consider $1/2 \leq r < s \leq 1$. By Lemma 3.19 it is $I_{1/2} \subseteq I_r \subset I_1$ (the case $1/2 = r$ is trivial), using the Lemma again then shows $I_r \subset I_s \subseteq I_1$, finishing the first part of c).
To show the second part of c), it is $0 \in I_s$ for all $s \in (0, 1]$. By Lemmas 3.15-3.17 it is $0 \in \overline{I_1}$, hence, because $0 \notin \operatorname{image}\gamma_1$, we have $0 \in I_1$. Let $m := \lceil -\log_2 s \rceil$, $r := 2^{-m}$. Then $0 \in \lambda^m I_1 = I_r$ and, as we have already shown: $I_r \subset I_s$.

□

Now to the last topological issue we consider here,

Theorem 3.20. *If ψ is injective, the sets $\psi(r\,\mathbf{S}_n)$ are simply connected for every $r \in [0, 1]$.*

Proof. Let $r \in [0, 1]$ be fixed. To see why the image Θ_r of $r\mathbf{S}_n$ under ψ is simply connected, let

$$\mathbb{S}^1 := \{(x, y) \in \mathbb{R}^2 : x^2 + y^2 = 1\},$$
$$\mathbb{D} := \{(x, y) \in \mathbb{R}^2 : x^2 + y^2 \leq 1\}$$

be the unit sphere and -disk. Further, $g : \mathbb{S}^1 \to \Theta_r$ shall be a continuous function. We must show that there is a mapping $e : \mathbb{D} \to \Theta_r$, which extends the domain of g onto the complete unit disk, i.e. $e_{|\mathbb{S}^1} = g$, and which is continuous.

For $r = 0$, by (3.15) it is $\psi(r\,\mathbf{S}_n) = \{0\}$, which is a simply connected set. Now assume $r > 0$. Then $\tilde{g} := \psi^{-1} \circ g$ is a continuous mapping from $\mathbb{S}^1$ to $r\mathbf{S}_n$ (Corollary 3.9). By Theorem 3.18a) and c) there is some $\tau > 0$ such that $\tau\mathbb{D} \subset \Theta_r$. Compactness of Θ_r and $\psi(2^{-m}\cdot) = \lambda^m\psi$, $m \in \mathbb{N}$, yield the

existence of $\rho_0 \in (0, r)$ such that $\psi(\rho_0 \mathbf{S}_n) \subset \tau\mathbb{D}$. Define

$$\begin{aligned}
\tilde{e}(\rho, t) &:= \rho\tilde{g}(t), \quad \rho \in [\rho_0, r], t \in \mathbb{S}^1, \\
e_1(\rho, t) &:= \frac{\rho}{\rho_0}\tilde{e}(\rho_0, t), \quad \rho \in [0, \rho_0], t \in \mathbb{S}^1, \\
e_2(\rho, t) &:= \psi \circ \tilde{e}(\rho, t), \quad \rho \in [\rho_0, r], t \in \mathbb{S}^1, \\
e(\rho, t) &:= \begin{cases} e_1(\rho, t), & \text{if } \rho \in [0, \rho_0], \\ e_2(\rho, t), & \text{if } \rho \in [\rho_0, r]. \end{cases}
\end{aligned}$$

e_1, e_2 are continuous, their domains closed, and e_1, e_2 are identical on the intersection of their domains. Continuity of e follows by the same argument as for d (see the proof of Lemma 3.13). This finishes the proof. □

Chapter 4

C^2 schemes

4.1 Historical note

The first C^2 schemes were *Freeform Splines* [53] and *TURBS* [58, 59]. The former was developed by H. Prautzsch, the latter one by U. Reif. *Freeform Splines* are a generalization of *TURBS*, although it should be noted that both contain the key elements needed for C^2-schemes (see [53, Remark 8] and [59, Chapter 4.5]).

Crucial point of C^2 subdivision algorithms is the extension of *quadratic polynomials*

$$(\chi_1)^i(\chi_2)^j, \quad 0 \leq i+j \leq 2, \tag{4.1}$$

from one spline ring onto the next inner one. χ_1 and χ_2 are the two component functions of the characteristic map, χ.

Both, necessity *and* sufficiency of this property, have first been clearly identified in [56, 57, Chapter 5.1]. The result can also be found in [49], where it is discussed from a more geometrical point of view. Remarkably, the paper did put more emphasis on necessity, perceiving it as an obstacle towards C^2 continuity at extraordinary points rather than including it into the construction of the subdivision algorithm.

Freeform Splines, as well as TURBS are in fact more than merely subdivision schemes: they allow to connect n polynomial patches[1] of degree six [2] such that the surface is curvature continuous at an extraordinary point. The existence of a representation by finitely many polynomial patches is advantageous for CAGD systems.

TURBS

The main building block of TURBS are D^k-patches, n of which are arranged around an extraordinary point of valency n:

1. Each D^k-patch has a singularity of order k at the central point.

[1] For *Freeform Splines*, these n patches correspond to the surface cap in item 4 in *Freeform Splines* below.

[2] Actually, both concepts allow for the construction of G^k (Freeform Splines), resp. C^k splines (TURBS). This is pointed out in both papers. However, the motivation of both has been the G^2/C^2 case, which both take up as instructive example. This is wise when explaining a concept that would be too sophisticated in its most general form, and we choose this course here also.

2. The joining of D^k-patches is single-sheeted[3] at the central point.

3. Finally, the local graph of the D^k-patch is required to be k-times differentiable in an environment of the central point.

D^k-patches are constructed by means of local reparametrizations[4], one of which is assigned to each extraordinary point. These local reparametrizations are typically polynomials of bi-degree $(k+1)$ and have themselves singularities of order k in the central point (i.e. their centermost $(k+1)$ rings of Bézier points coincide at the origin). For $k = 2$, the n D^k-patches are combined in the central point such that the local graph can be any quadratic polynomial, the exact shape of which can be controlled by *quasi control points*.
For more details please refer to [58, 59].

Freeform Splines

Freeform Splines take a different route. They are described in a more geometrical fashion; with terms from [53] translated to our notation, its steps are:

1. A planar filling $y : 2^{-1}\mathbf{S}_n \to \mathbb{R}^2$ for the re-parametrized parameter domain is constructed. It has to C^2 connect to a planar ring $x : \mathbf{S}_n^0 \to \mathbb{R}^2$ which, for instance, can be given by the characteristic ring of the Catmull-Clark scheme.

2. C^k-smoothness of the reparametrization y near the central point is recognized to be irrelevant. Consequently, only C^0 is demanded[5].

3. The filling $q : \mathbb{R}^2 \to \mathbb{R}^3$ for the surface is then defined on the image of y. q is to be a polynomial of total-degree ≤ 2.

4. The surface *cap* is $q \circ y$. Its degree is six (or, possibly, higher).

---

[3]The property is defined equivalently to Definition 2.11 in [50].

[4]The term used in [59, Chapter 6, Section 4.4] is "lokale Darstellungen".

[5]In comparison, TURBS do C^k-connect their n patches at the extraordinary point (the $k+1$ rings of innermost control points coincide in the origin). Thus, for TURBS the surface cap (see item 4) $q \circ y : 2^{-1}\mathbf{S}_n \to \mathbb{R}^3$ is in $C^2(2^{-1}\mathbf{S}_n, \mathbb{R}^3)$. This is why in [59, Chapter 4.5] Reif remarks that *Freeform Splines* are only G^2-connected at the extraordinary point.

5. The three innermost rings of Bézier points of the surface ring $r : \mathbf{S}_n^0 \to \mathbb{R}^{1\times 3}$ are now C^2 connected to the cap $q \circ y$.

From our point of view, the following sentence from [53, Section 3] is essential to the construction. However, it is difficult to understand in its context; with terms replaced to match those from above:

> "Now, let $q : \mathbb{R}^2 \to \mathbb{R}^3$ be any suitable polynomial of total degree ≤ 2. Then $q \circ x$ and $q \circ y$ together form a bisextic spline surface with C^2- and G^∞-joints, respectively."

Let us explain:

1. The pieces of $q \circ x$ join C^2.

2. The pieces of $q \circ y$ join G^∞ because by re-parametrizing this function with y^{-1}, i.e. changing domain to (a subset of) $\mathbb{R}^2$, the surface is a polynomial of total degree ≤ 2.

3. $q \circ x$ and $q \circ y$ join C^2 (since there are typically some s in the intersection of both their domains, i.e. $s \in \mathbf{S}_n^0 \cap 2^{-1}\mathbf{S}_n = 2^{-1}\partial\mathbf{S}_n$, at which $q \circ x$ is merely C^2). But this is not what Prautzsch meant–at this point, he did not yet get to describing how to connect $q \circ y$ and r.

Again, for a further description we refer to the original paper, [53].

Remark on the two concepts

Both *Freeform Splines* and *TURBS* aim for the number of polynomial pieces of a subdivision surface to be constant (note the distinction between "polynomial piece" and "knot interval"; in this context, the number of the former remains constant under subdivision). This lead to the concept of geometric continuity and is in accordance with a majority of works that were published until the mid 1990-ties, cf. [10, 12, 18, 21, 23, 22, 25, 33, 26, 31, 46, 65].

While this is indeed a quite worthwhile achievement, it puts limitations on the surface near the central point. Some of these limitations need sophisticated techniques to overcome. Subsequent *Guided Subdivision Surfaces* [28] aim for a smoother transition to the quadratic polynomial describing the subdivision surface in the vicinity of its central point, which is its key innovation versus *TURBS* and *Freeform Splines*.

Schemes with smoother decay of higher order terms

If we design a stationary subdivision scheme with a smoother transition of higher order terms, we start with a function $\chi : \mathbf{S}_n \to \mathbb{R}^2$ that has all the properties that we require of the characteristic map of a C^2 scheme (see Section 3.3 for a detailed description for how χ may be constructed). We re-parametrize the parameter domain by χ. Recall that all quadratic polynomials have to extended (cf. (4.1)).

In contrast to *Freeform Splines* and TURBS, *more* functions than merely $(\chi_1)^i(\chi_2)^j$, $0 \leq i + j \leq 2$ are extended onto the next inner surface ring. Typically, these will include but not be limited to some approximations of $(\chi_1)^i(\chi_2)^j$ when $i + j > 2$ (as these functions themselves will usually not be contained within the span of the generating rings b_k^0). The additional functions have to decay uniformly faster than the quadratic polynomials towards the extraordinary point.

On the other hand, because of the infinite sequence of spline rings, the surface can no longer be represented by a finite number of polynomial patches. In a purely subdivision context, this carries no weight. But for CAGD systems this has to be considered a severe disadvantage—at least nowadays a finite number of NURBS patches is desired for the representation of a surface.

In practice, the infinite sequence of spline rings can be truncated by passing into a cap, of course, once the spline rings have become flat enough (we expect at most five or six spline rings to be sufficient for this). The cap can be constructed, for instance, in the same fashion as for *Freeform Splines* (whose concept lies closer to the numeric model we propose for the subsequent PTER-scheme).

Finally, it should be noted that,

> *"Guided Subdivision Surfaces* are a fundamental revision and generalization of the ideas behind *Freeform Splines* and TURBS."

(J. Peters and U. Reif in *Subdivision Surfaces [50]* p.155, Bibliographical Notes, Remark 11). Consequently, many key elements of *Freeform Splines* and TURBS are contained in *Guided Subdivision Surfaces*. The same applies to the PTER-principle, which has been derived from *Guided Subdivision Surfaces* and is our main topic in Section 4.2.

4.2 Extending splinerings by the PTER-scheme

The book *Subdivision Surfaces*, [50], abstracted most techniques *Guided Subdivision Surfaces* base on to derive the PTER-scheme, a construction guidance for stationary subdivision matrices

1. which have quadratic precision, and
2. which extend more functions than merely $\chi_1^i \chi_2^j$ with $0 \leq i + j \leq 2$ onto the next inner surface ring[6], as noted in Section 4.1.

The original PTER-scheme is detailed in [50, Chapter 7]; we recommend this for a full description including variations. The book also contains a proof that the (stationary) subdivision matrices arising from it yield C^2 schemes, *if* they have the correct eigen-spectrum. This theorem is likewise applicable to the version of PTER we subsequently present.

To give a general overview beforehand, PTER extends the scalar valued generating rings, b_k^0, onto $\mathbf{S}_n^1$. The stationary subdivision matrix is then given in a reverse fashion by the Equation of Refinement,

$$B^1 =: B^0 A.$$

Note that we need the generating rings $b_k^0 : \mathbf{S}_n^0 \to \mathbb{R}$, $k = 0, \ldots, \bar{k}$, to be linearly independent to guarantee well-definition of A here.

As noted previously, some $0 < \lambda < 1$ and $\chi : \mathbf{S}_n \to \mathbb{R}^2$ must be given beforehand, so that χ can serve as the characteristic map of the scheme (A, B^0) to be built, to the eigenvalue λ (Section 3.3 describes how χ can be constructed).

Revised PTER-scheme

The original PTER-scheme allows the preliminary extention $\tilde{\beta}^1$ of a spline ring to be discontinuous with $\tilde{\beta}^0$. The spline ring x^1 is then – essentially

[6] In contrast to *Freeform Splines*: quoting [53, Remark 4],

> "Since the three outer control rings of r_i come from r^{i-1} or $q \circ \lambda^{i-1} x$, one has $r^i = q \circ \lambda^i x$. Thus the surface rings $r, r^1, r^2, \ldots$ form a G^2-surface."

(Most likely r_i is a typo and should mean r^i.) Thus, *Freeform Splines* extend only terms χ_1^i, χ_2^j with $0 \leq i + j \leq 2$ onto the next surface ring.
(Something analogous is true for TURBS; cf. their definition in [59, Definition 6.7].)

– constructed from a projection of $\tilde{\beta}^1$ into the subspace of rings that C^2 connect to x^0.

The purpose of this has most likely been to better capture the process to construct some of Jörg Peters' and K. Karciauskas' *guided rings*; and to include these surfaces within PTER.

We adapted the PTER-steps slightly to remove this issue. We feel that the result reflects better the process within (certain) guided schemes, too.

Let us abbreviate the image of the characteristic spline, respectively of its m-th ring by (see Figure 3.2 on page 75)

$$\Theta := \chi(\mathbf{S}_n), \quad \Theta^m := \lambda^m(\overline{\Theta \setminus \lambda\Theta}).$$

Further, denote

$$\Omega := \partial\Theta.$$

The PTER-steps now are

Reparametrization: The splinering B^0 is re-parametrized over Θ^0,

$$\beta^0(\omega) = B^0 \circ \chi^{-1}(\omega), \quad \omega \in \Theta^0.$$

β^0 is projected into a suitable function space $\mathcal{S} \subseteq \{f : \Theta^0 \subseteq \mathbb{R}^2 \to \mathbb{R}\}$, yielding $\tilde{\beta}^0$. $\mathcal{S}$ is required to contain the subspace

$$\mathcal{S}_{[2]} := \{\omega \mapsto \sum_{i+j\leq 2} c_{i,j}\omega_1^i\omega_2^j : \quad c_{i,j} \in \mathbb{R}\}$$

of quadratic polynomials.

Extension: $\tilde{\beta}^0$ is extended continuously to the next-inner ring Θ^1. The quadratic polynomials in $\mathcal{S}_{[2]}$ have to be preserved. Following [50, Chapter 7], we require the mapping $\beta^0 \mapsto \tilde{\beta}^1$ to be linear.

Turn-back: The preliminary extension $\tilde{\beta}^1$ is turned back into a splinering $\tilde{B}^1$ with domain $\mathbf{S}_n^0$, i.e. the inverse of the first substep of **R** is applied.

Projection: $\tilde{B}^1$ is projected back onto the function space available to the next splinering, finally yielding B^1.

(As operators most commonly are chosen to act from the left side, the acronym PTER encodes successive steps from the right to the left.)

The changes

We changed step "R" to be both reparametrization and projection on $\mathcal{S}$. Now polynomials that are bi-quadratic in χ_1, χ_2 lie within the respective function spaces in steps "R" and "P". They persist under the projections automatically. Guided-surfaces, for instance, identify the spline ring $\mathbf{x}^0$ with a set of Hermite-samples taken at specific positions. $\tilde{\beta}^0$ is assigned from these Hermite samples, possibly in a non-linear fashion. Its extention $\tilde{\beta}^1$ does not have to connect continuously to β^0, but to the projection $\tilde{\beta}^0$ (beware the tildes!). Thus, *guided rings* lie well within the framework when $\beta^0 \mapsto (\tilde{\beta}^0, \tilde{\beta}^1)$ is linear, without the need to allow discontinuity between $\tilde{\beta}^0$ and $\tilde{\beta}^1$.

Most likely, the acronym PTER is to acknowledge Jörg Peters for discovering his route to C^2 subdivision algorithms. However, understanding a subdivision surface as a graph parametrized over its characteristic map is centermost to constructing subdivision schemes. The final projection "P" is typically done with this in mind in order to be sound geometrically. We feel it is better placed *before* the turn-back onto the domain $\mathbf{S}_n^0$. The scope of the resulting subdivision schemes is identical, anyway. However, we do not want to create a new acronym, and therefore left the order of steps unchanged.

Accelerating schemes

Accelerating schemes dispense with stationarity of the algorithm as it necessitates polynomials of degree higher than two times the degree of χ (Ulrich Reif's degree-estimate, [57]). The idea is to replace the quadratic monomials, $(\chi_1)^i(\chi_2)^j, i+j=2$, by ever finer approximations, so that oszillations of second derivatives decay (at least) as they do for surfaces that are C^2 at the extraordinary point. The basic idea to this type of schemes is due to Jörg Peters and Kestutis Karciauskas[47]. For L-domains, the number of polynomial patches is doubled in each tensor direction. The acceleration to the approximations is a parameter that can be adapted as part of an algorithm's design. It has yet to be seen what is sufficient to guarantee good surface quality without bloating memory requirements. Most likely, the acceleration for L-domains exceeds the requirements for "good" surfaces.

Polar schemes are of particular advantage for these schemes. Since their characteristic maps can be linear in the radial direction (see Section 3.3), one

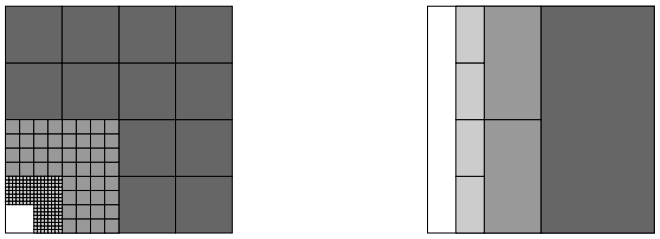

(a) L-domain (cardinal cubics).

(b) Polar-domain.

Figure 4.1: Possible patch-layout for accelerating schemes. For cardinal cubics on L-domains, we want the characteristic ring to both remain the same in each step and scale with eigenvalue $\lambda = 1/2$. Hence, we begin with 3×4 polynomial pieces, instead of only three as in the Catmull-Clark setting, where $\lambda = 1/2$ cannot be achieved.

merely has to accelerate in the circular one. Thus, the number of polynomial pieces is generally only the square root of those needed for L-shaped domains.

It is sensefull to base the construction of accelerating schemes on a non-accelerating scheme that has polynomial degree six or higher. The exponential increase of polynomial pieces per spline ring can quickly cause problems with computer memory if a new ring is computed (which typically also must take into account a number of successive rings). If we follow this course, then spline ring $m \in \mathbb{N}$ of the accelerating scheme is derived by approximating the respective ring of the degree-six-C^2 scheme, in a (typically) local fashion, by $3 * 4^{m+1}$ cubic pieces (for L-domains, cf. Figure 4.1a on page 113). For polar schemes. the number of such polynomial pieces needs only to be 2^m.

The A_n-bases of Section 2.5 are an alternative to acceleration, without the need to grow the number of polynomial pieces of successive spline rings exponentially.

Calculating derivatives of $\mathbf{x} \circ \chi^{-1}$

To implement the PTER (or, most likely, any C^2-) scheme, we need derivatives of the spline parametrized over the image of the characteristic map. Regularity of χ is indispensable here, as the complete set of derivatives of

χ^{-1} at any given degree $G \geq 1$ is defined if and only if χ is regular[7]. By the chain rule, if B and χ are differentiable up to total degree G at some $t_0 \in \mathbf{S}_n$, and $D\chi(t_0)$ is invertible, then $B \circ \chi^{-1}$ is differentiable up to and including total degree G.

On a historical note, Faà di Bruno's formula was the first one published that generalized the chain rule to higher derivatives. However, it exclusively does this for univariate functions. Recently, although after our work described here, a formula for the most generalized multivariate case,

$$h : x \in X \subset \mathbb{R}^\nu \xrightarrow{f} y \in Y \subset \mathbb{R}^\mu \xrightarrow{g} z \in \mathbb{R},$$

has been published [37].

The digital attachments contain the MATLAB routine

`Derivatives_f_circ_chiInv`.

It can calculate derivatives up to (incl.) total degree four. We verified its formulas symbolically. The program code is quite straightforward, and should be easy to adapt to other programming languages like C (a MATLAB -to-C compiler might also be an alternative).

There exists a bijection from partial derivatives to coefficients of the bivariate Taylor polynomial. Calculating the Taylor coefficients for $B \circ \chi^{-1}$ at $\chi(t_1, t_2, j)$ can be done as for any other bi-variate function, if the segment index $j \in \mathbb{Z}_n$ is considered fixed. Therefore, we disregard the segment number in the notations for the rest of this subsection. The first step to calculate derivatives of $B \circ \chi^{-1}$ is to calculate the

Taylor coefficients of χ^{-1}

Denote the component functions of χ by x, y, and those of χ^{-1} by u, v. To compute the coefficients up to degree G, set as outer functions

$$x = \sum_{g=1}^{G} \sum_{j=0}^{g} x_{g-j,j} u^{g-j} v^j, \quad y = \sum_{g=1}^{G} \sum_{j=0}^{g} y_{g-j,j} u^{g-j} v^j, \tag{4.2}$$

[7]This should not be difficult to prove for general degree, i.e. higher than those we computed explicitly (degree ten). Our programs did not require degrees more than four. However, we do not want to digress from the intended purpose, which is to extend spline rings by minimizing certain derivatives.

and substitute the inner functions

$$u = \sum_{g=1}^{G} \sum_{j=0}^{g} u_{g-j,j} X^{g-j} Y^j, \quad v = \sum_{g=1}^{G} \sum_{j=0}^{g} v_{g-j,j} X^{g-j} Y^j. \tag{4.3}$$

Using a computer algebra system like MATHEMATICA or MAPLE, comparing coefficients of $\chi \circ \chi^{-1}(X, Y) = (1 \cdot X,\, 1 \cdot Y)$, the $u_{i,j}, v_{i,j}$ can easily be solved for in successive degree $i + j$. As expected, for $G = 1$ we get

$$\begin{aligned} u_{1,0} &= \frac{y_{0,1}}{J}, & v_{1,0} &= -\frac{y_{1,0}}{J}, \\ u_{0,1} &= -\frac{x_{0,1}}{J}, & v_{0,1} &= \frac{x_{1,0}}{J}, \end{aligned}$$

where $J = x_{1,0}y_{0,1} - x_{0,1}y_{1,0}$ is the Jacobian determinant of χ. The formulas get longer the higher the degree, and they are not very interesting themselves. We list only one of degree two here, in order to give an idea of them:

$$\begin{aligned} u_{2,0} \;=\; & \frac{-x_{1,1}u_{1,0}v_{1,0}y_{0,1} + x_{2,0}u_{1,0}^2 y_{0,1} - x_{0,2}v_{1,0}^2 y_{0,1}}{J} \\ & + \frac{x_{0,1}y_{2,0}u_{1,0}^2 + x_{0,1}y_{0,2}v_{1,0}^2 + x_{0,1}y_{1,1}u_{1,0}v_{1,0}}{J}. \end{aligned}$$

It is possible to express the $u_{i,j}, v_{i,j}$ of degree G by $x_{i,j}, y_{i,j}$ with $i + j \le G$, substituting $u_{i,j}, v_{i,j}$ of lower degree. But since the next step essentially requires applying the chain rule, the latter are needed anyway.

Taylor coefficients of $f \circ \chi^{-1}$

Let f be the inner function (4.2), χ^{-1} the outer one, (4.3). Sorting out the respective coefficients in the composition is quite simple using a computer algebra system. Afterwards, we only have to go back from Taylor coefficients to partial derivatives.

As mentioned above, the MATLAB routine `Derivatives_f_circ_chiInv` provides functionality to calculate the derivatives of $f \circ \chi^{-1}$, taking derivatives of f, χ as input. In case we need only those of χ^{-1}, we can use $f = \mathrm{id}(\mathbb{R}^2)$.

4.3 Extension by quadratic forms

Peters and Reif [50, Section 7.4] proposed to take minimizers of a suitable semi-positive quadratic form $\boldsymbol{Q}$ as (preliminary) extension of a reparametrized

ring $\tilde{\beta} : \Theta^{m-1} \to \mathbb{R}^{1\times(\bar{k}+1)}$ to $\lambda^m\Theta$ in PTER's "E" step. Transferred to our version of PTER,

$$\tilde{\mathbf{y}} := \underset{f\in\mathcal{S} \text{ s.t. } f \text{ and } \tilde{\beta} \text{ join } C^{\tilde{k}}}{\operatorname{argmin}} \boldsymbol{Q}(f, \lambda^m\Theta), \tag{4.4}$$

where $\mathcal{S}$ is a sensible, usually finite, linear subspace of $C^2(\mathbb{R}^2, \mathbb{R})$ and $\tilde{k}$ is some non-negative integer, possibly as low as zero. This $\tilde{k}$ does not have to be the same as the degree of the C^k-conditions between successive spline rings (usually, the latter, k, will be at least two). The quadratic form $\boldsymbol{Q}$ is expected to be semi-positive. Note that we need to consider scalar-valued functions f only, the generating splines are to be of this type after all.

Before we proceed, we informally assert

Fact 4.1. *Extension by minimizing a quadratic form $\boldsymbol{Q}$ is well-defined if and only if the solution to the minimization problem* (4.4) *is unique.*

The reasoning is straightforward: the extension can be any minimizer of the quadratic form. However, the extension is a well-defined function of its input f if and only if it is uniquely determined from the latter.

Typically, the restriction of $\boldsymbol{Q}$ to the subspace of functions that C^k-connect to given $\tilde{\beta}$ is positive definite. Uniqueness of the solution of the minimization (i.e. 4.1) is usually verified easily in the computations. In the following, we will simply assume the solution to be uniquely determined.

For the following analysis, we will assume that the space of functions f in (4.4) is given by

$$\mathcal{S} := C^2(\mathbb{R}^2, \mathbb{R}).$$

The form of quadratic forms we examine will be

$$\boldsymbol{Q}(f, \mathcal{D}) := \int_{\mathcal{D}} \sum_{h=0}^{\bar{h}} \left(\sum_{g=1}^{\bar{g}_h} \sum_{j=0}^{g} q_{h,g,j} \partial_1^j \partial_2^{g-j} f \right)^2, \quad q_{h,g,j} \in \mathbb{R}, \tag{4.5}$$

for some $\bar{h}, \bar{g}_h \in \mathbb{N}$ and $\mathcal{D} \subset \mathbb{R}^2$.

A sufficient condition for quadratic precision

In their book, Peters and Reif [50] require the quadratic polynomials to be within the kernel of $\boldsymbol{Q}$ to guarantee that they are extended onto the next

spline ring by themselves. Otherwise, it is indeed possible that some of these polynomials are extended with differing functions, typically of corresponding eigenvalues less than λ^2. Consider

Example 4.2 (Reif's requirement violated: a quadratic form that does *not* yield quadratic precision)**.** Consider the quadratic form

$$\boldsymbol{Q}(f, \mathcal{D}) = \int_{\mathcal{D}} (\partial_1^2 f)^2 + (\partial_2^3 f)^2 d(x, y), \quad \mathcal{D} \subseteq \mathbb{R}^2. \tag{4.6}$$

Both xy, y^2 lie within its kernel and, indeed, are extended onto the next spline ring. x^2 however, does not. In the implementation we observed this $\boldsymbol{Q}$ does not yield full quadratic precision. For example, at valency six and $\lambda = 1/2$, the first six eigenvalues turn out to be

$$1.0000,\ 0.5000,\ 0.5000,\ 0.2500, 0.2500, 0.2374.$$

Consequently, the stationary subdivision matrix arising from it fails to model convex shapes in the limit, just like standard Catmull-Clark weights do at valencies greater than four.

Of course, for every quadratic polynomial to lie within $\ker \boldsymbol{Q}$, the scope of quadratic forms is limited to those containing only derivatives of at least degree three.

Clearly, we cannot choose any quadratic form to build our subdivision scheme on. But let us first introduce some notation and make concise how the stationary subdivision matrix is derived.

Notations

A function is C^k*-zero on* a subset $\tilde{\mathcal{D}}$ of its domain, written as

$$f \in Z^k(\tilde{\mathcal{D}}),$$

if for all $0 \leq |\alpha|_1 \leq k$ and $x \in \tilde{\mathcal{D}}$ it is $(\partial^\alpha f)(x) = 0$, with α a multi-index.

For $\tilde{\mathcal{D}} \subseteq \mathbb{R}^2$, let

$$\mathcal{S}_{|\tilde{\mathcal{D}}} := \{f_{|\tilde{\mathcal{D}}} : \quad f \in \mathcal{S}\}.$$

The unique minimizer of $\boldsymbol{Q}$ over a domain $\mathcal{D}$ that C^k-connects to some f_0 can now be denoted by

$$\mathcal{M}(f_0, \mathcal{D}) := \underset{\substack{f \in \mathcal{S}_{|\mathcal{D}} \\ f_0 - f \in Z^k(\partial\mathcal{D})}}{\operatorname{argmin}} \boldsymbol{Q}(f, \mathcal{D}). \tag{4.7}$$

Since we solve a quadratic program without inequality constraints, $\mathcal{M}(f_0, \mathcal{D})$ depends linearly on f_0.

Route to a stationary subdivision matrix

Recall that in the reparametrisation step of PTER, B^0 is parametrized over the outermost ring Θ^0. The resulting function β^0 is projected onto a suitable function space $\mathcal{S} \subseteq \{f : \mathcal{D} \subseteq \mathbb{R}^2 \to \mathbb{R}\}$, yielding $\tilde{\beta}$. If β^0 is fine— as we observed in our implementation—this projection can be omitted, letting $\tilde{\beta}^0 = \beta^0$:

1. We begin with C^k-boundary values for β at $\lambda\Omega$.
2. From C^k-boundary values taken from β at $\lambda\Omega$ we calculate the intermediate extension

   $$\widetilde{\beta} := \mathcal{M}(\beta, \Theta). \tag{4.8}$$

   Of these newly defined splinerings of $\widetilde{\beta} : \Theta \to \mathbb{R}$ we only keep the outermost one, assigning it to

   $$\beta := (\widetilde{\beta})_{|\Theta^1}.$$

   Next, we return to the domain $\mathbf{S}_n^1$:

   $$B_{|\mathbf{S}_n^1} := \beta \circ \chi_{|\Theta^1}.$$

   Recalling (3.1),

   $$b_j^m := b_j(2^{-m}\cdot)_{|\mathbf{S}_n^0},$$

   notice that the splinering b_k^m has been defined on the domain $\mathbf{S}_n^0$ for every ringindex $m \in \mathbb{N}$. Working our way through this somewhat tricky formalism, we arrive at

   $$B^1(t) = \left(B_{|\mathbf{S}_n^1}\right)(2^{-1}t), \quad t \in \mathbf{S}_n^0.$$

3. The subdivision matrix A is now defined from the equation of refinement,

$$B^1 =: B^0 A$$

(at this point, linear independence of the b_k^0, $k = 0, \dots, \bar{k}$, is crucial in order to unambiguously define the subdivision matrix).

We want our subdivision matrix to be shift- and flip-symmetric. Therefore, if r is any rotation or reflection of the plane $\mathbb{R}^2$, we demand

$$\mathcal{M}(f_0, \Theta) \circ r = \mathcal{M}(r \circ f_0, r(\Theta)). \tag{4.9}$$

Figuratively, the rotated minimizer must be identical to the minimizer of the rotated problem. For reflections, the analogous property is required. Before we look into differential operators suitable for this purpose, let us make sure the quadratic form lends itself for the construction of stationary subdivision matrices.

Restriction to homogeneous quadratic forms

In order to find out which quadratic forms lend themselves for the construction of stationary subdivision matrices, we need to decompose the domain $\Theta = \Theta^0 \cup \lambda\Theta$ and study the respective minimization problems over these subdomains.

If $f_1 : \mathcal{D}_1 \to \mathbb{R}, \dots, f_m : \mathcal{D}_m \to \mathbb{R}$ are functions with $f_i(x) = f_j(x)$ at all $x \in \mathcal{D}_i \cap \mathcal{D}_j$, let

$$\mathrm{pw}(f_1, \dots, f_m)(x) := \begin{cases} f_1(x) & , \text{ if } x \in \mathcal{D}_1, \\ \vdots & \vdots \\ f_m(x) & , \text{ if } x \in \mathcal{D}_m, \end{cases}$$

be the "joined", piecewise defined function from $\mathcal{D}_1 \dots \cup \mathcal{D}_m$ to $\mathbb{R}$. We can now write

$$\begin{aligned} \mathcal{M}(f_0, \Theta) &= \operatorname*{argmin}_{\substack{f \in \mathcal{S} \\ f - f_0 \in Z^k(\lambda\Omega)}} \boldsymbol{Q}(f, \lambda\Theta) \\ &= \mathrm{pw} \circ \operatorname*{argmin}_{\substack{(f_1, f_2) \in \mathcal{S}_{|\Theta^1} \times \mathcal{S}_{|\lambda^2\Theta} \\ f_0 - f_1 \in Z^k(\lambda\Omega) \\ f_2 - f_1 \in Z^k(\lambda^2\Omega)}} \left[\boldsymbol{Q}(f_1, \Theta^1) + \boldsymbol{Q}(f_2, \lambda^2\Theta) \right]. \end{aligned}$$

With yet unknown f_1, it is $f_2 = \mathcal{M}(f_1, \lambda^2\Theta)$, thus

$$\mathcal{M}(f_0, \lambda\Theta)_{|\Theta^1} = \underset{\substack{f_1 \in \mathcal{S}_{|\Theta^1} \\ f_0 - f_1 \in Z^k(\lambda\Omega)}}{\operatorname{argmin}} \left[\boldsymbol{Q}(f_1, \Theta^1) + \boldsymbol{Q}(\mathcal{M}(f_1, \lambda^2\Theta), \lambda^2\Theta) \right].$$

How is $\mathcal{M}(\cdot, \lambda^2\Theta)$ related to the current minimization $\mathcal{M}(\cdot, \lambda\Theta)$? (Notice that the former one has its C^k-conditions at $\lambda^2\Omega$!)

This is an important point that one should consider. Applying the resulting subdivision matrix A solves the minimization problem $\mathcal{M}(\cdot, \lambda\Theta)$, but only keeps the outermost ring of the solution (see (4.8)). For the successive spline ring, the restriction to $\lambda^2\Omega$ of the old minimizer should be a good starting point in the new minimization problem.

So when do the two minimization problems return identical solutions? If we set

$$\hat{f}_2 := f_2(\lambda\cdot) : \lambda^2\Theta \to \mathbb{R}$$

it is

$$\partial^\alpha \hat{f}_2 = \lambda^{-|\alpha|_1} \left(\partial^\alpha f_2\right)(\lambda\cdot).$$

With $\underline{g}$ the smallest (total-) degree of the derivatives that enter $\boldsymbol{Q}$ – the latter one defined by (4.5) – and

$$\hat{\boldsymbol{Q}}(f, \mathcal{D}) := \int_{\mathcal{D}} \sum_{h=0}^{\bar{h}} \left(\sum_{g=\underline{g}}^{\bar{g}_h} \lambda^{\underline{g}-g} \sum_{j=0}^{g} q_{h,g,j} \partial_1^j \partial_2^{g-j} f \right)^2, \tag{4.10}$$

we have

$$\boldsymbol{Q}(f_2, \lambda^2\Theta) = \lambda^{-2\underline{g}} \hat{\boldsymbol{Q}}(\hat{f}_2, \lambda\Theta). \tag{4.11}$$

Similarly, we transfer the C^k-conditions:

$$\begin{array}{rcl} f_1 - f_2 & \in & Z^k(\lambda^2\Omega) \\ \Leftrightarrow \quad (f_1 - f_2)(\lambda\cdot) & \in & Z^k(\lambda\Omega) \\ \Leftrightarrow \quad f_1(\lambda\cdot) - \hat{f} & \in & Z^k(\lambda\Omega). \end{array}$$

From now on explicitly specifying the quadratic form that is to be minimized, we obtain

$$\mathcal{M}_{\boldsymbol{Q}}\left(f_1, \lambda^2\Theta\right) = \mathcal{M}_{\hat{\boldsymbol{Q}}}\left(f_1 \circ (\lambda\cdot), \lambda\Theta\right) \circ (\frac{\cdot}{\lambda})$$

(concerning the right-hand side, recall that $\mathcal{M}$ returns a function).

Definition 4.3. A quadratic form $\boldsymbol{Q}$ is called *stationary under dilation of the domain* if it is

$$\Big(\mathcal{M}_{\boldsymbol{Q}}(\cdot, \lambda\Theta) - \mathcal{M}_{\hat{\boldsymbol{Q}}}(\cdot, \lambda\Theta)\Big)_{|\Theta^1} = 0.$$

Obviously, a quadratic form is stationary under dilation of the domain if it has the following property:

Definition 4.4 (Homogenous quadratic form)**.** A quadratic form $\boldsymbol{Q}$ is called *homogeneous* if $\boldsymbol{Q} = \hat{\boldsymbol{Q}}$.

Returning briefly to Example 4.2, at valency three the ten largest eigenvalues of the subdivision matrix in the implementation are, up to four digits after the decimal point,

$\boldsymbol{Q}$	$\hat{\boldsymbol{Q}}$
1.0000	1.0000
0.5000	0.5000
0.5000	0.5000
0.2500	0.2500
0.2500	0.2500
0.1936	**0.2122**
0.1131	0.1186
0.1107	0.1128
0.0842	0.1052
0.0804	0.1038.

We conjecture that only homogeneous quadratic forms are stationary under dilation of the domain, and thereby lend themselves to produce stationary subdivision matrices. Since homogeneous quadratic forms produce quite good subdivision matrices, there was no need to see if it is possible to broaden the scope of quadratic forms beyond this. From now on, we assume the quadratic form is homogeneous, i.e.

$$\boldsymbol{Q}(f, \mathcal{D}) := \int_{\mathcal{D}} \sum_{h=0}^{\bar{h}} \left(\sum_{j=0}^{g} q_{h,j} \partial_1^j \partial_2^{g-j} f \right)^2 dS, \quad q_{h,j} \in \mathbb{R}, \tag{4.12}$$

for some $g \in \mathbb{N}$.

The Euler-Lagrange equation

The Euler-Lagrange equation is a differential equation whose solutions are the functions for which a given functional is stationary. A differentiable functional is stationary at its local maxima and minima. So, the Euler-Lagrange equation is useful for solving optimization problems in which one seeks a function minimizing (or maximizing) some given functional. For an introduction we refer the reader to the classical *Methods of Mathematical Physics* by D. Hilbert and R. Courant [7].

Suppose we have some real-valued function

$$L(x_1, x_2, y, y_{1,0}, y_{0,1}, \ldots, y_{0,n}, \ldots, y_{n,0})$$

with continuous n-th derivatives. We want to find the function $f \in C^n(\mathbb{R}^2, \mathbb{R})$ that minimizes

$$\int_\Theta L(x_1, x_2, f, \partial_1 f, \partial_2 f, \ldots, \partial_1^0 \partial_2^n f, \ldots, \partial_1^n \partial_2^0 f) d(x_1, x_2). \tag{4.13}$$

With

$$y_{i,j} := \frac{\partial^{i+j} f}{(\partial x)^i (\partial y)^j}$$

the Euler-Lagrange equation of (4.13) then is

$$\begin{aligned} &\frac{\partial L}{\partial f} - \left(\frac{\partial}{\partial x_1} \left(\frac{\partial L}{\partial y_{1,0}} \right) + \frac{\partial}{\partial x_2} \left(\frac{\partial L}{\partial y_{0,1}} \right) \right) \\ \ldots + (-1)^n &\left(\frac{\partial^n}{\partial x_1^n \partial x_2^0} \left(\frac{\partial L}{\partial y_{n,0}} \right) + \ldots + \frac{\partial^n}{\partial x_2^0 \partial x_2^n} \left(\frac{\partial L}{\partial y_{0,n}} \right) \right) = 0. \end{aligned}$$

Returning to our quadratic forms (4.12), suppose the degree of homogeneity is $g \geq 2$. L depends on $y_{g-0,0}, y_{g-1,1}, \ldots, y_{0,g}$ only, but not on $y_{i,j}$ with $i+j \neq g$. Consequently, all $\frac{\partial L}{\partial y_{i,j}}, i+j \neq g$, vanish, and all $\frac{\partial L}{\partial y_{i,j}}, i+j = g = n$, are constants. Applying $\frac{\partial^g}{\partial x_1^{g-j} \partial x_2^j}, j \in \{0, \ldots, g\}$, to the latter also turns these to zero. The Euler-Lagrange equation simply is not very yielding if the Lagrange function L is a quadratic polynomial depending only on derivatives of order two or higher.

In practice, quadratic forms on first derivatives, that is $g = 1$, do fail to produce good results. In particular, they do not yield quadratic precision.

Sufficient conditions for invariance under Euclidean motions

A sufficient condition for (4.9) is that

$$\sum_{h=0}^{\bar{h}} \left(\sum_{j=0}^{g} q_{h,j} (\partial_1^j \partial_2^{g-j} f) \circ r \right)^2 = \sum_{h=0}^{\bar{h}} \left(\sum_{j=0}^{g} q_{h,j} \partial_1^j \partial_2^{g-j} (f \circ r) \right)^2, \qquad (4.14)$$

holds for any rotation or reflection $r : \mathbb{R}^2 \to \mathbb{R}^2$. The term within the brackets on the left-hand side is the integrand in the definition of $\boldsymbol{Q}$, evaluated at r.

(4.14) is easily achieved (or verified) for any reflection, say $y \mapsto -y$. From this point on, rotation-invariance is sufficient to imply invariance under all reflections of $\mathbb{R}^2$. Therefore, we restrict ourselves to the study of rotation invariance now.

Invariance under Euclidean motions guarantees both flip- and shift-invariance but is independent from valency. This leads to a consistent extension across valencies, which may ease a designer's work. Additionally, it should allow stationary subdivision matrices, or cappings, to be parametrized by segment and valency, in the same way as the mask by which the new extraordinary point in the Catmull-Clark setting is calculated.

As in previous sections, it is preferable to consider polynomials instead of bivariate derivatives. Let g be the degree of our homogeneous quadratic form. A basis for the polynomials of degree g in $\mathbb{R}[X, Y]$, whose elements are homogeneous, is $\beta_0, \ldots, \beta_g$,

$$\beta_{2j_1+j_0}(X,Y) := \begin{cases} \Re\left((X+iY)^{j_1}(X-iY)^{g-j_1}\right) & , \text{ if } j_0 = 0 \wedge 2j_1 + j_0 < g \\ \Im\left((X+iY)^{j_1}(X-iY)^{g-j_1}\right) & , \text{ if } j_0 = 1, \\ (X+iY)^{g/2}(X-iY)^{g/2} & , \text{ if } g \text{ even } \wedge 2j_1 + j_0 = g. \end{cases}$$

For example, for $g = 2$ it is

$$\beta_0 = X^2 - Y^2,\ \beta_1 = 2XY,\ \beta_2 = X^2 + Y^2.$$

With $c^{(0)} := [c_0^{(0)}; \ldots; c_g^{(0)}] \in \mathbb{R}^{(g+1)\times 1}$ consider

$$F(x,y) = \sum_{j=0}^{g} c_j^{(0)} \beta_j (x - x_0, y - y_0).$$

Let R_γ be the matrix which rotates row-vectors from $\mathbb{R}^{1\times 2}$ by the angle γ. If we set $(x, y) =: (\tilde{x}, \tilde{y})R_\gamma$, $(x_0, y_0) =: (\tilde{x}_0, \tilde{y}_0)R_\gamma$, by virtue of linearity of R_γ, there are $c^{(\gamma)} := [c_0^{(\gamma)}; \ldots; c_g^{(\gamma)}] \in \mathbb{R}^{(g+1)\times 1}$ such that

$$F(x, y) = \sum_{j=0}^{g} c_j^{(\gamma)} \beta(\tilde{x} - \tilde{x}_0, \tilde{y} - \tilde{y}_0) = F((\tilde{x}, \tilde{y})R_\gamma).$$

It is easy to see that $c^{(\gamma)}$ and $c^{(0)}$ are related by

$$c^{(\gamma)} = M_\gamma c^{(0)}, \tag{4.15}$$

where

$$M_\gamma := \begin{cases} \mathrm{diag}(R_{\gamma(g-0)}, R_{\gamma(g-2)}, \ldots, R_{\gamma\cdot 2}, 1) & , \text{ if } g \text{ is even,} \\ \mathrm{diag}(R_{\gamma(g-0)}, R_{\gamma(g-2)}, \ldots, R_{\gamma\cdot(-1)}) & , \text{ if } g \text{ is odd.} \end{cases}$$

Hence, we have

Lemma 4.5. *For odd g there is no linear operator composed solely of g-th derivatives that is invariant under all rotations. For even g, there is exactly one up to scaling, which is the $(g/2)$-th power of the Laplacian.*

Proof. By linear independence of the functions

$$\begin{aligned} &\{\gamma \mapsto \cos(\gamma(g - 2j)) : \ j \in \{0, 1, \ldots, \lfloor \frac{g}{2} \rfloor\}\} \\ &\cup \{\gamma \mapsto \sin(\gamma(g - 2j)) : \ j \in \{0, 1, \ldots, \lfloor \frac{g}{2} \rfloor\}\} \end{aligned} \tag{4.16}$$

and (4.15) there is exactly one linear operator composed exclusively of g-th derivatives for even degree, and none for odd degree. The Laplacian is invariant under rotations. By induction, $\triangle^{g/2}$ follows to exhibit that property, too. Therefore, up to scaling, $\triangle^{g/2}$ has to be the linear differential operator of degree g that is invariant under rotations of the domain. □

The analysis becomes more complex if we solely require the square of the value of the functional to be invariant under rotation:

Theorem 4.6. *Let z be a vector of coefficients with respect to the basis $\beta_0, \dots, \beta_g$. Then the real-valued, symmetric*[8] *quadratic forms $z^T N z$ which are invariant under all rotations are exactly given by*

$$N = \left[\begin{array}{ccc|c} \kappa_0 I_2 & 0 & 0 & 0 \\ 0 & \ddots & 0 & 0 \\ 0 & 0 & \kappa_{\frac{g}{2}-1} I_2 & 0 \\ \hline 0 & 0 & 0 & \kappa_{\frac{g}{2}} \end{array}\right], \kappa_0, \dots, \kappa_{\frac{g}{2}} \in \mathbb{R}, \quad \textit{if } g \textit{ is even.}$$

$$N = \begin{bmatrix} \kappa_0 I_2 & 0 & 0 \\ 0 & \ddots & 0 \\ 0 & 0 & \kappa_{\lfloor \frac{g}{2} \rfloor} I_2 \end{bmatrix}, \kappa_0, \dots, \kappa_{\frac{g-1}{2}} \in \mathbb{R}, \quad \textit{if } g \textit{ is odd.}$$

(The quadratic form is semi-positive if and only if all $\kappa_j \geq 0$).

Proof. If $N^{(1)}, N^{(2)}$ are real-valued, symmetric quadratic forms with

$$z^T N^{(1)} Z = z^T N^{(2)} z, \quad z \in \mathbb{R}^{m \times 1}$$

then

$$z^T (N^{(1)} - N^{(2)}) z = 0 \tag{4.17}$$

for all $z \in \mathbb{R}^{m \times 1}$. Further, $(N^{(1)} - N^{(2)})$ is real-valued and symmetric, too. Hence, there is an orthonormal basis such that the representation of $(N^{(1)} - N^{(2)})$ is diagonal. It follows from (4.17) that all entries on its diagonal are zero. Thus, $(N^{(1)} - N^{(2)}) = 0$, i.e. $N^{(1)} = N^{(2)}$.

Returning to our current problem, we conclude that

$$M_\gamma^T N M_\gamma = N, \quad \gamma \in \mathbb{R}.$$

We partition N into blocks $N_{i,j}$, $i, j \in \{0, \dots, \lfloor g/2 \rfloor\}$ corresponding to the size of the blocks on the diagonal of M_γ. Block (i, j) of $M_\gamma^T N M_\gamma$ calculates to

$$R_{\gamma(g-i)}^T N_{i,j} R_{\gamma(g-j)} \stackrel{!}{=} N_{i,j}.$$

The equation is equivalent to

$$N_{i,j} R_{\gamma(g-j)} - R_{\gamma(g-i)} N_{i,j} = 0.$$

[8]Note that non-symmetric quadratic forms $z^T N z$ can be transformed into symmetric ones, by $z^T (N^T + N) z / 2$.

We claim that

$$i = j \wedge 0 \leq i < \frac{g}{2} \implies N_{i,j} = \begin{bmatrix} \kappa_i & 0 \\ 0 & \kappa_i \end{bmatrix},\ \kappa_i \in \mathbb{R}, \tag{4.18}$$

$$i \neq j \wedge i, j \in \{0, \ldots, \lfloor g/2 \rfloor\} \implies N_{i,j} = 0. \tag{4.19}$$

(4.18) can be verified by simple calculation. With

$$\begin{bmatrix} c_k \\ s_k \end{bmatrix} := \begin{bmatrix} \cos(\gamma(g-k)) \\ \sin(\gamma(g-k)) \end{bmatrix}, \quad N_{i,j} =: \begin{bmatrix} n_{00} & n_{01} \\ n_{01} & n_{11} \end{bmatrix} \tag{4.20}$$

it is

$$N_{i,i} R_{\gamma(g-i)} - R_{\gamma(g-i)} N_{i,i} = \begin{bmatrix} -2n_{10}s_i & (n_{00}-n_{11})s_i \\ (n_{00}-n_{11})s_i & 2n_{10}s_i \end{bmatrix} \stackrel{!}{=} 0.$$

It follows immediately that $n_{10} = 0$ and $n_{00} - n_{11} = 0$, i.e. $n_{00} = n_{11}$.

For even g, block $N_{g/2,g/2}$ is of size 1×1. It is not included in assertion (4.18) anyway. $N_{g/2,g/2}$ can be any single real number $\kappa_{\frac{g}{2}}$ in that case, as asserted in the theorem.

We prove (4.19) by distinguishing two cases:

Case 1. Suppose g is even and either $i = g/2$, or $j = g/2$ but $i \neq j$. Linear independence of the functions in (4.16) implies $N_{i,j} = 0$.

Case 2. Let $i \neq j \wedge 0 \leq i, j < g/2$. Identifying $\mathbb{R}^{2\times 2} \cong \mathbb{R}^4$, we find that the matrix of the linear mapping

$$\hat{H}^{i,j,\gamma}(N_{i,j}) := N_{i,j} R_{\gamma(g-j)} - R_{\gamma(g-i)} N_{i,j},$$

is given by

$$H^{i,j,\gamma} = \begin{pmatrix} c_j - c_i & -s_j & -s_i & 0 \\ s_j & c_j - c_i & 0 & -s_i \\ s_i & 0 & c_j - c_i & -s_j \\ 0 & s_i & s_j & c_j - c_i \end{pmatrix}. \tag{4.21}$$

$H^{i,j,\gamma}$ operates on column-vectors $[n_{00}; n_{01}; n_{10}; n_{11}]$, defined as in (4.20); the c_k, s_k are also from (4.20). Trigonometric identities simplify the determinant of $H^{i,j,\gamma}$ to

$$\det H^{i,j,\gamma} = 4\left(\cos(\tilde{i}\gamma) - \cos(\tilde{j}\gamma)\right)^2, \quad \begin{bmatrix} \tilde{i} \\ \tilde{j} \end{bmatrix} := \begin{bmatrix} g-i \\ g-j \end{bmatrix}$$

Hence,

$$\det H^{i,j,\gamma} = 0 \Leftrightarrow \cos(\tilde{i}\gamma) - \cos(\tilde{j}\gamma) = 0.$$

$\tilde{i} \neq \tilde{j}$ and linear independence of the trigonometric polynomials now yield regularity of $H^{i,j,\gamma}$ for almost all $\gamma \in \mathbb{R}$. We can simply choose one such γ_0. Because $\hat{H}^{i,j,\gamma_0}$ is linear and injective, it follows that

$$\hat{H}^{i,j,\gamma_0}(N_{ij}) = 0 \Leftrightarrow N_{ij} = 0,$$

i.e. $N_{ij} = 0$, as claimed in (4.19).

The calculations can be found in the MATHEMATICA-notebook

`QFs_invariant_under_rotations-Theorem.nb`.

□

If we prefer the quadratic form to be defined on the vector of partial derivatives $\widetilde{z}$ instead, the transformation matrices T_g that produce

$$z = T_g \widetilde{z}, \quad \widetilde{z} = \begin{bmatrix} \partial_1^0 \partial_2^g f \\ \vdots \\ \partial_1^g \partial_2^0 f \end{bmatrix} \tag{4.22}$$

are listed in Table 4.1 on page 128 for $g \in \{1, \ldots, 4\}$. Their calculation, as well as a further verification that the quadratic forms of Theorem 4.6 are invariant under rotations, can be found in the attached MATHEMATICA-notebook

`QFs_invariant_under_rotations.nb`.

For example, for $g = 2, 3$ the quadratic forms $\widetilde{z}^T \tilde{N} \widetilde{z}$ that are invariant under rotation are given by

$$\begin{aligned} g = 2 &: \kappa_0 \left((\partial_1^2 f - \partial_2^2 f)^2 + (2\partial_1 \partial_2 f)^2 \right) + \kappa_1 (\partial_1^2 f + \partial_2^2 f)^2, \\ g = 3 &: \kappa_0 \left((\partial_1^3 f - 3\partial_1 \partial_2^2 f)^2 + (3\partial_1^2 \partial_2 f - \partial_2^3 f)^2 \right) \\ &\quad + \kappa_1 \left((3\partial_1^3 f + 3\partial_1 \partial_2^2 f)^2 + (3\partial_1^2 \partial_2 f + 3\partial_2^3 f)^2 \right), \end{aligned} \tag{4.23}$$

where $\kappa_0, \kappa_1 \in \mathbb{R}$ (cf. Table 4.1 and Theorem 4.6). In particular, there are now solutions when the degree is odd, in contrast to the situation for linear operators (cf. Lemma 4.5).

g	T_g
1	$\begin{pmatrix} 1 & 0 \\ 0 & 1 \end{pmatrix}$
2	$\begin{pmatrix} 1 & 0 & -1 \\ 0 & 2 & 0 \\ 1 & 0 & 1 \end{pmatrix}$
3	$\begin{pmatrix} 1 & 0 & -3 & 0 \\ 0 & 3 & 0 & -1 \\ 3 & 0 & 3 & 0 \\ 0 & 3 & 0 & 3 \end{pmatrix}$
4	$\begin{pmatrix} 1 & 0 & -6 & 0 & 1 \\ 0 & 4 & 0 & -4 & 0 \\ 4 & 0 & 0 & 0 & -4 \\ 0 & 8 & 0 & 8 & 0 \\ 3 & 0 & 6 & 0 & 3 \end{pmatrix}$

Table 4.1: Transformation matrices T_g for equation (4.22). T_g allows to calculate the vector z of coefficients of $\beta_0, \ldots, \beta_g$ from its vector $\tilde{z}$ of g-th derivatives, $z = T_g \tilde{z}$.

4.4 Implementation of the extension

In this section we describe the most important techniques we used in our implementation in MATLAB.

To calculate the extention of the generating splines on a computer, one must use a function space of finite dimension,

$$\mathcal{S} = \{\mathrm{pw}\left(\mathrm{pw}(\sum_{k=0}^{\bar{k}} x_k^{(m)} b_k^0 \circ (2^{-m}\cdot)_{|\mathbf{S}_n^m} : \quad m = 0, \ldots, \sharp r - 1),\right.$$
$$\left.\sum_{g=0}^{2}\sum_{k=0}^{g} x_k^{(\sharp r)} \left((\chi_1)^k (\chi_2)^{2-k}\right)_{|2^{-\sharp r}\mathbf{S}_n}\right) :$$
$$x_{\mathcal{I}}^{(m+1)} = S x^{(m)} \text{ for all } m = 0, \ldots, \sharp r - 1,\ M x^{(\sharp r)} = x^{(\sharp r - 1)}\}. \quad (4.24)$$

Our functions space consists of $\sharp r$ *spline rings*

$$x_k^{(m)} b_k^0 \circ (2^{-m}\cdot)_{|\mathbf{S}_n^m}, m = 0, \ldots, \sharp r - 1,$$

and a *cap*

$$\sum_{g=0}^{2}\sum_{k=0}^{g} x_k^{(\sharp r)}\left((\chi_1)^k(\chi_2)^{2-k}\right)_{|2^{-\sharp r}\mathbf{S}_n},$$

where only polynomials that are quadratic in χ_1, χ_2 are allowed. The remaining parameters are

m**:** a ringindex in the range of $0 \dots \sharp r - 1$, and $\sharp r$ to denote the cap[9].

$b_k^0 \circ (2^{-m}\cdot)_{|\mathbf{S}_n^m}$**:** one of the $\bar{k}+1$ functions of the generating rings which have been re-parametrized to $\mathbf{S}_n^m$.

$x^{(m)}$**:** the column vector of coefficients $x_0^{(m)}, \dots, x_{\bar{k}}^{(m)}$ for ring m.

$\mathcal{I}$**:** the indices $\subset \{0, \dots, \bar{k}\}$ of those coefficients that are inherited as a linear combination of a previous ring's coefficients.

S**:** $Sx^{(m)}$ gives exactly those coefficients of ring $m+1$ that are produced from the C^2 constraints of the preceding ring's coefficients.

M**:** is a matrix whose columns contain the coefficients of the monomials $\chi_1^j \chi_2^{g-j}, 0 \le j \le g$, for the cap.

If the differential operator is constructed solely of derivatives of degree three and higher, the integrand $f \circ \chi^{-1}$ is zero on $\lambda^{\sharp r}\Theta$ for all $f \in \mathcal{S}$. Otherwise, we might take any of three options:

1. Calculate the integral from the one on a single Θ^m and the geometric series, leveraging $\lambda^m \mathbf{S}_n = \Theta^m \cup (\lambda^{m+1}\Theta)$,
2. Since the number of rings will be reasonably large, usually, simply omit that part of the domain stemming from $\lambda^{\sharp r}\Theta$, or
3. Use some numeric integration techniques on the domain $\lambda^{\sharp r}\Theta$.

For $\boldsymbol{Q}(f, \mathcal{D}) = \int_{\mathcal{D}} (\triangle\ f)^2 \mathrm{d}X$, where $\triangle$ is the Laplacian, we replaced the monomials of degree two by the linear combinations

$$\chi_1^2 - \chi_2^2,\ \chi_1\chi_2, \quad \chi_1^2 + \chi_2^2.$$

[9]Note that in this section, the C^k conditions are at $\partial\mathbf{S}_n$ and the first spline ring of the extension is $\mathbf{S}_n^0$, not $\mathbf{S}_n^1$ as in Section 4.3.

Their images under the Laplacian are given by the constants $0, 0, 4$. This makes $\chi_1^2+\chi_2^2$ the only function whose integrand does not turn to zero on the cap. With the geometric series we can then easily calculate $\boldsymbol{Q}(\chi_1^2+\chi_2^2, \lambda^{\sharp r}\Theta)$ from its value on a single ring.

Numerical integration on a single ring

Let us assume that we have a homogeneous quadratic form

$$\boldsymbol{Q}(f, \mathcal{D}) := \int_{\mathcal{D}} \sum_{h=0}^{\bar{h}} \left(\sum_{j=0}^{g} q_{h,g,j} \partial_1^j \partial_2^{g-j} f \right)^2, \quad q_{h,j} \in \mathbb{R},\ \mathcal{D} \subset \mathbb{R}^2,$$

as discussed in Section 4.3. From Section 4.3 we know that

$$\boldsymbol{Q}(\cdot, \Theta^m) = \lambda^{2gm} \boldsymbol{Q}(\cdot, \Theta^0), \quad m \in \mathbb{N}. \tag{4.25}$$

Therefore, we only have to describe how $\boldsymbol{Q}$ is calculated on Θ^0.

Every segment of a spline ring can be partitioned into boxes

$$[\underline{s}, \overline{s}],$$

with $[\underline{s}, \overline{s}] \times \mathbb{Z}_n \subset \mathbf{S}_n$, such that the restriction of the ring to that box is a polynomial. The total number of pieces is usually small; for instance, L-domains with $\lambda = 1/2$ possess 12 pieces per segment.

The integral within $\boldsymbol{Q}$ on such a subdomain $\chi([\underline{s}, \overline{s}], j_0)$ can be turned into an integral on $[\underline{s}, \overline{s}]$ with the aid of the Transformation Theorem. Since $\boldsymbol{Q}$ is homogenous, we have

$$\int_{\chi([\underline{s},\overline{s}],j_0)} \sum_{h=0}^{\bar{h}} \left(\sum_{j=0}^{g} q_{h,j} \partial_1^j \partial_2^{g-j} \left[B^0 \circ \chi^{-1} \right] x^{(m)} \right)^2 \mathrm{d}X$$
$$= \sum_{h=0}^{\bar{h}} \int_{[\underline{s},\overline{s}]\times\{j_0\}} \left(\hat{B}_h x^{(m)} \right)^2 \mathrm{d}s, \tag{4.26}$$

with the row-vectors

$$\hat{B}_h := \sqrt{\det D\chi} \sum_{j=0}^{g} q_{h,j} \left[\partial_1^j \partial_2^{g-j} \left[B^0 \circ \chi^{-1} \right] \right] \circ \chi.$$

The attached MATLAB-routine `Derivatives_f_circ_chiInv` allows to evaluate the terms $\left[\partial_1^j \partial_2^{g-j} \left[B^0 \circ \chi^{-1}\right]\right] \circ \chi$ within $\hat{\bar{B}}_j$ comfortably. See Section 4.2 for more details.

A well known quadrature is

Remark 4.7 (Gaussian quadrature). Let $s_1, \ldots, s_{\widetilde{n^2}} \subseteq [\underline{s}, \overline{s}]$ be the sampling points, $w_1, \ldots, w_{\widetilde{n^2}}$ the weights of the Gaussian quadrature. Then it is

$$\begin{aligned} \int_{[\underline{s},\overline{s}]} \left[\sum_{j=0}^{\bar{j}} f_j(z) x_j\right]^2 \mathrm{d}z &\approx |Fx|_2^2, \\ F = W\tilde{F}, \quad x &= [x_0; \ldots; x_{\bar{j}}], \\ \tilde{F}_{i,j} := f_j(s_i), \quad W &= \operatorname{diag}(\sqrt{w_1}, \ldots, \sqrt{w_{n^2}}) \end{aligned}$$

(the weights w_j are non-negative). This rule of quadrature is exact for all integrands that are polynomials of order $2\widetilde{n}$.

Applying this technique here yields

$$\int_{[\underline{s},\overline{s}]\times\{j_0\}} \left(\hat{B}_h x^{(m)}\right)^2 \mathrm{d}s \approx \left|F^{(h)} x^{(m)}\right|_2^2$$

where

$$F^{(h)} := W \begin{bmatrix} \hat{B}_h(s_1) \\ \vdots \\ \hat{B}_h(s_{\widetilde{n^2}}) \end{bmatrix}.$$

Thus, we arrive at

$$\begin{aligned} \boldsymbol{Q}(f, \chi([\underline{s}, \overline{s}] \times \{j_0\})) &\approx \left|F^{([\underline{s},\overline{s}]\times\{j_0\})} x^{(m)}\right|_2^2, \\ F^{([\underline{s},\overline{s}]\times\{j_0\})} &:= \begin{bmatrix} F^{(0)} \\ \vdots \\ F^{(\bar{h})} \end{bmatrix}. \end{aligned}$$

The order $\widetilde{n}$ used in the Gaussian quadrature should be high enough for the integral to be exact on polynomials of the order n of the splines. The factor $\det D\chi$ has been observed to be unproblematic, χ^0 is almost an affine-linear function usually. An integration order of six proved sufficient.

Minimizing the quadratic functional

Stacking the $F^{([\underline{s},\overline{s}]\times\{j\})}$ of all polynomial pieces $[\underline{s},\overline{s}]\times\{j\}$ of the m-th ring rowwise within a single matrix $\tilde{F}_m$ finally produces

$$\boldsymbol{Q}(f,\Theta^m) \approx |\tilde{F}_m x^{(m)}|_2^2.$$

Putting all $\tilde{F}_m$ and the corresponding $\tilde{F}_{\sharp r}$ which belongs to the cap into a matrix F, all coefficients $x^{(0)},\ldots,x^{(\sharp r)}$ into the vector x yields

$$\boldsymbol{Q}(f,\Theta) \approx |Fx|_2^2.$$

Numeric tests using adaptive quadrature rules confirmed the values in the Gramnian F^TF to be very close to machine precision. Using these adaptive techniques leads, however, to much longer computation times, as well as numeric issues. The condition number of F^TF is roughly the square of that of F.

With terms from (4.24), the constraints are

$$\begin{gathered} x_{\mathcal{I}}^{(m+1)} = Sx^{(m)} \text{ for all } m = 0,\ldots,\sharp r-1, \\ Mx^{(\sharp r)} = x^{(\sharp r-1)}. \end{gathered}$$

Thus, x is given by some $\tilde{x}$,

$$x = R\tilde{x},$$

for some reduction matrix R constructed of blocks S, M and the identity. On the subspace of control points that are free of C^2 constraints, R acts as the identity. By including a permutation to R, if necessary, we may assume $\tilde{x} = [\tilde{x}_0;\tilde{x}_1]$. Here, $\tilde{x}_0$ are the input coefficients given by the C^2 constraints on ring zero, while $\tilde{x}_1$ contains all those that are still free. Denote the corresponding blocks of R by R_0, R_1.

Theoretically, one can solve the resulting least-squares problem,

$$|FR\begin{bmatrix}\tilde{x}_0\\ \tilde{x}_1\end{bmatrix}|_2^2 = |FR_0\tilde{x}_0 + FR_1\tilde{x}_1|_2^2$$

via the normal equation,

$$\tilde{x}_1 = -\left(R_1^TF^TFR_1\right)^{-1}R_1^TF^TFR_0\tilde{x}_0.$$

However, this is a cardinal sin numerical-wise. Additionally, the sparse structure of FR that we have here is destroyed, vastly increasing memory requirements. It is therefore better to calculate $\tilde{x}_1$ from a QR- or singular-value decomposition. In MATLAB, this can be done automatically with

$$\tilde{x}_1 = -(FR_1)\backslash FR_0\tilde{x}_0.$$

Using $\tilde{x}_0 = \mathrm{id}$ produces the operator to compute $\tilde{x}_1$ from any $\tilde{x}_0$. Note that the extension depends only on those control points of the previous spline ring which enter the C^2 constraints.

4.5 Results

In this section we show the extensions of various spline rings under the differential operators given in Theorem 4.6. We will briefly discuss some key data of the extensions of the generating rings. Of course, the extension depends continuously on the parameters κ_j of the differential operator used. It seems that the differential operators lead to different extensions (as indicated by the selected key data).

In the calculations, we typically use $\sharp r \approx 10$ spline rings before capping the surface. For differential operators of degree 2, it is possible to go as high as $\sharp r \approx 20$ if the valency is not too large. This is due to the fact that weighting of coefficients of the spline rings toward the center is not as strong as for degree three; cf. (4.25). Consequently, the underlying linear systems in general have smaller (numeric) condition numbers for lower degrees.

Although it is of course possible to calculate extensions for the Catmull-Clark setting with degree raised to six or seven, it is preferable to have subdominant eigenvalue $\lambda = 1/2$. All examples shown in the following are based on subdivision algorithms with characteristic maps to $\lambda = 1/2$.

Differential operators of degree 3

If our differential operator is of degree three or higher, all polynomials that are quadratic in χ_1, χ_2 lie in its kernel. Hence, they are extended by themselves, and the subdivision matrices derived from them have quadratic precision automatically.

Three example surfaces

Figures 4.2–4.4 show three sample surface-rings that have been extended by the differential operator (4.23), $(\kappa_0, \kappa_1) = (0, 1)$. In the first example, the spline ring might be given by the corner of some house joining the ground; the valency of the extraordinary point is $n = 3$. From the vertical edge of the wall, as well as the two horizontal edges where they meet the ground, one would expect the surface to be of hyperbolic shape at the extraordinary point. See Figure 4.2 on page 135 for how the extension turns out.

The second example is presented in Figure 4.3 on page 136. The initial surface ring is a multi-saddle here: the number of local maxima/minima, circularwise, is four. This is difficult to extend inwardly, because for a C^2 extension, spline rings near the extraordinary point must only have two local maxima. (The local graph at the extraordinary point has to be a quadratic form with the main curvatures as eigenvalues.)

The third example shows the extension of an initial ring with convex shape and which has been modelled by relatively high valency, $n = 16$. Notice that the layout of knot intervals is visible in the Gaussian curvature plot of the initial ring, cf. Figure 4.4 on page 137. Clearly, that ring is lacking in surface quality. Its curvature tends to be high at the knot lines, even points where it is negative exist. In the extension, curvature is quickly smoothed out, and is distinctly positive at the extraordinary point. No points with negative Gaussian curvature occur in the extension of the surface.

Extensions of the generating rings

First, recall from Section 4.4 that only those generating rings, for which not all of the derivatives of bi-degree ≤ 2 vanish at $2^{-1}\partial\mathbf{S}_n$, enter the extension. Therefore, only the three innermost rings of B-splines have non-zero extensions.

Figures 4.9–4.11 at the end of the section, on page 143, show the extensions of the degree raised, cubic B-splines. We present these here for the reasons given in 2.4. Although negative values of small magnitude are attained, too, the extensions seem to do quite fine.

Generator splines of the full spline space (order seven) can be found in Figures 4.12–4.16, on page 146. It can be observed that the magnitude of the negative function values is larger here, compared to the maximum value of the function.

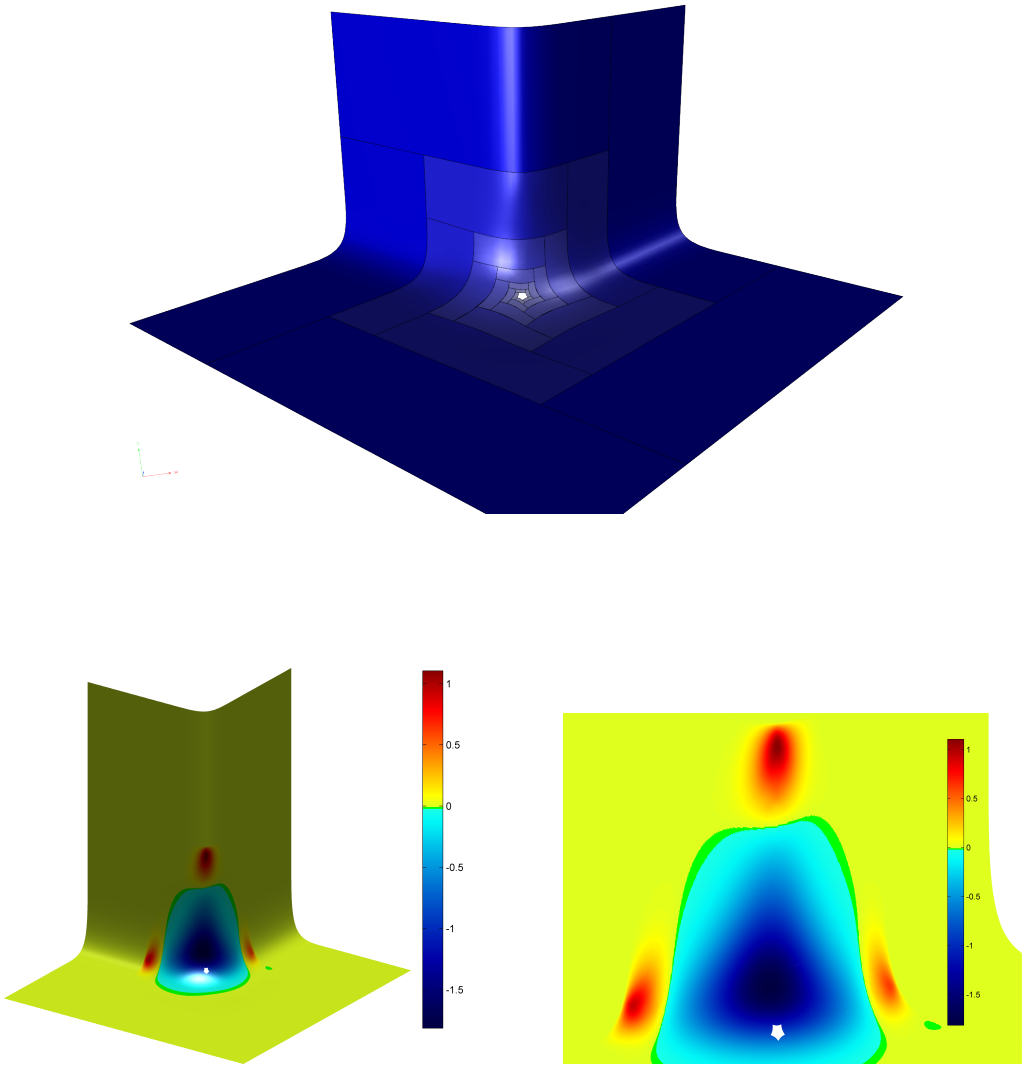

Figure 4.2: Extension of a house corner meeting the ground by a differential operator of degree three. The valency of the extraordinary point is $n = 5$. *Top:* interactive figure with shading of individual spline rings. *Bottom:* the surface colored by Gaussian curvature, which takes only small values from roughly -1.75 to 1.1. To the left, we see the complete surface. As we might expect from the initial spline ring, the surface turns out to be of hyperbolic shape at the extraordinary point (Gaussian curvature< 0). The right-hand side provides a zoomed view. Lighting has been turned off in this image.

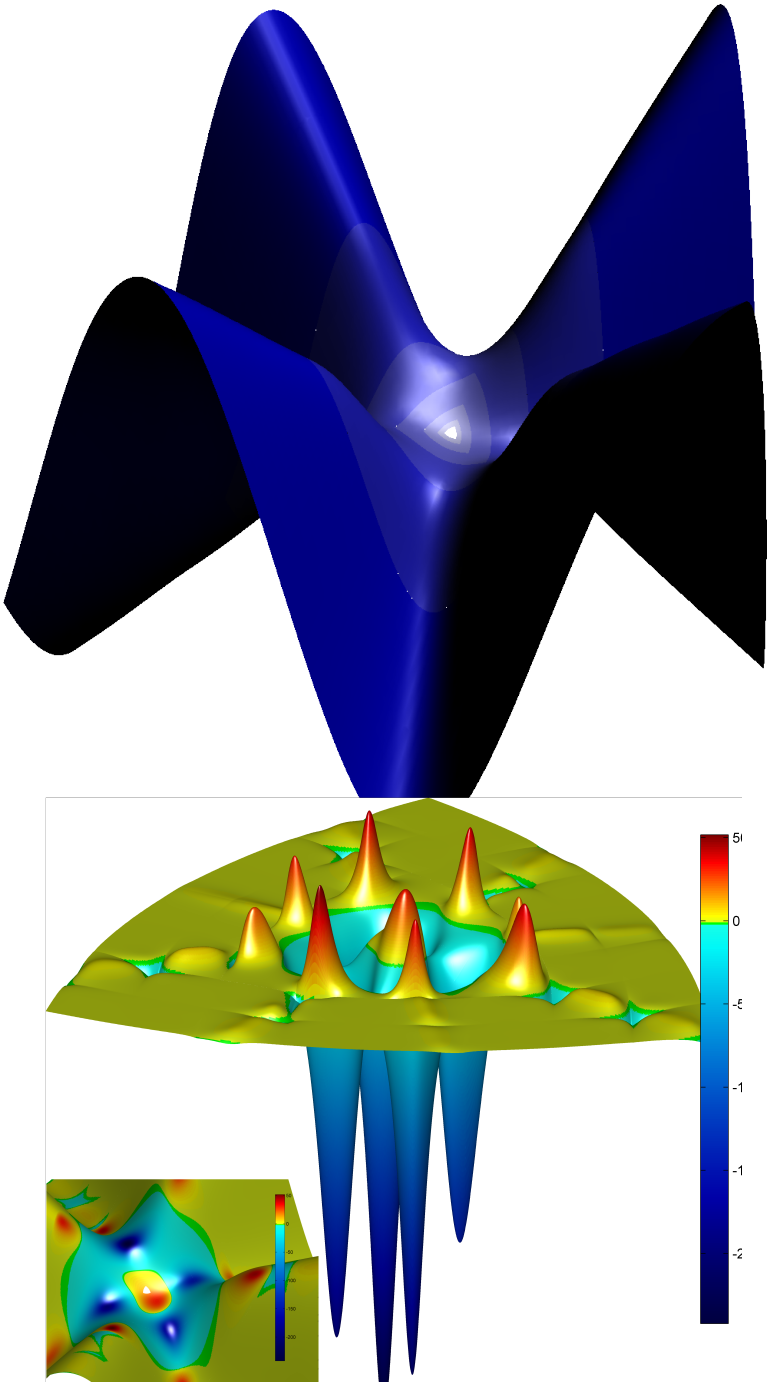

Figure 4.3: Extension of a multi-saddle by a differential operator of degree three. The valency of the extraordinary point is just $n = 3$. *Top:* an interactive figure with shading of individual spline rings. *Bottom:* zoom-in of the surface colored by Gaussian curvature (left-hand side), respectively the surface with z-coordinate replaced by Gaussian curvature (to the right). The surface turns out to be of convex shape close to the extraordinary point (Gaussian curvature> 0, though very close to zero).

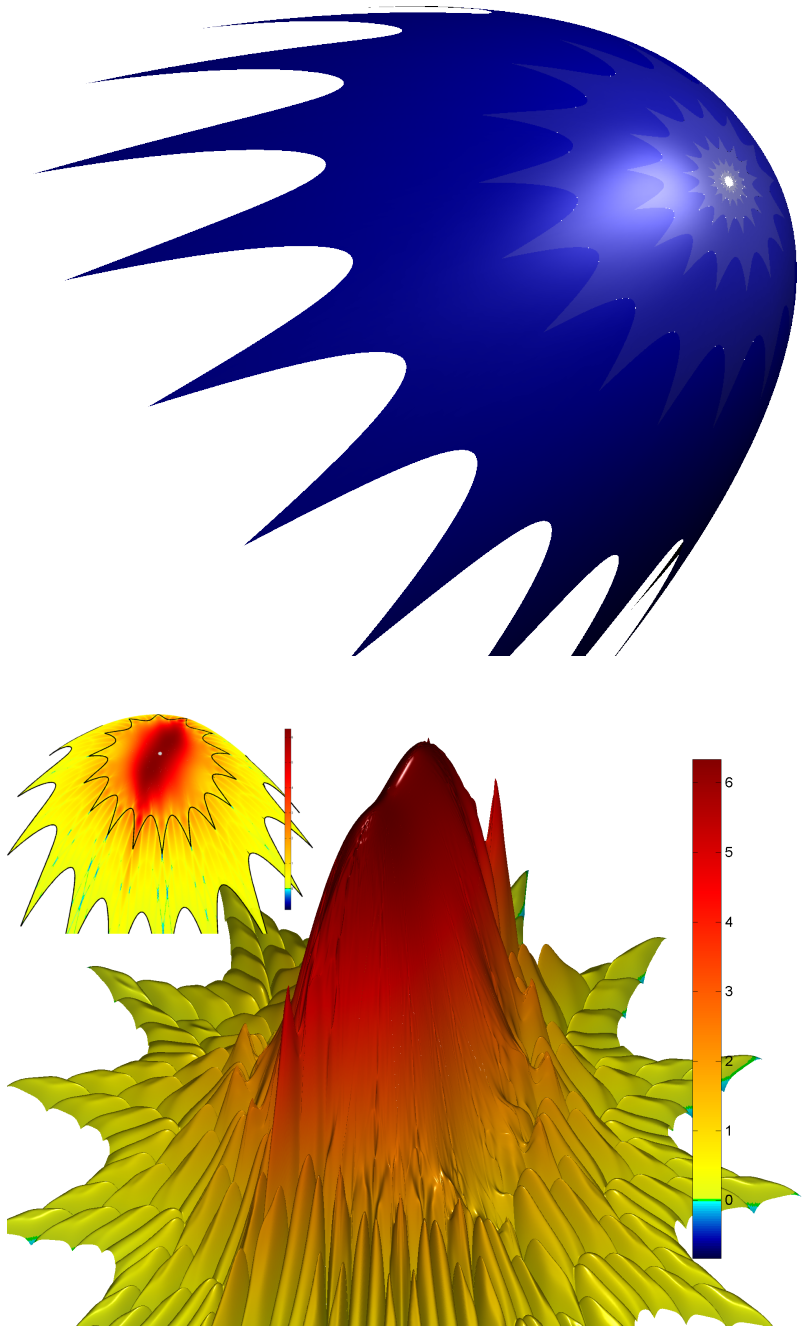

Figure 4.4: With x, y the X-/Y-components of the degree raised characteristic map of valency $n = 16$, we have set the control points of the initial spline ring to $[x,\ y,\ |x|\ .\hat{}\ 1.75 + 1.5 * |y|\ .\hat{}\ 2.2]$. The extension is done by minimizing a differential operator of degree three.
Top: an interactive figure with individual spline rings shaded differently.
Bottom: the surface with its z-coordinate replaced by Gaussian curvature. The small image on the left side shows the surface colored in the same way. The initial ring that we prescribed is highlighted by lines here.

Dependence on differential operator used

For degrees two and three, the quadratic forms given in (4.23) have two parameters, $\kappa_0, \kappa_1 \geq 0$. Since both have to be non-negative, we simply set $\kappa_1 = 1 - \kappa_0$. As Figure 4.5 on page 139 shows by a simple overview of two properties of the generating splines, the extensions do depend on the parameter we use in the differential operator. For example, for $\kappa_0 = 1$ the maximum of the red generating spline is about 10% higher than for $\kappa_0 = 0$. It should be noted that for order eight the maximas are generally slightly larger, too (the maximums of the respective generating B-splines are nearly the same, see Figure 2.11 on page 38).

We preferred our generating splines to have a smaller maximum, so we chose $\kappa_0 = 0$. Still, whether this choice is optimal will have to be revealed by a more detailed examination.

Differential operators of degree 2

For differential operators of degree two, it is not clear beforehand that all quadratic polynomials are extended by themselves. A very promising candidate among these differential operators is the Laplacian:

1. Minimizing the square of its value minimizes tension of the surface.

2. The maximum principle that typically holds for its solutions guarantees non-negative function values for the generating splines. Thus, the surface automatically lies within the convex hull of its control points.

Polynomials $x^i y^j$ of degree $i + j \leq 1$, as well as $x^2 - y^2, xy$ lie within its kernel. $x^2 + y^2$, however, does not: it is mapped by $\triangle$ to the constant function 4. Still, it turns out that the kernel property required by Reif is not necessary: $x^2 + y^2$ is still extended by itself onto the next spline ring. When we take a look at the resulting generator functions, we find that

1. Indeed, they obtain non-negative values only.

2. Their support is smaller than it generally has been for differential operators of degree three.

3. The generating splines look more similar to bi-variate tensor product B-splines.

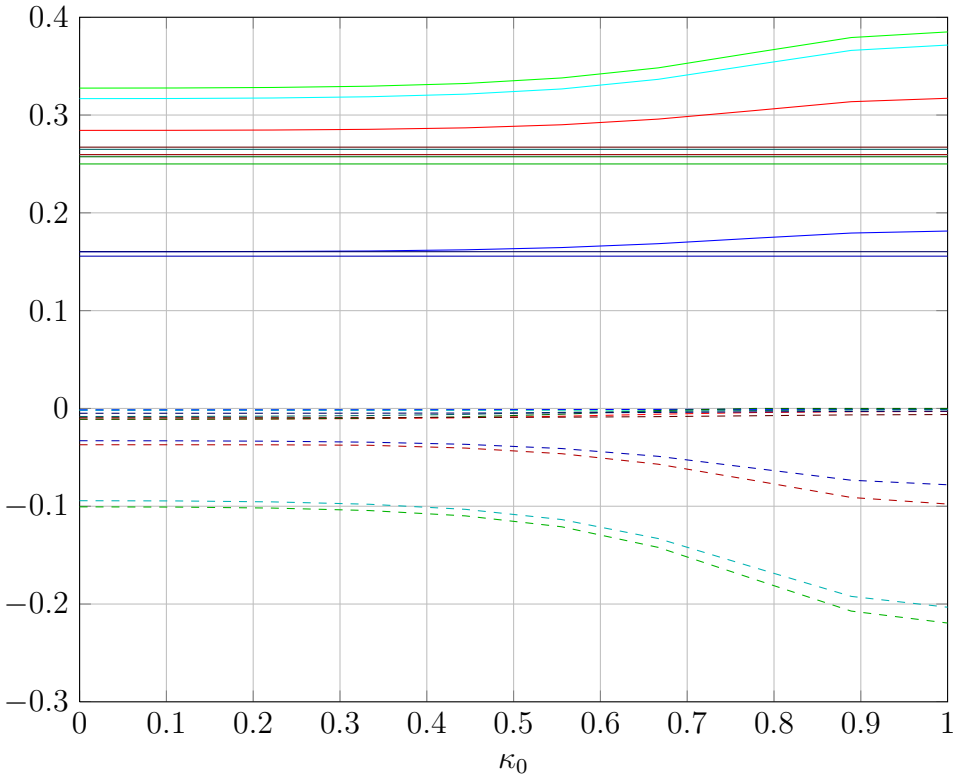

Figure 4.5: Maximas and minimas (dashed) of rings $0, \ldots, 5$ of the generating splines of order seven by parameter κ_0 used for the differential operator of degree three. Colors match the respective control coefficients indicated in Figure 4.12 on page 146.
Note that the generating functions of the second and third rows (towards the center) are descending if we go towards $2^{-1}\partial\mathbf{S}_n$ in $\mathbf{S}_n^0$ (cf. Figures 4.12–4.16). They attain their maximum on ring zero (ring 1 is the first one extended by the quadratic form).

4. However, there is a weird bump in some of the resulting generating splines; cf. Figure 4.6 on page 141.

Aside from the last item, the resulting generating splines were ideal candidates for an extension! Can we get that last issue straight?

Using an extended patch layout

First, extensive consistency checks and a thorough search for an error in our programs all point to the fact that this is, indeed, the correct solution of the minimization problem. We put forth the hypothesis that the finite function space we minimize in might be too small. Using a patch layout as indicated in Figure 4.7 on page 141 seems[10] mostly to remove the bump. However, there are still surfaces exhibiting high variation of curvature at parameters $(s, t, j) \in \mathbf{S}_n$ with $0.75 \leq \max(s, t) \leq 1$, i.e. exactly where we have allowed more flexibility to the surface (cf. Figure 4.7 on page 141). Using the extended function space merely alleviated the problem – it did not remove it.

It turns out that if the extension only has to C^1-connect to the B-splines, without any other additional knots as in the extended layout, there is no bump in the extension. We conclude that the solution of the minimization problem to the Laplacian does not lie in a space of functions that are C^2 everywhere. This is highly unfortunate, but apparently the Laplacian is not suitable to derive C^2 extensions at extraordinary points.

[10] On a historical note, the subdivision surfaces I presented at the *Workshop on Industry Challenges in Geometric Modeling, CAD and Simulation, 2010,* were based on this function space.

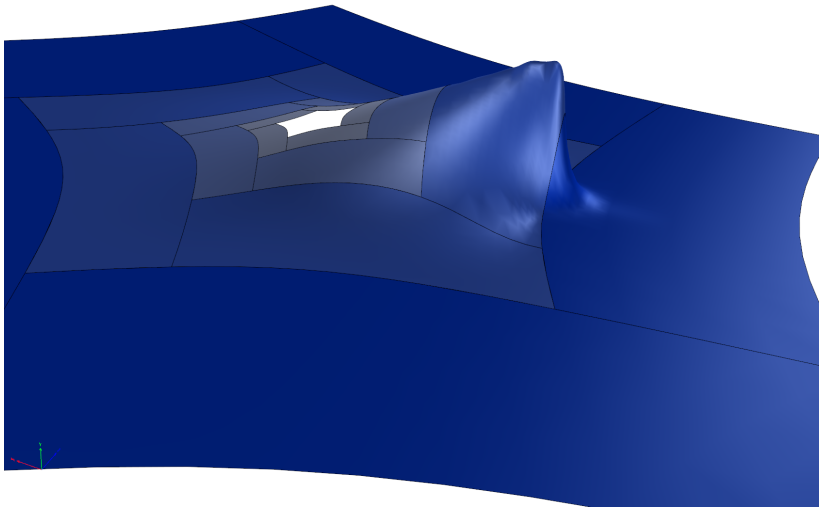

Figure 4.6: The bump in the generating splines when extending by the differential operator $\triangle$ (Laplacian).

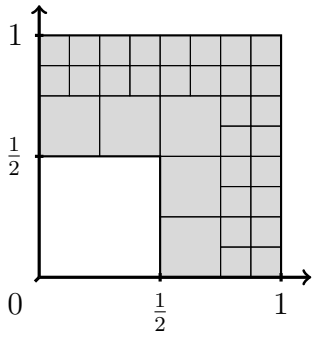

Figure 4.7: To provide more flexibility to the extension by the Laplacian, we increase the number of knot intervals in each spline ring.

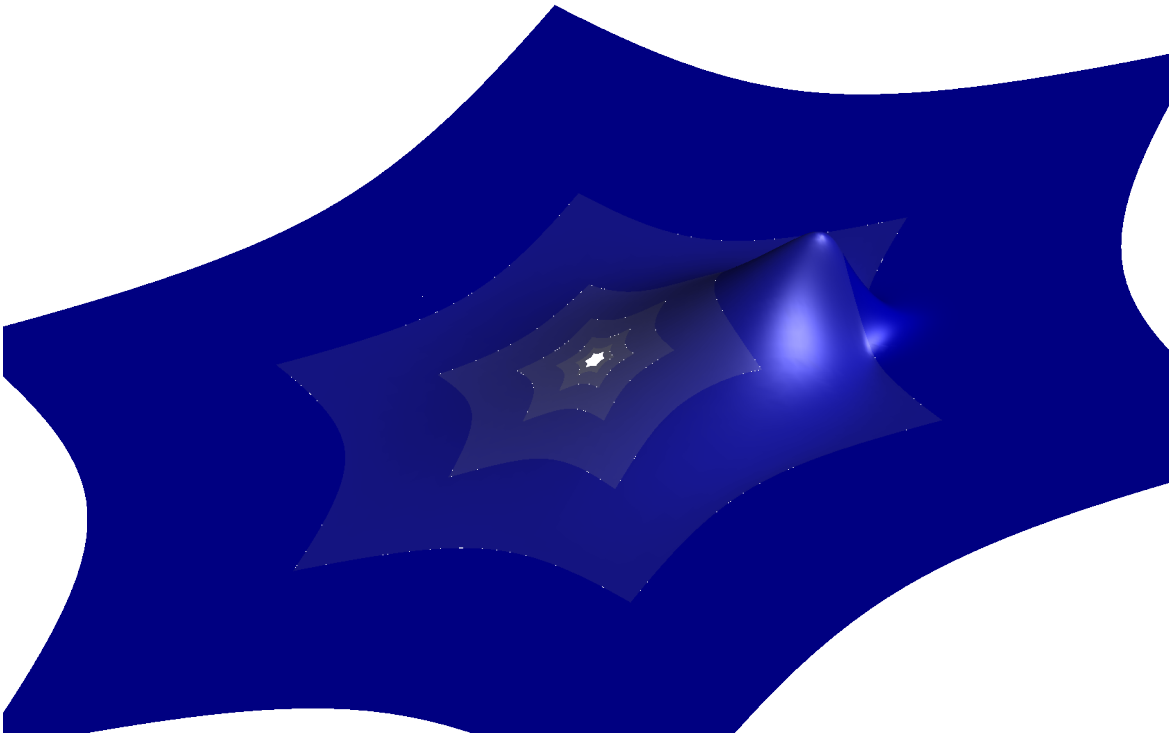

Figure 4.8: The bump in the generating splines when extending by $\triangle$ does not occur if we calculate the extension only under C^1-constraints to the B-splines on the outer ring.

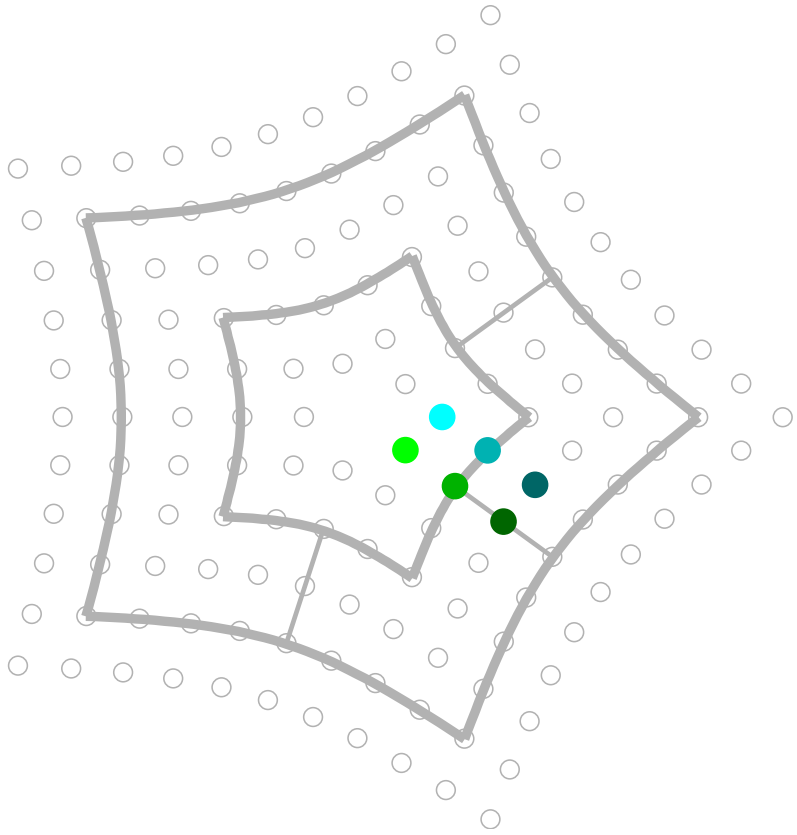

Figure 4.9: The extensions of the degree-raised, cubic generating splines that are presented in Figures 4.10–4.11. We have used a differential operator of degree three to compute these, to $(\kappa_0, \kappa_1) = (0, 1)$.

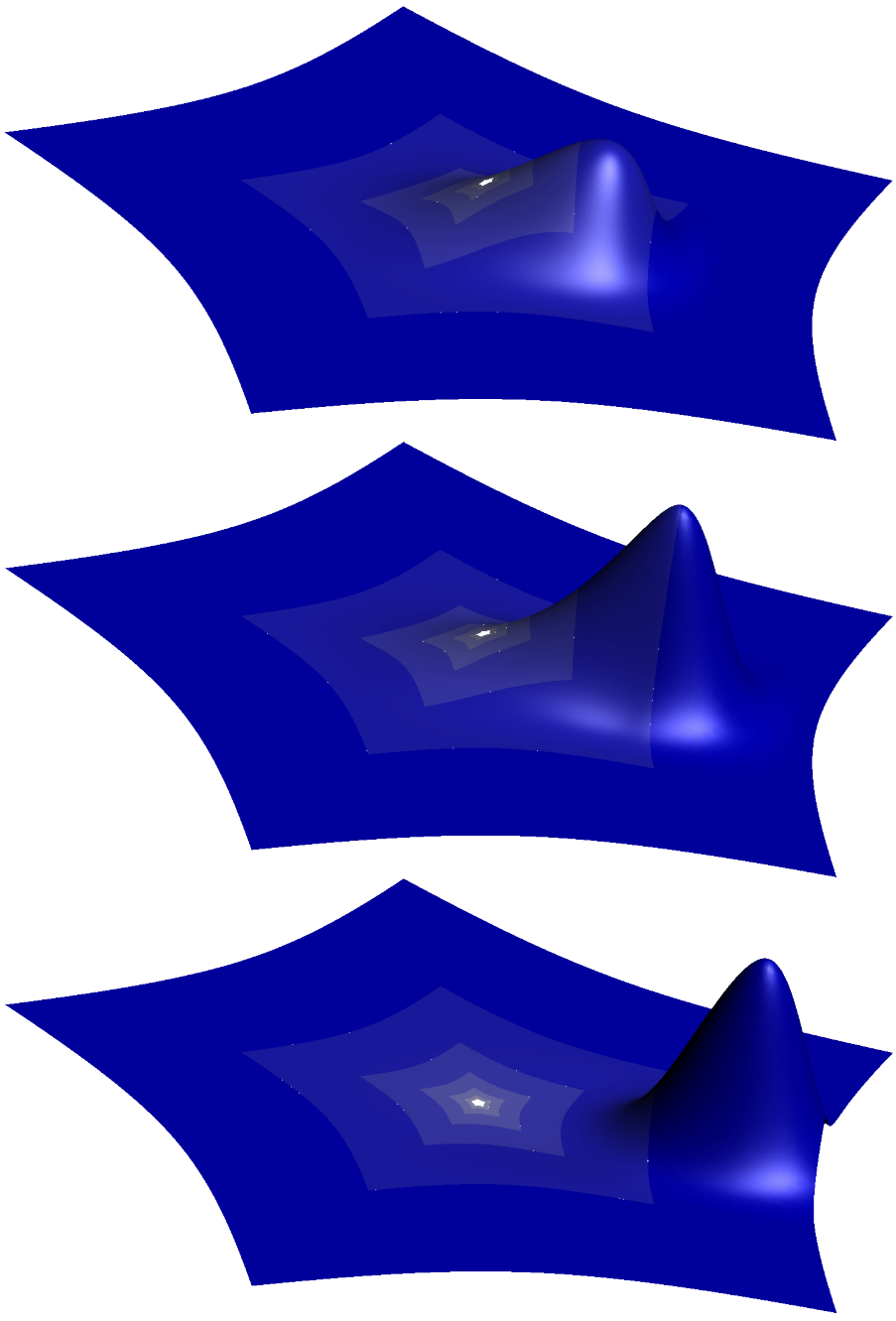

Figure 4.10: Extensions of the degree-raised, cubic splines ●, ●, ●, that are identified by green circles in Figure 4.9 on page 143.

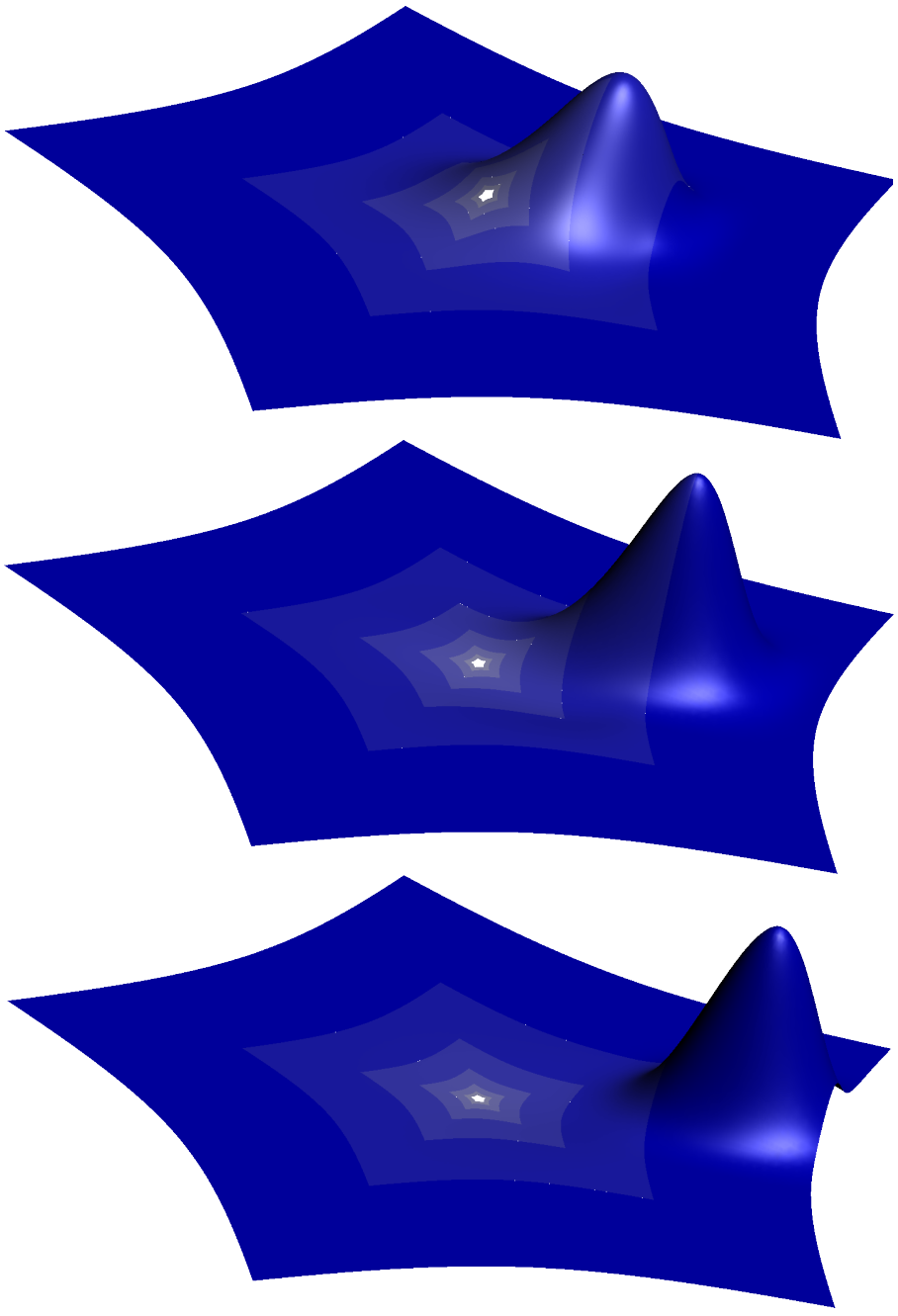

Figure 4.11: Extensions of the degree-raised, cubic splines ●, ●, ●, given by turquoise markers in Figure 4.9 on page 143.

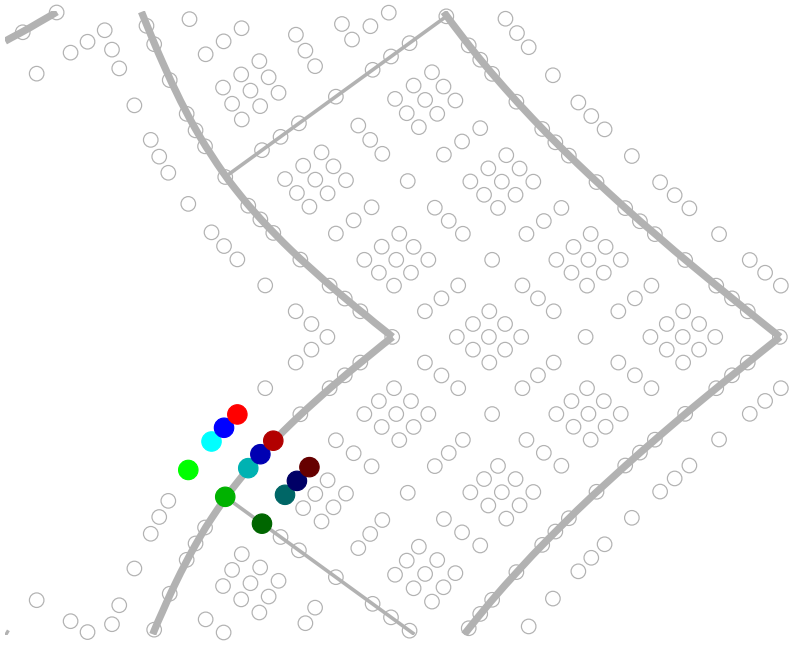

Figure 4.12: The generating splines of order 7 which we present in Figures 4.13–4.16. Again, we have used a differential operator of degree three to compute these, to parameters $(\kappa_0, \kappa_1) = (0, 1)$. In the circular direction, the colors match those that we used to plot a bundle of C^2 B-splines of order seven, cf. Figure 2.11 on page 38.

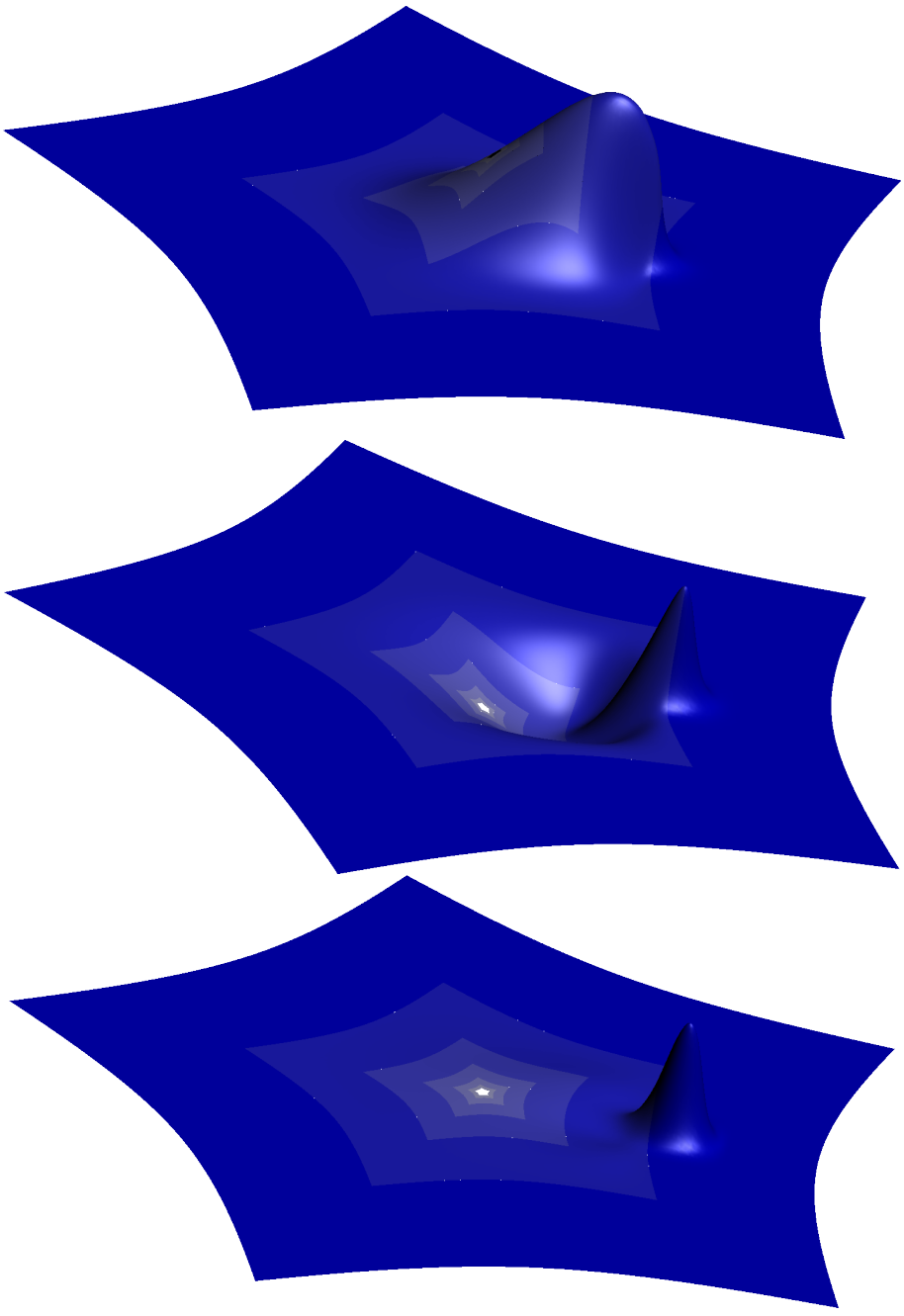

Figure 4.13: Generating splines ●, ●, ● of order 7 marked green in Figure 4.12 on page 146.

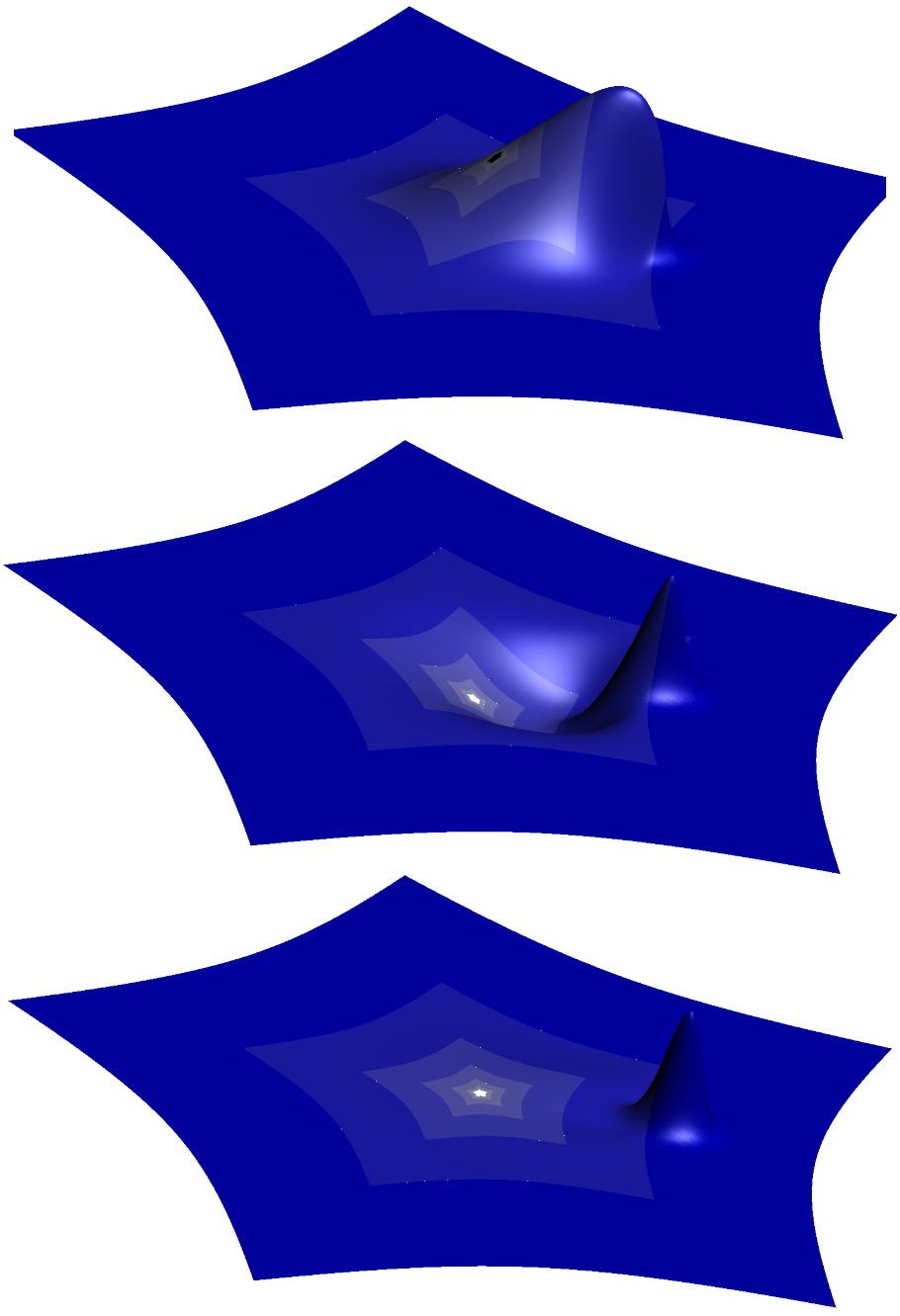

Figure 4.14: Generating splines ●, ●, ● of order 7, identified by turquoise markers in Figure 4.12 on page 146.

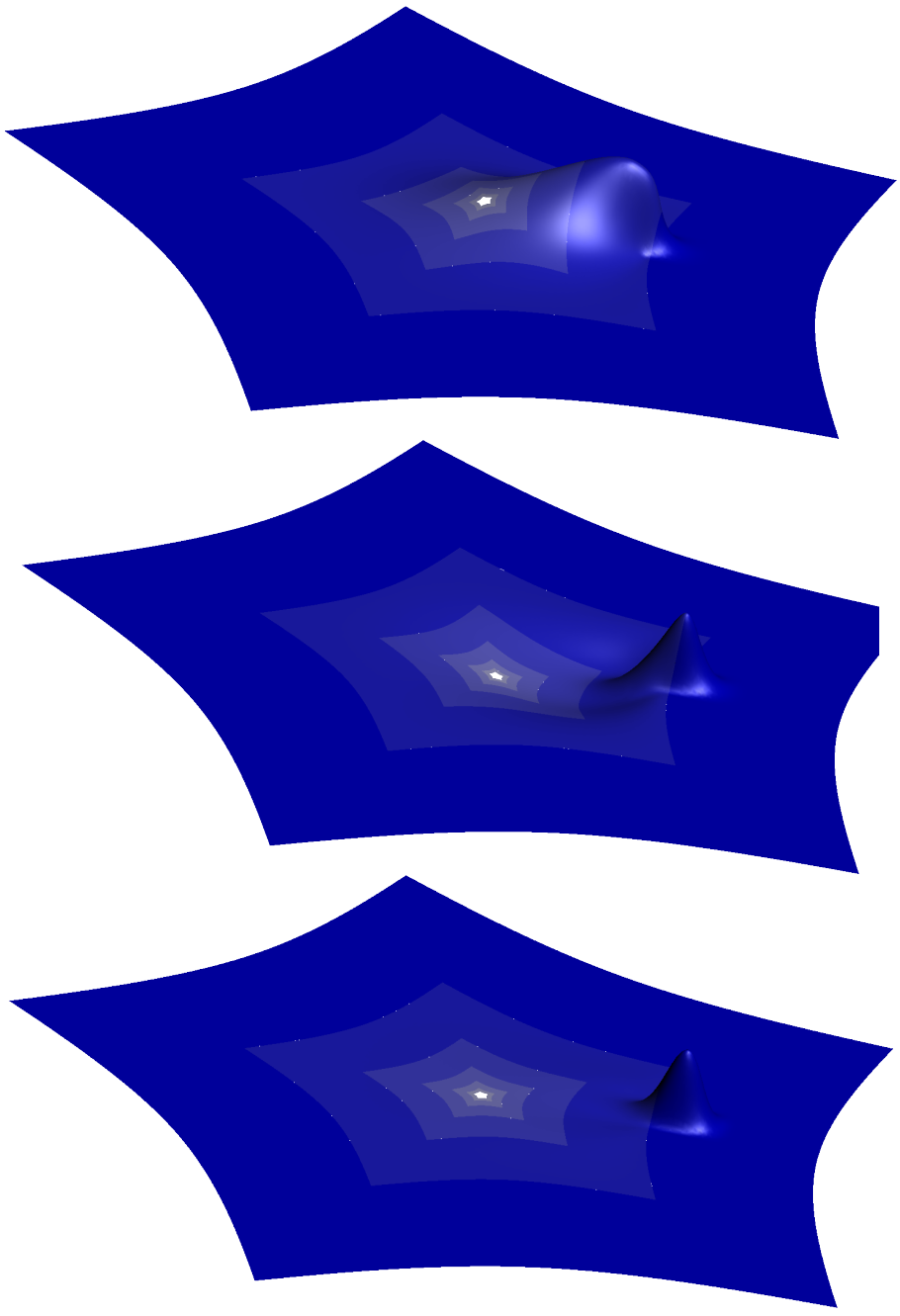

Figure 4.15: Generating splines ●, ●, ● of order 7, which are marked blue in Figure 4.12 on page 146.

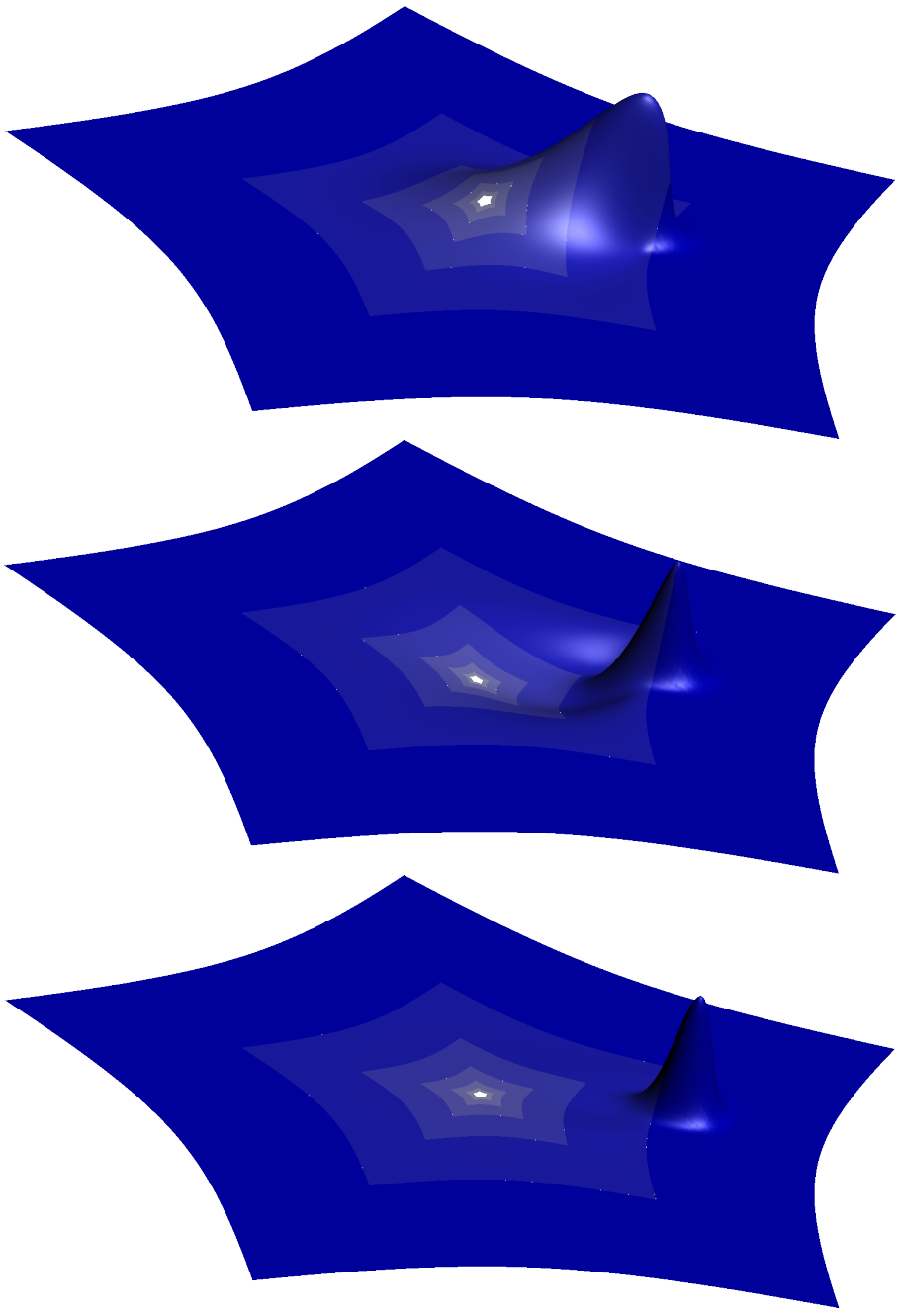

Figure 4.16: Generating splines ●, ●, ● of order 7, as identified in Figure 4.12 on page 146 by red.

Chapter 5

Proxies of subdivision surfaces

Although of a more general nature, proxies capture the crucial properties that make (bi-)linear control meshes approximate subdivision surfaces. They are the abstract structure that allows us now to examine the decay of various types of distances between control net and surface, as well as between their unit normals.

Throughout this chapter, we presuppose terms and assumptions of Section 3.1.

5.1 Defining extraordinary proxies

The issue of convergence rates of subdivision surfaces near extraordinary points has been studied in form of *control polyhedrons*—which are (bi-)linear interpolants—by Jörg Peters and Xiaobin Wu [51]. In the book *Subdivision Surfaces* [50] the concept is developed into *proxy splines*. This formulation identifies and includes the essential properties within the definition of the approximands. We further build on it:

Definition 5.1 ((Extraordinary) proxies)**.** $\breve{B}_\ell = [\breve{b}_{\ell 0}, \dots, \breve{b}_{\ell \bar{k}}]$ with $\breve{b}_{\ell k} \in C^0(\mathbf{S}_n, \mathbb{C})$ for $k \in \{0, \dots, \bar{k}\}$ form a sequence of *generating proxies* at successive refinement levels $\ell \in \mathbb{N}$ of the standard subdivision algorithm (A, B) if

1. there exist constants $\left[c_0^0, \dots, c_{\bar{k}}^0\right] =: c^0$ and $0 \le q < 1$ independent of ℓ such that

$$\sum_{k=0}^{\bar{k}} \breve{b}_{\ell,k} = 1 \tag{5.1}$$

$$\breve{B}_\ell = \breve{B}_{\ell+1}(2^{-1}\cdot)A \tag{5.2}$$

$$\|(B^0 - \breve{B}_\ell^0)v_k\|_\infty \le c_k^0 q^\ell \quad \text{for all } 0 \le k \le \bar{k}, \tag{5.3}$$

2. there are $\breve{m}_\ell$, $m_\ell \in \mathbb{N}$ with $\sup_{\ell\in\mathbb{N}} m_\ell < \infty$ such that

$$\chi(\mathbf{S}_n) \supseteq \breve{\chi}_\ell(2^{-\breve{m}_\ell}\mathbf{S}_n) \supseteq \chi(2^{-m_\ell}\mathbf{S}_n), \tag{5.4}$$

where $\breve{\chi}_\ell := \breve{B}_\ell[v_1, v_2]$ is the *characteristic proxy* at (refinement) level ℓ.

We assume that subsequent $\breve{m}_\ell$ have not been artificially increased beyond the following bound:

$$\breve{m}_{\ell+\Delta} \leq \breve{m}_\ell + \Delta, \quad \Delta \in \mathbb{N}. \tag{5.5}$$

(5.1),(5.2) and (5.3) are referred to as *Partition of Unity*, *Equation of Refinement* (towards the center) and *Convergence on the Outermost Ring*.

The differentiation of "extraordinary" proxies from those proxies in regular regions, which we examined in Chapter 2, will not be used in this chapter. All proxies are of the extraordinary type here.

Remark 5.2. For a polynomial spline, the parametric distance to a control polyhedron at uniform refinement level ℓ is proportional to $4^{-\ell}$ (see Theorem 2.13). Thus, (5.3) is typical for polynomial splines. Constants of proportionality can be found in [54, 45, 60], while [9] lists them for the more general box splines.

In this work we solely focus on developing the theory, leaving a verification of the defining properties of proxies for specific subdivision schemes to future work, and possibly to fellow researchers. However, by Remark 5.2 the main remaining difficulty of this verification consists of (5.4). The topological properties of the image of χ that we have presented in Section 3.5, for instance simple connectedness, may be useful at this point.

Remark 5.3. Condition (5.5) is only required to exclude artificial bloating of the $\breve{m}_\ell$. (5.3) yields

$$\breve{\chi}_{\ell+\Delta}(2^{-(\breve{m}_\ell+\Delta)}\mathbf{S}_n) = \lambda^\Delta \breve{\chi}_\ell(2^{-\breve{m}_\ell}\mathbf{S}_n).$$

By (5.4) $\breve{\chi}_\ell(2^{-\breve{m}_\ell}\mathbf{S}_n) \subseteq \chi(\mathbf{S}_n) = \lambda^{-\Delta}\chi(2^{-\Delta}\mathbf{S}_n)$. Hence,

$$\breve{\chi}_{\ell+\Delta}(2^{-(\breve{m}_\ell+\Delta)}\mathbf{S}_n) \subseteq \chi(2^{-\Delta}\mathbf{S}_n) \subseteq \chi(\mathbf{S}_n),$$

which shows that it is possible to have $\breve{m}_{\ell+\Delta} \leq \breve{m}_\ell + \Delta$.
A similar case could be made for the m_ℓ but is not needed in the following[1].

In practice, $\breve{m}_\ell, m_\ell$ often do not depend on the refinement level ℓ. For example, $\breve{m}_\ell = m_\ell \equiv 1$ for the Catmull-Clark or Loop algorithms and their generalizations, when a (bi-) linear interpolation of the control net is used as proxy.

[1]For those readers who are already familiar with Section 5.4: (5.5) is only important for the domains of the s_ℓ (cf. (5.15)), in order to permit (5.20).

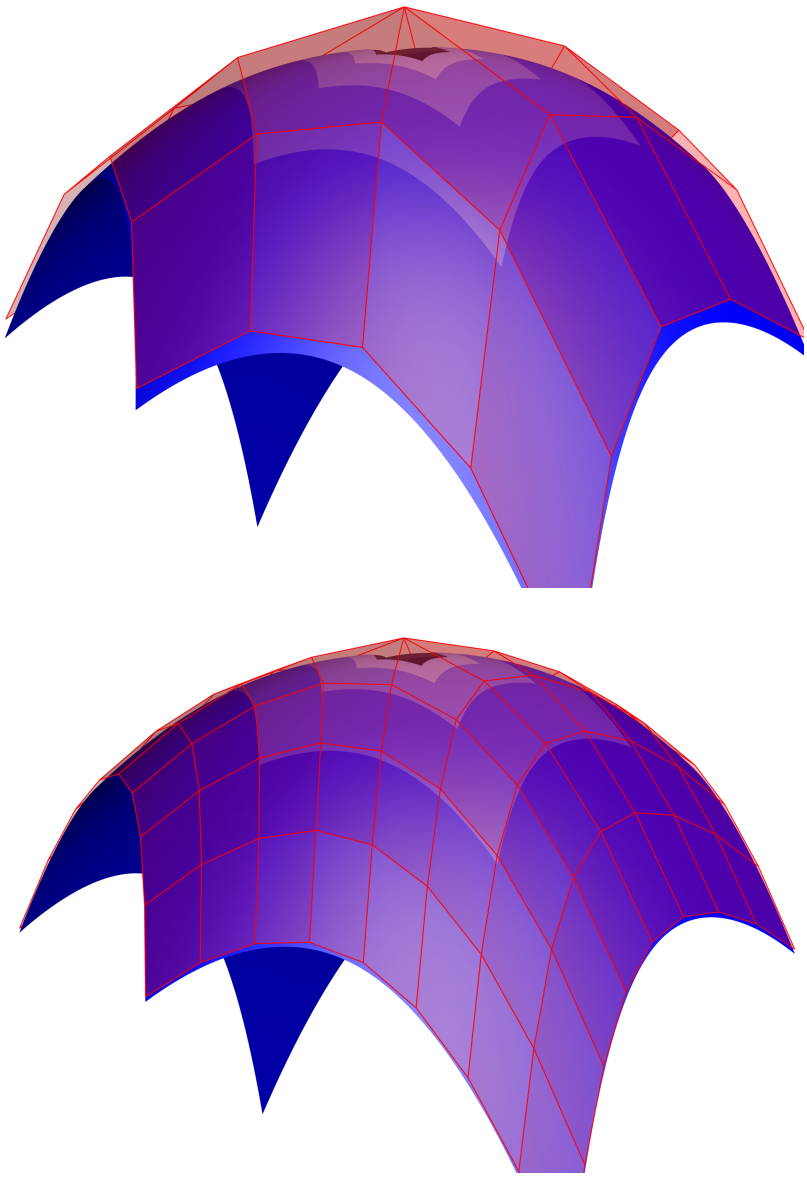

Figure 5.1: The same region of a subdivision surface near an extraordinary point at successive refinement levels. In both cases, part of the bi-linear control net is used to approximate the surface. Aside from linear approximations this is the type of *proxy* most commonly used. *Top:* coarse control net at refinement level $\ell = 0$. *Bottom:* the level of subdivision has been raised by one. One question is: how quickly does the difference of proxy and limit surface decay when ℓ approaches infinity?

Remark 5.4. While we need to include $\sup_\ell m_\ell < \infty$ among the assumptions, the analogous property for the $\breve{m}_\ell$ is already implicit. We will need this fact later on:

Lemma 5.5. *The sequence $(\breve{m}_\ell)_{\ell\in\mathbb{N}}$ is bounded, i.e. $\breve{m}_* := \sup_\ell \breve{m}_{\ell\in\mathbb{N}} < \infty$.*

Proof. $\breve{\chi}_\ell(2^{-\breve{m}_\ell}\mathbf{S}_n) \supseteq \chi(2^{-m_\ell}\mathbf{S}_n)$ implies

$$\| \left(\breve{\chi}_\ell\right)_{|2^{-\breve{m}_\ell}\mathbf{S}_n} \|_\infty \geq \|\chi_{|2^{-m_\ell}\mathbf{S}_n}\|_\infty. \tag{5.6}$$

We are now going to find upper bounds of $\|\chi(2^{-m}\cdot)\|_\infty$ and $\|\breve{\chi}_\ell(2^{-m}\cdot)\|_\infty$ in terms of the ringindex m. Since the m_ℓ are bounded, the right-hand side of (5.6) has a minimum that is greater than zero. As we will see, the left-hand side clusters at zero, if the $\breve{m}_\ell$ are unbounded.

χ is continuous and $\mathbf{S}_n^0$ compact, so $\chi(\mathbf{S}_n^0)$ is compact. Since χ is injective, with $\chi(0) = 0$, it follows that

$$C_0 := \|\chi^0\|_\infty > 0.$$

(5.3) implies $\chi(2^{-m}\cdot) = \lambda^m\chi$, therefore

$$\|\chi_{|2^{-m}\mathbf{S}_n}\|_\infty = \lambda^m C_0. \tag{5.7}$$

Now, let us consider the characteristic proxy. By (5.3), there is some $\ell_0 \in \mathbb{N}$ such that $\|\breve{\chi}_\ell^0 - \chi^0\|_\infty < C_0, \quad \ell \geq \ell_0$. We may ignore the finitely many levels ℓ below ℓ_0 for showing the claim of Lemma 5.5.

With (5.2), we arrive at

$$\|\breve{\chi}_\ell^m - \chi^m\|_\infty < \lambda^m C_0, \quad \text{for all } \ell - m \geq \ell_0.$$

Using this together with (5.7) yields

$$\|\breve{\chi}_\ell^m\|_\infty < 2\lambda^m C_0, \quad m \in \{0, \ldots, \ell - \ell_0\}. \tag{5.8}$$

It remains to estimate $\| \left(\breve{\chi}_\ell\right)_{|2^{-m}\mathbf{S}_n} \|_\infty$ for $m > \ell - \ell_0$. Let

$$C_1 := \|\breve{\chi}_{\ell_0}\|_\infty.$$

(5.3) yields

$$\| \left(\breve{\chi}_{\ell_0+m}\right)_{|2^{-m}\mathbf{S}_n} \|_\infty = \lambda^m C_1, \quad m \in \mathbb{N},$$

or, for $m = \ell - \ell_0$,

$$\| (\breve{\chi}_\ell)_{|2^{-(\ell-\ell_0)}} \|_\infty = \lambda^{\ell-\ell_0} C_1, \quad \ell \geq \ell_0. \tag{5.9}$$

Combining (5.8) and (5.9) yields

$$\begin{aligned} \| (\breve{\chi}_\ell)_{2^{-m}\mathbf{S}_n} \|_\infty &\leq \max \left\{ \max_{m \leq \widetilde{m} < \ell - \ell_0} \| \breve{\chi}_\ell^{\widetilde{m}} \|_\infty, \| (\breve{\chi}_\ell)_{|2^{-(\ell-\ell_0)}} \|_\infty \right\}, \quad \ell \geq \ell_0, \\ &\leq \lambda^m C_2, \quad \ell \geq \ell_0, \end{aligned}$$

where $C_2 := \max\{2C_0, C_1\}$.

Returning to (5.6), we find that

$$\lambda^{\breve{m}_\ell} C_2 \geq \| (\breve{\chi}_\ell)_{2^{-\breve{m}_\ell}\mathbf{S}_n} \|_\infty \geq \| \chi_{|2^{-m_\ell}\mathbf{S}_n} \|_\infty \geq \lambda^{m_*} C_0.$$

Hence, $\breve{m}_\ell \leq m_* \left(\log_\lambda C_0 - \log_\lambda C_2 \right)$.

□

5.2 Parametric distance

Let $H = [h_0, \ldots, h_{\bar{k}}]$ be a vector of splines or rings and $R = [r_0; \ldots; r_{\bar{k}}]$, where $r_j \in \mathbb{C}^{1\times d}$. If $h_0 = \ldots = h_{i-1} = 0$ then we have

$$\|HR\|_\infty \leq \langle [\|h_0\|_\infty, \ldots, \|h_{\bar{k}}\|_\infty], \mathcal{N}(R) \rangle_i, \quad \mathcal{N}(R) := \begin{pmatrix} |r_0| \\ \vdots \\ |r_{\bar{k}}| \end{pmatrix}, \tag{5.10}$$

where

$$\langle y, z \rangle_i := \sum_{k=i}^{\bar{k}} y_k z_k.$$

Notice that the operator $\mathcal{N}$ replaces the control points by their norm, its name is intended to hint at this.

At this point we recommend to briefly revisit Section 3.1 and refresh the fundamental definitions we have made there. For example, J and $V = [v_0, \ldots, v_{\bar{k}}]$ have been defined such that

$$A = VJV^{-1}$$

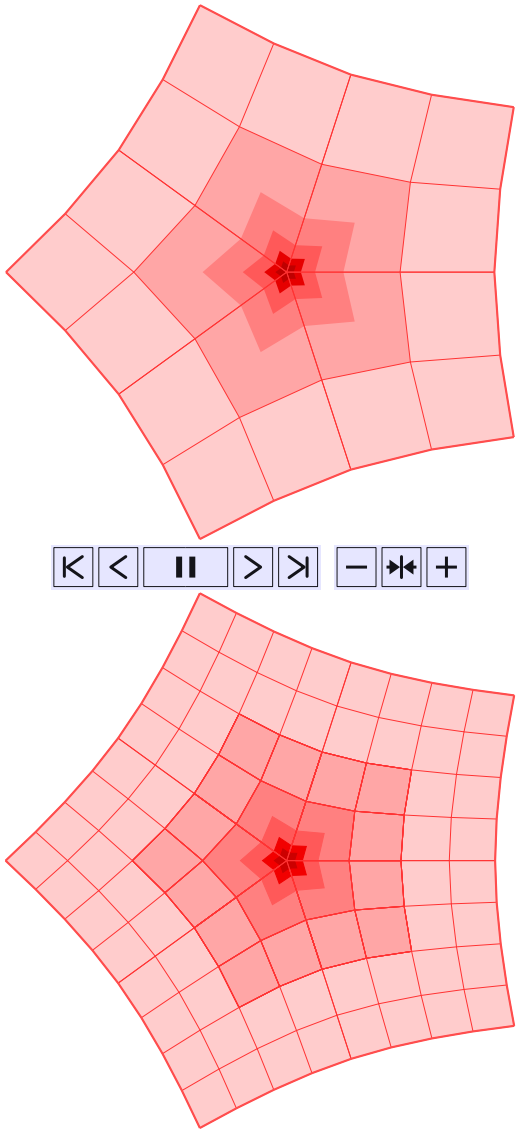

Figure 5.2: *Top*: animated sequence of the images of $\breve{\chi}_\ell$, $\ell \in \{0, \ldots, 4\}$, using part of the linearly interpolated control net of the Catmull-Clark algorithm. *Bottom*: image of $\breve{\chi}_1$ (for the print-out). Thin lines indicate the place where bi-linear pieces of the proxy join.
As in Figure 3.2 on page 75, which shows χ, at identical scaling, shadings indicate the image of successive rings $\breve{\chi}_\ell^m$. As the equation of refinement prescribes, $\lambda\breve{\chi}_0$ is nested within the next-outer ring of $\breve{\chi}_1$ (and so forth for successive levels ℓ). The outermost rings of $\breve{\chi}_\ell$ seem to be pretty close to χ. This, however, becomes less and less the case towards the center. The rings of $\breve{\chi}_\ell$ retain their polygonal edges, whereas those of χ are curved smoothly even toward the center.

is a Jordan decomposition of the subdivision matrix A.

Analogously to the definition

$$E := [e_0, \ldots, e_{\bar{k}}] := BV,$$

of eigensplines in Section 3.1 we define eigenproxies,

$$\breve{E}_\ell := [\breve{e}_{\ell 0}, \ldots, \breve{e}_{\ell \bar{k}}] := \breve{B}_\ell V.$$

We first take a look at the parametric difference between a spline and its proxy.

Theorem 5.6 (Estimate of parametric distance)**.** *Let*

$$c^{\geq 0} := [\|e_0 - \breve{e}_{00}\|_\infty, \ldots, \|e_{\bar{k}} - \breve{e}_{0\bar{k}}\|_\infty].$$

The parametric distance between a spline $\mathbf{x} = B\mathbf{Q}$ *and its proxy* $\breve{\mathbf{x}}_\ell = \breve{B}_\ell \mathbf{Q}$ *is bounded by*

$$\|\mathbf{x} - \breve{\mathbf{x}}_\ell\|_\infty \leq \max\left\{\lambda^\ell \langle c^{\geq 0}, \mathcal{N}(J^\ell \lambda^{-\ell}\mathbf{P})\rangle_1, \max_{0 \leq m < \ell} \lambda^m q^{\ell - m} \langle c^0, \mathcal{N}(J^m \lambda^{-m}\mathbf{P})\rangle_1\right\}.$$

Remark 5.7. We have factored out dominating terms in Theorem 5.6. The remaining factors, $\langle c^0, \mathcal{N}(J^m\lambda^{-m}\mathbf{P})\rangle_1$, $\langle c^{\geq 0}, \mathcal{N}(J^\ell\lambda^{-\ell}\mathbf{P})\rangle_1$, are bounded sequences for every fixed vector of initial control points $\mathbf{Q} = V\mathbf{P}$.

Proof of Theorem 5.6. Since B and $\breve{B}_\ell$ both form a partition of unity, $1 = \breve{e}_{\ell 0} = e_0$. Hence, the first component of $E - \breve{E}_\ell$ vanishes. Consider ring m of $\mathbf{x}, \breve{\mathbf{x}}_\ell$:

Case 1. Suppose $m \geq \ell$: by (5.2) and (5.10) with $i = 1$ we have

$$\begin{aligned} \mathbf{x}^m - \breve{\mathbf{x}}_\ell^m &= (E^m - \breve{E}_\ell^m)\mathbf{P} = (E^{m-\ell} - \breve{E}_0^{m-\ell})J^\ell \mathbf{P}, \\ \|\mathbf{x}^m - \breve{\mathbf{x}}_\ell^m\|_\infty &\leq \lambda^\ell \langle c^{\geq 0}, \mathcal{N}(J^\ell\lambda^{-\ell}\mathbf{P})\rangle_1. \end{aligned}$$

Case 2. Let $m < \ell$: again, by (5.2) and (5.10), and finally by (5.3):

$$\begin{aligned} \mathbf{x}^m - \breve{\mathbf{x}}_\ell^m &= (E^m - \breve{E}_\ell^m)\mathbf{P} \\ \|\mathbf{x}^m - \breve{\mathbf{x}}_\ell^m\|_\infty &\leq \langle [\|e_0^0 - \breve{e}_{\ell-m,0}^0\|_\infty, \ldots, \|e_{\bar{k}}^0 - \breve{e}_{\ell-m,\bar{k}}^0\|_\infty], \mathcal{N}(J^m\mathbf{P})\rangle \\ &\leq \lambda^m q^{\ell-m}\langle c^0, \mathcal{N}(J^m\lambda^{-m}\mathbf{P})\rangle_1. \qquad \square \end{aligned}$$

The reader should be familiar with the relations $\preccurlyeq, \sim, \precsim \prec$ and the definition of *convergence class* introduced in Subsection 2.1, starting on page 12. If this is not the case, we recommend to revisit their introduction[2].

Let us briefly discuss the qualitative change of the upper bounds in Theorem 5.6. Let (ℓ, m) be the pair of refinement level and ringindex m. For any fixed m, the parametric distance decays at least as q^ℓ. Conversely, for all rings m with $m \geq \ell$, the estimation decays like λ^ℓ. Going from one ring to the next at the same refinement level ℓ, powers of q and λ are traded evenly.

Are these upper bounds indeed the convergence class of $\|\mathbf{x}^m - \breve{\mathbf{x}}_\ell^m\|_\infty$ – or is our estimate too generous?

Theorem 5.8. *Assume that $\|\chi^0 - \breve{\chi}_\ell^0\|_\infty \sim q^\ell$ (which is typical) and let the subdominant eigen-coefficients have rank two. Then there exists some $\widetilde{m} \in \mathbb{N}$ such that*

$$\|\mathbf{x}^m - \breve{\mathbf{x}}_\ell^m\|_\infty \sim \lambda^m q^{\ell-m}$$

holds for $(\ell, m) \in \mathcal{D}_{\widetilde{m}} := \{(\ell, m) \in \mathbb{N} \times \mathbb{N} : \ \ell \geq m \geq \widetilde{m}\}$. (See Figure 5.3 on page 160 for an overview of $\mathcal{D}_{\widetilde{m}}$.)

Proof. It is $\mathcal{D}_0 \subseteq \mathcal{D}_1 \subseteq \mathcal{D}_2 \ldots$: we begin by examining $\mathcal{D}_0$, and adapt $\widetilde{m}$ as necessary along the way.

By Theorem 5.6, and as discussed in the preceding text, it is

$$\|\mathbf{x}^m - \breve{\mathbf{x}}_\ell^m\|_\infty \preccurlyeq \lambda^m q^{\ell-m}, \quad (\ell, m) \in \mathcal{D}_0 \subseteq \mathcal{D}_{\widetilde{m}}.$$

It remains to find $\widetilde{m}$ for which $\succcurlyeq$ holds on the domain $\mathcal{D}_{\widetilde{m}}$.

Denote by

$$M := \begin{bmatrix} \mathbf{p}_1 \\ \mathbf{p}_2 \end{bmatrix}$$

the subdominant eigencoefficients. The image of the unit circle under $y \mapsto yM$ is compact. Since M has full rank, it cannot contain zero. Therefore,

$$C_1 := \min_{y \in \mathbb{C}^{1\times 2}, |y|=1} |yM| > 0,$$

[2]In fact, the topics of this chapter first motivated the definitions of Subsection 2.1

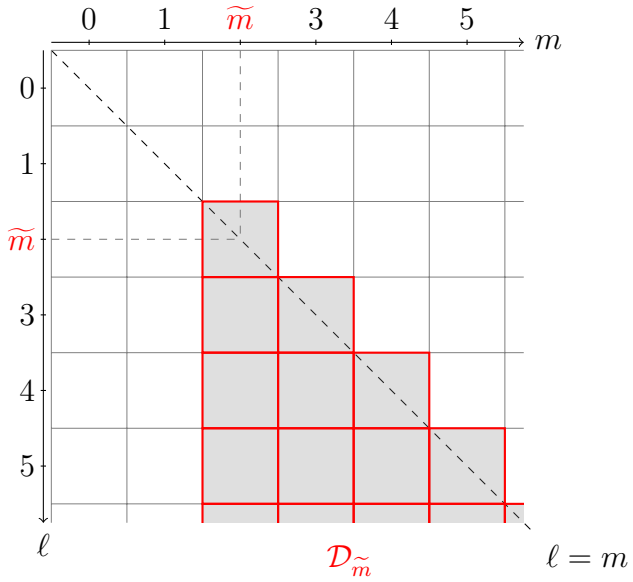

Figure 5.3: Sketch of the domain $\mathcal{D}_{\widetilde{m}}$ that is the topic of Theorem 5.8. The parameter is given by $\widetilde{m} = 2$ here.

and

$$|yM| \geq C_1|y| \quad \text{for all } y \in \mathbb{C}^{1\times 2}. \tag{5.11}$$

In the following, we will assume $(\ell, m) \in \mathcal{D}_0$ at least. The Jordan decomposition and reverse triangle inequality produce

$$\begin{aligned}\|\mathbf{x}^m - \breve{\mathbf{x}}^m_\ell\|_\infty &\geq \|\left(\chi^m - \breve{\chi}^m_\ell\right) M\|_\infty - \|\sum_{k=3}^{\bar{k}} \left(e^m_k - \breve{e}^m_{\ell k}\right) |\mathbf{p}_k|\|_\infty, \\ &\geq \|\chi^m - \breve{\chi}^m_\ell\|_\infty C_1 - \sum_{k=3}^{\bar{k}} \|e^m_k - \breve{e}^m_{\ell k}\|_\infty |\mathbf{p}_k|. \end{aligned} \tag{5.12}$$

It is $|\chi^m - \breve{\chi}^m_\ell| = \lambda^m |\chi^0 - \breve{\chi}^0_{\ell-m}|$. By presupposition, $\|\chi^0 - \breve{\chi}^0_{\ell-m}\|_\infty \succcurlyeq q^{\ell-m}$. Thus, there is a constant $C_2 > 0$ such that $\|\chi^0 - \breve{\chi}^0_{\ell-m}\|_\infty \geq q^{\ell-m} C_2$ for all $\ell - m \in \mathbb{N}$. Hence, with $C_3 := C_1 C_2$,

$$\|\chi^m - \breve{\chi}^m_\ell\|_\infty C_2 \geq \lambda^m q^{\ell-m} C_3, \quad \text{for all } (\ell, m) \in \mathcal{D}_0.$$

By (5.3) and the Jordan decomposition of A, the second term on the right-hand side of (5.12) is $\preccurlyeq \mu^m q^{\ell-m}$. Consequently, there exists $C_4 > 0$ with

$$\sum_{k=3}^{\bar{k}} \|e_k^m - \breve{e}_{\ell k}^m\|_\infty |\mathbf{p}_k| \le C_4 \mu^m q^{\ell-m}, \quad \text{for all } (\ell, m) \in \mathcal{D}_0.$$

Substituting the latter two displays into (5.12) yields

$$\begin{aligned} \|\mathbf{x}^m - \breve{\mathbf{x}}_\ell^m\|_\infty &\ge \lambda^m q^{\ell-m} C_3 - C_4 \mu^m q^{\ell-m} \\ &= \lambda^m q^{\ell-m} C_3 \underbrace{\left(1 - \left(\frac{\mu}{\lambda}\right)^m C_4/C_3\right)}_{h_{\ell,m}}. \end{aligned} \tag{5.13}$$

As $\lim_{m\to\infty}(\mu/\lambda)^m = 0$, there is some $\widetilde{m} \in \mathbb{N}$ such that $1/2 \le h_{\ell,m} \le 1$ for $\ell \ge m \ge \widetilde{m}$. Consequently,

$$\|\mathbf{x}^m - \breve{\mathbf{x}}_\ell^m\|_\infty \ge \lambda^m q^{\ell-m} \frac{C_3}{2}$$

for all $(\ell, m) \in \mathcal{D}_{\widetilde{m}}$. This finishes the proof.

□

Corollary 5.9. *Under the assumptions of Theorem 5.8, it is*

$$\|\mathbf{x} - \breve{\mathbf{x}}_\ell\|_\infty \sim \max(\lambda, q)^\ell, \quad \ell \in \mathbb{N}.$$

Proof. By Theorem 5.8,

$$\begin{aligned} \|\mathbf{x}^{\widetilde{m}} - \breve{\mathbf{x}}_\ell^{\widetilde{m}}\|_\infty \sim q^\ell, \quad \text{and} \\ \|\mathbf{x}^\ell - \breve{\mathbf{x}}_\ell^\ell\|_\infty \sim \lambda^\ell. \end{aligned}$$

It is $\mathbf{S}_n^{\widetilde{m}}, \mathbf{S}_n^\ell \subseteq \mathbf{S}_n$. The maximum over all of $\mathbf{S}_n$, $\|\mathbf{x} - \breve{\mathbf{x}}_\ell\|_\infty$, is at least as large as the two terms on the left-hand side. □

Remark 5.10. It might come as a bit of a surprise that $\|\chi^0 - \breve{\chi}_\ell^0\|_\infty \sim q^\ell$ alone is sufficient slow decay of $\|\mathbf{x} - \breve{\mathbf{x}}_\ell\|_\infty$ to $\succcurlyeq q^\ell$. But, as (5.13) shows, a similar presupposition for the remaining eigenfunctions $e_k^0, \breve{e}_{\ell k}^0$, $k \ge 3$, is not necessary.

5.3 Lipschitz continuity of the eigenfunctions

In Section 5.4 we are going to study the Hausdorff distance of $\mathbf{x}$ and $\breve{\mathbf{x}}_\ell$ essentially by re-parameterizing $\mathbf{x}$. We need to assert some basic properties of the eigensplines to judge the effect of this, building on the two following two properties we will henceforth assume:

Assumption 5.11. *$B \circ \chi^{-1}$ is Lipschitz-continuous on $\chi(\mathbf{S}_n^0)$.*

For C^1-functions defined on some compact, convex domain, Lipschitz-continuity follows automatically. Typically, $\chi(\mathbf{S}_n^0)$ is not convex, however.

Assumption 5.12. *For every straight line $g \subseteq \mathbb{R}^2$, the number of connected components of*

$$g \cap \chi(\partial \mathbf{S}_n)$$

is finite.

Remark 5.13. There is some work that can be done here: Lipschitz continuity of B on the closure $\mathbf{S}_{n,j}^0$ of segment $j \in \mathbb{Z}_n$ implies Lipschitz continuity of $B \circ \chi^{-1}$ on $\chi(\mathbf{S}_n^0)$.

We turn $\mathbf{S}_n$ into a metric space by the metric

$$d^\chi(s,t) := |\chi(s) - \chi(t)|, \quad s,t \in \mathbf{S}_n.$$

In the following, all distances in $\mathbf{S}_n$ are in terms of $d^\chi(\cdot,\cdot)$. Note that Assumption 5.11 is equivalent to Lipschitz-continuity of B in $(\mathbf{S}_n^0, d^\chi)$.

Theorem 5.14 (Lipschitz continuity & decay of Lipschitz constants)**.** *With J, χ as introduced in Section 3.1, let $\underline{E} = [\underline{e}_0, \dots, \underline{e}_{\bar{k}}]$, $\underline{e}_k \colon \mathbf{S}_n \to \mathbb{C}$ be continuous and $\underline{E} \circ \chi^{-1}$ Lipschitz-continuous on $\chi(\mathbf{S}_n^0)$. Further, let $\underline{E}$ be compatible with J in the same way as E is:*

$$\underline{E}(2^{-m}\cdot) = \underline{E} J^m \quad \textit{and } \underline{e}_0 = \textit{constant.}$$

Then the $\underline{e}_k \colon \mathbf{S}_n \to \mathbb{C}$ are Lipschitz continuous on all of $\mathbf{S}_n$: there are Lipschitz-constants $c_k^L \geq 0$ such that for all $s,t \in 2^{-m}\mathbf{S}_n, m \in \mathbb{N}$

$$|\underline{e}_k(s) - \underline{e}_k(t)| \leq \begin{cases} 0 & \textit{if } k = 0, \\ c_k^L d^\chi(s,t) & \textit{if } k \in \{1,2\}, \\ c_k^L d^\chi(s,t)\tilde{\mu}^m & \textit{if } k \in \{3,\dots,\bar{k}\}, \end{cases}$$

where $\widetilde{\mu} := \frac{\mu}{\lambda}$.

Before we can get to the proof of Theorem 5.14, we need some additional preparation.

There is a factor of λ^m hidden in $d^\chi(s,t)$. To avoid confusion in later situations where only dependence on m is relevant, we formulate

Corollary 5.15. *Let*[3]

$$C^{(\chi)} := \max_{s,t\in\mathbf{S}_n} d^\chi(s,t).$$

Continuing with the situation of Theorem 5.14, it is

$$|\underline{e}_k(s) - \underline{e}_k(t)| \le \begin{cases} 0 & \text{if } k = 0, \\ \lambda^m C^{(\chi)} c_k^L & \text{if } k \in \{1,2\}, \\ \mu^m C^{(\chi)} c_k^L & \text{if } k \in \{3,\dots,\bar{k}\}. \end{cases}$$

for all $s,t \in 2^{-m}\mathbf{S}_n$ *and* $m \in \mathbb{N}$.

Proof. It is $\chi(2^{-m}\cdot) = \lambda^m\chi$. Hence,

$$\begin{aligned} d^\chi(2^{-m}s, 2^{-m}t) &= \lambda^m d^\chi(s,t) \\ &\le \lambda^m C^{(\chi)} \end{aligned} \tag{5.14}$$

and the assertion follows. □

The proof of Theorem 5.14 uses three tools, which we present as lemmas. The first one is

Lemma 5.16. *Presuppose assumptions of Theorem 5.14. Then there are constants* $c_k^L \ge 0$ *independent of* m *such that*

$$|\underline{e}_k(s) - \underline{e}_k(t)| \le c_k^L |\chi(s) - \chi(t)|\kappa_k^m \quad \text{for all } s,t \in \mathbf{S}_n^m, m \in \mathbb{N},$$

where $\kappa_k := \begin{cases} 0 & \text{if } k = 0, \\ 1 & \text{if } k \in \{1,2\}, \\ \widetilde{\mu} & \text{if } 3 \le k. \end{cases}$

[3]By Corollary 3.8, $\chi(\mathbf{S}_n)$ is compact, so the maximum exists.

Proof. We distinguish the three cases

Case 1. Suppose $k = 0$. By premise, $\underline{e}_0$ is constant. So $\underline{e}_0(s) - \underline{e}_0(t) \equiv 0$.

Case 2. Suppose $k \in \{1, 2\}$. For $s, t \in \mathbf{S}_n^0$,

$$|\underline{e}_k(2^{-m}s) - \underline{e}_k(2^{-m}t)| = \lambda^m |\underline{e}_k(s) - \underline{e}_k(t)|.$$

By premise, $|\underline{e}_k(s) - \underline{e}_k(t)| \leq c_k^L |\chi(s) - \chi(t)|$. With

$$\lambda^m |\chi(s) - \chi(t)| = |\chi(2^{-m}s) - \chi(2^{-m}t)|$$

it directly follows that

$$|\underline{e}_k(2^{-m}s) - \underline{e}_k(2^{-m}t)| \leq |\chi(2^{-m}s) - \chi(2^{-m}t)|.$$

Case 3. Suppose $k \in \{3, \ldots, \bar{k}\}$. Denote by $\widetilde{J}$ the matrix J, where the Jordan blocks to eigenvalues $1, \lambda$ have been turned to zeros, and the whole matrix divided by μ afterwards.
For $s \in \mathbf{S}_n^0$ and $m \in \mathbb{N}$, it is

$$\underline{E}(2^m s) = \underline{E}(s) J^m = \mu^m \underline{E}(s) \widetilde{J}^m.$$

Hence, if t also lies in $\mathbf{S}_n^0$, and by premise

$$\begin{aligned} |\underline{E}(2^m s) - \underline{E}(2^m t)| &\leq \mu^m |\underline{E}(s) - \underline{E}(t)||\widetilde{J}^m| \\ &\leq \tilde{\mu}^m \lambda^m d^\chi(s, t) |\widetilde{J}^m|. \end{aligned}$$

By construction, the sequence $\widetilde{J}^m$ is bounded, that is, there is $C_1 > 0$ such that $|\widetilde{J}^m| \leq C_1$ for all $m \in \mathbb{N}$. (5.14) produces $\lambda^m d^\chi(s, t) = d^\chi(2^{-m}s, 2^{-m}t)$, which finishes the proof.

□

Lemma 5.17. *Denote the straight line from $\chi(s)$ to $\chi(t)$ by*

$$L(\tau) := \chi(s)(1 - \tau) + \tau\chi(t), \quad \tau \in [0, 1].$$

If $0 \notin \operatorname{image} L$, then the number of rings $\chi(\mathbf{S}_n^k), k \in \mathbb{N}$, that L intersects is finite.

Proof. If $0 \notin \operatorname{image} L$, the minimal norm C_1 of points in the image of L is greater than zero. Conversely, $\max|\chi(\mathbf{S}_n^m)|$ converges to zero for $m \to \infty$, so there are at most finitely many $k \in \mathbb{N}$ with $\|\chi^k\|_\infty \geq C_1$. □

Lemma 5.18. *Let* $0 = \tau_0 \leq \tau_1 \ldots \leq \tau_{\bar{\jmath}} = 1$, $\bar{\jmath} \in \mathbb{N} \cup \{\infty\}$, *be any countable partition of* $[0,1]$ *with*

$$\tilde{\tau}_j := \chi^{-1}(L(\tau_j)) \in 2^{-m}\mathbf{S}_n.$$

If the condition

$$|\underline{e}_k(\tilde{\tau}_j) - \underline{e}_k(\tilde{\tau}_{j-1})| \leq \kappa_k^m c_k^L |L(\tau_j) - L(\tau_{j-1})|$$

holds for every $j \in \{1, \ldots, \bar{\jmath}\}$, *then*

$$|\underline{e}_k(s) - \underline{e}_k(t)| \leq \kappa_k^m c_k^L |\chi(s) - \chi(t)|.$$

Proof. It is

$$\begin{aligned} |\underline{e}_k(s) - \underline{e}_k(t)| &= \left| \sum_{j=1}^{\bar{\jmath}} \underline{e}_k(\tilde{\tau}_j) - \underline{e}_k(\tilde{\tau}_{j-1}) \right| \leq \sum_{j=1}^{\bar{\jmath}} |\underline{e}_k(\tilde{\tau}_j) - \underline{e}_k(\tilde{\tau}_{j-1})| \\ &\leq \kappa_k^m c_k^L \underbrace{\sum_{j=1}^{\bar{\jmath}} |L(\tau_j) - L(\tau_{j-1})|}_{T}. \end{aligned}$$

We claim that $T = |\chi(s) - \chi(t)|$. Because of

$$\begin{aligned} (\tau_j - \tau_{j-1})(\chi(s) - \chi(t)) &= -\left((1-\tau_j)\chi(s) + \tau_j\chi(t)\right) \\ &\quad + \left((1-\tau_{j-1})\chi(s) + \tau_{j-1}\chi(t)\right) \\ &= L(\tau_{j-1}) - L(\tau_j) \end{aligned}$$

and $\tau_{j-1} \leq \tau_j$ it follows that

$$\begin{aligned} \sum_{j=1}^{\bar{\jmath}} |L(\tau_j) - L(\tau_{j-1})| &= |\chi(s) - \chi(t)| \sum_{j=1}^{\bar{\jmath}} (\tau_j - \tau_{j-1}) \\ &= |\chi(s) - \chi(t)|. \end{aligned}$$

Hence, $T = |\chi(s) - \chi(t)|$, which finishes the proof. □

Proof of Theorem 5.14. For $s = t$ the assertion is correct (and trivial). Let us assume $s \neq t$, which, by injectivity of χ, is the same as $\chi(s) \neq \chi(t)$.

The case $k = 0$ is trivial. Its eigenspace is separated from that of the other eigenvalues. Without loss of generality, we may assume $\underline{e}_0 \equiv 0$ in the following. Figure 5.4 illustrates the three cases of the dichotomy we are going to consider now.

Case 1. First, suppose $0 \notin \operatorname{image} L$. For g any straight line in $\mathbb{R}^2$,

$$g \cap \chi(2^{-k}\partial\mathbf{S}_n) = \lambda^k(g/\lambda^k \cap \chi(\partial\mathbf{S}_n)).$$

By Assumption 5.12, $g/\lambda^k \cap \chi(\partial\mathbf{S}_n)$ consists of finitely many connected components. As $g \mapsto g/\lambda^k$ is a bijection from the set of straight lines of $\mathbb{R}^2$ into itself, $g \cap \chi(2^{-k}\partial\mathbf{S}_n)$ follows to consist of at most finitely many connected components. By Lemma 5.17, L intersects only finitely many $\chi(\mathbf{S}_n^k)$, $k \in \mathbb{N}$. Hence,

$$L([0,1]) \cap \bigcup_{\substack{k\in\mathbb{N},\\ k\geq m}} \chi(2^{-k}\partial\mathbf{S}_n)$$

consists of only finitely many connected components $c_1, \ldots, c_N$, $N \in \mathbb{N}$. Because $\chi(s) \neq \chi(t)$, the mapping

$$c_j \mapsto L^{-1}(c_j) =: \tilde{c}_j$$

is bijective. We set

$$\tau_j := \begin{cases} 0, & \text{for } j = 0, \\ \sup \tilde{c}_j, & \text{for } 1 \leq j \leq N, \\ 1 & \text{for } j = N+1. \end{cases}$$

Without loss of generality, we may assume that the c_j are ordered so that the τ_j are ascending. Let

$$\tilde{\tau}_j := \chi^{-1}(L(\tau_j)).$$

Consecutive $\tilde{\tau}_j$ must lie in the same ring $\chi(\mathbf{S}_n^{k_j})$ for some $k_j \in \mathbb{N}^{\geq m}$. Suppose there was an intermediate $\chi(2^{-k}\partial\mathbf{S}_n)$, $k \in \mathbb{N}^{\geq m}$, in-between. By the Jordan Curve Theorem, $L_{|[\tau_j,\tau_{j+1}]}$ has to cross $\chi(2^{-k}\partial\mathbf{S}_n)$. This results in an

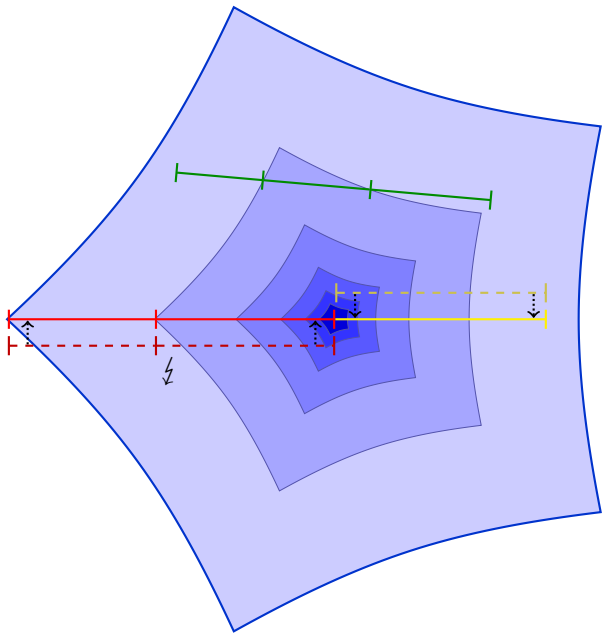

Figure 5.4: The three main cases we have to take care of in the proof of Theorem 5.14. The endpoints of the respective lines are always pairs $\chi(s), \chi(t)$. *Green*: partitioning into intersections with the rings of χ. *Yellow*: $0 \in \text{image}\, L$ but the image of L is contained in the set of interior points of the image of χ. *Red* : here we can neither shift into the direction of the normal, nor the reverse direction, because image L contains points from $\partial\chi(\mathbf{S}_n)$. A similar hazard occurs for the union of the red and yellow lines.

additional connected component between $\tilde{c}_j$ and $\tilde{c}_{j+1}$. But we have excluded this by putting the τ_j into ascending order.

All in all, we have partitioned the straight line $L(\tau)$ into those points at which $L(\tau)$ leaves one ring of $\chi(2^{-m}\mathbf{S}_n)$ and enters another, or goes into $\mathbb{R}^2 \setminus \chi(2^{-m}\mathbf{S}_n)$. Lemmas 5.16 and 5.18 now imply the claim of Theorem 5.14.

Case 2. Next, assume $0 \in \text{image}\, L$ and that the image of L contains only interior points of $\chi(2^{-m}\mathbf{S}_n)$ (that is, no points from $\partial\chi(2^{-m}\mathbf{S}_n)$). Let $\mathbf{n}$ be a unit normal to L. There is some $\bar{\varepsilon} > 0$ such that the images of all

$$L_\varepsilon(\tau) := L(\tau) + \varepsilon\mathbf{n}, \qquad 0 < \varepsilon \leq \bar{\varepsilon},$$

still contain only interior points of $\chi(2^{-m}\mathbf{S}_n)$, but do *not* contain 0. Denote

$$s_\varepsilon = s + \varepsilon\mathbf{n}, \quad t_\varepsilon = t + \varepsilon\mathbf{n}.$$

By the previous case it is

$$|\underline{e}_k(s_\varepsilon) - \underline{e}_k(t_\varepsilon)| \leq \kappa_k^m c_k^L |\chi(s_\varepsilon) - \chi(t_\varepsilon)|.$$

Taking the limit $\varepsilon \to 0$ on both sides yields the assertion of Theorem 5.14.

Case 3. Finally, the remaining case is when $0 \in \text{image}\, L$ but the image of L contains some boundary point of $\chi(2^{-m}\mathbf{S}_n)$. Let $\tau_* = L^{-1}(0)$ and define the partition

$$\begin{aligned}
&\tau_0 := 0,\\
&\tau_1 := \inf\{\tau \in [\frac{\tau_*}{2}, \tau_*] : \quad L((\tau, \tau_*]) \subseteq \operatorname{int}\chi(2^{-m}\mathbf{S}_n)\},\\
&\tau_2 := \tau_*,\\
&\tau_3 := \sup\{\tau \in [\tau_*, \frac{\tau_*+1}{2}] : \quad L([\tau_*, \tau)) \subseteq \operatorname{int}\chi(2^{-m}\mathbf{S}_n)\}\\
&\tau_4 := 1.
\end{aligned}$$

First, we claim that if $\tau_* \neq 0$ then $0 < \tau_1 < \tau_*$. *Proof:* It is $\tau_* \in (0, 1]$. By construction, $\tau_1 \in [\frac{\tau_*}{2}, \tau_*]$, that is $0 < \tau_1$. Because 0 is an interior point of $\chi(2^{-m}\mathbf{S}_n)$ (cf. 3.11) it has some open environment $U \subseteq \chi(2^{-m}\mathbf{S}_n)$. By continuity of L, $L^{-1}(U)$ is open. Per definition of τ_1, it must be

$$\tau_1 < \frac{\inf L^{-1}(U) + \tau_*}{2} \leq \tau_*.$$

Thus, $0 < \tau_1 < \tau_*$, as claimed.

In an analogue manner, one can show that $\tau_* \neq 1$ implies $\tau_* < \tau_3 < 1$.

Now, if $0 < \tau_* < 1$, we can partition L into the three segments

$$L_1 := L_{|[0,\tau_1]},\ L_2 := L_{|[\tau_1,\tau_3]},\ L_3 := L_{|[\tau_3,1]}.$$

Lemma 5.18 and the previous two cases yield the assertion of Theorem 5.14.

Finally, the cases $\tau_* \in \{0, 1\}$ are handled by partitioning the line segment $L([0, 1])$ similarly – either the "left-", or the "right-most" segment, L_1 or L_3, is not there then.

□

5.4 Hausdorff distance

One is usually more interested in the *geometric deviation* between a spline $\mathbf{x} = B\mathbf{Q}$ and a proxy $\breve{\mathbf{x}}_\ell = \breve{B}_\ell\mathbf{Q}$. We understand geometric distance as the Hausdorff distance of $\mathbf{x}, \breve{\mathbf{x}}_\ell$:

$$\mathcal{H}_\ell(\mathbf{Q}) := \max\left\{\max_{s\in\mathbf{S}_n}\min_{t\in\mathbf{S}_n}|(B(s)-\breve{B}_\ell(t))\mathbf{Q}|, \max_{t\in\mathbf{S}_n}\min_{s\in\mathbf{S}_n}|(B(s)-\breve{B}_\ell(t))\mathbf{Q}|\right\}.$$

Given s, it is usually very difficult to find $t_{\mathbf{Q},\ell}(s)$ such that $|(B(s)-\breve{B}_\ell(t))\mathbf{Q}|$ is minimized. The same is true for t and $s_{\mathbf{Q},\ell}(t)$. But we can simply use *any* $t = t(s) \in \mathbf{S}_n$ to that given s to estimate

$$\max_{s\in\mathbf{S}_n}\min_{t\in\mathbf{S}_n}|(B(s)-\breve{B}_\ell(t))\mathbf{Q}| \le \max_{s\in\mathbf{S}_n}|(B(s)-\breve{B}_\ell(t(s)))\mathbf{Q}|.$$

For the second term in $\mathcal{H}_\ell(\mathbf{Q})$ we proceed analogously. All in all, without needing any particular properties that simplify the problem, we have produced an estimate of the Hausdorff distance.

We can gather all pairs (s,t) that we used—either for the first, or the second term of $\mathcal{H}_\ell(\mathbf{Q})$—in a relation $R \subseteq \mathbf{S}_n \times \mathbf{S}_n$.

More generally, we call *any* relation $R \subseteq \mathbf{S}_n \times \mathbf{S}_n$ *feasible* if and only if

- for every s in $\mathbf{S}_n$ there is some $t \in \mathbf{S}_n$ such that $(s,t) \in R$ and,
- for every t in $\mathbf{S}_n$ there is $s \in \mathbf{S}_n$ with $(s,t) \in R$.

A feasible relation R allows to estimate Hausdorff distance safely,

$$\mathcal{H}_\ell(\mathbf{Q}) \le \mathcal{H}_\ell(\mathbf{Q}, R),$$

where

$$\mathcal{H}_\ell(\mathbf{Q}, R) := \max_{(s,t)\in R}|(B(s)-\breve{B}_\ell(t))\mathbf{Q}|.$$

We will also use the notation $\mathcal{H}_\ell(\mathbf{Q}, R)$ for subsets R of feasible relations which are not feasible themselves.

The fundament

Recall $\breve{m}_\ell, m_\ell$ from the definition of proxies. If we evaluate $\breve{\mathbf{x}}_\ell$ at t and $\mathbf{x}$ at

$$s_\ell(t) := \chi^{-1} \circ \breve{\chi}_\ell(t), \quad t \in 2^{-\breve{m}_\ell}\mathbf{S}_n. \tag{5.15}$$

Then, due to

$$\breve{\chi}_\ell(t) = \chi \circ s_\ell(t), \quad t \in 2^{-\breve{m}_\ell}\mathbf{S}_n, \tag{5.16}$$

we have

$$\begin{aligned}
\mathbf{x} \circ s_\ell - \breve{\mathbf{x}}_\ell &= \left(E(s_\ell) - \breve{E}_\ell(t)\right)\mathbf{P}, \\
E(s_\ell) - \breve{E}_\ell(t) &= \begin{bmatrix} 1-1 \\ \chi \circ s_\ell(t) - \breve{\chi}_\ell(t) \\ e_3(s_\ell(t)) - \breve{e}_{\ell 3}(t) \\ \vdots \end{bmatrix}^T = \begin{bmatrix} 0 \\ 0_{2\times 1} \\ e_3(s_\ell(t)) - \breve{e}_{\ell 3}(t) \\ \vdots \end{bmatrix}^T.
\end{aligned}$$

Thus, we have removed the subdominant components that govern decay of the parametric distance (cf. Corollary 5.9). We set

$$R_{\ell,1} := \left\{(s_\ell(t), t) : \ t \in 2^{-\breve{m}_\ell}\mathbf{S}_n\right\}.$$

To make $R_{\ell,1}$ feasible, we extend it by

$$R_{\ell,2} := \{(s, s) \in \mathbf{S}_n \times \mathbf{S}_n : \ \varrho(s) < m_\ell^{\max}\}$$

where

$$m_\ell^{\max} := \max\left(\breve{m}_\ell, m_\ell\right)$$

and m_ℓ is from the definition of proxies (notice that $R_{\ell,2}$ contains points from the domains of rings $0, \ldots, m_\ell^{\max} - 1$ only!).
It can easily be seen that

$$R_\ell := R_{\ell,1} \cup R_{\ell,2}$$

is feasible:

- For $t \in 2^{-\breve{m}_\ell}\mathbf{S}_n \supseteq 2^{-m_\ell^{\max}}\mathbf{S}_n$, the pair $(s_\ell(t), t)$ lies in $R_{\ell,1}$.

- When t is from $\mathbf{S}_n$ and of ringindex $< m_\ell^{\max}$, it is $(t,t) \in R_{\ell,2}$.
- If s is in $\mathbf{S}_n^0 \cup \ldots \cup \mathbf{S}_n^{m_\ell^{\max}-1}$, then (s,s) is contained in $R_{\ell,2}$.
- For $s \in 2^{-m_\ell}\mathbf{S}_n \supseteq 2^{-m_\ell^{\max}}\mathbf{S}_n$, by (5.4) there is a $t \in \mathbf{S}_n$ with $s = s_\ell(t)$. The pair (s,t) lies in $R_{\ell,1}$.

Yet the gain towards the center would be devaluated if $R_{\ell,2}$ throttled decay on the outer rings to less than q^ℓ – which is the speed of the parametric distance there. We must be certain that this does not occur:

Theorem 5.19. *Let*

$$\begin{aligned}
\mathfrak{h}_\ell^{(m)} &:= [\mathfrak{h}_{\ell,k}^{(m)}, \ldots, \mathfrak{h}_{\ell,\bar{k}}^{(m)}],\\
&:= \frac{1}{\mu^{\min(\ell,m)} q^\ell}[\|e_0 \circ s_\ell^m - \breve{e}_{\ell,0}^m\|_\infty, \ldots, \|e_{\bar{k}} \circ s_\ell^m - \breve{e}_{\ell,\bar{k}}^m\|_\infty],\\
\mathfrak{h}_{\bar{0}}^{\geq \breve{m}_*} &:= \frac{1}{\mu^{\breve{m}_*}}[\|(e_0 \circ s_0 - \breve{e}_{00})_{|\lambda^{\breve{m}_*}\mathbf{S}_n}\|_\infty, \ldots, \|(e_{\bar{k}} \circ s_0 - \breve{e}_{0\bar{k}})_{|\lambda^{\breve{m}_*}\mathbf{S}_n}\|_\infty].
\end{aligned}$$

Then there is a constant vector $\mathfrak{h}_*^{(*)} \in \mathbb{R}^{1\times\bar{k}}$ independent of ℓ such that

$$\mathfrak{h}_\ell^{(m)} \leq \mathfrak{h}_*^{(*)}, \quad \ell \in \mathbb{N},\, 0 \leq m \leq \breve{m}_*,$$

holds (componentwise).

The constants $\mathfrak{h}_\ell^{(m)}, \mathfrak{h}_{\bar{0}}^{\geq \breve{m}_*}$ will be part of an estimate of Hausdorff distance shortly, hence their name.

The proof of Theorem 5.19 will be done at the end of this subsection, as it relies on a theorem that we will also need later on. Essentially, we assert that the re-parametrization s_ℓ is sufficiently "local". As ringindices cluster around $0 \in \mathbf{S}_n$, this locality—relative to level ℓ—is better reflected by

Definition 5.20 (Capped ringindex ϱ_ℓ)**.** The *capped ringindex at level ℓ,* denoted by $\varrho_\ell \colon \mathbf{S}_n \to \mathbb{N}$, is derived from the standard ringindex via

$$\varrho_\ell(t) := \min(\ell, \varrho(t)).$$

While the equivalence classes/iso-sets of ϱ partition $\mathbf{S}_n$ into an infinite sequence of rings (plus 0), ϱ_ℓ produces $\mathbf{S}_n^0, \ldots, \mathbf{S}_n^{\ell-1}$, plus the center-piece $2^{-\ell}\mathbf{S}_n$. The capped ringindex at level ℓ does not "distinguish" beyond ring ℓ.

Theorem 5.21. *There exists some $\ell_1 \in \mathbb{N}$ such that*

$$\sup_{\ell\in\mathbb{N}} \|\varrho_\ell - \varrho_\ell \circ s_\ell\|_\infty \le \ell_1. \tag{5.17}$$

The brunt of the proof of Theorem 5.21 is contained in

Lemma 5.22. *There exists $\ell_0 \in \mathbb{N}$ such that*

$$\varrho_\ell \circ s_\ell^m \in \varrho_\ell^m + \{-1, 0, 1\}$$

holds for all $\ell - \ell_0 \ge m \ge \breve{m}_\ell$. Further, ℓ_0 can be replaced by any natural number greater than the initial ℓ_0.

Remark 5.23. ℓ_1 in Theorem 5.21 and ℓ_0 from Lemma 5.22 are related by $\ell_1 = \ell_0 + \breve{m}_*$. We will see this in the proof of the lemma.

Proof. We first need to prepare a tool: for sets $S, T \subseteq \mathbb{C}^d$, define

$$\mathcal{M}(S, T) := \inf_{s\in S, t\in T} |s - t|.$$

Obviously, for compact $S, T \subseteq C^d$

$$\mathcal{M}(S, T) = 0 \iff S \cap T \ne \emptyset. \tag{5.18}$$

Further, if $f : S \to \mathbb{C}^d$ and $g, h : T \to \mathbb{C}^d$ are arbitrary functions, the inverse triangle inequality produces

$$\begin{aligned}\mathcal{M}(f(S), g(T)) &\ge \inf_{s\in S, t\in T} (|f(s) - h(t)| - |h(t) - g(t)|) \\ &\ge \mathcal{M}(f(S), h(T)) - \|h - g\|_\infty. \end{aligned}\tag{5.19}$$

Returning to the current problem, let

$$\begin{aligned} d_{1,m} &:= \begin{cases} \mathcal{M}(\chi(\mathbf{S}_n^m), \chi(\bigcup_{k=0}^{m-2} \mathbf{S}_n^m)), & \text{if } m \ge 2, \\ \lambda^{m-2} d_{1,2}, & \text{for } m \in \{0, 1\}, \end{cases} \\ d_{2,m} &:= \mathcal{M}(\chi(2^{-(m+2)}\mathbf{S}_n), \chi(\mathbf{S}_n^m)), \quad m \in \mathbb{N}, \\ d_m &:= \min(d_{1,m}, d_{2,m}). \end{aligned}$$

Since χ is injective $d_m > 0$ for every $m \in \mathbb{N}$. (It is $d_{1,m} = \lambda^m d_{1,0}$, $\quad d_{2,m} = \lambda^m d_{2,0}$ because $\chi(2^{-m}\cdot) = \lambda^m \chi$, but we do not need this fact.)

By (5.3), there is $\ell_0 \in \mathbb{N}$ such that

$$\|\breve{\chi}_\ell^0 - \chi^0\|_\infty \le \frac{d_0}{2}, \quad \ell \ge \ell_0.$$

$\breve{\chi}_\ell^m - \chi^m = \lambda^m(\breve{\chi}_{\ell-m}^0 - \chi^0)$, $m \le \ell$, further implies

$$\|\breve{\chi}_\ell^m - \chi^m\|_\infty \le \frac{d_m}{2}, \quad \ell - m \ge \ell_0.$$

If we replace $\chi(\mathbf{S}_n^m)$ in the definition of $d_{1,m}, d_{2,m}$ by $\breve{\chi}_\ell(\mathbf{S}_n^m)$, (5.19) produces

$$\begin{aligned}\mathcal{M}(\breve{\chi}_\ell(\mathbf{S}_n^m), \chi(\bigcup_{k=0}^{m-2} \mathbf{S}_n^k)) &\ge d_m - \|\breve{\chi}_\ell^m - \chi^m\|_\infty, \\ &\ge \frac{d_m}{2} > 0, \quad m \ge 2, \ell - m \ge \ell_0.\end{aligned}$$

Similarly,

$$\mathcal{M}(\chi(2^{-(m+2)}\mathbf{S}_n), \breve{\chi}_\ell(\mathbf{S}_n^m)) \ge \frac{d_m}{2} > 0, \quad m \in \mathbb{N}, \ell - m \ge \ell_0.$$

All arguments of the $\chi, \breve{\chi}_\ell$ in the latter two displays are compact subsets of $\mathbf{S}_n$. As $\chi, \breve{\chi}_\ell$ are continuous, their images retain compactness. (5.18) now implies

$$\begin{aligned}\breve{\chi}_\ell(\mathbf{S}_n^m) \cap \chi(\bigcup_{k=0}^{m-2} \mathbf{S}_n^k) = \emptyset, \quad m \ge 2, \ell - m \ge \ell_0, \\ \breve{\chi}_\ell(\mathbf{S}_n^m) \cap \chi(2^{-(m+2)}\mathbf{S}_n) = \emptyset, \quad m \in \mathbb{N}, \ell - m \ge \ell_0.\end{aligned}$$

The domain of s_ℓ is $2^{-\breve{m}_\ell}\mathbf{S}_n$ and $\breve{\chi}_\ell(\mathbf{S}_n^m) \subseteq \chi(\mathbf{S}_n)$ for $m \ge \breve{m}_\ell$ (cf. (5.4)). Consequently, for $m \ge \breve{m}_\ell$ and $\ell - m \ge \ell_0$,

$$\breve{\chi}_\ell(\mathbf{S}_n^m) \subseteq \chi(\bigcup_{k=m-1}^{m+1} \mathbf{S}_n^k).$$

Therefore,

$$\varrho_\ell \circ s_\ell^m \in \varrho_\ell^m + \{-1, 0, 1\}, \quad \text{for all } \ell - \ell_0 \ge m \ge \breve{m}_\ell,$$

as asserted in the lemma. □

Next, we are going to prove Theorem 5.21. Note that $\breve{\chi}_\ell(2^{-\Delta}\cdot) = \lambda^\Delta \breve{\chi}_{\ell-\Delta}$ for $\Delta \le \ell$, and $\chi(2^{-\Delta}\cdot) = \lambda^\Delta \chi$ imply

$$2^{-\Delta} s_\ell(t) = s_{\ell+\Delta}(2^{-\Delta}t), \quad \Delta \in \mathbb{N}, t \in 2^{-\breve{m}_\ell}\mathbf{S}_n. \tag{5.20}$$

(Because of (5.5), the domain of $s_{\ell+\Delta}(2^{-\Delta}\cdot)$ indeed contains the domain of s_ℓ, given by $2^{-\breve{m}_\ell}\mathbf{S}_n$!)

Proof of Theorem 5.21. Let ℓ_0 be as in Lemma 5.22, and

$$\ell_1 := \ell_0 + \breve{m}_*.$$

Further, let $\widetilde{t} \in 2^{-\breve{m}_\ell}\mathbf{S}_n$ and ℓ be fixed. We distinguish three cases:

Case 1. Let $\ell \le \ell_1$: By construction of ϱ_ℓ, it is

$$\|\varrho_\ell - \varrho_\ell \circ s_\ell\|_\infty \le \ell_1, \tag{5.21}$$

for $\ell \in \{0, \dots, \ell_1\}$.

Case 2. Let $\ell \ge \ell_1 \wedge \varrho(\widetilde{t}) \le \ell - \ell_0$: The case $\ell \ge \ell_0 \wedge \varrho(\widetilde{t}) \le \ell - \ell_0$ is done in Lemma 5.22. Due to $\ell_1 \ge \ell_0$, the current subcase is contained therein.

Case 3. Let $\ell \ge \ell_1 \wedge \varrho(\widetilde{t}) \ge \ell - \ell_0$: By (5.20) it is $\varrho \circ s_{\ell+\Delta}(2^{-\Delta}t) = \Delta + \varrho \circ s_\ell(t)$ for $t \in 2^{-\breve{m}_\ell}\mathbf{S}_n$, so

$$\varrho_{\ell+\Delta} \circ s_{\ell+\Delta}(2^{-\Delta}t) = \Delta + \varrho_\ell \circ s_\ell(t), \quad t \in 2^{-\breve{m}_\ell}\mathbf{S}_n.$$

Similarly, $\varrho(2^{-\Delta}t) = \Delta + \varrho(t)$ implies

$$\varrho_{\ell+\Delta} \circ s_{\ell+\Delta}(2^{-\Delta}t) = \Delta + \varrho_\ell \circ s_\ell(t), \quad t \in 2^{-\breve{m}_\ell}\mathbf{S}_n.$$

Combining the last two displays yields, in particular,

$$(\varrho_\ell \circ s_\ell - \varrho_\ell)\,(2^{-(\ell-\ell_1)}t) = (\varrho_{\ell_1} \circ s_{\ell_1} - \varrho_{\ell_1})\,(t), \quad t \in 2^{-\breve{m}_{\ell_1}}\mathbf{S}_n. \tag{5.22}$$

It is $\ell - \ell_1 + \breve{m}_* = \ell - \ell_0$. The scaling $\tau_\ell : 2^{-\breve{m}_*}\mathbf{S}_n \to 2^{-(\ell-\ell_1)}\mathbf{S}_n$,

$$\tau_\ell(t) := 2^{-(\ell-\ell_1)}t,$$

is obviously bijective. We can define $t \in 2^{-\breve{m}_*}\mathbf{S}_n \subseteq 2^{-\breve{m}_{\ell_1}}\mathbf{S}_n$ by

$$t := {\tau_\ell}^{-1}(\widetilde{t}).$$

(5.22) now yields

$$|(\varrho_\ell \circ s_\ell - \varrho_\ell)\,(\widetilde{t})| = |(\varrho_{\ell_1} \circ s_{\ell_1} - \varrho_{\ell_1}) \circ {\tau_\ell}^{-1}(\widetilde{t})|.$$

By (5.21), the right-hand side is at most ℓ_1.

□

Remark 5.24. Note that, in general Theorem 5.21 does not hold for ϱ instead of ϱ_ℓ. This conclusion is—under our assumptions—impossible:

If $\breve{\chi}_0(0) \neq 0$, the difference of (non-capped) ringindices is unbounded.

Even if it was $\breve{\chi}_0(0) = 0$, we would lack any premises that describe how fast $\breve{\chi}_0^m$ converges toward zero. For instance, suppose $\|\breve{\chi}_0^m\|_\infty = \lambda^{2m}\|\breve{\chi}_0^0\|_\infty$. This is double the speed that χ^m exhibits. Consequently (we do not fully go into the details),

$$\lim_{m\to\infty} \|\varrho^m - \varrho \circ s_\ell^m\|_\infty = \infty.$$

We finish the subsection with the

Proof of Theorem 5.19. To show that $\mathfrak{h}_\ell^{(m)}$ $(0 \leq m \leq \breve{m}_*)$ are bounded, it is sufficient to show that $\mathfrak{h}_\ell^{(m)}$ is bounded for every fixed m. Besides m being fixed, we may also assume $\ell \geq m$.

By Theorem 5.6 and (5.16)

$$|\chi(t) - \chi \circ s_\ell(t)| \preccurlyeq \lambda^{\varrho_\ell(t)} q^{\ell - \varrho_\ell(t)}. \tag{5.23}$$

The triangle inequality, Theorems 5.21 and 5.14 produce

$$\begin{aligned} q^\ell \mathfrak{h}_{\ell k}^{(m)} &= \|e_k \circ s_\ell^m - \breve{e}_{\ell k}^m\|_\infty \\ &\leq \|e_k^m - \breve{e}_{\ell k}^m\|_\infty + \|e_k \circ s_\ell^m - e_k^m\|_\infty \\ &\preccurlyeq \mu^m q^{\ell-m} + (\frac{\mu}{\lambda})^m |\chi - \chi \circ s_\ell| \\ &\preccurlyeq \mu^m q^{\ell-m} + \mu^m q^{\ell-m} \preccurlyeq q^\ell. \end{aligned}$$

Dividing by q^ℓ on both sides shows the boundedness of $\mathfrak{h}_\ell^{(m)}$, $m \in \breve{m}_\mathbb{N}$, as asserted. Figure 5.5 on page 176 gives a quick overview of the situation.

□

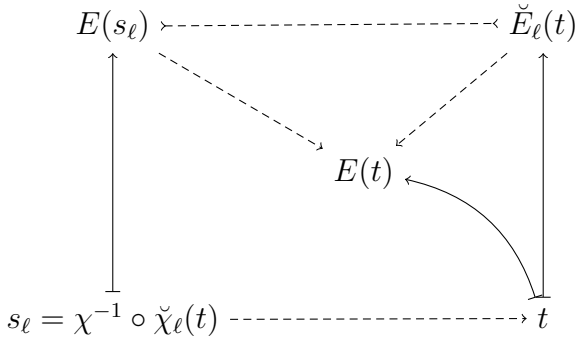

Figure 5.5: Illustration to the proof of Theorem 5.19. Convergence of $|E \circ s_\ell - \breve{E}_\ell| \preccurlyeq \lambda^{\varrho_\ell} q^{\ell-\varrho_\ell}$ follows from $|E - \breve{E}_\ell| \preceq \lambda^{\varrho_\ell} q^{\ell-\varrho_\ell}$, Lipschitz-continuity of E and the triangle inequality. Arrows "$\mapsto$" stand for "maps-to", while dashed ones indicate convergence toward the term the arrow's tip(s) point(s) at. Convergence classes are always at least $\lambda^{\varrho_\ell} q^{\ell-\varrho_\ell}$.

Estimate of Hausdorff distance

Abbreviate

$$\begin{aligned}
\kappa_1 &:= \max\left\{\langle c^0, \mathcal{N}(\mu^{-m} J^m \mathbf{P})\rangle_1 : \quad 0 \le m < \min(\ell, m_\ell^{\max})\right\},\\
\kappa_2 &:= \begin{cases} \langle c^{\ge 0}, \mathcal{N}(\mu^{-\ell} J^\ell \mathbf{P})\rangle_1, & \text{if } \ell < m_\ell^{\max},\\ 0, & \text{otherwise,}\end{cases}\\
\kappa_3 &:= \max\left\{\langle \mathfrak{h}_\ell^{(m)}, \mathcal{N}(\mathbf{P})\rangle_3 : \quad \breve{m}_\ell \le m < \breve{m}_*\right\},\\
\kappa_4 &:= \max\left\{\langle \mathfrak{h}_{\ell+\breve{m}_*-m}^{(\breve{m}_*)}, \mathcal{N}(J^{m-\breve{m}_*}\mathbf{P})\rangle_3 : \quad \breve{m}_* \le m < \breve{m}_* + \ell\right\},\\
\kappa_5 &:= \langle \mathfrak{h}_0^{\ge \breve{m}_*}, \mathcal{N}(J^{m-\breve{m}_*}\mathbf{P})\rangle_3
\end{aligned}$$

(we always suppress the dependence of the κ_j on ℓ in the notation).

Now we can estimate geometric deviation:

Theorem 5.25. *The Hausdorff distance $\mathcal{H}_\ell(\mathbf{P})$ is bounded as follows:*

$$\mathcal{H}_\ell(\mathbf{P}) \le \max\{\kappa_1, \ldots, \kappa_5\}. \tag{5.24}$$

Proof. In conjunction with (5.20), $B(2^{-h}\cdot) = BA^h$ implies

$$B \circ s_{\ell+h}(2^{-h}\cdot) = B \circ s_\ell A^h, \quad h \in \mathbb{N}. \tag{5.25}$$

Now let $(s,t) \in R_\ell$, $m := \varrho(t)$. We distinguish the cases

$m < m_\ell$, $s = t$: Theorem 5.6 is used to estimate $|\mathbf{x} - \breve{\mathbf{x}}_\ell|$ for $s = t \in \mathbf{S}_n^m$, $m = 0, \ldots, \breve{m}_\ell - 1$, yielding κ_1 and κ_2 in (5.24).

$\breve{m}_\ell \le m < \breve{m}_*$: using (5.10) it is $|(B \circ s_\ell - \breve{B}_\ell)\mathbf{Q}| = |(E \circ s_\ell - \breve{E}_\ell)\mathbf{P}| \le \mu^{\min(\ell,m)} q^{\ell - \min(\ell,m)} \langle \mathfrak{h}_\ell^{(m)}, \mathcal{N}(\mathbf{Q}) \rangle_3$.

$\breve{m}_* \le m < \breve{m}_* + \ell$: letting $h := m - \breve{m}_*$, it is $\ell > h$ and (5.25)

$$\begin{aligned} |(B \circ s_\ell(t) - \breve{B}_\ell(t))\mathbf{Q}| &= |(E \circ s_{\ell-h}(2^h t) - \breve{E}_{\ell-h}(2^h t)) J^h \mathbf{P}| \\ &\le \mu^h q^{\ell-h} \langle \mathfrak{h}_{\ell-h}^{(\breve{m}_*)}, \mathcal{N}(J^h \mathbf{P}) \rangle_3. \end{aligned}$$

$\breve{m}_* + \ell \le m$: using (5.25) we get

$$\begin{aligned} (B \circ s_\ell(t) - \breve{B}_\ell(t))\mathbf{Q} &= (E \circ s_0(2^\ell t) - \breve{E}_0(2^\ell t)) J^\ell \mathbf{P} \\ &\le \mu^\ell \langle \mathfrak{h}_0^{\ge \breve{m}_*}, \mathcal{N}(J^\ell \mathbf{P}) \rangle_3. \end{aligned}$$

□

5.5 Graphs over the subdominant component

In this section, we study an important subset of subdivision surfaces: those whose control points lie in

$$\begin{aligned} \mathcal{G} := \{ \mathbf{Q} \in \mathbb{C}^{(\bar{k}+1)\times d} :\ & \mathbf{P} = V^{-1}\mathbf{Q} \text{ is of form (5.26), and} \\ & \begin{bmatrix} \mathbf{P}_{1,0} & \mathbf{P}_{1,1} \\ \mathbf{P}_{2,0} & \mathbf{P}_{2,2} \end{bmatrix} \text{ is invertible} \}, \end{aligned}$$

where

$$\mathbf{P} = \left[\begin{array}{cc|ccc} * & * & * & \ldots & * \\ \hline * & * & 0 & \ldots & 0 \\ * & * & 0 & \ldots & 0 \\ \hline 0 & 0 & * & \ldots & * \\ \vdots & \vdots & \vdots & \ddots & \vdots \\ 0 & 0 & * & \ldots & * \end{array}\right]. \tag{5.26}$$

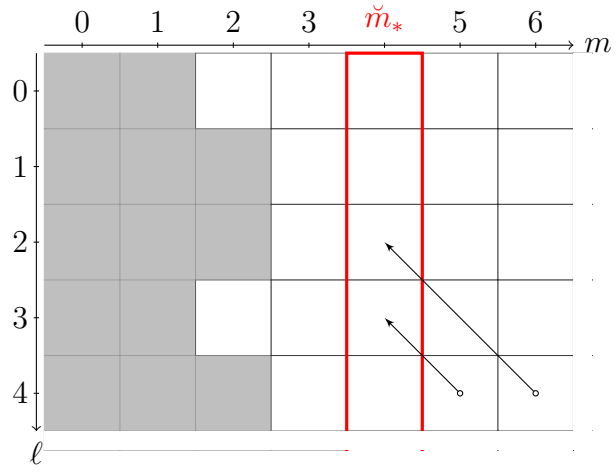

Figure 5.6: A hypothetical situation of pairs of refinement level ℓ and ringindex m. Shaded squares indicate pairs (ℓ, m) for which $m < \breve{m}_\ell$, i.e. s_ℓ cannot be defined. Therefore, one cannot apply the Equation of Refinement ("north-west" arrows) on s_ℓ without paying special attention first.
It is sensible not to use the Equation of Refinement beyond the left of $\breve{m}_*$, as we do not want having to take care of a possible raggedness of $(\ell, \breve{m}_\ell)$.

The placeholder $*$ in (5.26) stands for any complex number. We purposely allow the control points to be non-generic here. The set of central surfaces is a subset of $\mathcal{G}$.

Recall that $s_{\ell,\mathbf{Q}}(t)$ returns $s \in \mathbf{S}_n$ such that $|(B(s) - \breve{B}_\ell(t))\mathbf{Q}|$ is minimal. Analogously, $t_{\ell,\mathbf{Q}}(s)$ returns $s \in \mathbf{S}_n$ such that $|(B(s) - \breve{B}_\ell(t))\mathbf{Q}|$ is minimal for that given $s \in \mathbf{S}_n$.

Theorem 5.26. *Let $|\cdot| = |\cdot|_1$. There exists a constant $\varepsilon_* > 0$, depending on the Lipschitz constants from Theorem 5.14 for the eigensplines, such that*

$$(s_{\ell,\mathbf{Q}})_{|2^{-\breve{m}_\ell}\mathbf{S}_n} = s_\ell$$

for all $\mathbf{Q} \in \mathcal{G}$ with

$$\max_{3 \le k \le \bar{k}} |\mathbf{p}_k| < \varepsilon_* \frac{1}{|M^{-1}|}, \tag{5.27}$$

where $M := \begin{bmatrix} \mathbf{P}_{1,0} & \mathbf{P}_{1,1} \\ \mathbf{P}_{2,0} & \mathbf{P}_{2,2} \end{bmatrix}$ is constructed of—as in the definition of $\mathcal{G}$—subdominant eigen-coefficients.

Remark 5.27. For Theorem 5.26 it is crucial that the distance between spline and proxy is measured by the 1-norm. Conversely, by equivalency of norms on $\mathbb{C}^{1\times d}$, the norm in (5.27) can be replaced by any other norm, provided we adjust ε_* accordingly.

Proof. In the following, all functions are restricted to $2^{-\check{m}_\ell}\mathbf{S}_n$, which is the domain of s_ℓ.

Denote by

$$\mathbf{r} := \sum_{k=3}^{\bar{k}} e_k \mathbf{p}_k, \quad \check{\mathbf{r}}_\ell := \sum_{k=3}^{\bar{k}} \check{e}_{\ell k} \mathbf{p}_k$$

the "remainders" after the subdominant and constant terms have been removed.

For all subdivision surfaces whose control points lie in $\mathcal{G}$, the subdominant control points lie in coordinate planes separate from the subspace that is allowed for the $\mathbf{p}_k$, $k \geq 3$. Taking the 1-norm yields

$$|\mathbf{x} \circ s_{\ell,\mathbf{Q}} - \check{\mathbf{x}}_\ell|_1 = \underbrace{|(\chi \circ s_{\ell,\mathbf{Q}} - \check{\chi}_\ell)\, M|_1}_{T_1} + \underbrace{|\mathbf{r} \circ s_{\ell,\mathbf{Q}} - \mathbf{r} \circ s_\ell + \mathbf{r} \circ s_\ell - \check{\mathbf{r}}_\ell|_1}_{T_2}. \tag{5.28}$$

It is $|y| = |yNN^{-1}| \leq |yN||N^{-1}|$, so

$$|yN| \geq \frac{|y|}{|N^{-1}|}, \quad N \in \mathrm{GL}_m(\mathbb{C}), y \in \mathbb{C}^{1\times m}.$$

By definition of s_ℓ, it is $(\check{\chi}_\ell)_{|2^{-\check{m}_\ell}\mathbf{S}_n} = \chi \circ s_\ell$. Hence,

$$T_1 \geq |\chi \circ s_{\ell,\mathbf{Q}} - \chi \circ s_\ell|_1 \frac{1}{|M^{-1}|_1} = d^\chi(s_{\ell,\mathbf{Q}}, s_\ell) \frac{1}{|M^{-1}|_1}. \tag{5.29}$$

For T_2, the reverse triangle inequality shows that

$$T_2 \geq |\mathbf{r} \circ s_\ell - \check{\mathbf{r}}_\ell|_1 - |\mathbf{r} \circ s_{\ell,\mathbf{Q}} - \mathbf{r} \circ s_\ell|_1.$$

It is $\mathbf{r} \circ s_\ell - \check{\mathbf{r}}_\ell = \mathbf{x} \circ s_\ell - \check{\mathbf{x}}_\ell$, because $(\check{\chi}_\ell)_{|2^{-\check{m}_\ell}\mathbf{S}_n} = \chi \circ s_\ell$. Further, $|\mathbf{x} \circ s_\ell - \check{\mathbf{x}}_\ell|_1 \geq |\mathbf{x} \circ s_{\ell,\mathbf{Q}} - \check{\mathbf{x}}_\ell|_1$, by definition of $s_{\ell,\mathbf{Q}}$ (as minimizer). Thus,

$$T_2 \geq |\mathbf{x} \circ s_{\ell,\mathbf{Q}} - \check{\mathbf{x}}_\ell|_1 - \sum_{k=3}^{\bar{k}} \underbrace{|e_k \circ s_{\ell,\mathbf{Q}} - e_k \circ s_\ell|}_{T_{2,k}} |\mathbf{p}_k|_1.$$

By Theorem 5.14, there are Lipschitz constants $c_k^L \geq 0$ such that $T_{2,k} \leq d^\chi(s_{\ell,\mathbf{Q}}, s_\ell)c_k^L$. Therefore,

$$T_2 \geq |\mathbf{x} \circ s_{\ell,\mathbf{Q}} - \breve{\mathbf{x}}_\ell|_1 - d^\chi(s_{\ell,\mathbf{Q}}, s_\ell) \sum_{k=3}^{\bar{k}} c_k^L |\mathbf{p}_k|_1. \tag{5.30}$$

Returning with (5.29)–(5.30) to (5.28), we find that

$$\begin{aligned}
|\mathbf{x} \circ s_{\ell,\mathbf{Q}} - \breve{\mathbf{x}}_\ell|_1 &\geq |\mathbf{x} \circ s_{\ell,\mathbf{Q}} - \breve{\mathbf{x}}_\ell|_1 + d^\chi(s_{\ell,\mathbf{Q}}, s_\ell) \left(\frac{1}{|M^{-1}|_1} - \sum_{k=3}^{\bar{k}} c_k^L |\mathbf{p}_k|_1 \right) \\
&\geq |\mathbf{x} \circ s_{\ell,\mathbf{Q}} - \breve{\mathbf{x}}_\ell|_1 \\
&\quad + d^\chi(s_{\ell,\mathbf{Q}}, s_\ell) \Bigg(1 - |M^{-1}|_1 \underbrace{\left(\sum_{k=3}^{\bar{k}} c_k^L \right)}_{T_3 :=} \max_{3 \leq k \leq \bar{k}} |\mathbf{p}_k|_1 \Bigg).
\end{aligned}$$

For $\varepsilon_* := 1/T_3$ and

$$\max_{3 \leq k \leq \bar{k}} |\mathbf{p}_k|_1 < \frac{1}{|M^{-1}|_1} \varepsilon_*$$

the coefficient of $d^\chi(s_{\ell,\mathbf{Q}}, s_\ell)$ is positive. (In the unrealistic scenario that T_3 is zero, one could choose $\varepsilon_* := \infty$. But in this case any positive number is OK for ε_*, too.) It follows that $d^\chi(s_{\ell,\mathbf{Q}}, s_\ell) = 0$, i.e. $s_{\ell,\mathbf{Q}} = s_\ell$. □

Although there are other norms for which Theorem 5.26 can be formulated, among the p-norms, the 1-norm is the only one that allows to explicitly solve $s_{\ell,\mathbf{Q}}$ as in the preceding proof. As Theorem 5.26 is more an intermediate step for the analysis of super-converging proxies, we do not present the exact point at which the arguments of Theorem 5.26 fail for other p-norms.

5.6 Super-converging proxies

A tuple of generating proxies is called *super-converging* if its Hausdorff distance decays uniformly faster than μ^ℓ,

$$\mathcal{H}_\ell(\mathbf{Q}) \prec \mu^\ell.$$

As noted in Section 2.1, convergence classes are independent of the norm used. Thus, the convergence class of $\mathcal{H}_\ell(\mathbf{Q})$ is the same for any norm by which we measure distances.

With $s_{\ell,\mathbf{Q}}, t_{\ell,\mathbf{Q}}$ as defined in Section 5.4 (as respective minimizer), let

$$R^{\mathrm{opt}}_{\ell,\mathbf{Q}} := \{(s_{\ell,\mathbf{Q}}(t), t) : \quad t \in \mathbf{S}_n\} \cup \{(s, t_{\ell,\mathbf{Q}}(s)) : \quad s \in \mathbf{S}_n\}.$$

By definition of $s_{\ell,\mathbf{Q}}, t_{\ell,\mathbf{Q}}$,

$$\mathcal{H}_\ell(\mathbf{Q}) = \mathcal{H}_\ell(\mathbf{Q}, R^{\mathrm{opt}}_{\ell,\mathbf{Q}}). \tag{5.31}$$

Super-converging proxies are possible

Defining eigenproxies is equivalent to defining generating proxies. Setting the eigenproxies identical to the eigensplines up to subsub-dominant components—suppose $q < \mu$ here—yields proxies whose convergence is indeed faster than μ^ℓ. The extreme case is $\breve{B}_\ell = B$.

So we can construct proxies that converge as fast as we want. But are there any of practical relevance which are super-converging? To answer this question, we must look into the implications of super-converging proxies.

Examination of super-converging proxies

The following theorem characterizes super-converging eigenproxies. To formulate it, we need a definition,

Definition 5.28 (Ring-zero-part)**.** For any relation $R \subseteq \mathbf{S}_n \times \mathbf{S}_n$, we denote by the *ring-zero-part*

$$\pi^0(R) := \{(s,t) \in R : \quad s \in \mathbf{S}^0_n \vee t \in \mathbf{S}^0_n\}$$

its subset of pairs $(s,t) \in R$ where at least one of s, t lies in $\mathbf{S}^0_n$.
If we have a sequence R_ℓ of relations—one relation to each level ℓ—we define its ring-zero-part canonically, i.e. by the sequence $\pi^0(R_\ell)$.

Theorem 5.29 (Characterization of super-converging proxies)**.** *Let j_0 be such that $|\lambda_{j_0}| > |\lambda_{j_0+1}|$. Set*

$$\underline{E} := [e_0, \dots, e_{j_0}], \quad \underline{\breve{E}}_\ell := [\breve{e}_{\ell,0}, \dots, \breve{e}_{\ell,j_0}].$$

and $\underline{J} := J_{0\dots j_0,\,0\dots j_0}$ *be the corresponding submatrix of* J*. Further, let*

$$\widetilde{s}_\ell(t) := s_{\ell+\breve{m}_*}(2^{-\breve{m}_*}t), \quad t \in \mathbf{S}_n.$$

Then the following two properties are equivalent:

a) $\mathcal{H}_\ell(\mathbf{Q}) \prec |\lambda_{j_0}|^\ell$ *holds for all initial control points* $\mathbf{Q}$*.*

b) The eigenproxies of indices $0, \dots, j_0$ *are given by*

$$\underline{\breve{E}}_\ell(t) = \underline{E} \circ \widetilde{s}_\ell(t)\, \underline{J}^{-\breve{m}_*}, \tag{5.32}$$

and the ring-zero-part of $R^{opt}_{\ell,\mathbf{Q}}$ *fulfills*

$$\mathcal{H}_\ell(\mathbf{Q}, \pi^0(R^{opt}_{\ell,\mathbf{Q}})) \prec |\lambda_{j_0}|^\ell.$$

In particular, for Theorem 5.29 we have in mind the case $\lambda_{j_0} = \mu$, $j_0 = 2 + \sharp\mu$, i.e. super-convergent proxies.

Due the length of its proof and the rather differing nature of the argumentation for a) $\Longrightarrow$ b) and b) $\Longrightarrow$ a), we separate the proof into two separate lemmas:

Lemma 5.30. *Presuppose assumptions of Theorem 5.29 and let* $\mathcal{H}_\ell(\mathbf{Q}) \prec |\lambda_{j_0}|^\ell$ *for all initial control points* $\mathbf{Q}$*.*
Then it is

$$\underline{\breve{E}}_\ell(t) = \underline{E} \circ \widetilde{s}_\ell(t)\, \underline{J}^{-\breve{m}_*}. \tag{5.33}$$

Furthermore, the ring-zero-part of $R^{opt}_{\ell,\mathbf{Q}}$ *fulfills*

$$\mathcal{H}_\ell(\mathbf{Q}, \pi^0(R^{opt}_{\ell,\mathbf{Q}})) \prec |\lambda_{j_0}|^\ell.$$

Proof. Suppose $\mathcal{H}_\ell(\mathbf{Q}) \prec |\lambda_{j_0}|^\ell$ holds for all initial control points $\mathbf{Q}$.

It is $\pi^0(R^{\mathrm{opt}}_{\ell,\mathbf{Q}}) \subset R^{\mathrm{opt}}_{\ell,\mathbf{Q}}$, hence

$$\mathcal{H}_\ell(\mathbf{Q}, \pi^0(R^{\mathrm{opt}}_{\ell,\mathbf{Q}})) \le \mathcal{H}_\ell(\mathbf{Q}, R^{\mathrm{opt}}_{\ell,\mathbf{Q}}) = \mathcal{H}_\ell(\mathbf{Q}) \prec |\lambda_{j_0}|^\ell,$$

so $\mathcal{H}_\ell(\mathbf{Q}, \pi^0(R^{\mathrm{opt}}_{\ell,\mathbf{Q}})) \prec |\lambda_{j_0}|^\ell$.

Now to (5.33): since convergence classes are independent of the norm used, we can switch to the 1-norm. We may scale the (possibly generalized)

eigenvectors $v_3, \dots, v_{j_0}$ such that the 1-norms of $\mathbf{p}_k$, $3 \le k \le \bar{k}$ are at most $\varepsilon_*/2$, where ε_* is as per Theorem 5.26. Consequently, we can replace $s_{\ell,\mathbf{Q}}$ by s_ℓ.

Let $\ell_0 \in \mathbb{N}$ be any fixed level. Abbreviate

$$h := \breve{m}_*.$$

Because of $s_{\ell,\mathbf{Q}} = s_\ell$ and (5.20), we have

$$\begin{aligned} |\lambda_{j_0}|^\ell &\succ \left(\underline{\breve{E}}_{\ell+\ell_0+h} - \underline{E} \circ s_{\ell+\ell_0+h}\right)(2^{-(\ell+h)}t) \\ &= \underbrace{\left(\underline{\breve{E}}_{\ell_0+h} - \underline{E} \circ s_{\ell_0+h}\right)(2^{-h}t)}_{\Delta(\ell_0,t)}\, \underline{J}^\ell, \end{aligned} \tag{5.34}$$

where $t \in \mathbf{S}_n$.

Let $0 \le k_0 \le k_1 \le j_0$ be such that v_{k_0} is head of the Jordan chain of v_{k_1}, to the eigenvalue λ_{k_0}.

First, assume $k_1 = k_0$. Component k_0—with indexing beginning at 0—of the right-hand side of (5.34) is then

$$\left(\underline{\breve{E}}_{\ell+\ell_0+h} - \underline{E} \circ s_{\ell+\ell_0+h}\right)_{k_0}(2^{-(\ell+h)}t) = (\lambda_{k_0})^\ell \Delta_{k_0}(\ell_0, t)$$

(we refer to component $j \in \{0, 1, \dots, \bar{k}\}$ of Δ directly by Δ_j). $\Delta_{k_0}(\ell_0, t)$ is independent of ℓ. By (5.34), both sides are $\prec |\lambda_{j_0}|^\ell$. Because of $|\lambda_{k_0}| > |\lambda_{j_0}|$, it follows that $\Delta_{k_0}(\ell_0, t) = 0$.

Next, let $k_1 > k_0$ be such that

$$\Delta_k(\ell_0, t) = 0, \quad \text{for all } t \in \mathbf{S}_n,\ k \in \{k_0, \dots, k_1 - 1\}.$$

Because the preceding $\Delta_k(\ell_0, t)$, $k_0 \le k < k_1$ are all zero each, we have again

$$\left(\underline{\breve{E}}_{\ell+\ell_0+h} - \underline{E} \circ s_{\ell+\ell_0+h}\right)_{k_1}(2^{-(\ell+h)}t) = (\lambda_{k_0})^\ell \Delta_{k_1}(\ell_0, t).$$

By the same argument as above, $\Delta_{k_1}(\ell_0, t)$ follows to be zero for all $t \in \mathbf{S}_n$.

Renaming ℓ_0 to ℓ in $\Delta(\ell_0, t)$, we have shown that

$$\left(\underline{\breve{E}}_{\ell+h} - \underline{E} \circ s_{\ell+h}\right)(2^{-h}\cdot) = 0.$$

It is $\underline{\breve{E}}_{\ell+h}(2^{-h}\cdot) = \underline{\breve{E}}_\ell \underline{J}^h$. Further, $s_{\ell+h}(2^{-h}\cdot) =: \widetilde{s}_\ell$. Since $\underline{J}$ is invertible, we have

$$\underline{\breve{E}}_\ell(t) = \underline{E} \circ \widetilde{s}_\ell(t)\, \underline{J}^{-h}, \quad t \in \mathbf{S}_n,$$

as claimed in the lemma. □

Lemma 5.31. *Continue with terms and presuppositions of Theorem 5.29. The eigenproxies of indices* $0, \dots, j_0$ *shall be given by*

$$\breve{\underline{E}}_\ell(t) = \underline{E} \circ \widetilde{s}_\ell(t)\, \underline{J}^{-\breve{m}_*}.$$

Further, let the ring-zero-part of $R^{opt}_{\ell,\mathbf{Q}}$ *fulfill*

$$\mathcal{H}_\ell(\mathbf{Q}, \pi^0(R^{opt}_{\ell,\mathbf{Q}})) \prec |\lambda_{j_0}|^\ell.$$

Then $\mathcal{H}_\ell(\mathbf{Q}) \prec |\lambda_{j_0}|^\ell$ *holds for all initial control points* $\mathbf{Q}$*.*

Proof. We can assume $\ell \geq m_\ell^{\max}$ for the following proof.

We define the relations

$$T_\ell := T_\ell^{\geq \breve{m}_\ell} \cup \bigcup_{m=0}^{m_\ell^{\max}} T_\ell^m$$

by

$$\begin{aligned} T_\ell^m &:= 2^{-m}\pi^0(R^{\text{opt}}_{\ell-m,\mathbf{Q}}), \quad 0 \leq m \leq m_\ell^{\max}, \\ T_\ell^{\geq \breve{m}_\ell} &:= \{(s_\ell(t), t) :\ t \in 2^{-\breve{m}_\ell}\mathbf{S}_n\}. \end{aligned}$$

(Notice the similarity in the construction of T_ℓ and R_ℓ in Subsection 5.4.) To deduce that $\mathcal{H}_\ell(\mathbf{Q}) \prec |\lambda_{j_0}|^\ell$ holds, we show that

1. T_ℓ is a sequence of feasible relations, and
2. it is $\mathcal{H}_\ell(\mathbf{Q}, T_\ell) \prec |\lambda_{j_0}|^\ell$.

T_ℓ is feasible: if $s \in \mathbf{S}_n^m$ for some $m \in \{0, \dots, m_\ell\}$, we can set $t = 2^{-m}t_{\ell-m,\mathbf{Q}}(2^m s)$ and (s,t) lies in T_ℓ. Similarly, for $t \in \mathbf{S}_n^m$, $m \in \{0, \dots, \breve{m}_\ell\}$, we can set $s = 2^{-m}s_{\ell-m,\mathbf{Q}}(2^m t)$. Again, the pair (s,t) is in T_ℓ.

The two cases $s \in 2^{-m_\ell}\mathbf{S}_n$, $t \in 2^{-\breve{m}_\ell}\mathbf{S}_n$ are the same as for R_ℓ at the beginning of Section 5.4.

It is $\mathcal{H}_\ell(\mathbf{Q}, T_\ell) \prec |\lambda_{j_0}|^\ell$: distinguish the two cases

Case 1. Suppose $(s,t) \in T_\ell^{\geq \breve{m}_\ell}$, i.e. $s = s_\ell(t)$. By premise and the definition of $\widetilde{s}_\ell$,

$$\begin{aligned} \breve{\underline{E}}_\ell(t) &= \underline{E} \circ \widetilde{s}_\ell(t)\, \underline{J}^{-\breve{m}_*} \\ &= \underline{E} \circ s_{\ell+\breve{m}_*}(2^{-\breve{m}_*}t)\underline{J}^{-\breve{m}_*}. \end{aligned}$$

Because of (5.20), we can replace $s_{\ell+\breve{m}_*}(2^{-\breve{m}_*}t) = 2^{-\breve{m}_*}s_\ell(t)$.

$$\begin{aligned}\underline{\breve{E}}_\ell(t) &= \underline{E}(2^{-\breve{m}_*}s_\ell(t))\underline{J}^{-\breve{m}_*},\\ &= \underline{E}\circ s_\ell(t)\underline{J}^{\breve{m}_*}\underline{J}^{-\breve{m}_*}\\ &= \underline{E}\circ s_\ell(t).\end{aligned}$$

Thus, at $s = s_\ell(t)$ we have

$$\underline{\breve{E}}_\ell(t) - \underline{E}(s) = 0$$

and all components of $\breve{E}_\ell(t) - E(s)$ (beware these terms are without the underlines) that correspond to eigenvalues whose magnitude is larger than $|\lambda_{j_0+1}|$ vanish. It follows that $\mathcal{H}_\ell(\mathbf{Q}, T_\ell^{\geq\breve{m}_\ell}) \prec |\lambda_{j_0+1}|^\ell$.

Case 2. For $(s,t) \in T_\ell^m$ we have

$$\begin{aligned}|E(s) - \breve{E}_\ell(t)| &= |(E(2^m s) - \breve{E}_{\ell-m}(2^m t))J^m|\\ &\leq |E(2^m s) - \breve{E}_{\ell-m}(2^m t)||J|^m\\ &= \mathcal{H}_{\ell-m}(\mathbf{Q}, \pi^0(R^{\text{opt}}_{\ell-m,\mathbf{Q}}))|J|^m\\ &\prec |\lambda_j|^{\ell-m}|J|^m.\end{aligned}$$

Since $m \leq m_\ell^{\max}$ is bounded, we can replace $\prec |\lambda_j|^{\ell-m}|J|^m$ by $\prec |\lambda_j|^\ell$.

□

Proof of Theorem 5.29. The Theorem follows directly from Lemmas 5.30–5.31.

□

Remark 5.32. The necessary condition

$$\underline{\breve{E}}_\ell(t) = \underline{E}\circ\widetilde{s}_\ell(t)\,\underline{J}^{-\breve{m}_*}$$

of Theorem 5.29 can be checked easily to narrow down the convergence class of Hausdorff distance.

A result closely related to Theorem 5.29, which we will likewise need in the next section, is

Corollary 5.33. *Continue with the scenario of Theorem 5.29. Suppose that* $\mathcal{H}_\ell(\mathbf{Q}) \prec |\lambda_{j_0}|^\ell$ *holds for all initial control points* $\mathbf{Q}$*. Then*

$$\breve{\chi}_\ell(t) = \breve{\chi}_\ell(t') \implies \underline{\breve{E}}_\ell(t) = \underline{\breve{E}}_\ell(t'),$$

i.e. the function

$$\tilde{\underline{E}}_\ell(\omega) := \underline{\breve{E}}_\ell \circ \breve{\chi}_\ell^{-1}(\omega), \quad \omega \in \breve{\chi}_\ell(\mathbf{S}_n),$$

is welldefined.

Proof. Let $t_1, t_2 \in \mathbf{S}_n$ with $\breve{\chi}_\ell(t_1) = \breve{\chi}_\ell(t_2)$. Then

$$\begin{aligned}\underline{\breve{E}}_\ell(t_1)\underline{J}^{+\breve{m}_*} &= \underline{E} \circ \widetilde{s}_\ell(t_1) = \underline{E} \circ \chi^{-1} \circ 2^{-\breve{m}_*}\breve{\chi}_\ell(t_1) \\ &= \underline{E} \circ \chi^{-1} \circ 2^{-\breve{m}_*}\breve{\chi}_\ell(t_2) \\ &= \underline{\breve{E}}_\ell(t_2)\underline{J}^{+\breve{m}_*}.\end{aligned}$$

□

Super-convergent, piecewise (bi-) linear proxies imply unusable central surfaces

In Remark 5.32, we conclude from eigensplines on properties of the respective super-converging eigenproxies. We use equation (5.32) in the opposite direction now:

Theorem 5.34. *Suppose the generating proxies* $\breve{B}_\ell$ *are super-convergent. Further, let there exist some* $\ell_0 \in \mathbb{N}$ *and* $S \subseteq \mathbf{S}_n$ *such that the restriction of* $\breve{B}_{\ell_0}$ *to* S *is a polynomial of total order two. Then for all central surfaces*[4]

$$[\chi M, \sum_{k=3}^{2+\sharp\mu} e_k\alpha_k], \quad M \in GL_2(\mathbb{C}),\, \alpha_k \in \mathbb{C},$$

the height-function

$$h(\omega) := \sum_{k=3}^{2+\sharp\mu} \alpha_k e_k \circ \chi^{-1}(\omega M^{-1}), \quad \omega \in \lambda^{\breve{m}_*}\breve{\chi}_{\ell_0}(S)M, \tag{5.35}$$

is a polynomial of total order two.

[4]Central surfaces were first introduced in [49].

Proof. Obviously this statement is true if and only if it holds for $M = I_2$. It is $\widetilde{s}_\ell(t) := \chi^{-1} \circ \breve{\chi}_{\ell+\breve{m}_*}(2^{-\breve{m}_*}t) = \chi^{-1}(\lambda^{\breve{m}_*}\breve{\chi}_\ell(t))$. Along with Theorem 5.29 for $j_0 = 2 + \sharp\mu$, this yields

$$\underline{\breve{E}}_{\ell_0}(t) = \underline{E} \circ \chi^{-1}(\lambda^{\breve{m}_*}\breve{\chi}_{\ell_0}(t))\, \underline{J}^{-\breve{m}_*}.$$

By Lemma 5.33, the function $\underline{\breve{E}}_{\ell_0} \circ \breve{\chi}_{\ell_0}^{-1}$ is well-defined. Hence,

$$\underline{\breve{E}}_{\ell_0} \circ \breve{\chi}_{\ell_0}^{-1}\ \underline{J}^{+\breve{m}_*} = \underline{E} \circ \chi^{-1}(\lambda^{\breve{m}_*}\cdot).$$

By premise, the restriction to $\breve{\chi}_{\ell_0}(S)$ of the left-hand side is a polynomial of total order 2. Therefore, $\underline{E} \circ \chi^{-1}(\lambda^{\breve{m}_*}\cdot)$ restricted to $\breve{\chi}_{\ell_0}(S)$ is a polynomial of total order two.

It follows that $\mathbf{x} \circ \chi^{-1}(\cdot M^{-1})$ restricted to $\lambda^{\breve{m}_*}\breve{\chi}_{\ell_0}(S)M$ is a polynomial of total order two, and also

$$h(\omega) = \sum_{k=3}^{2+\sharp\mu} e_k \circ \chi^{-1}(\omega M^{-1}), \quad \omega \in \lambda^{\breve{m}_*}\breve{\chi}_{\ell_0}(S)M,$$

as claimed. □

Let us discuss the impact of Theorem 5.34:

- First, if the generating proxies are of total order two on some piece $P \subseteq \mathbf{S}_n$, the height mapping $h(\omega)$ in the corollary is affine-linear on $\omega \in \breve{\chi}_{\ell_0}(P)$. This is unusable for central surfaces, which should at least have curvature $\neq 0$ somewhere within topological interior of P.

- Second, enter the scenario when the generating proxies are of bi-order two, piecewise. Typically, the $\breve{B}_\ell$ are linear on the parameter lines,

$$[0,1] \times \{y_2\} \times \mathbb{Z}_n, \quad , \{y_1\} \times [0,1] \times \mathbb{Z}_n, \tag{5.36}$$

  where $y_j \in [0,1]$. (Figure 5.7 presents those parallels where one of the y_j is in $\{i/5 : i \in \{0,\dots,5\}\}$.)
  Consider, for instance, the third spline ring of Figure 5.7. Each segment of $\chi(\mathbf{S}_n^0)$ is covered completely by a single bi-linear piece of the characteristic proxy. In practice, a scheme is useless if the central surfaces are linear on these lines (also, we should not forget that only few of these lines can be shown in the illustration!).

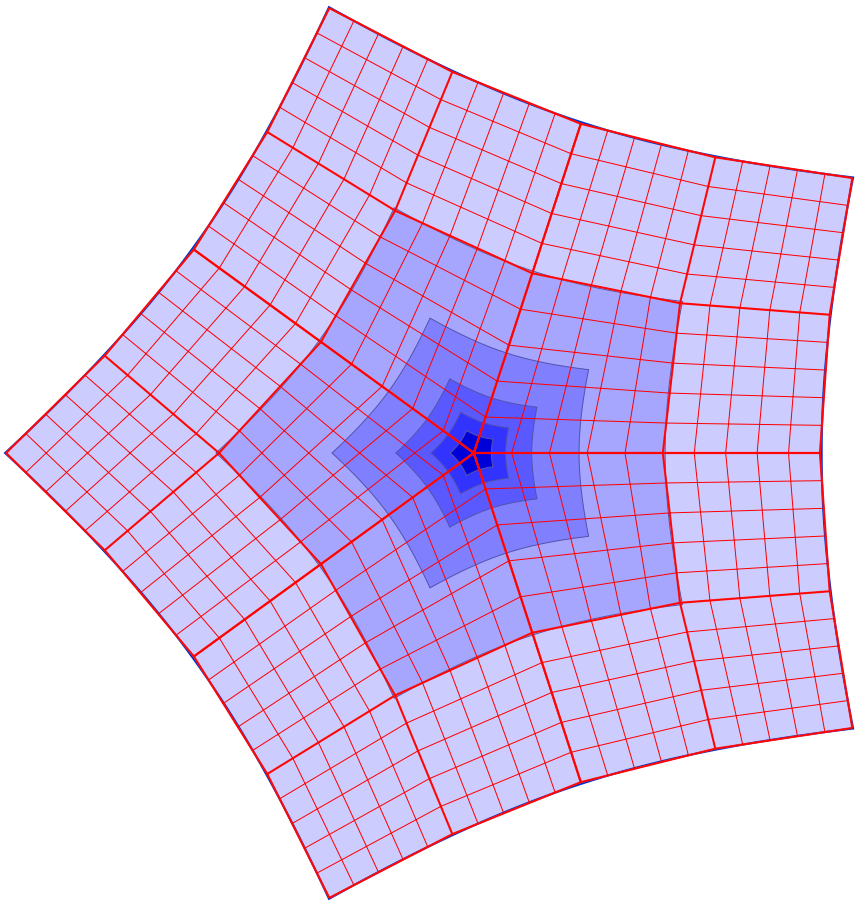

Figure 5.7: The situation of bi-linear proxies in Corollary 5.34 for the typical case: (some) lines $\tilde{L}_{y_2,j}(\cdot) = \breve{\chi}_0(\cdot, y_2, j)$, $\bar{L}_{y_1,j}(\cdot) = \breve{\chi}_0(y_1, \cdot, j)$ on whose image the height function $h(\omega)$ is affine-linear for every central surface. Thicker lines indicate linear pieces of the proxy at level 0: bends only can occur at these transitions.

- Even if only the bi-order is 2, one can typically conclude that central surfaces would have to have linear height maps. In Figure 5.7, the radial parameterlines of $\breve{\chi}_0$ that are plotted across χ^0 and χ^1 are not parallel. Consequently, the height-mapping $h(\omega)$ of a central ring follows to be linear in *three* directions (two of which are linearly independent). The entire piece of the central surface would have to be of total order two.

Except for the rate of decay of the parametric distance to its spline, we

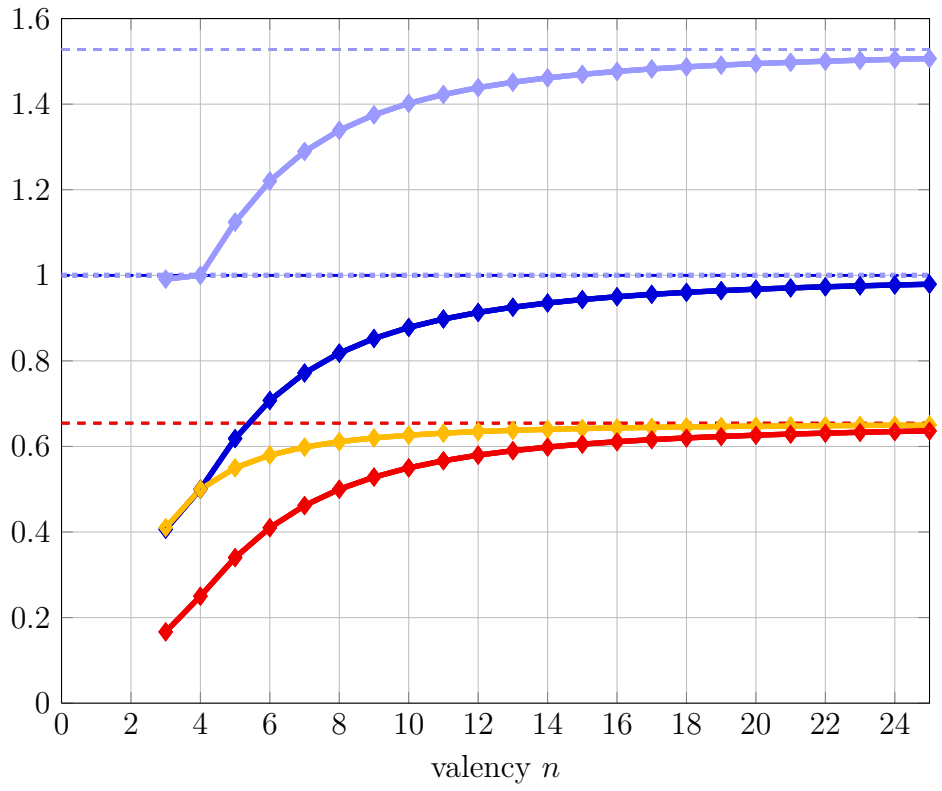

Figure 5.8: Overview of eigenvalues resulting from the standard weights of the Catmull-Clark algorithm: $\lambda_n, \mu_n, \frac{\mu_n}{\lambda_n}$ and $\frac{\mu_n}{\lambda_n{}^2}$. The lower dashed line indicates the limit $(\sqrt{5}+3)/8 \approx 0.655$ of μ_n and λ_n for $n \to \infty$. The middle one marks the threshold of $\frac{\mu_n}{\lambda_n{}^2}$ for bounded/unbounded curvature at 1 (less or equal, respectively greater than). The uppermost dashed line is the limit of μ/λ^2 for $n \to \infty$, $\frac{8}{\sqrt{5}+3} \approx 1.528$.

did not require any special properties of the refinement operation $\breve{B}^0_\ell \mapsto \breve{B}^0_{\ell+1}$. Usually, it can be described by a local proxy of regular valence – we will say $\breve{B}_\ell$ *incorporates the regular case*. The convergence class of $\|\chi^0 - \breve{\chi}^0_\ell\|_\infty$ is then q^ℓ for some easily determined $0 < q < 1$, the subsub-dominant eigenvalue of the regular case (also cf. Theorem 2.13 for polynomial schemes). It should be noted that the parameter q is an additional check on the decay of Hausdorff distance then.

Figure 5.8 on page 189 shows which convergence classes are to be expected from the Catmull-Clark algorithm. It becomes apparent why this algorithm has so slow convergence. Even for valency eight, the convergence class of Hausdorff distance is merely $\left(\frac{1}{2}\right)^\ell$, as opposed to $\left(\frac{1}{4}\right)^\ell$ that would be possible (and is convergence class for the regular case, valency four).

5.7 Convergence class of unit normals

There are few publications on normals of subdivision surfaces. Ginkel et al. [19] examine whether the cone of normals of a control polyhedron encloses surface normals, and points out that this conjecture is false. However, as far as is known to us, no estimate of convergence rate has been made for normals near extraordinary points. In this section, we estimate convergence speed of *unit*-normals of a subdivision surface, i.e. normals of length 1.

Assumptions

In this section, let $|\cdot|$ be the Euclidean norm. Further, we require $\mathbf{Q} \in \mathbb{R}^{(\bar{k}+1)\times 3}$. Without loss of generality, we can then fix scaling of $\mathbf{P}$ and rotate the coordinate-system such that

$$\mathbf{p}_1 \times \mathbf{p}_2 = \begin{bmatrix} 1 \\ 0 \\ 0 \end{bmatrix}.$$

The generating proxies are to be at least piecewise differentiable, their first derivatives on the first ring converging as

$$\|D(B^0 - \breve{B}^0_\ell)\|_\infty \preccurlyeq q_1^\ell \tag{5.37}$$

for some $q_1 \in (q, 1)$. Further, $\partial_0 B^0, \partial_1 B^0$ are assumed to be Lipschitz-continuous.

Goal of the section

The quadratic operator $\overset{\times}{\nabla}$ assigns to any function $g\colon \mathbb{R}^2 \to \mathbb{C}^3$ its crossed gradients,

$$\overset{\times}{\nabla} g := (\partial_0 g) \times (\partial_1 g).$$

The unit normals are then given by

$$\mathbf{n}(s) := \frac{\overset{\times}{\nabla}\mathbf{x}}{|\overset{\times}{\nabla}\mathbf{x}|}(s), \quad \breve{\mathbf{n}}_\ell(t) := \frac{\overset{\times}{\nabla}\breve{\mathbf{x}}_\ell}{|\overset{\times}{\nabla}\breve{\mathbf{x}}_\ell|}(t).$$

A well-known rule is: if $f_0, \dots, f_n : \mathbb{R}^2 \to \mathbb{R}$ are arbitrary differentiable functions which are weighted by coefficients $\mathbf{a}_0, \dots, \mathbf{a}_n \in \mathbb{C}^{1\times 3}$, it is

$$\overset{\times}{\nabla} \sum_{i=0}^{n} f_i \mathbf{a}_i = \sum_{0\le i<m\le n} \det D[f_i, f_m](\mathbf{a}_i \times \mathbf{a}_m). \tag{5.38}$$

This section aims toward

Theorem 5.35 (Convergence class of unit normals)**.** *Let* $\min\det D\breve{\chi}_\ell > 0$ *and* (5.37)*. Then unit normals of proxy and spline converge according to*

$$|\mathbf{n}(s) - \breve{\mathbf{n}}_\ell(t)| \preccurlyeq \widetilde{\mu}^{\varrho_\ell} q_1^{\ell-\varrho_\ell}, \quad \widetilde{\mu} := \left|\frac{\mu}{\lambda}\right|. \tag{5.39}$$

Remark 5.36. Comparing unit normals at matching points in the tangent plane would be more interesting than the parametric difference we consider in Theorem 5.35. However, the problem becomes more complicated then, and will be a topic for future research.

Dissection

Separating control points into eigen-components was sufficient in the previous sections. Decay of the difference in derivatives between spline and proxy is an additional aspect now. Additionally, $\overset{\times}{\nabla}$ is a quadratic operator, which means that these two factors intermix.

We can arrange summands in a two dimensional matrix

$$\begin{aligned} F &:= \begin{bmatrix} F_0 \\ F_1 \end{bmatrix} := \begin{bmatrix} f_{00} & \dots & f_{0\bar{k}} \\ f_{10} & \dots & f_{1\bar{k}} \end{bmatrix} \\ &:= \left[\begin{array}{ccc|cc} e_0(s) & \dots & e_2(s) & \dots & e_{\bar{k}}(s) \\ \hline \breve{e}_{\ell 0}(t) - e_0(s) & \dots & \breve{e}_{\ell 2}(t) - e_2(s) & \dots & \breve{e}_{\ell\bar{k}}(t) - e_{\bar{k}}(s) \end{array}\right] \end{aligned} \tag{5.40}$$

(we will get to the partitioning in the display shortly). Usually, we suppress dependence upon ℓ, s, t in the notation of the f_{jk}. With the renamed terms,

we have the situation

$$\mathbf{x} = F_0\mathbf{P} = \sum_{k=0}^{\bar{k}} f_{0k}\mathbf{p}_k,$$
$$\breve{\mathbf{x}}_\ell = \mathbf{x} + F_1\mathbf{P} = \sum_{j=0}^{1}\sum_{k=0}^{\bar{k}} f_{jk}\mathbf{p}_k.$$

Let

$$\begin{array}{rcl} i_0 & := & (j_0, k_0), \\ i_1 & := & (j_1, k_1), \end{array} \tag{5.41}$$

where the k_m range from 0 to $\bar{k}$, while the row indices j_0, j_1 are in $\{0, 1\}$. We can order the f_{jk} linearly in the lexicographic way,

$$i_0 \overset{\text{lex}}{<} i_1 \Leftrightarrow (k_0 < k_1 \vee k_0 = k_1 \wedge j_0 < j_1)\,.$$

Now, rule (5.38) can be applied, but with $\overset{\text{lex}}{<}$ in place of $<$.

Each of the summands in $\overset{\times}{\nabla}\mathbf{x}, \overset{\times}{\nabla}\breve{\mathbf{x}}_\ell$ is then identified by the pair of its indices,

$$i := (i_0, i_1). \tag{5.42}$$

We will use the names in (5.41)-(5.42) for the rest of the section.

We classify the various multi-indices i from (5.42) into sets $\mathcal{I}_{gh}$, according to the two criteria

1. Whether the summand vanishes when the refinement level ℓ goes to infinity,
   - $j_0 = j_1 = 0$ shall be if and only if $g = 0$ (no decay – stable), versus
   - at least one factor vanishes ($g = 1$). The whole summand becomes $\preccurlyeq q_1^\ell$.
2. Their decay towards the central point,
   - both $k_0, k_1 \in \{0, 1, 2\}$ shall be if and only if $h = 0$,
   - otherwise ($h = 1$): at least one of k_0, k_1 is from $\{3, \ldots, \bar{k}\}$.

   Actually, when $k_0 = 0$ or $k_1 = 0$, the respective factor is zero (the derivative of $e_0 = \breve{e}_{\ell 0} = 1$).

Display (5.40) indicates this partitioning. We summarize:

$$\begin{aligned}\mathcal{I}_{gh} := \{i : \text{ with (5.41)(5.42), } & k_0, k_1 \in \{0, \ldots, \bar{k}\},\ j_0, j_1 \in \{0,1\},\ i_0 \overset{\text{lex}}{<} i_1,\\ & j_0 = j_1 = 0 \text{ if and only if } g = 0,\\ & \{k_0, k_1\} \subset \{0,1,2\} \text{ if and only if } h = 0\}, \quad g, h \in \{0,1\}.\end{aligned}$$

The $\mathcal{I}_{gh}$ define

$$\nu_{gh} := \frac{1}{\det D\chi} \sum_{i \in \mathcal{I}_{gh}} \det D[f_{i_0}, f_{i_1}](\mathbf{p}_{k_0} \times \mathbf{p}_{k_1}).$$

By rule (5.38) – with the standard linear order $<$ replaced by $\overset{\text{lex}}{<}$ (lexicographic) –

$$\nu_{00} = \mathbf{p}_1 \times \mathbf{p}_2 = \begin{bmatrix} 1 \\ 0 \\ 0 \end{bmatrix},$$

$$\frac{\overset{\times}{\nabla}\mathbf{x}}{\det D\chi} = \nu_{00} + \nu_{01}, \tag{5.43}$$

$$\frac{\overset{\times}{\nabla}\breve{\mathbf{x}}_\ell}{\det D\chi} = \nu_{00} + \nu_{01} + \nu_{10} + \nu_{11}. \tag{5.44}$$

Similarly - (5.38) backwards, then forwards -

$$\begin{aligned}\nu_{00} + \nu_{10} &= \frac{1}{\det D\chi} \sum_{i \in \mathcal{I}_{00} \cup \mathcal{I}_{10}} \det D[f_{i_0}, f_{i_1}](\mathbf{p}_{k_0} \times \mathbf{p}_{k_1})\\ &= \frac{\overset{\times}{\nabla}\breve{\chi}_\ell}{\det D\chi} = \frac{\det D\breve{\chi}_\ell}{\det D\chi}(\mathbf{p}_1 \times \mathbf{p}_2).\end{aligned} \tag{5.45}$$

We partition the domain $\mathcal{D} = \mathbb{N} \times \mathbf{S}_n$ into three disjoint subdomains,

$$\mathcal{D}_1 := \mathbb{N} \times \left(\bigcup_{m=0}^{\bar{m}-1} \mathbf{S}_n^m \right), \qquad \bar{m} \text{ "outermost rings".}$$

$$\mathcal{D}_2 := \{0\} \cup \bigcup_{\substack{m \geq \bar{m},\\ m - \ell > \bar{\ell} + \bar{m}}}^{\infty} \{\ell\} \times \mathbf{S}_n^m, \qquad \text{"central point region",}$$

$$\mathcal{D}_3 := \bigcup_{\substack{m \geq \bar{m},\\ \ell - m \geq \bar{\ell} + \bar{m}}} \{\ell\} \times \mathbf{S}_n^m, \qquad \text{"region of transition"}$$

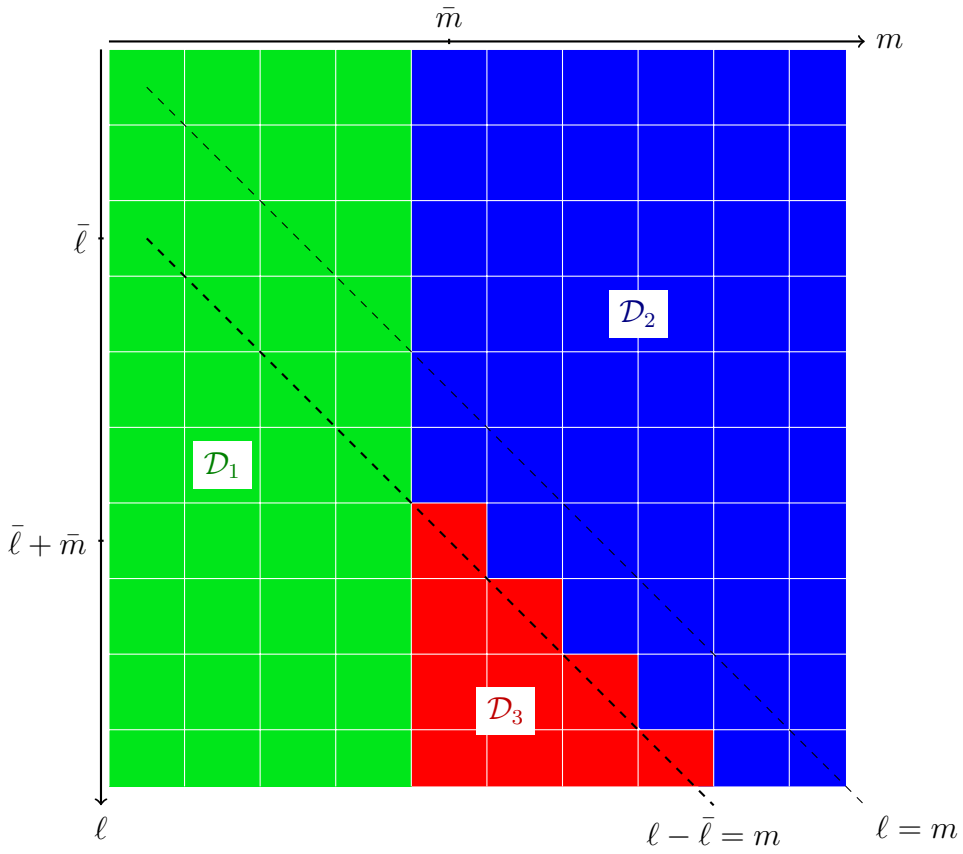

Figure 5.9: Partitioning of the domain into regular region, central point region and region of transition for arbitrary parameters $\bar{\ell}, \bar{m} \in \mathbb{N}$. ℓ is the refinement level, m the ringindex.

(Figure 5.9 on page 194 shows the situation at a glance). The parameters $\bar{\ell}, \bar{m} \in \mathbb{N}$ will be adjusted (only upwards) during the discussion.

Following this, we use the simple principle

Lemma 5.37. *Let f, g be functions from $\mathcal{D} \to \mathbb{C}^d$ for some domain $\mathcal{D}$, $d \in \mathbb{N}$. Further,*

$$\mathcal{D} = \mathcal{D}_1 \cup \ldots \cup \mathcal{D}_m,$$

to some fixed $m \in \mathbb{N}$. Then

$$f \preccurlyeq g \;\Leftrightarrow \left(f_{|\mathcal{D}_j} \preccurlyeq g_{|\mathcal{D}_j} \text{ for all } 1 \le j \le m\right)$$

(and similarly for $\succcurlyeq$ and $\sim$).

Proof. "$\Rightarrow$": $f \preccurlyeq g$ implies there is some $C > 0$, such that $f(x) \le g(x)C$ for all $x \in \mathcal{D}$. Hence, $f_{|\mathcal{D}_j}(x) \le g_{|\mathcal{D}_j}(x)$ for every $x \in \mathcal{D}_j$, which is the definition of $f_{|\mathcal{D}_j} \preccurlyeq g_{|\mathcal{D}_j}$

"$\Leftarrow$": by definition of $\preccurlyeq$, there are $C_1, \ldots, C_m > 0$ such that $f(x) \le g(x)C_j$ for all $x \in \mathcal{D}_j$. Let $C := \max_{1 \le j \le m} C_j$. It follows that $f(x) \le g(x)C$ for all $x \in \mathcal{D}$. □

The stepping stone

Starting point for the proof of Theorem 5.35 are the convergence classes of the ν_{gh},

Lemma 5.38. *If (5.37) holds then the restrictions of ν_{gh} to $\mathcal{D}_1 \cup \mathcal{D}_3$ fulfill*

$$\begin{array}{llll} \nu_{00} & \sim 1 & \nu_{01} & \preccurlyeq \widetilde{\mu}^{\varrho_\ell} \\ \nu_{10} & \preccurlyeq q_1^{\ell-\varrho_\ell} & \nu_{11} & \preccurlyeq \widetilde{\mu}^{\varrho_\ell} q_1^{\ell-\varrho_\ell}. \end{array} \tag{5.46}$$

Furthermore, if the initial control points are (componentwise) real-valued, the above decomposition is so, too: $\nu_{00}, \nu_{01}, \nu_{10}, \nu_{11} \in \mathbb{R}^{1\times 3}$.

Proof. Let $v \in \{0, 1\}$ denote the variable number we are differentiating for. It is $\partial_v e_0 = 0$. For $t \in 2^{-m}\mathbf{S}_n$ it is $E(t) = E(2^m t)J^m$. So,

$$\left(\partial_v E\right)(t) = 2^m \left(\partial_v E\right)(2^m t)\, J^m, \quad m \in \mathbb{N}, t \in 2^{-m}\mathbf{S}_n.$$

With $m = \varrho_\ell(t)$ this can be written in the more compact form

$$\partial_v E = 2^{\varrho_\ell} \left(\partial_v E\right) \left(2^{\varrho_\ell} \cdot\right) J^{\varrho_\ell}. \tag{5.47}$$

The $\nu_{h0} \cdot (\det D\chi)$, $h \in \{0, 1\}$, are sums of products whose factors both stem from subdominant components, or else vanish. On the other hand, for ν_{h1}, $h \in \{0, 1\}$, it is $k_0 \geq 3 \vee k_1 \geq 3$. The terms 2^{ϱ_ℓ} in each of the two factors cancel with their counterpart $2^{2\varrho_\ell}$ from $1/\det D\chi$. The first row of (5.46) follows.

The $\nu_{1h} \cdot (\det D\chi)$, $h \in \{0, 1\}$, in the bottom row are sums of products where one of the two factors is provided by the proxy. Regardless which one it is, let $k \in \{0, \ldots, \bar{k}\}$ denote its eigen-component. Analogously to the statement above, $\partial_v \breve{e}_{\ell 0} \equiv 0$ and

$$\begin{aligned} \left(\partial_v \breve{E}_\ell\right)(t) &= 2^m \left(\partial_v \breve{E}_{\ell-m}\right)(2^m t)\, J^m, \quad 0 \leq m \leq \ell, t \in 2^{-m}\mathbf{S}_n, \\ \partial_v \breve{E}_\ell &= 2^{\varrho_\ell} \left(\partial_v \breve{E}_{\ell-\varrho_\ell}\right)(2^{\varrho_\ell} t)\, J^{\varrho_\ell}. \end{aligned}$$

Hence,

$$\partial_v f_{1k} = \partial_v(\breve{e}_{\ell k} - e_k) \preccurlyeq \begin{cases} \lambda^{\varrho_\ell} q_1^{\ell-\varrho_\ell} & \text{if } k \in \{0, 1, 2\} \\ \mu^{\varrho_\ell} q_1^{\ell-\varrho_\ell} & \text{if } k \geq 3. \end{cases} \tag{5.48}$$

The bottom row of (5.46) follows immediately.

If $\mathbf{Q} \in \mathbb{R}^{1\times 3}$ then the subdominant eigencoefficients have to be reals as well – otherwise, because they dominate decay toward the central point, the surface would exhibit complex function values near the central point. Hence, the components of ν_{00} and ν_{10} are reals. Since $\overset{\times}{\nabla}\mathbf{x}$ and $\overset{\times}{\nabla}\breve{\mathbf{x}}_\ell$ lie in $\mathbb{R}^{1\times 3}$, by equations (5.43)-(5.44) ν_{01}, ν_{11} must be vectors of reals as well. □

All functions on $\mathbb{N} \times \mathbf{S}_n$ are restricted to the respective $\mathcal{D}_j$ in the following dichotomy of the $\mathcal{D}_j$. To make inspection easy we have refrained from restricting the functions each individually.

Regular region on outermost rings

First, what happens on the regular region of the subdivision surface? Consider the first $\bar{m}$ rings,

$$\mathcal{D}_1 := \mathbb{N} \times \left(\bigcup_{m=0}^{\bar{m}-1} \mathbf{S}_n^m \right).$$

Since $m \in \{0, \dots, \bar{m} - 1\}$ is bounded in this case, it is enough to show that the difference of unit normals is $\preccurlyeq q_1^\ell$. If we let

$$1 + \tau := \frac{|\nu_{00} + \nu_{01} + \nu_{10} + \nu_{11}|}{|\nu_{00} + \nu_{01}|}$$

then $|\tau| \in [0, \frac{|\nu_{10}+\nu_{11}|}{|\nu_{00}+\nu_{01}|}]$. By Lemma 5.38 the ν_{1h} are $\preccurlyeq q_1^\ell$ while the ν_{0h} are inherently independent of ℓ, so $\tau \preccurlyeq q_1^\ell$. Further, we can assume the level ℓ to be high enough that $|\tau| < 1$. Using the geometric series

$$\frac{1}{1+z} = \sum_{k=0}^{\infty} (-1)^k z^k =: 1 + H(z) \tag{5.49}$$

yields

$$\frac{\overset{\times}{\nabla}\check{\mathbf{x}}_\ell}{|\overset{\times}{\nabla}\check{\mathbf{x}}_\ell|} = \frac{1}{|\nu_{00} + \nu_{01}|}(1 + H(\tau))\left(\nu_{00} + \nu_{01} + \nu_{10} + \nu_{11}\right).$$

The terms $H(\tau), \nu_{10}, \nu_{11}$ are all $\equiv 0 \bmod q_1^\ell$. Thus,

$$\frac{\overset{\times}{\nabla}\check{\mathbf{x}}_\ell}{|\overset{\times}{\nabla}\check{\mathbf{x}}_\ell|} \equiv \frac{\nu_{00} + \nu_{01}}{|\nu_{00} + \nu_{01}|} \bmod q_1^\ell = \frac{\overset{\times}{\nabla}\mathbf{x}}{|\overset{\times}{\nabla}\mathbf{x}|},$$

i.e. the difference of unit normals is $\preccurlyeq q_1^\ell$ and therefore $\preccurlyeq \widetilde{\mu}^{\varrho_\ell} q_1^{\ell-\varrho_\ell}$on $\mathcal{D}_1$, too.

Towards the central point

For some maximal refinement level $\bar{\ell} \in \mathbb{N}$, let us examine what happens on

$$\mathcal{D}_2 := \{0\} \cup \bigcup_{\substack{m \geq \bar{m}, \\ m - \ell > \bar{\ell} + \bar{m}}}^{\infty} \{\ell\} \times \mathbf{S}_n^m.$$

One can argue in a manner similar to the previous case.

For the proxy,

$$1 + \check{\tau} := \frac{|\nu_{00} + \nu_{10} + \nu_{01} + \nu_{11}|}{|\nu_{00} + \nu_{10}|}$$

fulfills $|\breve{\tau}| \in [0, \frac{|\nu_{01}+\nu_{11}|}{|\nu_{00}+\nu_{10}|}]$. By construction of the ν_{gh}, the denominator contains only summands of factors from at most subdominant terms, while in the numerator at least one of the factors decays faster than that. Consequently, $|\breve{\tau}| \preccurlyeq \widetilde{\mu}^{\varrho_\ell}$, and by the same argument $\nu_{01} + \nu_{11} \preccurlyeq \widetilde{\mu}^{\varrho_\ell}$. Again assuming ϱ_ℓ to be high enough that $|\breve{\tau}| < 1$, it is $H(\tau) \preccurlyeq \widetilde{\mu}^{\varrho_\ell}$, too. So,

$$\begin{aligned}\frac{\overset{\times}{\nabla}\breve{\mathbf{x}}_\ell}{|\overset{\times}{\nabla}\breve{\mathbf{x}}_\ell|} &= \frac{1 + H(\breve{\tau})}{|\nu_{00} + \nu_{10}|}\left(\nu_{00} + \nu_{10} + \nu_{01} + \nu_{11}\right) \\ &\equiv \frac{\nu_{00} + \nu_{10}}{|\nu_{00} + \nu_{10}|} \bmod \widetilde{\mu}^{\varrho_\ell}.\end{aligned}$$

With (5.45) and $\det D\breve{\chi}_\ell > 0$,

$$\frac{\overset{\times}{\nabla}\breve{\mathbf{x}}_\ell}{|\overset{\times}{\nabla}\breve{\mathbf{x}}_\ell|} \equiv \nu_{00} \bmod \widetilde{\mu}^{\varrho_\ell}.$$

For $\mathbf{x}$, set

$$1 + \tau := |\nu_{00} + \nu_{01}|.$$

Then $\tau \preccurlyeq \widetilde{\mu}^{\varrho_\ell}$, and proceeding completely analogously as above,

$$\begin{aligned}\frac{\overset{\times}{\nabla}\mathbf{x}}{|\overset{\times}{\nabla}\mathbf{x}|} &= \left(1 + H(\tau)\right)\left(\nu_{00} + \nu_{01}\right) \\ &\equiv \nu_{00} \bmod \widetilde{\mu}^{\varrho_\ell}.\end{aligned}$$

Hence, the norm of the difference of unit normals is $\preccurlyeq \widetilde{\mu}^{\varrho_\ell}$ on $\mathcal{D}_2$.

We have seen that towards the center, both spline's and proxy's unit normals are $\mathbf{p}_1 \times \mathbf{p}_2/|\mathbf{p}_1 \times \mathbf{p}_2|$ modulo $\widetilde{\mu}^{\varrho_\ell}$.

Region of Transition

Finally, let us consider

$$\mathcal{D}_3 = \bigcup_{\substack{m \geq \bar{m}, \\ \ell - m \geq \bar{\ell} + \bar{m}}} \{\ell\} \times \mathbf{S}_n^m.$$

Define the x_{gh}, y_{gh}, z_{gh} by

$$\nu_{10} =: \begin{bmatrix} x_{10} \\ 0 \\ 0 \end{bmatrix}, \ \nu_{01} =: \begin{bmatrix} x_{01} \\ y_{01} \\ z_{01} \end{bmatrix}, \ \nu_{11} =: \begin{bmatrix} x_{11} \\ y_{11} \\ z_{11} \end{bmatrix}. \tag{5.50}$$

From Lemma 5.38 we know the components of the ν_{gh} to be real, so let the difference of unit normals be called

$$\mathbf{d} := \frac{\nu_{00} + \nu_{01} + \nu_{10} + \nu_{11}}{\sqrt{(\nu_{00} + \nu_{01} + \nu_{10} + \nu_{11})^T(\nu_{00} + \nu_{01} + \nu_{10} + \nu_{11})}} - \frac{\nu_{00} + \nu_{01}}{\sqrt{(\nu_{00} + \nu_{01})^T(\nu_{00} + \nu_{01})}}.$$

Note that, for arbitrary $m \in \mathbb{N}$ and $G : \mathbb{R}^m \to \mathbb{R}$, applying the univariate Mean Value Theorem to $h_{(u)}(\tau) := G(u\tau)$, $\tau \in [0, 1]$, yields the existence of $\vartheta = \vartheta(u) \in (0, 1)$ such that $G(u) - G(0) = \vartheta \cdot \langle u, \operatorname{grad} G(0)\rangle$.

Transferred to our current problem, $\mathbf{d}^T\mathbf{d}$ evaluates to zero if $\nu_{10} = \nu_{01} = \nu_{11} = 0$. Using a computer algebra system we calculated $\langle u, \operatorname{grad} G(0)\rangle$ of $G = \mathbf{d}^T\mathbf{d}$ in regard to the seven variables defined in (5.50). Then we put terms onto a common denominator. The denominator turned out to be continuous in $(x_{10}, x_{01}, x_{11}, y_{01}, y_{11}, z_{01}, z_{11})$ and is 1 at zero (in fact it is some multiple of powers of the denominators in the definition of $\mathbf{d}$). With α in place of $q_1^{\ell-\varrho_\ell}$ and β for $\widetilde{\mu}^{\varrho_\ell}$, for all $(g, h) \in \{0, 1\}^2$ we applied the following substitutions to the numerator N

$$x_{gh} \mapsto \alpha^g\beta^h X_{gh}, \quad Y_{gh} \mapsto \alpha^g\beta^h Y_{gh}, \quad Z_{gh} \mapsto \alpha^g\beta^h Z_{gh}.$$

Dividing the result by $(\alpha\beta)^2$ and determining the successive new denominator yields a value of one, so N is a multiple of $(\alpha\beta)^2$, thus

$$\mathbf{d}^T\mathbf{d} \preccurlyeq (\widetilde{\mu}^{\varrho} q_1^{\ell-\varrho_\ell})^2.$$

(Interestingly, dividing N by $(\alpha\beta)^3$ produces a denominator of $\alpha\beta$.) Taking the square root on both sides of the last display ($\sqrt{\cdot}$ is a strictly monotonic increasing function) yields $\sqrt{\mathbf{d}^T\mathbf{d}} \preccurlyeq \widetilde{\mu}^{\varrho} q_1^{\ell-\varrho_\ell}$, which finishes the proof of the theorem.

In the digital attachments, the MATHEMATICA notebook

`unit-normals-of-proxies.nb`

as well as a PDF-version can be found for those who are interested.

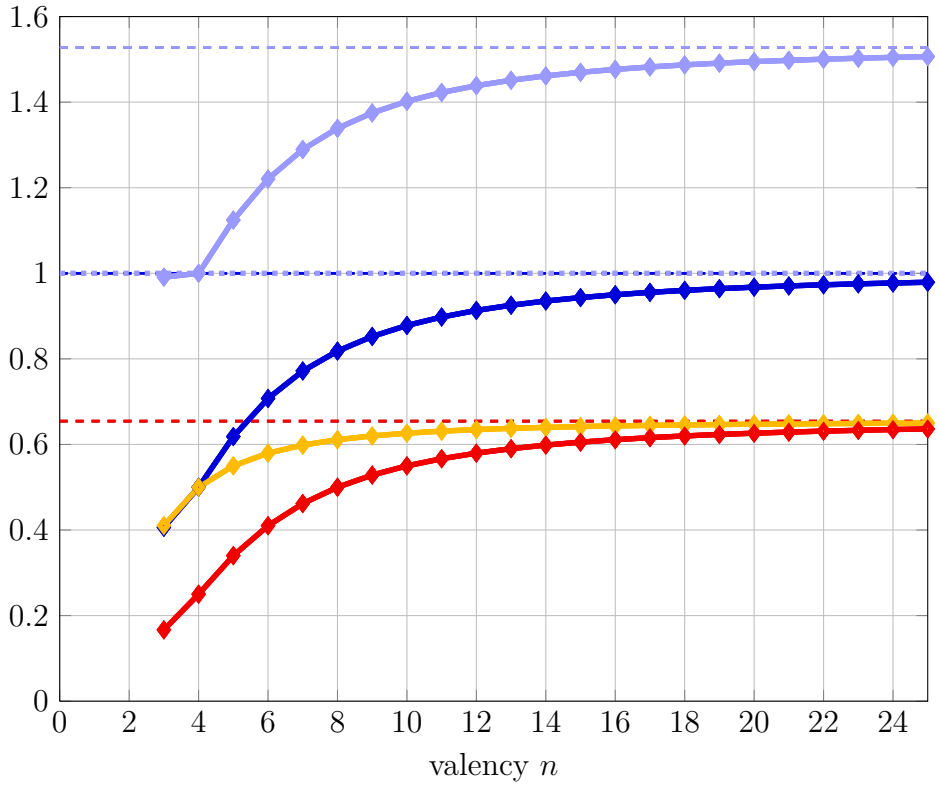

Figure 5.10: Eigenvalues of the Catmull-Clark algorithm (standard weights). $\lambda_n, \mu_n, \frac{\mu_n}{\lambda_n}$ and $\frac{\mu_n}{\lambda_n{}^2}$. The lower dashed line indicates the limit $(\sqrt{5}+3)/8 \approx 0.655$ of μ_n and λ_n for $n \to \infty$. The middle one marks $\frac{\mu_n}{\lambda_n{}^2}$'s threshold for bounded/unbounded curvature at 1 (less or equal, respectively greater than). The uppermost dashed line is the limit of μ/λ^2 for $n \to \infty$, $\frac{8}{\sqrt{5}+3} \approx 1.528$.
(The figure has been repeated from Section 5.6)

5.8 Postproxies: how convergence for Catmull-Clark proxies can be put straight

The Catmull-Clark algorithm can still be useful where C^2-surfaces are simply not needed. In particular, this applies to

1. computer-animated films, and

2. the gaming industry.

In this section, we present a concept which allows to circumvent the slow convergence of proxies toward subdivision surface.

To avoid complications that would not be relevant in practice anyway, the theory of this section presupposes

Assumption 5.39. *It is* $[0,1]\chi(\mathbf{S}_n) = \chi(\mathbf{S}_n)$ *where* $[0,1]\chi(\mathbf{S}_n) := \{\tau\omega : \tau \in [0,1], \omega \in \chi(\mathbf{S}_n)\}$.

While Assumption 5.39 certainly holds for all practically relevant schemes, one can construct artificial characteristic maps for which it is violated. However, we refrain from describing such a scenario here, as it is irrelevant in practice.

Basic principles

The previous sections have shown why convergence of (bi-) linear control polygons as proxy to its Catmull-Clark subdivision surface is so slow. The subdominant components of spline and proxy shackle $\chi(s)$ to $\breve{\chi}_\ell(t)$. Otherwise, convergence is essentially throttled to $\lambda^{\varrho_\ell} q^{\ell-\varrho_\ell}$ (cf. Theorem 5.8).

Any bilinear *proxy* would share the same flaw. But foregoing part of proxies' internal structure – the Equation of Refinement, (5.2) – can put this back in order. For example, we might proceed along the following steps:

1. First, we replace the characteristic proxy by one whose tesselation is "better" spaced: $\hat{\chi}_\ell$. In most cases, "better" would mean to choose $\hat{\chi}_\ell$ such that the images of its polynomial cells (which tesselate the tangent plane for the proxy) are evenly spaced. On the other hand, it might even make sense to thin tesselation locally sometimes, in particular when the algorithm generates only flat points at extraordinary vertices.

2. Let us assume we wished our new proxies – we call them *postproxies* – to come from the same function space $\mathcal{S}_\ell$ that is spanned by $\breve{b}_{\ell,0}, \ldots, \breve{b}_{\ell,\bar{k}}$. For the postproxies to be really useful in practice, they have to depend linearly on the input control points. We simply replace the remaining eigenproxies by "better" approximations $\hat{e}_{\ell,k}, k \geq 3$, taylored to $\hat{\chi}_\ell$ specifically. On the other hand, it is preferable in practice to define

the $\hat{b}_{\ell,k}$ instead.
Two methods are particularly straightforward to achieve this:

a) *Proxies-by-Interpolation*: Let $\hat{s}_\ell := \chi^{-1} \circ \hat{\chi}_\ell$ and $\mathcal{G}_\ell$ denote the set of Greville-abscissae of the proxy at refinement level ℓ (cf. Section 3.2). Set $\hat{b}_{\ell,k}$ as the bi-linear interpolant given by

$$\hat{b}_{\ell,k}(g) := b_k \circ \hat{s}_\ell(g), \quad g \in \mathcal{G}_\ell. \tag{5.51}$$

Note that each function value $\hat{b}_{\ell,k}(g)$ in (5.51) directly represents the value of the control point to which the Greville-abscissa g belongs. (We preferred this notation because it is easier to write down.)

b) *Proxies-as-Minimizer*: $\hat{\chi}_\ell$ is usually constructed to be injective and regular[5]. The function space it is derived from consists of piecewise C^1 functions only. Hence, with $\|\cdot\|$ any norm induced by a scalar product on functions $\mathbb{R}^2 \to \mathbb{R}$, let

$$\hat{b}_{\ell,k} := \operatorname*{argmin}_{y \in \mathcal{S}_\ell} \|y \circ \hat{\chi}_\ell^{-1} - b_k \circ \chi^{-1}\|^2. \tag{5.52}$$

The minimizer of a quadratic form $y^T Q y$ is linear in y. Thus, postproxies still depend on their control points in a linear fashion.

Both strategies reproduce $\hat{\chi}_\ell$. Defining the $\hat{b}_{k,\ell}$ directly, versus the remaining eigenproxies $\hat{e}_{\ell,k}$, $3 \leq k$ only, is preferable in the practical implementation.

Proxies-as-Minimizer allows to factor in first and/or second derivatives $\partial/\partial\chi_k$ (see Section 4.2 how these derivatives can be calculated). They would probably serve equally well for convex and hyperbolical shapes – elliptical shapes are typically a weak point for interpolatory approximands.

On the other hand, *Proxies-by-Interpolation* is extremely easy to implement. These could be applied even in regular regions. This would certainly leave transitions between proxies in regular and irregular regions of the mesh undetectable. Still, it remains to be seen whether this is actually an issue for *Proxies-as-Minimizer*.

[5]The $\hat{\chi}_\ell$ suggested in Example 5.8 apparently have these properties, too; however, we do not wish to stray into a proof here.

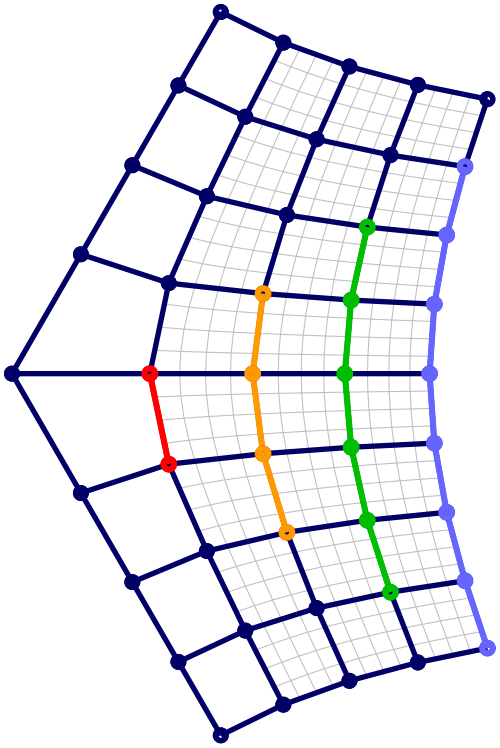

Figure 5.11: Control point rings $r \in \{1, 2, 3, 4\}$ of the Catmull-Clark proxy at level $\ell = 1$, segment j. Thin gray lines in the background indicate parameter lines of the corresponding part of the characteristic map.

Constructing a subdominant postproxy

The radial sampling function

A bi-linear proxy at level ℓ can be identified with its $2^{\ell+1}$ rings[6] of control points. Note that the outermost control-point (cp) -ring, which is needed to define the spline, is not part of the irregular point's (post-) proxy. Going outwards from the innermost cp-ring adds 2 points in every segment per ring: cp-ring $r \in \{1, \ldots, 2^{\ell+1}\}$ consists of $2r$ control points per segment.

[6]The central control point is not considered part of any cp-ring here; although one might consider it to be cp-ring "zero".

Please consult Figure 5.11 on page 203 for an overview. Counting from their bottom ends[7], the c^{th} control point in ring r is replaced by

$$\rho_\ell(\frac{r}{2^\ell})\chi(1,\, \frac{2(c-1)}{r} - 1,\, j), \quad r = 1 \dots 2^\ell,\, c = 1 \dots 2r, \tag{5.53}$$

for some *radial sampling function* $\rho_\ell : [0,1] \to [0,1]$, possibly depending on the refinement level ℓ. Notice

- the "circular" coordinate c samples the outer boundary of $\chi(\mathbf{S}_n)$ in a roughly equidistant fashion,
- the "radial" variable r controls scaling towards the center.

For example, choosing $\rho_\ell^{\text{Id}}(\tau) := \tau$ would result in polynomial pieces in $\hat{\chi}_\ell$ whose diameters roughly decay like $1/2^\ell$.

Scaling exponent

The *scaling exponent* of a subdivision scheme is defined as

$$\mathfrak{e} := \log_\lambda \mu = \frac{\ln \mu}{\ln \lambda}.$$

Going towards zero by a factor of $\tau \in \{\lambda^m :\ m \in \mathbb{N}\}$ within

$$\Omega := \chi(\mathbf{S}_n) \setminus \{(0,0)\},$$

the (total-degree-) g-th derivatives of

$$\tilde{b}_k := \left(b_k \circ \chi^{-1}\right)_{|\Omega}$$

scale by a factor of $\tau^{\mathfrak{e}-g}$. Figure 5.12 on page 205 gives an overview of $\mathfrak{e}$ for various valencies.

If the subdivision scheme is of relevance for practice, the following certainly holds:

Assumption 5.40. *For every $g \in \{0,1\}$ there is some $k \in \{3, \dots, 2 + \#\mu\}$, $(v_1, v_2) \in \{0, \dots, g\}^2$ with $g = v_1 + v_2$ and some $\omega \in \chi(\mathbf{S}_n^0)$ at which $\left(\partial_1^{v_1}\partial_2^{v_2}\tilde{e}_k\right)(\omega) \neq 0$.*

[7] In the `irP`-structure's redundant representation, their position (i, j) within segment j's matrix of control points has $i < j$, or equivalently, their Greville-absciassa in the second tensor-direction is < 0.

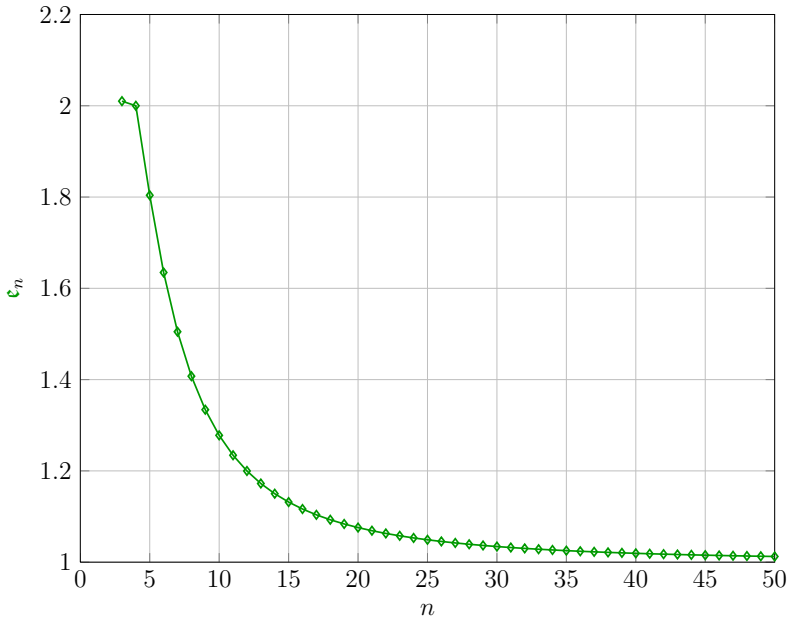

Figure 5.12: Scaling exponents $\mathfrak{e}$ of the Catmull-Clark scheme for various valencies.

We will presuppose Assumption 5.40 henceforth.

Suppose we wish to distribute the radial samples such that the maximal error in (total-degree-) g-th derivatives is minimal, $g \in \{0, 1\}$. Let $g = v_1 + v_2$, where v_j is the multiplicity by which variable j is differentiated for. It is typically

$$\max_{\omega \in \chi(\mathbf{S}_n^0)} \left| \left(\partial_1^{v_1} \partial_2^{v_2} \tilde{b}_k \right) (\tau\omega) \right| \sim \tau^{e-(v_1+v_2)}, \quad \tau \in (0, 1] \tag{5.54}$$

(this is where Assumption 5.40 comes in, yielding $\succcurlyeq$). Hence, the magnitude of g-th derivatives is essentially given by $\tau^{g-\mathfrak{e}}$, the radial values coming from $\tau \in (0, 1]$. How should the radial samples $\tau_{\ell,1} < \tau_{\ell,2} \ldots < \tau_{\ell,2^\ell}$ be placed within $[0, 1]$ in order to minimize

$$\max_{\tau \in [0,1]} \min_{1 \le j \le 2^\ell} |\tau^{g-\mathfrak{e}} - \tau_{\ell,j}|?$$

Remark 5.41. If $f : [0,1] \to \mathbb{R}$ is a strictly monotonic, continuous function – such as ρ_ℓ above– the sample points $0 = \tau_1 < \tau_2 \ldots < \tau_m = 1$ minimizing

$$\max_{\tau\in[0,1]} \min_{1\le j\le m} |f(\tau) - \tau_j| =: g(\tau_1, \ldots, \tau_m)$$

are given by

$$\tau_j = F^{-1}(\frac{j-1}{m-1}), \quad j \in \{1, \ldots, m\},$$

where $F(\tau) := \frac{f(\tau)-f(0)}{f(1)-f(0)}$. The value of the target function is then

$$g(\tau_1, \ldots, \tau_m) = \frac{1}{2(m-1)}.$$

The simple proof of this is left to the reader (the $f(\tau_j)$ are centers of closed balls of radius $1/(2(m-1))$ that – except for endpoints, disjointly – cover the image of f).

Using this on our current problem, we arrive at radial sampling functions

$$\rho_\ell(r) = r^{\frac{1}{\mathfrak{e}-g}}. \tag{5.55}$$

Remark 5.42 (A puzzle for $\mathfrak{e} = 2$?). C^2-schemes naturally have scaling exponent $\mathfrak{e} = 2$. Yet, when minimizing the deviation in function values, equation (5.55) prescribes $\tilde{\rho}(r) = \sqrt{r}$ as radial sampling function - which is *not* equidistant spacing (exactly given by ρ_ℓ^{Id}). The reason is that when sampling a parabola, equidistant spacing of sampling points (on the x-axis) is not optimal; near the apex, fewer samples are necessary. But when minimizing deviation of derivatives for these schemes ($g = 1$), we do indeed obtain the radial sampling function ρ_ℓ^{Id} as optimum.

Reasoning behind the construction

When maximum distance of the function values is minimized in this fashion ($g = 0$), the resulting postproxies are classified as $\mathcal{H}$-*postproxies* (for Hausdorff-distance). For $g = 1$ they will be referred to as $\mathbf{n}$-*postproxies*.

The accompanying figures demonstrate the benefits postproxies can bring. We used the technique *postproxies by interpolation*.

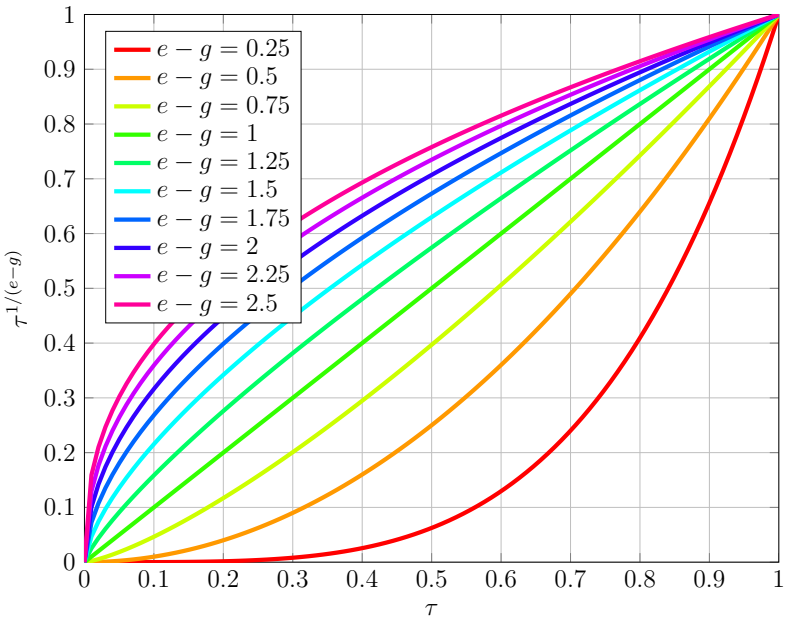

Figure 5.13: Radial sampling functions resulting from various differences $\mathfrak{e} - g$.

By (5.54) and Remark 5.41, the convergence of first derivatives of **n**-postproxies constructed with the interpolation technique should be restored to $\preccurlyeq 1/2^\ell$. By a similar argumentation as for the regular region of proxies, the convergence class of normals should follow to be $1/2^\ell$.

For $\mathcal{H}$-postproxies based on interpolation, the distance between function values at neighboring sample points follows to be $\preccurlyeq 1/2^{-\ell}$. At the sample points themselves, deviation is zero. In-between, the values are interpolated bi-linearly. Unfortunately, this is where the situation becomes more sophisticated. If $B \circ \chi^{-1}$ was C^2 everywhere in $\chi(\mathbf{S}_n)$, the error would be quadratic in $1/2^{-\ell}$, so it should be relatively straightforward to show that its convergence class is $\preccurlyeq 1/4^{-\ell}$. But second derivatives diverge towards the central point for the Catmul-Clark scheme. Therefore, an analysis must take a different route.

It is indeed unlikely that the *parametric* difference of function values has convergence class $1/4^\ell$. We conjecture its Haussdorff distance decays at this rate.

Anyway, **n**-postproxies are likely the more important ones: deviation

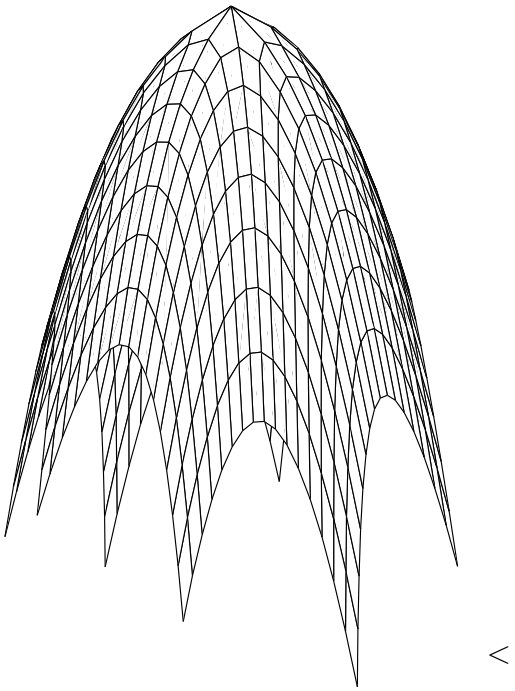

Figure 5.14: Standard Catmull-Clark proxy at refinement level $\ell = 2$, valency 8. (Interactive figure)

of function values tends to be less visible than differently sloped, adjacent facets of the control polygon. This is a topic that only further study can reveal.

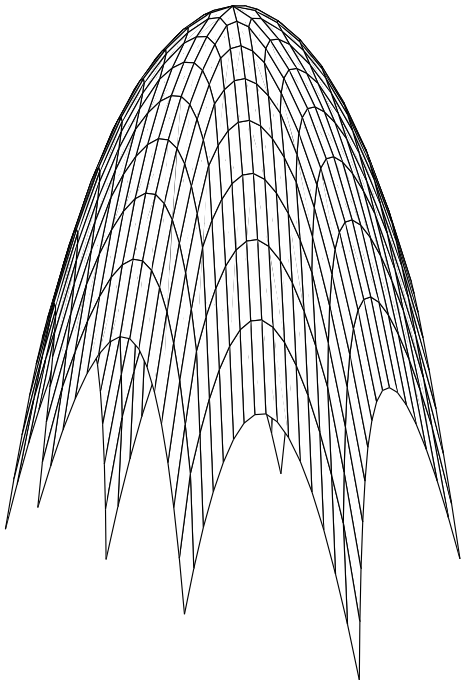

Figure 5.15: Postproxy for the Catmull-Clark scheme at refinement level $\ell = 2$, valency 8 and radial sampling function $\rho_\ell = \mathrm{id}$. This radial sampling function leads to facettes of the characteristic postproxy having roughly identical size. The number of facettes is identical to that of the standard proxy displayed in Figure 5.14. The approximation to the limit surface is much better, however. (Interactive figure)

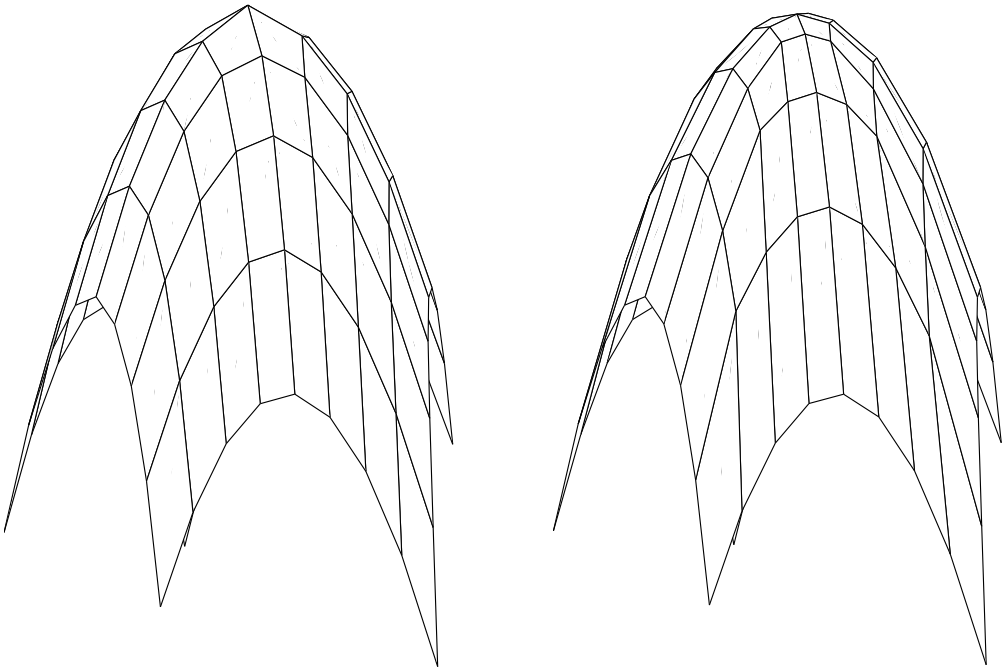

(a) Standard Proxy. **(b)** **n**-Postproxy.

Figure 5.16: Comparison between proxy and postproxy at refinement level $\ell = 1$ (at level zero no subdivisions have been applied). Here, the Catmull-Clark scheme is shown at valency five.

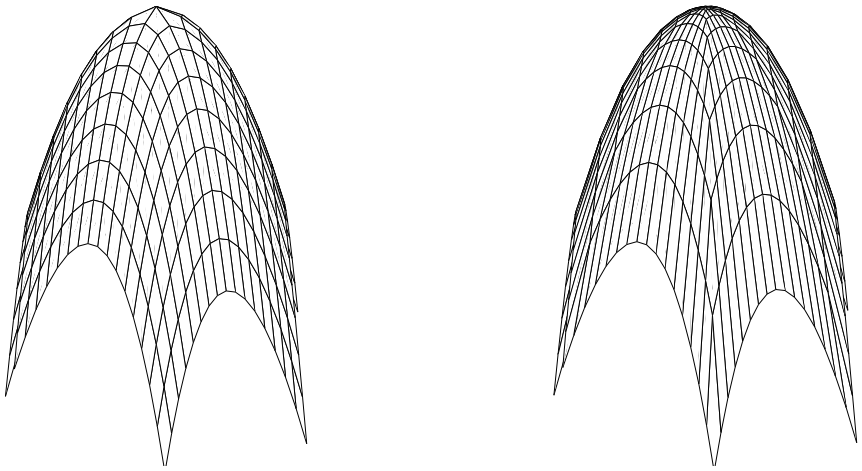

(a) Proxy. **(b)** **n**-Postproxy.

Figure 5.17: Comparison between proxy and postproxy at subdivision level $\ell = 2$. Both for the Catmull-Clark scheme at valency six.

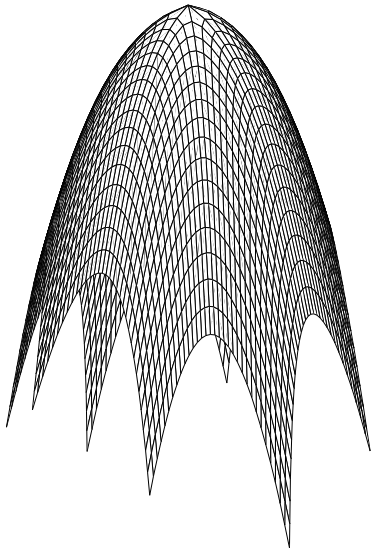

(a) Proxy.

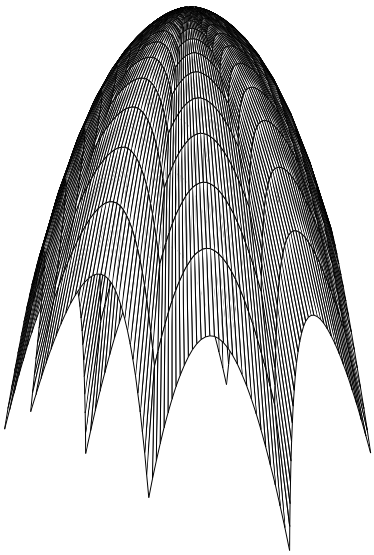

(b) **n**-Postproxy.

Figure 5.18: Comparison between proxy and **n**-postproxyat level $\ell = 3$; the Catmull-Clark scheme at valency eight.

Chapter 6

Conclusion and outlook

Chapter 2 uncovered the general mechanism which makes proxies in regular regions converge toward the limit curve/surface. Further, we introduced a new basis to decompose the space of C^2 splines of orders 7–8 into the shape-defining subspace of cubic splines, plus details of higher degree to allow for C^2 continuity in the irregular setting. Crucial questions that arise for the new bases, such as convergence of the cubic part, or their application to non-tensor product domains, have been answered. In combination with the bundle paradigm, this allows binary subdivision of splines of degrees 6–7 to proceed with masks not larger than for cardinal cubic B-splines.

In Chapter 3, we showed how characteristic maps χ to any eigenvalue $\lambda \in (0, 1)$ can be constructed; a parametrized solution is included in the digital attachments of this work. Injectivity of a characteristic map can be proved for infinitely many valencies more easily now. We also laid some groundwork regarding the topology of the image of χ, that is indispensable for proving more advanced assertions.

In Chapter 4, the PTER-scheme for extending generating rings by minimization of some quadratic functional has been tested. Our high expectations were not met. In particular, the Laplacian has been identified as unsuitable for C^2 extensions, as its solutions only C^1 connect to the outermost ring. Still, we obtained usable subdivision matrices for stationary C^2 schemes for quadratic functionals of degree three.

By our discussion with Kestutis Karciauskas, we know that he encountered similar difficulties, before turning to the principle of guides at extraordinary points. Thus, it seems likely that the subdivision matrices we obtain here mark the limit of what is possible when extending generating splines by a stationary subdivision matrix. As far as is known to us, no other stationary subdivision matrices for the examined type of C^2 schemes have been published until today.

Chapter 5 streamlined the concept of proxies as generalized approximations to subdivision surfaces near extraordinary points. We proved that the parametric distance of a subdivision surface to its control net is indeed governed by the subdominant eigenvalue λ (as has been alluded to in [50]). For Hausdorff-distance, vanishing the subdominant component by pairs $(s,t) \in \mathbf{S}_n \times \mathbf{S}_n$ with

$$\chi(s) = \breve{\chi}_\ell(t) \tag{6.1}$$

has been brought about by inverting the characteristic map, for which injectivity can be presupposed by the known requirements of C^1 algorithms. Furthermore, we have shown that there are no practical subdivision schemes with bi-linear proxies for which the distance converges faster than μ^ℓ, μ the subsubdominant eigenvalue.

Convergence speed of unit normals near extraordinary points has been estimated. The quotient μ/λ and q_1, the convergence factor for first derivatives in regular regions, are the governing terms of our estimate for extraordinary points. Proving sharpness of this estimate is a topic for future research. As proof of this might turn out to be too sophisticated, some select case studies could be more sensible.

Comparison of unit normals at matching points of the tangent plane, i.e. pairs $(s,t) \in \mathbf{S}_n \times \mathbf{S}_n$ with (6.1), likewise will be the subject of future study. Our work here can serve as a basis onto which that work can be built.

Finally, post-proxies provide a concept to restore better convergence rates to Catmull-Clark schemes, in addition to giving a broader view on proxies. Post-proxies can be highly beneficial in areas such as computer-animation films (for example “Shrek”, “Toy story”...), as well as computer games where C^2 continuity is irrelevant.

Appendix A

Additional contents

A.1 Tools for univariate splines

For working with univariate splines, the following MAPLE-functions proved useful for symbolic calculations:

MonomCoeff(s,I,n) This low-level tool is used to decide equality of splines. Given such a spline $s(x)$ with polynomial intervall I (i.e. $s_{|I}$ is a polynomial), this function returns the monomial or Bézier coefficients of $s_{|I}$ up to order n. The coefficients are computed by interpolation.

SplCoeffs(s,I,steplength,n,alpha,cond) solves $s(x) = 0$ for the unknowns $\alpha = (\alpha_1, \ldots, \alpha_{\#\alpha})$ under (optional) additional conditions **cond**. The remaining parameters, **I,steplength,n** , are needed to determine which sub-intervalls to pass to MonomCoeff when checking for equality. The intervalls handed over to it are $[I_1, I_1 + steplength], \ldots, [I_2 - steplength, I_2]$ (I and $steplength$ must be compatible).

TransLincomb(A,nofA,I,steplength) creates linear combinations of the **nofA** functions $A_1, \ldots, A_{nofA}$, using the coefficient α_j for A_j. Additional functions are created automatically by translating the block A by substituting $x_{old} = x_{new} - x_0$, with x_0 from I_1 to I_2 at **steplength**.

The package *CurveFitting* contains definitions of B-splines. For example,

```
n := 8;
nofB8 := 5;
for k from 1 to 5 do
 B8[k] := BSpline(n,x,knots=[0$(5-k), 1$min(5,4+k),
    2$min(5,k-1),3$min(5,k-6)]);
od:
```

assigns the block of five B-splines of order eight shown on the right-side of Figure 2.11 on page 38 to the vector `B8`. To represent these by their subdivided cousins, we first create a linear combination $s(x)$ of them:

```
IG :=[0,1];
s,nofalpha := TranslLincomb(map2(subs,x=2*x,B8), nofB8, IG, 1/2):
```

Then, to find the representation of `B8[j]`, $j = 1 \ldots 5$, solve $s - B8[j] = 0$ for the α_k,

```
l := SplKoeffs(s - B8[j],[-5,10],1/2,n, seq(alpha[k],    k=1..nofalpha),);
assign( l );
```

Assigning α_k to $S^{(8)}_{k,j}$ results in the subdivsion matrix $S^{(8)}$ presented in Table 2.2 on page 37.[1]

[1]Note that if one already have values assigned to the α_k, thus also to s, they need to be unassigned in MAPLE before solving for a different `B8[j]`. One can do this with `unassign('alpha','s'):`, then repeat the steps above.

Bibliography

[1] U. H. Augsdörfer, N. A. Dodgson, and M. A. Sabin. Variations on the four-point subdivision scheme. *Comput. Aided Geom. Des.*, 27:78–95, January 2010. ISSN 0167-8396. doi: 10.1016/j.cagd.2009.09.002. URL `http://portal.acm.org/citation.cfm?id=1655416.1655576`. 12

[2] A.A. Ball and D.J.T. Storry. Conditions for tangent plane continuity over recursively generated B-spline surfaces. *ACM Trans. on Graphics*, 7:83–102, 1988. 9

[3] C. Fix C. de Boor. Spline approximation by quasiinterpolants. *Journal of Approximation Theory*, 8, 1973. 16, 60

[4] E. Catmull and J. Clark. Recursively generated B-spline surfaces on arbitrary topological meshes. *Computer Aided Design*, 10:350–355, 1978. 9

[5] A.S. Cavaretta, W. Dahmen, and C.A. Micchelli. Stationary subdivision. *Memoirs of the American Mathematical Society*, 93(453):1–186, 1991. 12

[6] E. Cohen and L. L. Schumaker. Rates of convergence of control polygons. *Computer Aided Geometric Design*, 2(1-3):229 – 235, 1985. ISSN 0167-8396. doi: DOI:10.1016/0167-8396(85)90029-9. URL `http://www.sciencedirect.com/science/article/B6TYN-45FKS4W-11/2/a101839bae4e5caa99f843eb245b075b`. 16

[7] R. Courant D. Hilbert. *Methods of Mathematical Physics*. Interscience Publishers, New York, 1953. 122

[8] C. de Boor. *A Practical Guide to Splines*. Springer-Verlag, 1978. 16

[9] C. de Boor, K. Höllig, and S. Riemenschneider. *Box splines*, volume 98 of *Applied Mathematical Sciences*. Springer-Verlag, New York, 1993. 9, 16, 153

[10] W. L.F. Degen. Explicit continuity conditions for adjacent bézier surface patches. *Computer Aided Geometric Design*, 7(1-4):181 – 189, 1990. ISSN 0167-8396. doi: DOI:10.1016/0167-8396(90)90029-Q. URL http://www.sciencedirect.com/science/article/B6TYN-45FSNKC-G/2/8b911b8eb7f7698356a54e529754f394. 108

[11] D. Doo and M. Sabin. Behaviour of recursive division surfaces near extraordinary points. *Computer Aided Design*, 10(6):356–360, 1978. 9

[12] W.-H. Du and F. J.M. Schmitt. On the g1 continuity of piecewise bézier surfaces: a review with new results. *Computer-Aided Design*, 22(9):556 – 573, 1990. ISSN 0010-4485. doi: DOI:10.1016/0010-4485(90)90041-A. URL http://www.sciencedirect.com/science/article/B6TYR-481DYKN-1DH/2/9e14e7208d58d716a5aaa0e8ee189a8e. 108

[13] N. Dyn and D. Levin. Stationary and non-stationary binary subdivision schemes. In T. Lyche and L.L. Schumaker, editors, *Mathematical Methods in Computer Aided Geometric Design II*, pages 209–216. Academic Press, 1992. 12

[14] N. Dyn, J.A. Gregory, and D. Levin. Analysis of uniform binary subdivision schemes for curve design. *Constructive Approximation*, 7(2):127–148, 1991. 12

[15] N. Dyn, D. Levin, and D. Liu. Interpolatory convexity-preserving subdivision schemes for curves and surfaces. *Computer-Aided Design*, 24(4):211 – 216, 1992. ISSN 0010-4485. doi: DOI:10.1016/0010-4485(92)90057-H. URL http://www.sciencedirect.com/science/article/B6TYR-4829XYB-40/2/298a069c07c74f02b381edb45c93a070. 12

[16] G. E. Farin. *Curves and surfaces for CAGD, a practical guide*. Academic Press, 2002 (5th ed.). 16

[17] J. Hoschek G. Farin and M.-S. Kim, editors. *Handbook of Computer Aided Geometric Design*. Elsevier Science B.V., 2002. 16

[18] T. Garrity and J. Warren. Geometric continuity. *Computer Aided Geometric Design*, 8(1):51 – 65, 1991. ISSN 0167-8396. doi: DOI:10.1016/0167-8396(91)90049-H. URL `http://www.sciencedirect.com/science/article/B6TYN-45FJYC9-6/2/d88c1292cffbc33eeb07a754da691d8d`. 108

[19] I. Ginkel, J. Peters, and G. Umlauf. Normals of subdivision surfaces and their control polyhedra. *Computer Aided Geometric Design*, 24 (2):112 – 116, 2007. ISSN 0167-8396. doi: DOI:10.1016/j.cagd.2006.10.005. URL `http://www.sciencedirect.com/science/article/B6TYN-4MJBTCT-1/2/29a0d73562f67d05ecdcfb8c2de93406`. 190

[20] R. N. Goldman and T. D. Derose. Recursive subdivision without the convex hull property. *Computer Aided Geometric Design*, 3(4): 247 – 265, 1986. ISSN 0167-8396. doi: DOI:10.1016/0167-8396(86)90002-6. URL `http://www.sciencedirect.com/science/article/B6TYN-484N6H3-2/2/c370a02608fc0963f2b670cd03a3929b`. 12

[21] T.N.T Goodman. Closed surfaces defined from biquadratic splines. *Constr. Approx.*, 7:141–160, 1991. 108

[22] J.A. Gregory. Geometric continuity. *Mathematical Methods in Comput. Aided Geom. Des.*, pages 353–371, 1989. 108

[23] J.N. Gregory and J.M. Hahn. A C^2 polygonal surface patch. *Computer-Aided Geometric Design*, 6(1):69–75, 1989. 108

[24] W. Boehm H. Prautzsch and M. Paluszny. *Bezier and B-Spline techniques*. Springer-Verlag, 2002. Springer, 2002. 16

[25] J. M. Hahn. Geometric continuous patch complexes. *Computer Aided Geometric Design*, 6(1):55 – 67, 1989. ISSN 0167-8396. doi: DOI:10.1016/0167-8396(89)90006-X. URL `http://www.sciencedirect.com/science/article/B6TYN-45S986C-6/2/6cafa259a2f41302c7f4393b0546a066`. 108

[26] B. Juettler and P. Wassum. Some remarks on geometric continuity of rational surface patches. *Computer Aided Geometric Design*, 9(2):

143 – 157, 1992. ISSN 0167-8396. doi: DOI:10.1016/0167-8396(92)90013-F. URL http://www.sciencedirect.com/science/article/B6TYN-45D9TSW-Y/2/bc3514edd1bb96bea0ffe380faa42bc2. 108

[27] K. Karčiauskas and J. Peters. Guided subdivision. *Computer-Aided Geometric Design*, 2006. accepted subject to revision. 9

[28] K. Karčiauskas and J. Peters. Concentric tessellation maps and curvature continuous guided surfaces. *Computer-Aided Geometric Design*, 24(2):99–111, 2007. 108

[29] L. Kobbelt. Using the discrete Fourier-transform to analyze the convergence of subdivision schemes. *Appl. Comp. Harmonic Anal.*, 5: 68–91, 1998. 12

[30] F. Kuijt and R.M.J. van Damme. Smooth interpolation by a convexity preserving nonlinear subdivision algorithm. *Surface Fitting and Multiresolution Methods*, pages 219–224, 1996. URL http://purl.org/utwente/31162. 12

[31] S. L. Lee, H. H. Tan, and A. A. Majid. Smooth piecewise biquartic surfaces from quadrilateral control polyhedra with isolated n-sided faces. *Computer-Aided Design*, 27(10):741 – 758, 1995. ISSN 0010-4485. doi: DOI:10.1016/0010-4485(94)00024-8. URL http://www.sciencedirect.com/science/article/B6TYR-3YF4NGC-K/2/dac5db19d320f1d9890625031a2078c4. 108

[32] A. Li. Interpolatory convexity preserving subdivision schemes for curves. In *Proceedings of the Geometric Modeling and Processing 2004*, GMP '04, pages 379–, Washington, DC, USA, 2004. IEEE Computer Society. ISBN 0-7695-2078-2. URL http://portal.acm.org/citation.cfm?id=977398.977764. 12

[33] D. Liu and J. Hoschek. Gc1 continuity conditions between adjacent rectangular and triangular bézier surface patches. *Computer-Aided Design*, 21(4):194 – 200, 1989. ISSN 0010-4485. doi: DOI:10.1016/0010-4485(89)90044-4. URL http://www.sciencedirect.com/science/article/B6TYR-481DX7H-SC/2/79619f8339254b3ec66005e2636ba445. 108

[34] C. Loop. Smooth subdivision surfaces based on triangles. Master's thesis, Department of Mathematics, University of Utah, 1987. 9

[35] D. Lutterkort and J. Peters. Tight linear bounds on the distance between a spline and its B-spline control polygon. *Numerische Mathematik*, 89:735–748, 2001. 15

[36] T. Lyche and L. L. Schumaker, editors. *Mathematical Methods for Curves and Surfaces: Oslo 2000*. Vanderbilt University, Nashville, TN, USA, 1 edition, 2001. ISBN 0-8265-1378-6. 16

[37] T.-W. Ma. Higher chain formula proved by combinatorics. *The Electronic Journal of Combinatorics*, 16:#21, 2009. 114

[38] R. Maehara. The jordan curve theorem via the brouwer fixed point theorem. *The American Mathematical Monthly*, 91(10):pp. 641–643, 1984. ISSN 00029890. URL `http://www.jstor.org/stable/2323369`. 94

[39] A. Le Méhauté and F. I. Utreras. Convexity-preserving interpolatory subdivision. *Computer Aided Geometric Design*, 11(1): 17 – 37, 1994. ISSN 0167-8396. doi: DOI:10.1016/0167-8396(94)90023-X. URL `http://www.sciencedirect.com/science/article/B6TYN-45DHVYX-3/2/bdefe41dbfb89b71492e98863b8b622f`. 12

[40] C. Micchelli and H. Prautzsch. Computing surfaces invariant under subdivision. *CAGD*, 4:321–328, 1987. 12

[41] C.A. Micchelli and H. Prautzsch. Computing curves invariant under halving. *Computer-Aided Geometric Design*, 4:133–140, 1987. 12

[42] C.A. Micchelli and H. Prautzsch. Uniform refinement of curves. *Linear Algebra Appl.*, 114/115:841–870, 1989. 12

[43] M. E. Mortensen. *Geometric Modeling*. John Wiley & Sons, Inc., New York, NY, USA, 1985. ISBN 0471818720. 16

[44] J. Munkres. *Topology*. Prentice Hall, December 1999. ISBN 0131816292. 94

[45] D. Nairn, J. Peters, and D. Lutterkort. Sharp, quantitative bounds on the distance between a polynomial piece and its Bézier control polygon. *Computer-Aided Geometric Design*, 16(7):613–633, 1999. ISSN 0167-8396. 153

[46] J. Peters. Joining smooth patches around a vertex to form a c^k surface. *Computer Aided Geometric Design*, 9(5):387 – 411, 1992. ISSN 0167-8396. doi: DOI:10.1016/0167-8396(92)90032-K. URL `http://www.sciencedirect.com/science/article/B6TYN-45DHS9D-D/2/6ddfb6acc3c8222229ed5d4c5a60c8e3`. 108

[47] J. Peters and K. Karciauskas. An introduction to guided and polar surfacing. In *Mathematics of Curves and Surfaces*, pages 1–26. Seventh International Conference on Mathematical Methods for Curves and Surfaces, Toensberg, June-July 2008. Norway. 112

[48] J. Peters and U. Reif. Analysis of algorithms generalizing B-spline subdivision. *SIAM Journal on Numerical Analysis*, 35(2):728–748, 1998. 89

[49] J. Peters and U. Reif. Shape characterization of subdivision surfaces—basic principles. *Comput. Aided Geom. Design*, 21(6):585–599, 2004. ISSN 0167-8396. 106, 186

[50] J. Peters and U. Reif. *Subdivision Surfaces*, volume 3 of *Geometry and Computing*. Springer-Verlag, New York, 2008. 9, 10, 74, 75, 82, 89, 107, 109, 110, 111, 115, 116, 152, 214

[51] J. Peters and X. Wu. The distance of a subdivision surface to its control polyhedron. *Journal of Approximation Theory*, 161(2):491 – 507, 2009. ISSN 0021-9045. doi: DOI:10.1016/j.jat.2008.10.012. URL `http://www.sciencedirect.com/science/article/B6WH7-4V0MTF4-1/2/8e87bf9b5a95035b51a6ef3ae048a8d9`. 152

[52] L. Piegl and W. Tiller. *The NURBS Book*. Springer, 1995. 16

[53] H. Prautzsch. Freeform splines. *Computer-Aided Geometric Design*, 14(3):201–206, 1997. 106, 107, 108, 110

[54] H. Prautzsch and L. Kobbelt. Convergence of subdivision and degree elevation. *Advances in Computational Mathematics*, 2:143–154, 1994. 153

[55] U. Reif. *Neue Aspekte in der Theorie der Freiformflächen beliebiger Topologie*. PhD thesis, Universität Stuttgart, 1993. 9

[56] U. Reif. On constructing topologically unrestricted B-splines. *Zeitschrift für Angewandte Mathematik und Mechanik*, 76:73–74, 1996. Suppl. 1. 106

[57] U. Reif. A degree estimate for subdivision surfaces of higher regularity. *Proc. AMS*, 124(7):2167–2174, 1996. 33, 106, 112

[58] U. Reif. TURBS—topologically unrestricted rational B-splines. *Constructive Approximation*, 14(1):57–77, 1998. 106, 107

[59] U. Reif. *Analyse und Konstruktion von Subdivisionsalgorithmen für Freiformflächen beliebiger Topologie*. Shaker Verlag, 1999. Habilitationsschrift. 74, 89, 106, 107, 110

[60] U. Reif. Best bounds on the approximation of polynomials and splines by their control structure. *Comput. Aided Geom. Des.*, 17(6):579–589, 2000. doi: 10.1016/S0167-8396(00)00014-5. 15, 153

[61] Malcolm A. Sabin, Neil A. Dodgson, M. Sabin, and N. Dodgson. A circle-preserving variant of the four-point subdivision scheme. In *Mathematical Methods for Curves and Surfaces: Tromsø 2004, Modern Methods in Mathematics*, pages 275–286. Nashboro Press, 2005. 12

[62] I. J. Schoenberg. Contributions to the problem of approximation of equidistant data by analytic functions. *Quarterly of Applied Mathematics*, 4:44–99, 112–141, 1946. 15

[63] L. L. Schumaker. *Spline Functions Basic Theory*. Cambridge University Press, 2007 (3rd ed). 16

[64] D. J. T. Storry and A. A. Ball. Design of an n-sided surface patch from Hermite boundary data. *Comput. Aided Geom. Design*, 6(2): 111–120, 1989. ISSN 0167-8396. doi: 10.1016/0167-8396(89)90014-9. URL `http://dx.doi.org/10.1016/0167-8396(89)90014-9`. 9

[65] T. Varady. *The Mathematics of Surfaces II*. Clarendon Press, Oxford, 1987. 108

[66] O. Veblen. Theory on plane curves in non-metrical analysis situs. *Transactions of the American Mathematical Society*, 6(1):pp. 83–98, 1905. ISSN 00029947. URL http://www.jstor.org/stable/1986378. 94

René Hartmann

Year of birth:	*1977*	Nationality:	*german*
Place of birth:	*Penang Island/Malaysia*		

School and career

March 2011	Defense of PhD thesis at Technical University Darmstadt
2005–2010	Scientific Assistant at Technical University Darmstadt
2000, 3 months	Exchange student at the Imperial College, London.
1998–2005	Study of mathematics at Technical University Darmstadt.
1997–1998	Alternative civilian service.
1996	A-levels (germ., Allgemeine Hochschulreife) at Max-Planck-School, Gr. Umstadt.